High Speed Optical Wireless Communication Systems

Safwan Hafeedh Younus Fasola

Submitted in accordance with the requirements for the degree of Doctor of Philosophy

University of Leeds
School of Electronic and Electrical Engineering
June 2019

The candidate confirms that the work submitted is his own, except where work which has formed part of jointly authored publications has been included. The contribution of the candidate and the other authors to this work has been explicitly indicated below. The candidate confirms that appropriate credit has been given within the thesis where reference has been made to the work of others.

The work in Chapter 2 of the thesis has appeared in publications as follows:

1. S. H. Younus, and J.M.H. Elmirghani, “A survey of Visible Light Communication Systems” IEEE Communications Surveys and Tutorials, (to be submitted), 2019.

My contribution: literature review that covered most optical wireless (OW) systems and summarised new areas of research in OW, deserve further investigations and produced the paper.

Professor Elmirghani: Helped with the preparation of paper.

The work in Chapter 4 of the thesis has appeared in publications as follows:

1) S. H. Younus, A. T. Hussein, M. Thamer Alresheedi, and J. M. Elmirghani, "CGH for Indoor Visible Light Communication System," *IEEE Access,* vol. 5, pp. 24988-25004, 2017.
2) S. H. Younus, A. T. Hussein, M. Thamer Alresheedi, and J. M. Elmirghani, "VLC Systems with CGHs," *International Conference in Transparent Optical Network (ICTON),* accepted, 2019.

My contribution: literature review, designed three VLC systems based on computer generated holograms (CGHs) with two types of receiver. The CGHs

was used with imaging receivers to enhance system performance and enable VLC systems to operate at an aggregate data rate of 40 Gb/s.

Dr. A.T. Hussein and M. T. Alresheedi: helped with the development of the idea of CGHs and the preparation of papers.

Professor Elmirghani: Originator of the ideas of computer generated holograms and beam steering, developed the system models and helped with the preparation of the papers.

The work in Chapter 5 of the thesis has appeared in publications as follows:

1) S. H. Younus, A. Al-Hameed, A. T. Hussein, M. T. Alresheedi and J. M. Elmirghani, "Parallel Data Transmission in Indoor Visible Light Communication Systems," *IEEE Access,* vol. 7, pp. 1126-1138, 2019.

My contribution: literature review and introduced the idea of using subcarrier multiplexing (SCM) tones for parallel data transmission in indoor VLC systems with using imaging receiver in two indoor rooms. In addition, proposed a novel optical receiver to distinguish between SCM tones. As well as, simulation of the proposed idea in Matlab and produced results.

A. Al-Hameed: helped with the development of the idea of using SCM tones.

Dr. A.T. Hussein and M. T. Alresheedi: helped with preparation of paper.

Professor Elmirghani: Originator of the idea of SCM tones, developed the optical receiver and helped with the preparation of the paper.

The work in Chapter 6 of the thesis has appeared in publications as follows:

1) S. H. Younus, A. Al-Hameed, A. T. Hussein, M. T. Alresheedi and J. M. Elmirghani, "WDM for Multi-user Indoor VLC Systems with SCM," *IET Communication,* submitted, 2018.

My contribution: literature review and using subcarrier multiplexing (SCM) tones as resource allocations with WDM to realise a high data rate multiuser indoor VLC systems. In addition, proposed and designed two novel receivers: non-imaging receiver (NI-R) and non-imaging angle diversity receiver (NI-ADR). As well as, simulation of the proposed idea in Matlab and produced results with considering the effect of mobility and co-channel interference (CCI).

A. Al-Hameed, Dr. A.T. Hussein and M. T. Alresheedi: helped with preparation of paper.

Professor Elmirghani: Originator of the idea, developed the optical receivers and helped with the preparation of the paper.

2) S. H. Younus and J. M. Elmirghani, "WDM for high-speed indoor visible light communication system," in *Transparent Optical Networks (ICTON), 2017 19th International Conference on*, 2017, pp. 1-6.

My contribution: literature review and using WDM to realise a high data rate indoor VLC system. In addition, proposed and designed a novel imaging diversity receiver (IMDR) to obtain a data rate of 10 Gb/s. As well as, simulation of the proposed idea in Matlab and produced results considering mobility and diffuse reflections.

Professor Elmirghani: Originator of the idea, developed the optical receivers and helped with the preparation of the paper.

The work in Chapter 7 of the thesis has appeared in publications as follows:

1) S. H. Younus, A. Al-Hameed, A. T. Hussein, M. T. Alresheedi and J. M. Elmirghani, "Multi-Branch Transmitter for Indoor Visible Light Communication Systems," *IEEE Access*, 2018, submitted.

My contribution: literature review and proposed and designed a multi branch transmitter (MBT) to improve the performance of the indoor channel of the VLC systems to support a single user and multi-user. In addition, using SCM tones as resource allocations and WDM to obtain high data rate. As well as, simulation of the proposed ideas in Matlab and produced results with considering t of mobility and diffuse reflections.

A. Al-Hameed, Dr. A.T. Hussein and M. T. Alresheedi: helped with preparation of papers.

Professor Elmirghani: Originator of the idea, developed the optical receivers and helped with the preparation of the papers.

My parents, brothers, sisters, my wife and my children (Mustafa and Yousif), this work is dedicated to you.

Acknowledgements

First and foremost, all praise to Almighty Allah, for endowing me with health, patience, and knowledge to complete this work. I would like to acknowledge my supervisor, Professor Jaafar Elmirghani for his guidance and patience through my PhD journey. I am very grateful for his teaching and friendship. He has offered me invaluable opportunities and continuously kept faith in me. I feel very honoured to have had the chance to work with him.

I am very grateful and thankful to the Ministry of Higher Education and Scientific Research (MOHESR) in Iraq for fully funding my PhD. I also thank the University of Mosul and University of Ninevah in Iraq for their financial support.

I would like to express my appreciation to my beloved family back home, my mother, sisters and brothers. I don't have enough words to thank them for supporting me in all possible ways. They are the reason behind my life achievements and have always shown me by example that everything is doable. I hope I made them proud.

Finally, I am very grateful and thankful to my young family. My best achievement (My children), Mustafa (Our superhero) and Yousif (Our baby). Their smiles and innocent gazes have changed the definition of life for me. I thank them for making my life so fulfilled and rewarding and for making every day so special. I dedicate my final acknowledgements to the love of my life, my dear wife Sahar, without her kindness, sacrifices, and patience I would not have been able to pursue my dreams. I truly appreciate her standing by my side and thank her for her love, support and attention.

Abstract

Visible light communication (VLC) systems have become promising candidates to complement conventional radio frequency (RF) systems due to the increasingly saturated RF spectrum and the potentially high data rates that can be achieved by VLC systems. Over the last decade, significant research efforts have been directed towards the development of VLC systems due to their numerous advantages over RF communication systems, such as the availability of simple transmitters (light emitting diodes, (LEDs)) and receivers (silicon photo detectors), better security at the physical layer, improved energy efficiency due to the dual functionally (i.e., illumination and communication) and hundreds of THz of license-free bandwidth. However, several challenges face VLC systems to achieve high data rates (multi gigabits per second). These challenges include the low modulation bandwidth of the LEDs, inter symbol interference (ISI) due to multipath propagation, co-channel interference (CCI) and the light unit (i.e., VLC transmitter) should be ‘‘ON’’ all the time to ensure continuous communication.

This thesis investigates a number of techniques to design robust high-speed indoor VLC systems that support a single user and multi-users. Light engines composed of RYGB laser diodes (LDs) are used for communication and illumination. The main goal of using LDs is to enable the VLC system to achieve high data rates while using simple modulation techniques (such as on off keying (OOK)), which adds simplicity to VLC systems.

Three VLC systems based on the computer generated holograms (CGHs) are proposed in this thesis, which are single beam static CGH-VLC system, static CGH-VLC system and adaptive CGH-VLC system. Whereas in the first and the second systems a single photodetector is used (added simplicity), an imaging receiver is used in the third one to obtain spatial multiplexing. We consider the lighting constraints where illumination should be at an acceptable level and should consider diffuse reflections (up to second order) to find the maximum data rate that can be offered by each system. In the first system, the CGH is used to produce one fixed broad beam from the best light unit and focus it to a specific area on the communication floor. In the second system,

the CGH generates 100 beams (all these beams carry same data) from the best transmitter and directs these beams to an area of 2 m × 2 m on the communication floor. In the third system, the CGH is used to generate eight beams from the best transmitter and steer these beams to the receiver's location. In addition, each one of these eight beams carries a different data stream.

This thesis also presents an indoor VLC system in conjunction with an imaging receiver with parallel data transmission (spatial multiplexing) to reduce the effects of inter-symbol-interference (ISI). To distinguish between light units (transmitters) and to match the light units used (to convey the data) with the pixels of the imaging receiver, we proposed the use of subcarrier multiplexing (SCM) tones. Each light unit transmission is multiplexed with a unique tone. At the receiver, a SCM tone decision system is utilised to measure the power level of each SCM tone and consequently associate each pixel with a light unit.

We proposed a high data rate single user VLC system based on wavelength division multiplexing (WDM) in this thesis. An imaging diversity receiver (IMDR) is used as an optical receiver. Based on the location of the IMDR, each colour of the RYGB LDs sends a different data stream at a different rate where the variable data rates are attributed mainly to the different power levels assigned to the colours to yield the desired white colour. Each pixel of the IMDR is covered by a specific colour optical filter.

WDM in conjunction with the SCM tones are used to realise a high data rate multi-user VLC system in this thesis. The SCM tones are used to allocate an optimum transmitter to each user and to calculate the co-channel interference (CCI). Two novel optical receivers are used to evaluate the performance of the VLC systems: an array of non-imaging receivers (NI-R) and an array of non-imaging angle diversity receivers (NI-ADR).

This thesis proposes a multi-branch transmitter (MBT) as a solution that can improve the VLC system performance over an indoor channel and support multi-user operation. The MBT has many transmitter branches (TBs) where each branch is directed to a specific area. By reducing the semi angle of each TB, the effect of multipath propagations is reduced and the received optical

power is improved. The performance of the MBT is evaluated with a single user VLC system using a wide field of view (W-FOV) receiver and then with an angle diversity receiver (ADR). The results show that this system can provide a data rate of 4 Gb/s and 10 Gb/s when using wide FOV receiver and ADR, respectively. In addition, the performance of the MBT is evaluated in a multi-user scenario. We used the MBT with WDM and SCM tones to realise a high data rate multiuser indoor VLC system. Four colour laser diodes (RYGB LDs) are used as sources of illumination and data communication. One colour of these four colours is used to convey the SCM tones at the beginning of the connection to set up the connection. When the connection is set up, the data is transmitted in parallel through the RYGB LDs.

Contents

List of Figures

List of Tables

List of Abbreviations

ADR	Angle diversity receiver
APD	Avalanche photodetector
AM	Amplitude modulation
AWGN	Additive white Gaussian noise
BCM	Beam clustering method
BER	Bit error rate
BPF	Band pass filter
BN	Background noise
CAP	Carrier less amplitude and phase
CCI	Co-channel interference
CDF	Cumulative distribution function
CDMA	Code division multiple access
CDS	Conventional diffuse system
CF	Communication floor
CGHs	Computer generated holograms
CPC	Compound parabolic concentrator
CNR	Carrier to noise ratio
DAT	Delay adaptation technique
DMT	Discrete multi-tone modulation
D&C	Divide and conquer
EGC	Equal gain combining
El	Elevation
FEC	Forward error correction
FOV	Field of view

FSO	Free space optical
HPF	High pass filter
IoT	Internet of things
IM	Intensity modulation
IMDR	Imaging diversity receiver
ISI	Inter-symbol interference
LD	Laser diode
LED	Light emitting diode
LOS	Line of sight
LPF	Low pass filter
LSD	Light shape diffuser
LSMS	Line strip multi-beam system
MBT	Multi branch transmitter
MCFA	Multispectral colour filter array
MFTP	Maximum flickering time period
MIMO	Multiple input multiple output
MISO	Multiple input single output
MRC	Maximum ratio combining
MRI	Magnetic resonance imaging
NI-ADR	Non imaging angle diversity receiver
NI-R	Non imaging receiver
NLOS	Non light of sight
NOMA	Non orthogonal multiple access
NRZ	Non return to zero
OFDM	Orthogonal frequency division multiplexing
OOK	On off keying

OW	Optical wireless
PAT	Power adaptation technique
PD	Photodetector
PDF	Probability density function
PIA	Position identification algorithm
PIN	Positive intrinsic negative
PPM	Pulse position modulation
PWM	Pulse width modulation
QAM	Quadrature amplitude modulation
QoS	Quality of service
RF	Radio frequency
RZ	Return to zero
SBA	Select the best algorithm
SC	Selection combining
SCM	Subcarrier multiplexing
SDMA	Space division multiple access
SINR	Signal to interference and noise ratio
SLM	Spatial light modulator
SNR	Signal to noise ratio
TB	Transmitter branch
TDD	Time division duplexing
ToA	Time of arrival
UVC	Ultra violet communication
UWB	Ultra-wide band
VLC	Visible light communication
WDD	Wavelength division duplexing

WDM	Wavelength division multiplexing
ZF	Zero forcing

List of Symbols

δ	Angle of incidence with respect to the receiver normal
$A_{eff}(\delta)$	The effective signal-collection area
$g(\delta)$	Concentrator gain
ψc	The semi-angle of the concentrator
R	Responsivity of the photodiode
c	Speed of light
q	The electronic charge
$h(t)$	The impulse response
$n(t)$	Background noise
n	Lambertian emission order
P_s	Total average transmitted optical power
α	Angle of incidence with respect to the transmitter's normal
P_{LOS}	Received optical power due to LOS
P_{1st}	Received optical power due to first order reflections
P_{2nd}	Received optical power due to second order reflections
R_d	Direct link distance between receiver and transmitter
$\widehat{n_t}$	Normal of the transmitter
$\widehat{n_r}$	Normal of the receiver
Rt	Location of the transmitter
Rr	Location of the receiver
β	Angle between the incident ray from the transmitter and the reflective element's normal

γ	Angle between the reflective element's normal and the reflected ray
d_{A1}	Area of the first reflective element
d_{A2}	Area of the second reflective element
ρ_1	Reflection coefficient of the first reflective element
ρ_2	Reflection coefficient of the second reflective element
ne	Reflection coefficient of the reflective element
R_1	Distance between the transmitter and the first reflective element
R_2	Distance between the first reflective element and the second reflective element
R_3	Distance between the receiver and the second reflective element
Δt	Time bin
D	Delay spread
μ	The mean delay
Q	Gaussian function
P_{s1}	Power associated with logic 1
P_{s0}	Power associated with logic 0
σt	Standard deviation of the total noise
σ_{bn}	Standard deviation of background shot noise component
σ_s	Standard deviation of shot noise component associated with the received signal
σ_{pr}	Standard deviation of preamplifier noise component
$I(0)$	Centre luminous intensity of the LD
R_l	Load resistor
C_d	Photodetector's capacitance

w	Detector thickness
$T_c(\delta)$	Transmission factor of the imaging concentrator
$H(u,v)$	Complex transmittance of the hologram
$A(u,v)$	Amplitude distribution of the hologram
$\Phi(u,v)$	Hologram's phase distribution
PL	Path loss
$I_m(t)$	Input current to RYGB LDs
I_{bais}	The bias current
$H(f_m)$	Channel frequency response
I_{bn}	Background photocurrent
$p(a)$	Probability density function of the desired signal
$p(b)$	Probability density function of the undesired signal
m_{ds}	Mean value of the desired SCM tone
σ_{ds}	Standard deviation of the desired SCM tone
m_{us}	Mean value of the undesired SCM tone
σ_{us}	Standard deviation of the undesired SCM tone
opt_th	Optimum threshold
$Pcds$	Probability of correct decision of the desired SCM tone
$Pfus$	Probability of false alarm of the undesired SCM
$Pcus$	Probability of the correct decision in the undesired SCM tone
Pcd	Probability that SCM identification system makes a correct decision
S	Electrical power of the SCM tone
I	Co-channel interference

1. Introduction

Using light to transmit information between two points is an old idea. In fact, optical wireless (OW) communication has been in use for more than three centuries. Techniques such as ship flags, semaphore and fire beacons were the earliest stages of OW. Long time ago holy days were announced by using bonfires on the tops of mountains. Smoke and fire were used in America for communication between Indian tribes. The reflection of sunlight by mirrors is another early method of optical communication. In this system, mirror movement produces light flashes that can be used to send Morse code [1]. In the 19th century, this system was a very effective instrument for optical communication over a distance of 50 miles or more. The major uses of this device were in surveys, forest protection work and by the military. It was in use until 1935 [1].

Alexander Graham Bell and Sumner Trainer developed and patented the photophone in 1880. This photophone was utilised to convey sound on a beam of light [2] as shown in Figure 1.1. It was based on electronic detection where a receiver that comprised of a selenium crystal converted an optical signal into an electrical current. The photophone used the conductivity of selenium crystals, where the electrical conductivity depends on the intensity of the light it is exposed to [2]. The photophone is widely regarded as the precursor to modern fibre optics. Today, such technology transports more than 80% of the world's telecommunication traffic [1], with much higher data rates and with a quality of service (QoS) that exceeds the old methods [3].

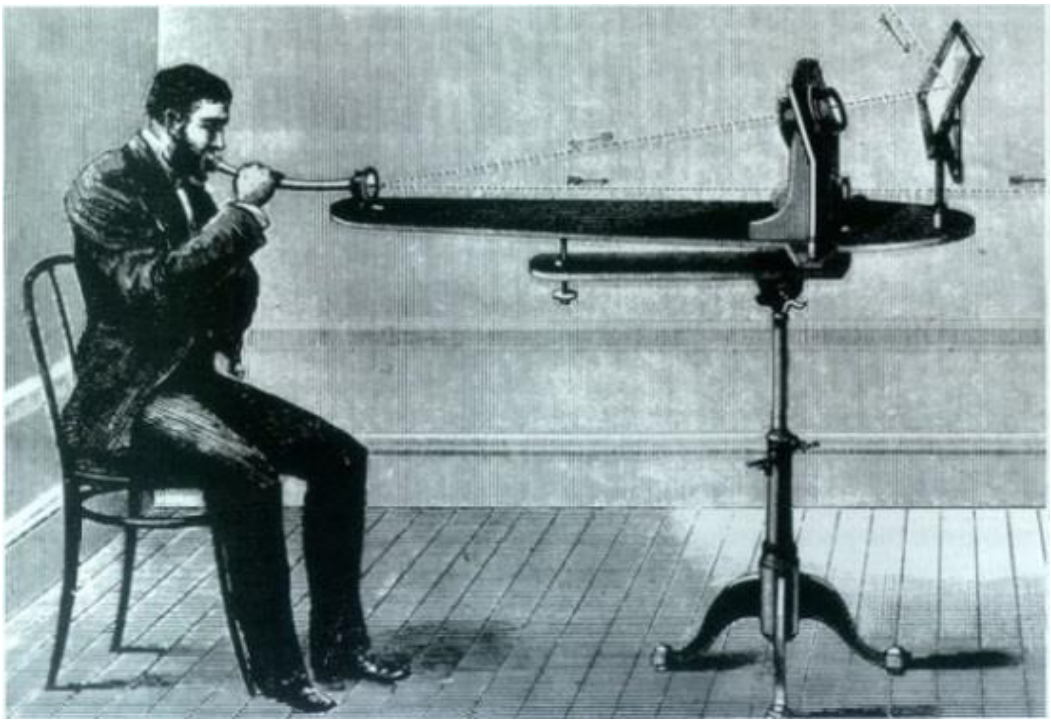

(a)

(b)

Figure 1-1: photophone, (a) transmitter, (b) receiver [2].

Modern telecommunication has experienced exponential growth in applications and research over the past decades. Wired physical connections have been established to convey information between different devices. However, physical connections introduce difficulties in installation, re-wiring and maintenance. An alternative method that can achieve the same performance in such systems is wireless communication based on radio frequency (RF) transmission. The RF band is the basis of most currently used wireless communication systems. Unfortunately, the growth in demand for more frequencies, high data rate services, better QoS and lower cost components has reduced the available RF spectrum. These demands have forced researchers to find other options. Figure 1.2 shows the electromagnetic spectrum.

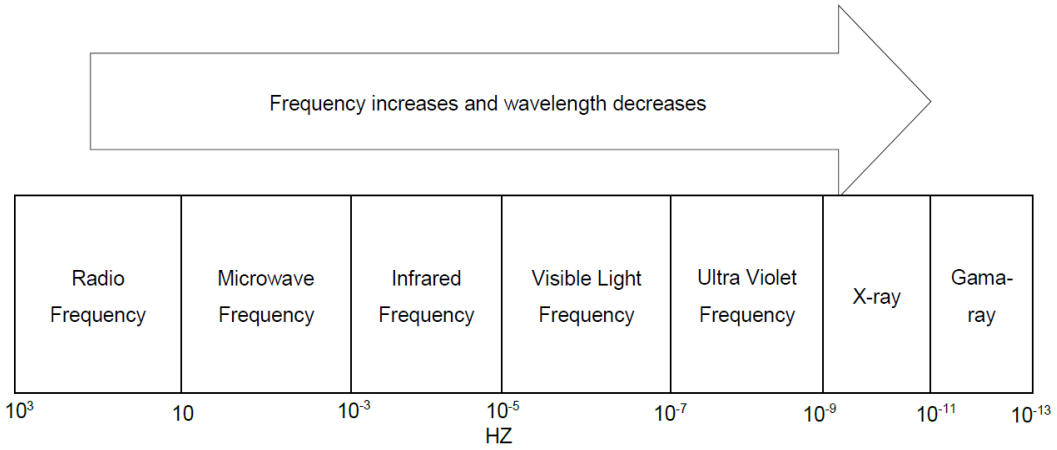

Figure 1.2: The electromagnetic spectrum.

Realising very high data rates (multi gigabits per second) using the relatively narrow bandwidth of RF systems is challenging. According to a GreenTouch research study, mobile Internet traffic over this decade (2010-2020) is expected to increase by 150 times [4]. Given this expectation of dramatically growing demand for data rates, the quest is already underway for alternative spectrum bands beyond microwaves and millimetre waves (RF spectrum). Different technology candidates have entered the race to provide ultra-fast wireless communication systems for users, such as OW systems for indoor and outdoor use [5], ultra-wideband wireless system (UWB) [6], 60 GHz band for local wireless multimedia access [7] and terahertz (THz), which has been studied as a new alternative in this race [8].

Modern OW communication systems coincided with the invention of the first laser in 1960 [9]. However, this technology was not deployed until the 1990s when the transmitter and the receiver components became available at low cost [10]. OW communication systems include outdoor systems, such as free-space optical (FSO), ultra violet communication (UVC) and underwater communications, while indoor systems are those such as infrared data association (IrDA) systems, infrared optical wireless communication (IROW) systems and visible light communication (VLC) systems [3].

The term ‘visible light communication’ (VLC) refers to the use of light waves in free-space propagation in the visible band as a transmission medium for communication. Visible signals are part of the electromagnetic radiation whose wavelengths are located between those of IR and UV. Visible radiation has wavelengths between 380 nm and 780 nm [11].

Along with radio, the term wireless is also applicable to systems which utilise other regions of the electromagnetic spectrum, such as infrared. It has been more than three decades since OW systems were introduced [5]. OW offers a number of advantages over its radio frequency counterpart, such as abundance of unregulated bandwidth, no multipath fading and cost effective systems at data rates well beyond 100 Mb/s [12]. To an extent, RF and OW may be viewed as complementary rather than competitive media. For example, if a wireless LAN is required to cover a large area, where users can roam freely and remain connected to the network at all times, then radio is the only cost-effective medium which can achieve this. If, however, a wireless LAN is required to cover a more modest area, but deliver advanced high bandwidth multimedia network services such as video conferencing and video on demand, then OW is a good medium which truly has the bandwidth available to deliver this [3]. A comparison between the properties of RF and OW is shown in Table 1.1. So far, commercially available OW systems have not come close to delivering the high data rates which are potentially available from the OW spectrum, the reasons for this are more to do with the limited range, difficultly to operate outdoor, high power requirement and cost constraints rather than any fundamental limitations of the core technology.

Table 1-1: Comparison between RF system and OW system.

Parameters	Radio Frequency System	OW System
Band Width	Regulated	Unregulated
Pass through obstacles	Yes	No
Distances	Long	Short
Security	Low	High
Cost	High	Low
Noise sources	From other users	From ambient light
Multipath fading	Suffer from fading	Freedom from fading

OW is a good communications medium, however there are numerous considerations which must be taken into account when designing high speed indoor OW links. Non-directed line-of-sight (LOS) and diffuse links incur a high optical path loss and must also contend with multipath propagation. Whilst multipath propagation does not result in multipath fading in indoor OW systems, since the optical detector sizes are huge in comparison with the wavelength, it does give rise to inter symbol interference (ISI), which is one of the primary impairments to achieving high speed OW communication [12]. In addition, OW links must be capable of operating in environments where intense ambient light levels exist, which degrades the link performance in two ways. Firstly, the average power of the background radiation generates shot noise in the receiver, which is independent of the transmitted signal, and secondly, artificial sources of ambient light generate a periodic interference signal, which can contain harmonics into the MHz region for fluorescent lamps driven by electronic ballasts [5].

1.1. Motivation and Research Objectives

Significant research effort is being directed towards the development of VLC systems due to their numerous advantages over RF systems, such as:

- Immunity against interference caused by adjacent channels with the possibility of frequency reuse in different parts of the same building, which means abundant capacity.

- Improved security at the physical layer as light cannot penetrate walls and opaque objects, thus the signal remains in the communication environment.
- Availability of simple front-end devices at low cost.
- Improved realise energy efficiency in VLC systems as communications is a by-product illumination.
- License-free bandwidth, hundreds of terahertz of bandwidth.
- Harmless radiation for humans and other electronic devices.
- Easy to integrate into the existing lighting infrastructure.

There are however several challenges hindering the development of VLC systems. These challenges include:

- The low modulation bandwidth of light emitting diodes (LEDs).
- Multipath propagation, which may cause inter-symbol-interference (ISI).
- Multiple transmitters, which may cause co-channel interference (CCI).

The primary objectives of this work were to:

1- Propose and evaluate new techniques to enhance the performance of VLC systems under the influence of multipath dispersion and mobility.
2- Investigate the benefits of using computer generated holograms (CGHs) in indoor VLC systems.
3- Evaluate parallel data transmission in indoor VLC systems.
4- Design WDM VLC system that enable high data rates.
5- Investigate the use of WDM to realise high data rate multi-user VLC systems.

1.2. Research Contributions

The author has:

1- Designed, investigated and evaluated the use of CGHs for indoor VLC systems. The CGHs was used to reduce the effects of ISI and increase the received optical power without increasing the transmitted optical

power. This led to improvement in the 3-dB channel bandwidth of the indoor VLC system and helped realise a high data rate system. The author has designed and evaluated different VLC systems based on CGHs:

- Single beam static CGH-VLC system.
- Static CGH-VLC system.
- Adaptive CGH-VLC system.

The performance of the three systems were evaluated in two rooms: an empty room and a realistic room. In these systems, the effect of diffuse reflections and mobility were taken into account. In addition, the effect of co-channel interference was considered for the adaptive CGH-VLC system.

2- Developed an indoor VLC system in conjunction with an imaging receiver with parallel data transmission (spatial multiplexing) to reduce the effects of ISI. To distinguish light units (transmitters) and to match the light units used to convey the data with the pixels of the imaging receiver, SCM tones were proposed. These tones were used to identify each light unit, to match each light unit with the pixel(s) of the imaging receiver and to calculate the CCI level. The author also designed a novel receiver to evaluate the ability of the SCM tones to match each light units with its pixel(s). The author has also evaluated the performance the VLC system in the empty room and in a realistic room where physical partitions introduce shadowing and signal blockage, windows cause signal loss and bookshelves, chairs and cabinets are present and cause additional reflections.

3- Proposed a WDM VLC system with an imaging diversity receiver (IMDR) to enable high data rates. The author has designed and evaluated a novel IMDR, which has three faces. Each pixel was covered by a specific optical filter. Thus, each pixel responds to a certain colour. The author investigated this system with a single user when operating at a data rate of 10 Gb/s.

4- Proposed a high data rate multi user WDM VLC system. The author used SCM tones to allocate an optimum transmitter to each user. This system was investigated with two novel optical receivers: non-imaging receiver (NI-R) and non-imaging angle diversity receiver (NI-ADR). This system was investigated in an empty room considering the effects of diffuse reflections, mobility and CCI level.

5- Proposed and evaluated the performance of the MBT with a high data rate single user VLC system. The author obtained the delay spread, 3-dB channel bandwidth and SNR of the user. The author evaluated the performance of this system with two types of receivers: wide field of view (W-FOV) receiver and an angle diversity receiver (ADR). The author considered the effects of multipath propagation, mobility and illumination constraints in this system.

6- Used a multi-beam transmitter (MBT) with WDM and SCM tones to realise a high data rate multiuser indoor VLC system. Each branch can be used to send different data; therefore, many users can be served simultaneously. The author used SCM tones to assign the best branch to each user. The author used WDM to increase the data rate of each user. The multiuser VLC system was investigated with the NI-ADR. The effect of the CCI, mobility, diffuse reflection (up to second order) components and lighting constraints (acceptable illumination level in the room) are considered in this system.

1.3. Publications

The original contributions are supported by the following publications:

Journals

1) S. H. Younus, A. T. Hussein, M. Thamer Alresheedi, and J. M. Elmirghani, "CGH for Indoor Visible Light Communication System," *IEEE Access,* vol. 5, pp. 24988-25004, 2017.

2) S. H. Younus, A. Al-Hameed, A. T. Hussein, M. T. Alresheedi and J. M. Elmirghani, " Parallel Data Transmission in Indoor Visible Light Communication Systems," *IEEE Access,* vol. 7, pp. 1126-1138, 2019.
3) S. H. Younus, A. Al-Hameed, A. T. Hussein, M. T. Alresheedi and J. M. Elmirghani, "WDM for Multi-user Indoor VLC Systems with SCM," *IET Communication,* submitted, 2018.
4) S. H. Younus, A. Al-Hameed, A. T. Hussein, M. T. Alresheedi and J. M. Elmirghani, "Multi-Branch Transmitters for Indoor Visible Light Communications," *IEEE Access,* submitted, 2019.

Conferences

5) S. H. Younus and J. M. Elmirghani, "WDM for high-speed indoor visible light communication system," *19th International Conference on Transparent Optical Networks (ICTON)*, 2017, pp. 1-6.
6) S. H. Younus, A. T. Hussein, M. Thameralresheedi, and J. M. Elmirghani, "VLC Systems with CGHs," *21st International Conference on Transparent Optical Networks (ICTON)*, submitted, 2019.

1.4. Overview of the Thesis

The next chapter provides a general review of indoor visible light communication systems. Comparison between VLC and RF systems is presented. It also presents the VLC systems structure, including transmitter and receiver components and VLC link configurations. In addition, the chapter outlines the design challenges of indoor VLC systems and signal modulation techniques.

Chapter 3 presents the VLC channel model used in all the systems designed and presented in this work. It also provides an analysis of the impulse

response, delay spread and SNR of a VLC system with W-FOV receiver, ADR and imaging receiver.

Chapter 4 introduces three VLC systems based on CGHs. The CGHs-VLC systems were investigated with W-FOV receiver and imaging receiver. The chapter focuses on designing a high-speed indoor VLC system. The results show significant improvements in terms of data rate.

Chapter 5 introduces an 8 Gb/s mobile VLC system that employs parallel data transmission and imaging receivers. It also introduces SCM tones to identify each light unit, to match each light unit to pixels of the imaging receiver and to the level of the CCI. In addition, it introduces a novel receiver designed to make use of the ability of the SCM tones to find the optimum transmitter for each pixel. The proposed systems are examined in two different room scenarios: an empty room and a realistic room.

Chapter 6 proposes two VLC systems based on WDM: a single user WDM-VLC system and a multi-user WDM-VLC system. The single user WDM-VLC system is investigated with a novel IMDR that has three faces. Each pixel is covered by an optical filter, which enables each pixel to sense a specific colour. This system achieves a data rate of 10 Gb/s. The multi-user WDM VLC system is evaluated with two novel receiver, NI-R and NI-ADR. In addition, in this system SCM tones are used to allocate the optimum receiver to each user. The effects of the mobility, diffuse reflections and CCI on the performance of the multi-user VLC system are taken into account.

Chapter 7 Proposes two VLC systems (single user VLC system and multi-user VLC system) based on MBT. Both systems are investigated in an empty room considering the effects of mobility and lighting constraints as well as the effects of diffuse reflections. The results show that the MBT improves the 3-dB channel bandwidth to support high data rates with a good communication link. In addition, the MBT enables the VLC system to support many users with a high data rate.

Chapter 8 summarises the contributions of the work and outlines possible directions of future work.

2. Review of Visible Light Communication Systems

2.1 Introduction

It is generally accepted that wireless communication has become a very important part of our daily lives. Recent research by Cisco has shown that by 2017, it is expected that more than 11 Exabytes of data will have to be transferred through mobile networks every month. In addition, it is estimated that the data traffic will grow tenfold by 2020 [13]. It can be seen that the demand for wireless data communication is increasing dramatically. Radio frequency (RF) communication is used to convey the data. However, due to the increasing demand for wireless data transmission and the fact that most of the RF spectrum is occupied, the RF spectrum congestion has significantly increased recently [14], [15]. Consequently, the RF spectrum is not enough to cover the growing demand for wireless data transmission. Different alternative technology candidates have been proposed to provide high data rate services for users. One of the suggested solutions to overcome the congestion of the low RF spectrum is the use of the high-frequency spectrum (beyond 10 GHz) [16]. However, by using this spectrum, the infrastructure of the entire mobile systems will need to be recreated to be compatible with this new wavelength band in terms of antennas, needs for line of sight and alternate modulation, coding and signal processing [14]. Furthermore, using these spectrum bands might lead to an increase in the path loss and increase in the probability of signal blockages due to shadowing [16]. Visible light communication (VLC) systems are among the promising solutions to the bandwidth limitation problem faced by RF systems.

Since the RF spectrum is expensive and limited, new and complementary wireless transmission techniques are required to relieve the RF spectrum. There is a potential band of the electromagnetic spectrum (i.e., the optical band) available that is able to provide tens of gigabits per second for users in

the near future [17], especially for indoor users. It has been more than three decades since the first OW systems were proposed as an alternative technology to RF systems to support high data rates [5]. Since then, a large and growing body of research in this area has emerged, and in the last ten years OW communication has gone from strength to strength as a potential high speed method for local area networks [5], [18], [19]. OW systems are candidates for high data rates in the last mile of access networks. One of the most promising OW systems for realising ubiquitous wireless networks are VLC systems based on white LEDs, because LEDs can be simultaneously used for illumination and data communications [20].

The VLC systems are proposed as a complementary systems to RF systems [21], which helps to overcome the RF spectrum congestions issue. The VLC systems have gained attention during the last decade due to the growing use of energy efficient LEDs for indoor illumination. It is expected that LEDs will be used to provide 75% of all illumination in the world by 2030 instead of conventional sources of illumination such as fluorescent and incandescent lamps [22]. LEDs have several advantages compared with traditional lighting sources (incandescent and fluorescent), such as longer lifetime, lower power consumption and higher brightness. Moreover, LEDs can be used for both illumination and data communication, while traditional lighting sources are used for illumination only [20].

Generally, two main approaches are used to generate white light from LEDs. The first method uses a phosphor layer (yellow light is emitted) that is coated on blue LEDs, while the second method uses a combination of red, green and blue (RGB) colours LEDs [23], [24]. The blue-chip LED requires one electrical driven source, which makes it cheaper and simpler than an RGB LED. However, the blue-chip LED has low bandwidth because the yellow phosphor has slow response. The RGB LED offers higher bandwidth, but is more expensive and more complex than the blue-chip LED, as it requires three electrical drive sources [24]. Figure 2.1 depicts the methods of generating white light from the LEDs.

Following this introduction, this chapter is organised as follows. Section 2.2 gives a comparison between VLC systems and RF systems. The indoor

VLC system structure is described in Section 2.3. Design challenges in indoor VLC systems, such as ISI, multipath dispersion and photodetector high capacitance, are discussed in Section 2.4. Next, signal modulation techniques and VLC standards are presented in Sections 2.5 and 2.6, respectively. The chapter concludes by describing current indoor VLC systems.

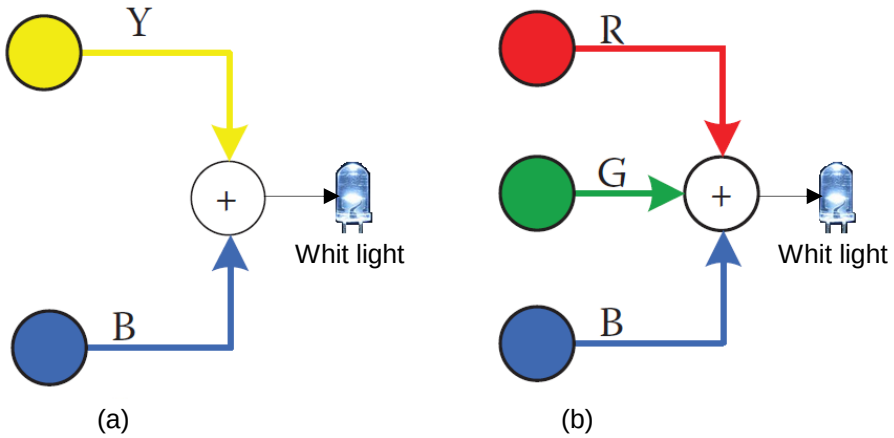

Figure 2.1 : Two white emissions approaches from LEDs, (a) phosphor LED method and (b) RGB method.

2.2 Comparison of Visible Light Communication and Radio Frequency Communication

VLC and RF systems are complementary transmission techniques, with distinguishing characteristics that can make either one individually more suited to different applications than the other. For example, for applications requiring the transmission of data through walls or other large physical objects and where user mobility over wide geographic coverage is essential, RF is the preferred medium distance. On the other hand, VLC is favoured in short to medium link applications where aggregate system capacity must be maximised at minimal cost or receiver signal processing complexity must be minimised.

RF technology is widely used and is the basis of most of the current wireless communication systems. However, the RF spectrum is crowded due to the rapidly growing demand for wireless access. Thus, the available bandwidth of

the RF spectrum may fail to meet the requirements [25]. Thus, researchers begin to look for other solutions. One of the suggested solutions to overcome the congestion of the low RF spectrum is the use of millimetre wave (mmWave), which has high-frequency spectrum (beyond 10 GHz) [16]. In mmWave, carrier frequencies are higher than the existing wireless communication techniques. Hence, many benefits can be obtained by using the mmWave. These advantages are 1) huge bandwidth, 2) high quality of the transmission, 3) ability to obtain narrow beams and 4) mmWave devices lead to make large antenna arrays to be packed in small size [26]. However, by using this spectrum, the infrastructure of the entire mobile systems will need to be recreated to be compatible with this new wavelength band in terms of antennas, needs for line of sight and alternate modulation, coding and signal processing [14]. Furthermore, using these spectrum bands might lead to an increase in the path loss and increase in the probability of signal blockages due to shadowing [16]. Besides that, the maximum data rate that has been obtained by mmWave (at 60 GHz) is 7 Gb/s while using OFDM.

Fortunately, by using the existing illuminating devices, VLC can be utilised as one of the promising alternative methods for RF-based communication, especially in indoor communications [25]. VLC offers several significant advantages over RF. For example, rapid deployment, low start-up operational costs and high bandwidth similar to fibre optic. The VLC spectral region offers virtually unlimited bandwidth (380nm~780 nm) that is an unregulated worldwide spectrum, and this leads to reduced system cost [27].

The nature of light gives VLC systems immunity against interference caused by adjacent channels with the possibility of frequency reuse in different parts of the same building, which means abundant capacity. The VLC systems also offer high security in the physical layer. This is due to the fact that light does not penetrate through opaque barriers, which means that eavesdropping is not possible as with radio systems [25]. The availability of simple front-end devices at low cost, the provision of energy efficiency, hundreds of terahertz of license-free bandwidth, being potentially harmless as radiation to humans and other electronic devices and being easy to integrate into the existing lighting infrastructure are also benefits. The detector (photodiode) is very large

in size, typically tens of thousands of wavelengths, hence VLC systems are free from fading [28], [29] and the freedom from fading can greatly simplify the design of VLC systems. VLC systems are not without disadvantages.

Due to its properties, light cannot penetrate through walls from one room to another. Therefore, access points that are interconnected via a wired backbone will need to be installed. In addition, the spread in the received pulse due to multipath dispersion degrades the eye opening and hence the SNR.

Multipath dispersion is attributed to reflective surfaces, such as walls, windows, doors and ceilings. Since these reflective elements act as small emitters that reflect (diffuse) the signal in the form of a Lambertian pattern, the transmitted data arrives at the receiver from multiple different paths, which makes the transmitted pulses spread [12]. Furthermore, the received signal at the receiver includes shot noise induced by intense ambient light sources (sunlight and other light sources), and this leads to signal corruption by background noise [30]. Moreover, the available current modulation bandwidth of the transmitters (LEDs) is very low compared with the VLC spectrum, which means the transmission bandwidth is limited by the LED bandwidth. In addition, using white lighting LEDs for communication is naturally one direction communication (downlink), useful for applications such as background music transmission, therefore, providing an uplink to a portable transmitter structure can be a big challenge. Besides, to improve the performance of the VLC systems, a photodetector that has a large area is required. However, this leads to increase in the internal capacitance of the photodetector as it is directly proportional to its area. Consequently, the available bandwidth in the receiver decreases [31]. Table 2.1 summarises the comparison between VLC and RF systems.

Table 2-1: Comparison between VLC and RF systems in indoor wireless.

	VLC systems	RF systems
Advantages	• Unlimited and license-free bandwidth. • Signals contained within the room of origin, which leads to high security against eavesdropping. • Freedom from multipath fading. • Inexpensive technology.	• Transmission through walls and other objects is possible. • High flexibility and mobility for users.
Disadvantages	• Sensitive to ambient light. • Multipath dispersion leads to ISI. • Signal to noise ratio different according to the receiver location. • High path loss. • Installation of access points for communication between rooms.	• Interference from other users and systems. • Regulated bandwidth. • Low security. • Multipath fading.

2.3 Structure of the Indoor VLC system

Figure 2.2 shows a block diagram of an indoor VLC system. The VLC system consists of (1) a transmitter, which can be LED or LD, (2) a propagation medium (VLC channel) and (3) a receiver that employs a photodetector (PD). Electronic circuitry receives information (input data) in the form of digital data and modulates the transmitting light source (LED or LD). The optical power from the light source propagates into the free space medium. The photodetector converts the received optical power into an electrical current. This electrical current is then amplified by the preamplifier and passes through a bandpass filter (BPF) and a demodulator circuit to detect the data.

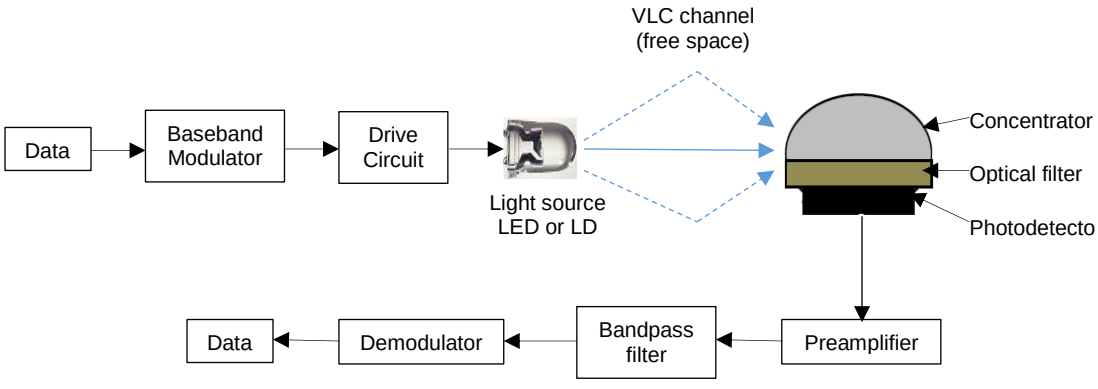

Figure 2-2: A block diagram of an indoor VLC system.

2.3.1 VLC system transmitter

LEDs and LDs are the two main sources for indoor VLC transmission. The main function of the VLC transmitter is to convert the input electrical signal into an optical form and then launch the resulting optical signal into the free space channel. Currently, LEDs are utilised in indoor VLC transmission [32]. White LEDs are available at low cost, with high energy efficiency compared to the traditional lighting sources, and are characterised by long life and eye-safety [14], [33]. Despite the LEDs having several advantages, they are also have some drawbacks, including:

- Low modulation bandwidth (typically tens of MHz) [34].
- Low electro-optic power conversion efficiency [35].
- Non linearity.

On the other hand, LDs may be considered as alternatives to LEDs in VLC systems due to their numerous advantages, which include:

- Wide modulation bandwidth [36].
- High electro-optic power conversion efficiency [35].
- Linear electrical to optical signal conversion characteristics [12].

However, LD are more expensive than LEDs as well as requiring a more complex drive circuit.

2.3.2 Propagation Medium and VLC Transmission Links Design

Generally, the indoor VLC system is classified according to two criteria: (1) the existence of a directed path between transmitter and receiver and (2) the degree of transmitter and receiver directionality. The second classification is based on the radiation pattern of the transmitter and the field of view (FOV) of the receiver. Figure 2.3 illustrates the link classification schemes of the indoor VLC system.

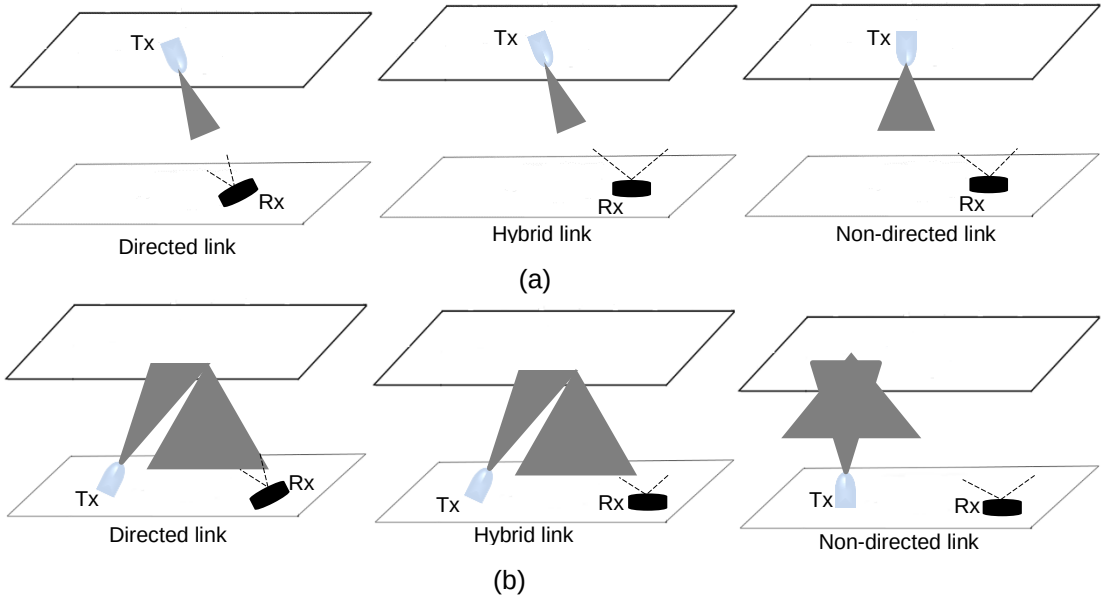

Figure 2-3: The main types of VLC links, (a) LOS transmission configurations and (b) NLOS transmission configurations.

Line of sight (LOS) and non LOS (NLOS) transmission configurations represent the two main types of indoor VLC links [37], [38], [39]. LOS links provide a direct path between the transmitter and receiver, minimise multipath dispersion and enhance the power efficiency of the VLC communication system. However, LOS links suffer from shadowing. On the other hand, NLOS links rely on reflections from the walls, ceiling and other objects. They play an important role in environments where mobility is a key factor and where obstructions and the effects of shadowing are also present. However, they are severely affected by multipath dispersion, which results in ISI and pulse spread [40]. In a VLC system, LOS communication can be achieved with many light units on the ceiling. However, the optical path differences between the light units results in ISI. In this thesis, both LOS and NLOS links are considered.

LOS and NLOS, both can be further categorised according to the transmitter and receiver FOV and radiation pattern into directed, non-directed and hybrid [41], [42]. The system is classified as directed when the emitted beam from the transmitter and FOV of the receiver are narrow, which demands alignment between the transmitter and receiver. A hybrid link can be formed either by a transmitter with a narrow radiation beam and a receiver that is non-directed, or vice versa. Contrary to directed systems, when the transmitter has

a wide emission beam and if the receiver has a wide FOV, the system is non-directed. The three classifications of LOS and NLOS configurations are shown in Figures 2.3 (a) and (b).

2.3.3 VLC Receiver Components

The receiver of the VLC system includes a photodetector and a pre-amplifier circuit that are placed behind a front end. The front end consists of a concentrator and an optical filter (see Figure 2.2). The photodetector converts the received optical power into an electrical signal. The concentrator increases the amount of received signal power at the receiver [43], [44]. The optical filter reduces the amount of collected ambient light captured by removing the captured light outside the signal optical spectral band [45]. The main components of a VLC receiver are discussed next.

2.3.3.1 Concentrators

The main function of the optical concentrator is to guide light rays incident at large area into light rays that come out of a smaller area. It is important to note that concentrators not only collect the desired optical signal power, but also collect background noise from daylight and artificial light sources.

There are two types of concentrators that may be used in VLC systems: an imaging concentrator and a non-imaging concentrator. The effective signal-collection area can be written as [12]:

$$A_{eff}(\delta) = \begin{cases} Acos(\delta) & 0 \le \delta \le \frac{\pi}{2} \\ 0 & \delta > \frac{\pi}{2} \end{cases} \quad (2.1)$$

where δ is the angle of incidence with respect to the receiver normal and A is the physical area of the photodetector. The gain of the non-imaging concentrator has a relationship with the FOV. The maximum achievable concentrator gain is as follows [12]:

$$g(\delta) = \begin{cases} \dfrac{N^2}{\sin(\psi c)^2} & 0 \le \delta \le \psi c \\ 0 & \delta > \ \psi c \end{cases} \qquad (2.2)$$

where N is an internal refractive index and ψc is the semi-angle FOV of the concentrator (usually $\psi c \leq 90^o$). The above formula shows an inverse relation between the gain and FOV of the receiver. If the receiver's FOV is reduced, the gain is increased.

The non-directional hemispherical lens is an important non-imaging concentrator [12], [46]. It is widely studied in OW and VLC systems where it can achieve a wide FOV and omnidirectional gain. Therefore, it is ideal for non-directed links. A hemisphere can achieve an acceptance semi-angle (ψc) of 90^o and gain ($g(\delta)$) equal to N^2 over the entire FOV. A hemisphere-based receiver has an effective area of:

$$A_{eff}(\delta) = AN^2 cos(\delta) \qquad (2.3)$$

Figure 2.4 shows a non-directional hemispherical lens that employs a planar filter.

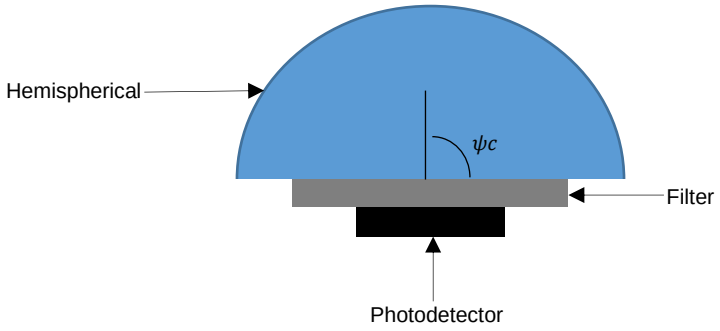

Figure 2-4: Non-directional hemispherical lens that employs a planar filter.

Another non-imaging concentrator studied widely in OW and VLC links is the compound parabolic concentrator (CPC) [47]. It can achieve greater gain than the hemispherical concentrator, but this comes at a reduction of FOV. A CPC is particularly appropriate for directed links. A CPC can be coupled with an optical filter on the front surface, as shown in Figure 2.5.

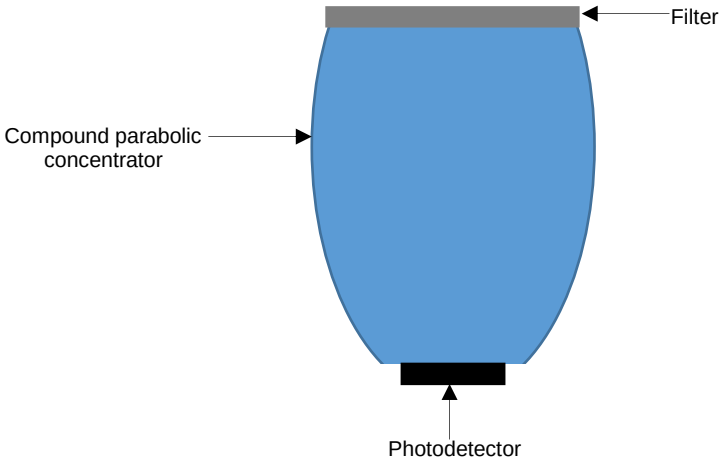

Figure 2-5: Compound parabolic concentrator (CPC) with planar filter.

2.1.1.1 Optical filters

In VLC systems, ambient light is a source of noise that can interfere with the desired signal. The VLC receivers collect both the desired optical signal and ambient light (natural and artificial) noise sources. Thus, to reduce the effect of unwanted noise components in the received electrical signal, an optical filter can be used prior to detection by the photodetector [5]. Day light, fluorescent and incandescent lamps are the major ambient light sources in indoor environments. Figure 2.6 illustrates a photodetector can capture some ambient light even with the use of a bandpass filter (BPF) or a daylight filter in front of its active area. The photodetector converts this light to an electronic signal.

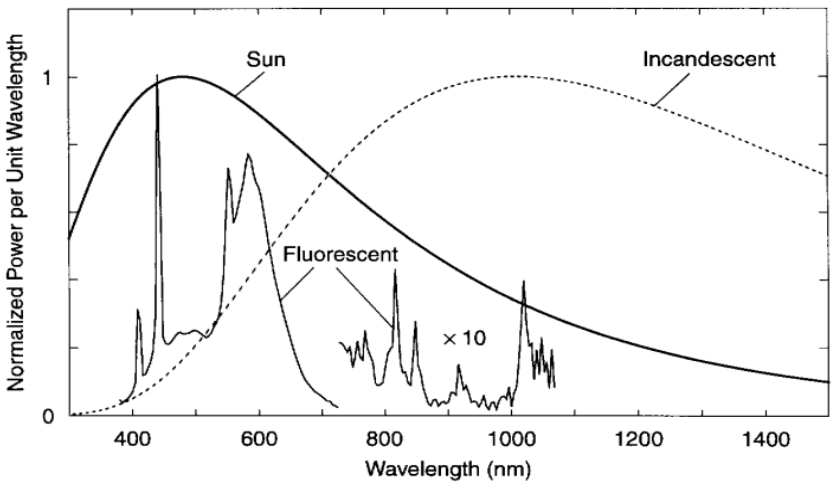

Figure 2-6: Relative spectral power densities of the three common ambient light [12].

A high pass filter (HPF) and a BPF are generally used in VLC systems. The HPF passes light at wavelengths higher than the cut off wavelength, and they are usually made of colour glass or plastic and their transmission characteristics are substantially independent of the angle of incidence [12]. The BPF is the other alternative that can be used to minimise the ambient light in VLC receivers. The BPF can have very narrow bandwidths (typically 1 nm). An imaging diversity receiver with a BPFs were used to obtain 10 Gb/s in an indoor VLC system [48].

2.3.3.2 Photodetectors

Photodetectors are optoelectronic transducers that generate an electrical signal, which is proportional to the incident optical power. Since, the received light the photodetector is generally weak, the photodetector must therefore meet important performance specifications, such as:

- High sensitivity at the operating frequency.
- High conversion efficiency within its operational range of wavelengths.
- High response speed.
- High reliability, low cost and small size.
- Low noise level.
- Low bias voltage required in portable devices together with tolerance to temperature fluctuations.

There are commonly two types of the photodetectors that can be used in VLC systems: positive-intrinsic-negative (PIN) photodiodes and the avalanche photodiodes (APDs). PIN photodiodes require less complex biasing than APDs and are cheaper and simpler to manufacture. However, PIN photodiodes are less sensitive than APDs. APDs provide an inherent current; hence, improving the SNR and reducing the effect of frontend noise. APDs are the preferred choice when the ambient induced shot noise is weak and the pre-amplifier noise is the major source of noise. However, when the shot noise due to the ambient light is large a PIN photodiode is considered to be the better option [12]. A photodiode should have a large bandwidth and a high responsivity. The bandwidth of the photodiode is limited by the transit time of

the carriers through the PN junction. Responsivity is a key parameter in photodiode models and is measured at the central optical frequency of operation. The responsivity of the photodiode can be expressed as [49]:

$$R = \frac{\eta q \lambda}{h_p c} \tag{2.4}$$

where q is the electronic charge (1.6×10^{-19}), η is the quantum efficiency of the device, λ and c are the wavelength and the speed of light respectively and h_p is the Planck constant. The internal quantum efficiency (η) is the probability of the incident photon producing an electron-hole pair. Typical values of η range from 0.7 to 0.9.

2.3.3.3 Preamplifiers

The preamplifiers that are used in the receivers can be categorised into three types: low impedance, high impedance and trans-impedance preamplifiers. The low impedance preamplifier offers a large bandwidth but has high noise and hence low receiver sensitivity. On the other hand, the high impedance preamplifier provides high sensitivity but an equaliser must be used to mitigate the limitations imposed on the frequency response by the front end RC time constant. In addition, due to their high input load resistance they also have a limited dynamic range [50], [51]. In contrast, a trans-impedance preamplifier provides a large dynamic range and avoids the need for an equaliser. Therefore, it is suitable in most OW link applications. However, it has lower sensitivity (high noise level) compared to a high impedance amplifier.

2.4 Design Challenges of Indoor VLC Systems

Over the last decade, significant research effort has been directed towards the development of VLC systems due to their numerous advantages over RF systems, such as the availability of simple transmitters and receivers.

However, several challenges facing it, especially for achieving high data rates and using VLC spectrum efficiently. These challenges include the low modulation bandwidth of the LEDs (VLC transmitters), provision of an uplink for VLC system, multipath dispersion and photodetector high capacitance. Figure 2.7 shows the main challenges of VLC systems in each component.

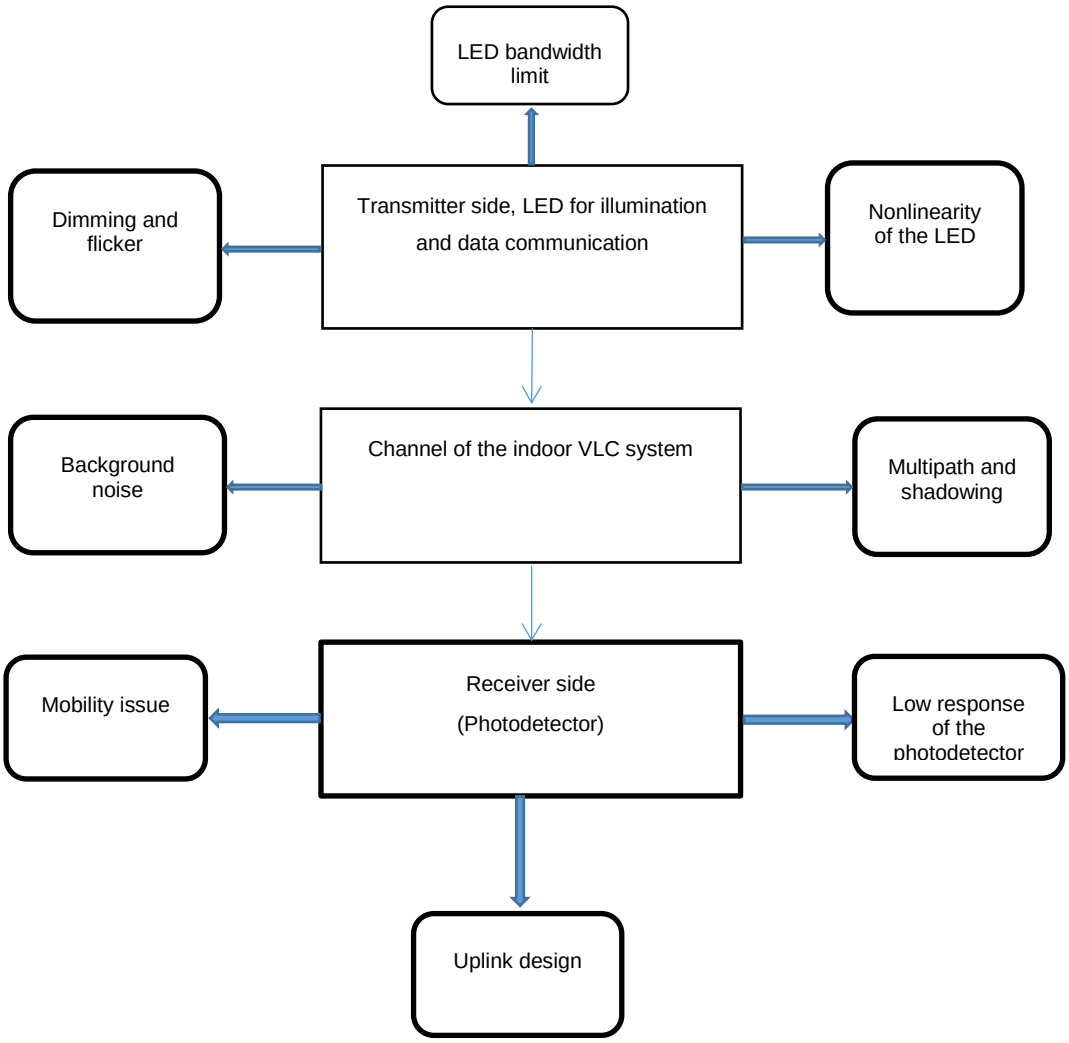

Figure 2-7: Main challenges in indoor VLC systems.

2.4.1 Modulation bandwidth of the LED

The modulation bandwidth available in the transmitters (LED) is typically less than the VLC channel bandwidth, which means that the former limits the transmission rates. Phosphor LEDs and RGB LEDs have limited modulation bandwidth, which is typically several megahertz for the phosphor LEDs and a few hundred megahertz for the RGB LED [52], [53] and this leads to limit the data rate. Many techniques have introduced to enhance the bandwidth of the

LED and increase the data rate such as, optical filters, pre and post equalisation (or both), complex modulation techniques for example, modulation formats that encode multiple bits per symbol and/or modulation formats able to operate at low system bandwidth, and parallel communication (multiple input and multiple output, MIMO). Data rates up to 32 Mb/s with a simple modulation scheme, non-return to zero on-off keying (NRZ-OOK), have been achieved with a simple equalizer at the receiver side [54]. Moreover, using a pre-equalizer at the transmitter side offered 40 Mb/s without using a blue filter [55]. By using a blue filter with complex pre-equalizer, a data rate up to 80 Mb/s was achieved in [56]. On the other hand, a MIMO technique and complex modulation, such as quadrature amplitude modulation (QAM) with orthogonal frequency division multiplexing (OFDM) or discrete multitone (DMT), are other approaches that were used to increase the data rate. More complex modulation formats have started to appear in VLC systems because the LED has a low modulation bandwidth and high SNR (results from the need to ensure the illumination level is at an acceptable level) [52]. A data rate exceeding 100 Mb/s was achieved by using a blue filter and applying DMT [57]. In addition, OFDM with MIMO and photodetector arrays offered a 220 Mb/s data rate [58]. By employing DMT with QAM and adaptive data loading technique, a data rate up to 513 Mb/s was achieved [59]. A 1 Gb/s rate was demonstrated experimentally in [20] by using the DMT technique. Using RGB LEDs with wavelength division multiplexing (WDM) and DMT achieved an aggregate data rate of 1.25 Gb/s in [60], 2.1 Gb/s in [61] and 3.4 Gb/s in [62]. A data rate of 2.3 Gb/s was demonstrated over a distance of 30 cm by using WDM with OFDM [63]. A three colours LED based WDM-VLC system was investigated with carrier-less amplitude and phase (CAP) modulation and adaptive equalization to achieve an aggregate data rate of 4.5 Gb/s. This data rate was obtained over 1.5 m with bit error rate (BER) of 3.8×10^{-3}, and consideration was given to use forward error correction (FEC) codes [64]. Commercial multicolour (RYGB) LEDs were used with discrete multi-tone (DMT) modulation to achieve an offline aggregate data rate of 5.6 Gb/s at BER = 3.8×10^{-3} [65]. A four channel WDM system with CAP modulation and hybrid post-equalizer was investigated experimentally obtaining a data rate of 8 Gb/s with BER = 3.8×10^{-3} [66]. A VLC system based WDM was reported using

commercial red LEDs, custom green LEDs and micro LEDs. It achieved a data rate of 11.28 Gb/s over 1.5 m [67].

Nonlinearity is another challenge at the transmitter side of the VLC system, which affect the system's performance. The LED is a major nonlinearity source at the transmitter side, as the modulation input current of the LED behaviour nonlinearity with the output power of the LED [53]. The baseband signal in optical system should be real and unipolar, to ensure forward biasing of the LED.

The bias voltage of the LED should be large than the turn on voltage of the LED so the current through the LED. Figure 2.8 illustrates the relationship between the input current and the output light of the LED. As can be seen the relationship between the input current and the light emission is not linear. Thus, to reduce the effect of nonlinearity of the LED, the biasing point of the LED should be chosen to operate at optimum point and the LED with a large range of linearity should be selected. To overcome this issue we used LDs in this thesis as will be explained in Chapter 3.

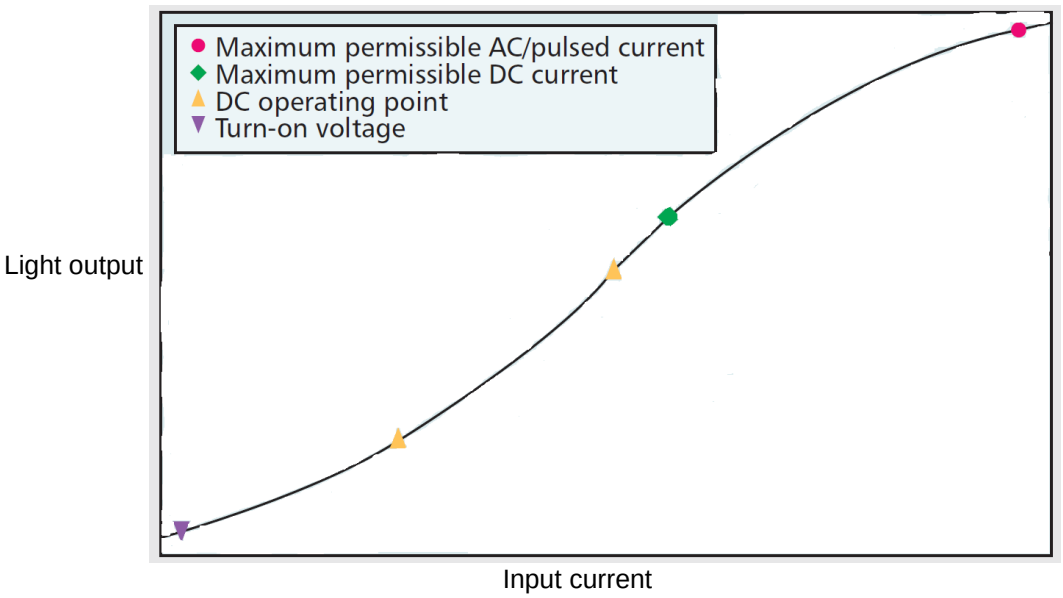

Figure 2-8: Output Characteristic of the LED [53].

2.4.2 Dimming control and flicker brightness of the VLC system

Brightness control for the LEDs in VLC systems is required. Light dimming is defined as controlling the perceived brightness of the light source according to the user's requirement [24]. The simplest method for dimming control is amplitude modulation (AM) where the luminous flux is controlled by controlling the input DC current. However, the chromaticity coordinates of the emitted light can be changed. Pulse width modulation (PWM) is another method to control the width of the current pulse as shown in Figure 2.9. The main feature in the PWM dimming method is that the amplitude of the pulse remains constant. The width of the pulse varies according to the dimming level, thus the result is that the emitted light spectrum is constant.

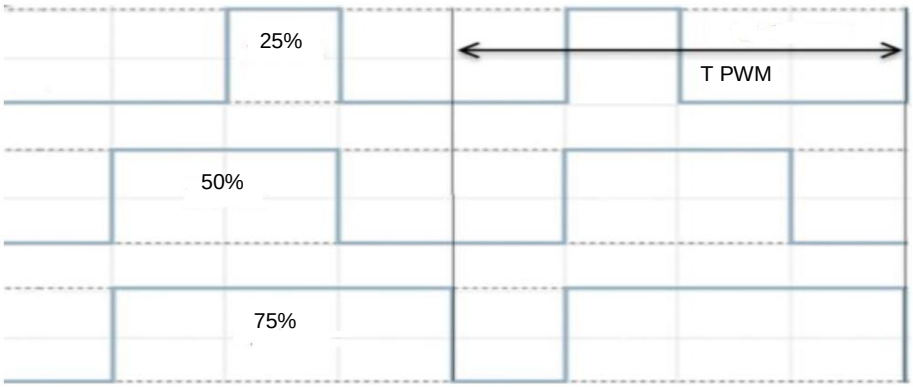

Figure 2-9: Dimming control using PWM.

Flicker in the VLC system can be defined as the fluctuations of the brightness of the LED light. The flicker occurs when the brightness changes over periods longer than the maximum flickering time period (MFTP). MFTP is the maximum time period that the light intensity can be changing, and it must be < 5 ms to be safe on the human [24], [68]. The flicker in VLC is classified into two groups according to its generation mechanism: intra-frame flicker and inter-frame flicker. Intra-frame flicker is defined as the perceivable brightness fluctuation within a frame. Inter-frame flicker is defined as the perceivable brightness fluctuation between adjacent frame transmissions

2.4.3 Multipath dispersion

Multipath dispersion is an important concern in designing a VLC system for an indoor environment. This is a result of the reflective proprieties of the VLC channel. Multipath dispersion occurs when the transmitted signal reaches the receiver through different paths at different times due to reflections from the ceiling, walls and other objects. Multipath dispersion causes the received pulse to spread, hence causing ISI. The channel root mean square (rms) delay spread is an important parameter to measure the ISI induced by multipath propagation [69]. The indoor channel characteristics of VLC systems have attracted great attention to devise techniques that can help alleviate multipath dispersion. VLC systems are subjected to ISI when operated at high data rates. Therefore, various techniques have been proposed to reduce the impact of ISI in VLC systems. In [70], cooperative transmission was used to synchronize the time of arrival (TOA) of multiple LEDs, which leads to a reduction in ISI in VLC systems. LED spotlights were used with narrow half power angle to decrease the delay spread of the indoor VLC system and to increase the data rate [71]. A holographic light shape diffuser (LSD) was used to reduce the ISI and to obtain a uniform power distribution over the entire room [72]. An angle diversity receiver (ADR) was studied in indoor VLC systems to reduce the delay spread and consequently, reduce the effect of ISI and enhance the system's performance [73], [74]. A delay adaptation technique (DAT) in conjunction with an imaging receiver were used to reduce the delay spread of the indoor VLC system. This enabled the system to work at high data rates with a good performance [75]. Another approached used to decrease ISI is the use of CGH in indoor VLC systems [76], [77], [78], [79].

2.4.4 Photodetector high capacitance

To collect an adequate optical signal the photodetector active area must be large, but the capacitance of the photodetector is directly proportional to its area. Therefore, a large photodetector area implies a large capacitance, which results in a restriction in the attainable bandwidth. The large capacitance at the input of the amplifier operates as a low pass filter (LPF), which means that

the received high frequency components will be attenuated. Although, a large capacitance acts as a LPF, it does not eliminate the dominant white thermal noise that is observed after the input stage. This noise may negatively affect the SNR at higher signal frequencies. When a white noise process following a LPF is fed back into the input of the filter, its power spectral density becomes quadratic in frequency and is often called f^2 noise [80]. Due to the f^2 noise variance being proportional to the square of the capacitance, an array of photodetectors can be used instead of a single photodetector (hence avoiding the photodetector's high capacitance) to reduce the effect of f^2 noise. The authors in [81] proposed the use of an array of photo detectors instead of a single photo detector to mitigate the effects of the large capacitance and to maximise the collected power at the same time. The photodetector's effective area can be enhanced by using a hemispherical lens, as suggested in [12]. Bootstrapping was proposed by the authors in [31] to minimise the effective capacitance of a large area photo detector. In this thesis, an ADR and an imaging receiver are employed to mitigate the impact of the large photodetector area and to improve the system's performance.

2.4.5 Provision of uplink for VLC system

In general, most of the researchers focusing on the downlink discretion of the VLC system, this is due to the future wireless internet services, the traffic volume is much higher than that in the uplink. However, in any communication system, it is important to establish an uplink direction to achieve communication in both directions (bi-directional communication) [82]. The RF and IR can be used in the uplink to avoid the interference between the uplink and the downlink, [53]. In addition, it is possible to use the visible light on the uplink, but this will require techniques to separate between the uplink and the downlink direction to avoid the interference [82]. Two methods may be used to support the bi-directionality of VLC system. Time-division duplexing (TDD) and Wavelength-division duplexing (WDD) [23]. In TDD, the uplink and the downlink direction have the same wavelength with different transmission time.

WDD offers a separation in frequency (wavelength) band between the transmitter and the receiver [82].

2.5 Signal Modulation Techniques

VLC system channels are completely different from traditional RF system channels, and this has resulted in different methods of modulation being used. Modulation schemes that fit well in RF channels do not necessarily perform well in the optical domain. There are four criteria for choosing a specific modulation technique for VLC systems. The most important criterion to be applied is the average power requirement used, due to eye hazards and power consumption. The second criterion is the receiver's electrical bandwidth requirements. The third factor is the complexity of modulation and power consumption in portable devices. The last factor is the physical limitations in the transmitter. In VLC systems, modulation occurs in two stages. In the first stage, the information to be transmitted is coded as waveforms and in the second stage these waveforms are modulated onto the instantaneous power of the carrier. This section firstly defines the intensity modulation and direct detection (IM/DD) channel, and then discusses the most common modulation schemes used over this channel: OOK and pulse position modulation (PPM).

2.5.1 IM/DD channel

IM/DD is the preferred transmission technique in OW systems [12]. IM is achieved by varying the bias current of the LD or the LED. In VLC systems, the transmitted signal power is always positive. Direct detection is the simplest method that can be used to detect an intensity modulated signal. The photodetector generates a current that is proportional to the incident the optical power intensity. A simple description for the IM/DD channel is given as [12]:

$$y(t) = Rx(t) \otimes h(t) + Rn(t) \tag{2.5}$$

where R is the photodetector responsivity (in amps per watt), $y(t)$ is the instantaneous photocurrent received, t is the absolute time, $\otimes$ denotes

convolution, $h(t)$ is an impulse response, $x(t)$ is the instantaneous transmitted power and $n(t)$ is the background noise (BN), which is modelled as white Gaussian noise, and the BN is independent of the received signal. One of the most important factors that should be considered when designing a communication system is the modulation scheme. The modulation scheme defines the power efficiency and bandwidth of the system, and these will affect the overall system performance. One of the main constraints in a mobile VLC transmitter is the power consumption. Therefore, power efficient modulation is required. OOK and PPM are the most popular modulation schemes applied in OW systems [83]. In this thesis, all the proposed systems employ an OOK modulation scheme that adds simplicity to the VLC system.

2.5.2 On-Off Keying (OOK)

In OOK modulation, each bit is simply sent by switching the light source (LDs or LEDs) ON or OFF during its bit period. A '1' bit is encoded when the light source is ON, and a '0' bit is encoded when no signal is transmitted. There are two types of OOK modulation: Non-Return to Zero (NRZ-OOK) and Return to Zero (RZ-OOK).

In NRZ-OOK, the transmission period (Tp) of the transmitted pulse is equal to the bit period (k=1). However, RZ-OOK, with k=0.5, represents 50% of the duty cycle. NRZ-OOK has several advantages, including simplicity of implementation and bandwidth efficiency. However, it requires a high average optical power compared to RZ-OOK. A basic NRZ-OOK and RZ-OOK with a 50% duty cycle is shown in Figure 2.10. A high bit rate in the VLC system can be offered using OOK modulation.

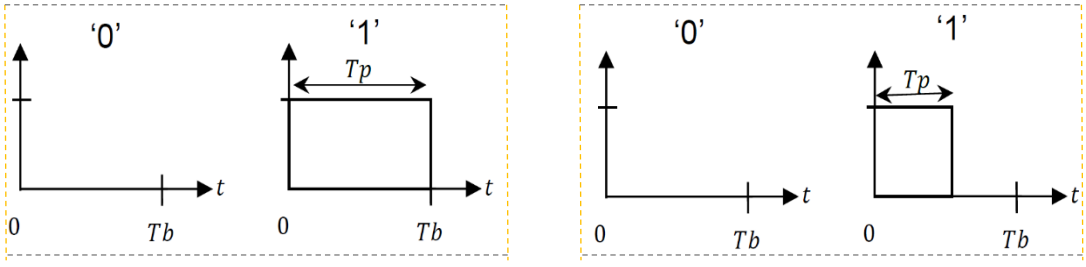

(a) NRZ-OOK (b) RZ-OOK

Figure 2-10: Basic NRZ-OOK and RZ-OOK signals.

2.5.3 Pulse position modulation (PPM)

Modulation techniques that use minimum average transmitter power and make high-speed digital transmission achievable are required for indoor optical wireless communication. PPM is a modulation scheme that offers high average power efficiency at the cost of relatively poor bandwidth efficiency [84], which makes it more sensitive than OOK to multipath dispersion. PPM is considered in optical communications due to its low average power requirements [85]. PPM is a modulation scheme in which data bits are conveyed by a single pulse in one of several possible positions. The positions are represented as slots, and *L*-PPM has slots in a single symbol time (frame). Each frame contains a pulse occupying one slot and empty slots. The pulse is located at a slot that is proportional to the binary value of the original digital symbol. Each frame can be concluded by a guard interval to avoid inter frame interference and for timing extraction purposes. The time used for communication is divided into equal blocks. Each block is equally divided again into *L* time slots. Figure 2.11 shows an example of 4-PPM modulation.

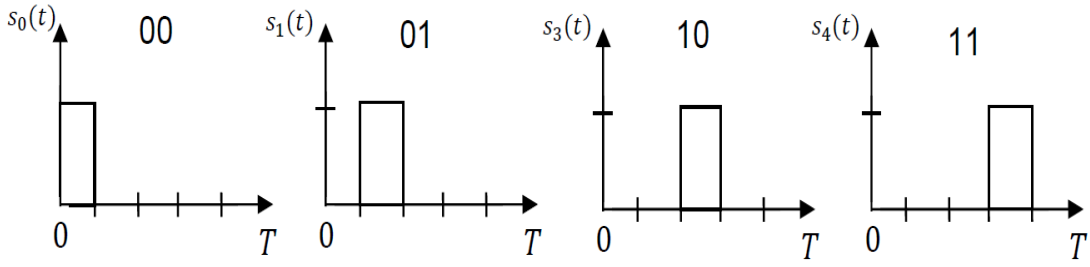

Figure 2-11: Example of 4-PPM code.

2.6 VLC Applications

VLC systems cover indoor to outdoor applications. Indoor applications could be data communications, indoor location estimation, indoor navigation for visually impaired people and accurate position measurements. The outdoor applications could be transportation, location information, information broadcast using the traffic light infrastructure. VLC systems can be used to transfer data within offices. User location can be estimated in an indoor environment using white LEDs, hallways are assumed to be illuminated by

LEDs with a unique ID for each LED. White LEDs in conjunction with geometric sensors integrated in smart phones could help visually impaired people move inside buildings [86]. Figure 2.12 shows a prototype of a navigation system for visually impaired people from [86]. RF signals can be undesirable inside hospital environments, especially in operating theatres and magnetic resonance imaging (MRI) scanners, therefore VLC systems can be potential solutions to such scenarios.

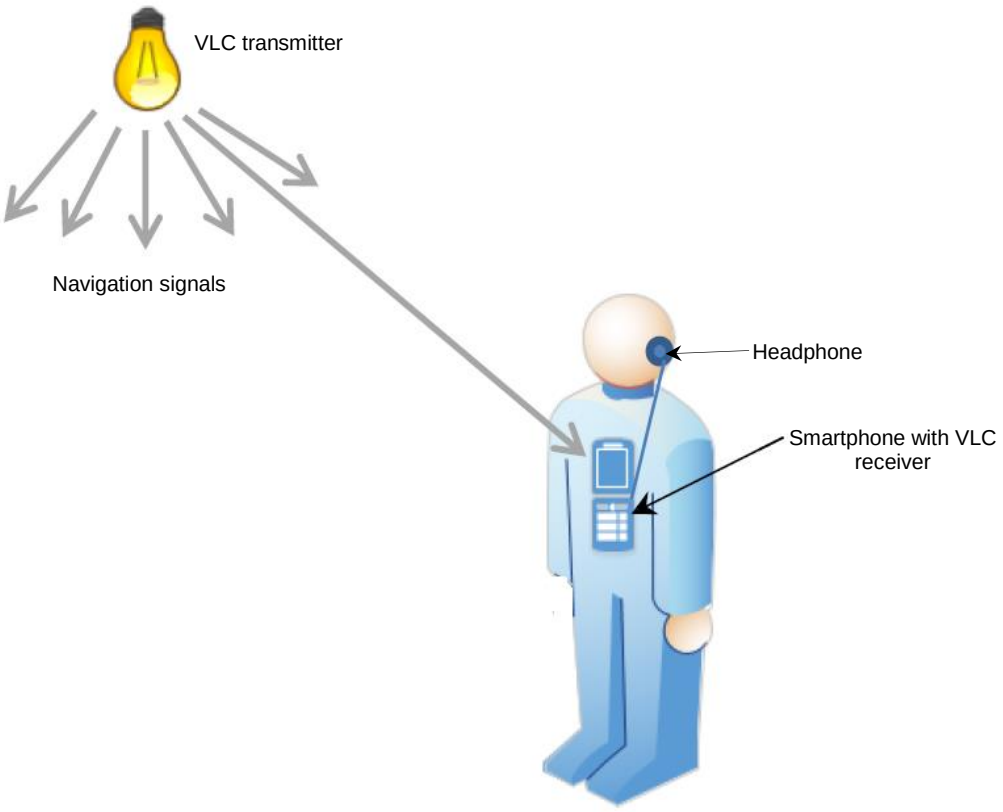

Figure 2-12: Indoor VLC navigation system for visually impaired people.

Recently, various approaches for VLC indoor positioning systems have been researched [87], [88]. VLC systems are a promising solution for indoor positioning due to many features. Firstly, there is better positioning accuracy compared to radio wave systems, since VLC suffers less from interference and multipath effects. Secondly, VLC positioning systems can be used in environments where radio positioning systems are restricted, such as in hospitals [88]. White LEDs can be used to transfer digital data in the

automotive field (car to car communication), head and tail LED lights can be used to communicate between cars, and also there is the possibility to communicate between cars and the traffic lights infrastructure [89]. In risk areas, such as oil rigs and mines, safe communication and illumination can be provided by VLC systems using LEDs. Nowadays, aircraft use white LEDs for illumination, which can also be used to provide media services to passengers instead of wires. This will reduce the weight and the cost of the aircraft.

2.7 Summary

This chapter has provided an overview of VLC systems. It has introduced a comparison between VLC and RF systems. It has also explained the VLC system structure including the transmitter and the receiver components In addition, to the classification of VLC links were presented. It has highlighted the significant challenges in VLC systems, such as low modulation bandwidth of transmitters (LEDs), multipath dispersion, photodetector high capacitance and the provision of an uplink. This chapter has also addressed the most common types of modulation schemes in VLC systems.

3. Channel Modelling of Indoor VLC Systems

3.1 Introduction

To evaluate the behavior of an indoor VLC link in terms of signal integrity, modelling the indoor channel of the VLC system is important. The characteristics of the indoor VLC system channel are fundamental to evaluate the VLC system performance and to address the design issues. In the indoor VLC system, the received optical signals are detected under the effect of surrounding noise sources, receiver noise, mobility and multipath dispersion. These aspects lead to degrade the received optical signals and consequently impair the performance of the indoor VLC system. Due to light rays cannot pass through opaque barriers, which results in multipath propagations, the indoor channel of the VLC system is assessed for different link configurations (LOS and NLOS). In this chapter, the tools that are used to simulate the indoor channel of the VLC system are described. Simulations and calculations reported in this thesis were carried out using MATLAB.

The indoor VLC communication channel is discussed in Section 3.2. The multipath propagation model is given in Section 3.3. The impulse response is given in Section 3.4. An analysis of delay spread of the received pulse is provided in Section 3.5. The SNR evaluation is given in Section 3.6. The simulation package is explained in Section 3.7. The results of the traditional VLC system with wide FOV receiver, angle diversity receiver and imaging receiver are summarised in Section 3.8. Section 3.9 gives the simulation set up of the proposed VLC systems. A summary is provided in Section 3.10.

3.2 Indoor VLC System Channel

Intensity modulation with direct detection (IM/DD) is the most suitable method for indoor optical wireless communication, including VLC system. This is due to low complexity and cost [12], [90]. As can be seen in Figure 3.1, IM

is used at the transmitter side to modulate the wanted signal into the instantaneous optical power by varying the intensity of the optical source. In addition, the receiver uses DD to generate the electrical current $(I(t))$, which is proportional to the instantaneous received optical power. In indoor VLC system, The typical detector area contains tens of millions of very short wavelengths of the received optical signal, and hence allows spatial diversity and prevents fading [12]. When using IM/DD, the indoor channel of the VLC system can be fully modelled by the impulse response $(h(t))$ of the channel [91]:

$$I(t, Az, El) = \sum_{k=1}^{L} R\, x(t) \otimes h_k(t, Az, El) + \sum_{k=1}^{L} R\, n_k(t, Az, El) \tag{3.1}$$

where $I(t, Az, El)$ is the instantaneous current received by the photodetector, t is the absolute time, Az and El are the arrival directions, L is the total number of receiving elements, R is the responsivity of the photodetector, $x(t)$ is the instantaneous optical power transmitted by the transmitter, $\otimes$ denotes convolution and $n(t, Az, El)$ is the background received noise, which can be modelled as additive white Gaussian noise (AWGN) [92]. In this theses, a ray tracing algorithm was used to compute the channel impulse response on the communication floor.

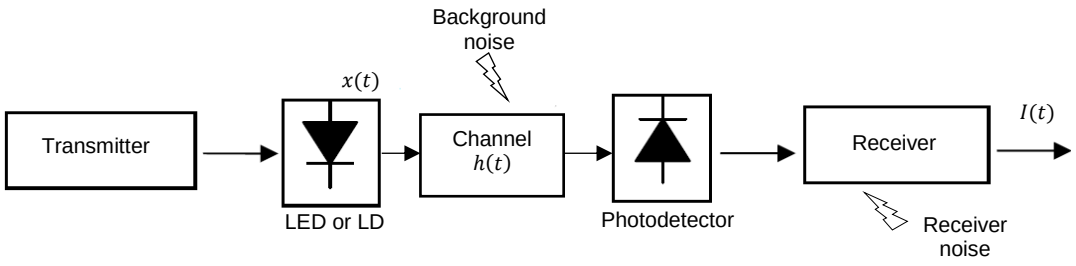

Figure 3-1: Block diagram of IM/DD VLC system.

The channel impulse response can be represented approximately as the sum of scaled and delayed Direct delta functions [12] and given as:

$$h(t) = \sum_{k=0}^{\infty} h^{(k)}(t) \tag{3.2}$$

where $h(t)$ is the impulse response due to LOS components and k^{th} reflections.

3.3 Multipath Propagation Model

The characteristics of the propagation of the indoor VLC channel depend on the relative positions of the transmitter, reflector elements and the receiver. Besides that, these characteristics depend on the patterns of the transmitter, reflector elements and the receiver (i.e., FOV for the transmitter and the receiver and reflection coefficient of the reflector elements). These characteristics are also subject to the movement of objects and people. However, those changes are slow in comparison with the transmission rate. Thus, the channel can be assumed as stationary for a given fixed configuration.

One of the main challenges in VLC systems when working at high data rates (several Gb/s) is multipath propagation, which leads to increase in the ISI and consequently degrades the system performance. When the dimensions of the indoor environment increase, this leads to increase the multipath dispersion. This is attributed to increase in the difference in paths length. Measurements to study the reflection coefficients for a number of materials normally used in indoor settings were taken by Gfeller and Bapst [5]. They have shown that the reflection coefficients (ratio of reflected power to incident power) ranged from 0.4 to 0.9. They also observed that the power reflected by either the walls or the ceiling of the room is in a form similar to that of a Lambertian pattern. Therefore, the reflecting elements for the walls, floor and ceiling were considered in their work and in this thesis as second transmitters that transmit the received signal in a form of a Lambertian pattern. The power radiated into a solid-angle element $d\Omega$ can be written as [93]:

$$dP = \frac{n+1}{2\pi} P_s \cos(\alpha)^n \, d\Omega \tag{3.3}$$

where $\frac{n+1}{2\pi}$ assures that integrating dP over a hemisphere surface results in the total average transmitted optical power P_s radiated by the source (i.e., LED or LD), α is the angle of incidence with respect to the transmitter's normal and the parameter n represents the mode number that determines the shape of

the radiated beam. The n mode number of the transmitted beam is related to the half-power semi-angle hps that can be given as [12]:

$$n = -\frac{ln(2)}{ln\,(cos(hps))} \tag{3.4}$$

It should be noted that sources with a narrow beam have a large value of n and this leads to focus the optical power at an area of interest. When n = 1, this leads to make an ideal Lambertian sources. Due to all surfaces are presumed to be rough, it is suitable to use n = 1, which agrees with experimental measurements [5]. Thus, in this work, we assume that the reflecting elements in a plaster surface have hps that is equivalent to 60◦, which corresponds to n = 1.

3.3.1 Received optical power calculations

Due to multipath propagation, more than one path may present between the transmitter and the receiver, which causes a temporal dispersion. To compute the received optical power at the receiver, the ray tracing algorithm can be used. The reflected optical rays from different reflectors are traced following all potential paths to the detector or other reflectors. Therefore, to implement the ray tracing, the reflective surfaces on the ceiling and walls were segmented into a number of equal square-shaped surface elements. Each one of these surface elements was treated as a Lambertian source with n = 1. Selecting a small size for these elements improves the accuracy of the impulse response, but the computation time increases exponentially.

Previous researchers [94], [52], [60] have taken into account only LOS components and reflection components up to first order. However, this may not give a full description of the system characteristics. Thus, in this thesis, up to second order reflections were considered in modelling the optical wireless channel, as second order reflections have a great impact on the system performance at the high data rate. In addition, references [95] and [96] found that most of the received optical power is within the first and second order reflections as when it goes beyond the second order signals are highly attenuated. Therefore, reflections up to the second order are considered in this

thesis. Figure 3.2 shows the ray tracing setup for the LOS component and first order and second order components.

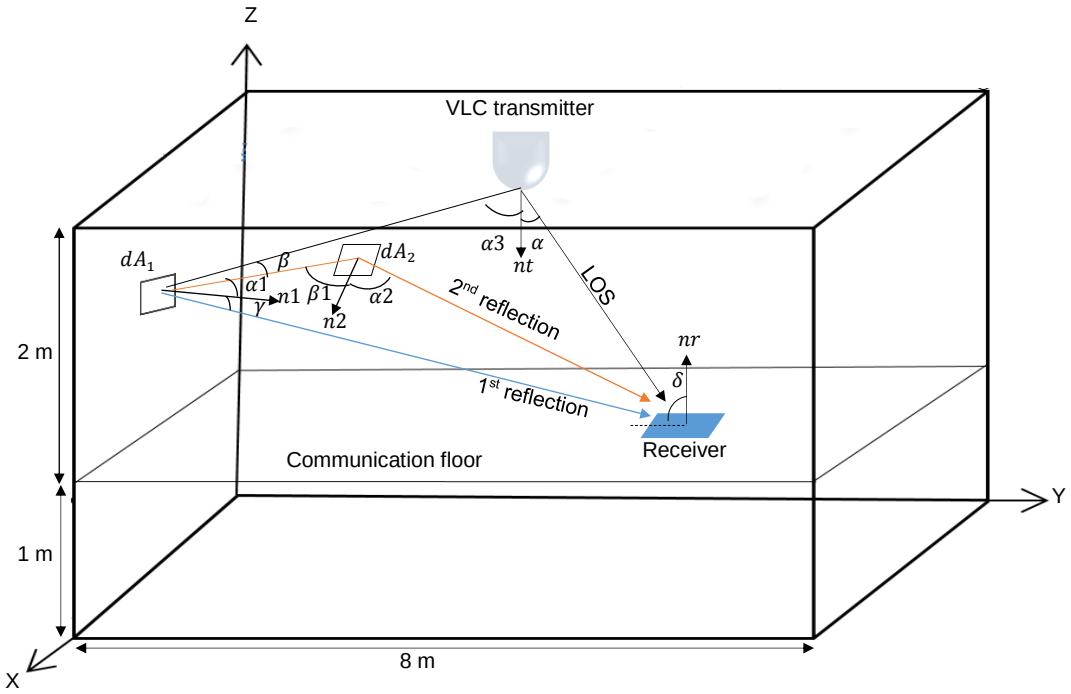

Figure 3-2: Ray tracing setup for LOS, first and second order reflections in VLC system.

The impulse response of the indoor VLC channel can be computed by tracing all potential light rays connecting the transmitter and the receiver. The total received optical power (P_r) at the receiver, considering the direct LOS component (P_{LOS}), first order reflection components (P_{1st}) and second order reflection components (P_{2nd}) can be expressed as:

$$P_r = \sum_{k=1}^{s} P_{LOS} + \sum_{i=1}^{l} P_{1st} + \sum_{d=1}^{f} P_{2nd} \tag{3.5}$$

where s is the number of rays due to LOS components, l is the number of rays due to the first reflection components and f is the number of rays due to the second reflection components.

3.3.1.1 Line-of-Sight (LOS) calculation

A LOS link exists when a direct path connects the transmitter and the receiver. When the VLC transmitter is located on the ceiling facing downwards (has an elevation angle of -90º) and the VLC receiver is placed on the communication floor facing upwards (has an elevation angle of -90º), this leads to create the LOS component between the transmitter and the receiver as shown in Figure 3.3. The P_{LOS} component can be written as:

$$P_{LOS} = \begin{cases} \frac{n+1}{2\pi {R_d}^2} \times P_s \times cos^n(\alpha) \times cos(\delta) \times A_r & 0 \le \delta \le \psi c \\ 0 & \delta > \psi c \end{cases} \quad (3.6)$$

where P_s represents the average optical power of the light source (LD or LED), δ is the angle between the normal of the photodetector and the incident ray. A_r is the area of the photodetector. α is the angle between the normal of the transmitter and the incident ray. R_d is the direct link distance between the receiver and the transmitter. If the received angle (δ) is larger than the acceptance semi-angle (ψc), then the direct LOS received power is zero as the light is only gathered by the receiver within the receiver's FOV (ψc). Thus, altering the receiver's FOV reduces the effect of the unnecessary signals.

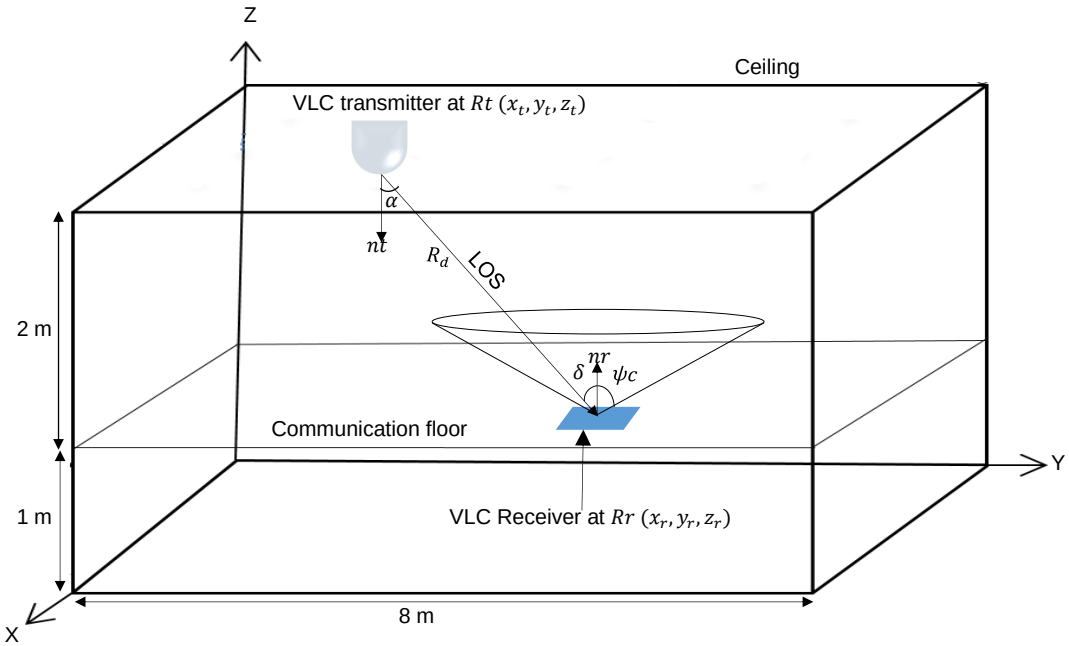

Figure 3-3: Ray tracing for LOS component.

As shown in Figure 3.3, the reception angle (δ) is first checked against the FOV of the receiver. The incident ray on the photodetector is inside the detector's FOV if the reception angle is smaller than or equivalent to the FOV of the photodetector. The receiving and transmitting angles (δ,α) are computed as follows:

$$\alpha = \cos^{-1}\left(\frac{\widehat{n_t}.(Rr - Rt)}{R_d}\right) \; and \; \delta = \cos^{-1}\left(\frac{\widehat{n_r}.(Rt - Rr)}{R_d}\right) \tag{3.7}$$

where the normal of the transmitter at location Rt is $\widehat{n_t}$ and $\widehat{n_r}$ is the normal of the receiver at locations Rr, respectively.

It should be noted that both angles in (α and δ) are equal if the receiver and transmitter are placed in parallel planes. This case when the transmitter is located on the ceiling while the receiver is on the communication floor (see Figure 3.3). But, if the walls which are at 90◦ to the communication plane are considered or a different elevation angle of the receiver with respect to the communication floor is considered, then the transmitting and receiving angles are different. R_d is the direct distance between the transmitter and the receiver, which can be given as:

$$R_d = \sqrt{(x_r - x_t)^2 + (y_r - y_t)^2 + (z_r - z_t)^2} \tag{3.8}$$

where x_r, y_r and z_r are the receiver coordinates and x_t, y_t and z_t are the transmitter coordinates. The vector length linking the receiver and transmitter is used to determine the time delay taken by the direct ray to reach the receiver. The speed of light rays travelling through air is 3×10^8 m/s. The time delay is the ratio of the link length (R_d) and the speed of light.

3.3.1.2 Analysis of the first order reflection

The ray tracing setup for the first order reflection is depicted in Figure 3.4. Plaster walls can be considered as Lambertian reflectors with ne = 1 [5]. The received optical power of the first order reflections can be obtained by using the Lambertian model in Equation 3.3 as:

$$P_{1st} = \begin{cases} \dfrac{(n+1)(n_e+1)}{4\pi^2 R_1^2 R_2^2} \times P_s \times dA_1 \times \rho_1 \times cos^n(\alpha) \times cos(\beta) \times cos^{ne}(\gamma) \times cos(\delta) \times A_r & 0 \le \delta \le \psi c \\ 0 & \delta > \psi c \end{cases}$$

(3.9)

where R_1 is the distance between the reflective element and transmitter, R_2 is the distance between the receiver and the reflective element, α is the angle between the normal of the transmitter and the irradiance ray, β is the angle between the incident ray from the transmitter and the reflective element's normal, γ is the angle between the reflective element's normal and the reflected ray and δ is the angle that joins the normal of the receiver and the incident ray. d_{A1}, ρ_1 and n_e are the area of the reflective element, the reflection coefficient of the reflective element and the Lambertian emission order of the reflective element, respectively.

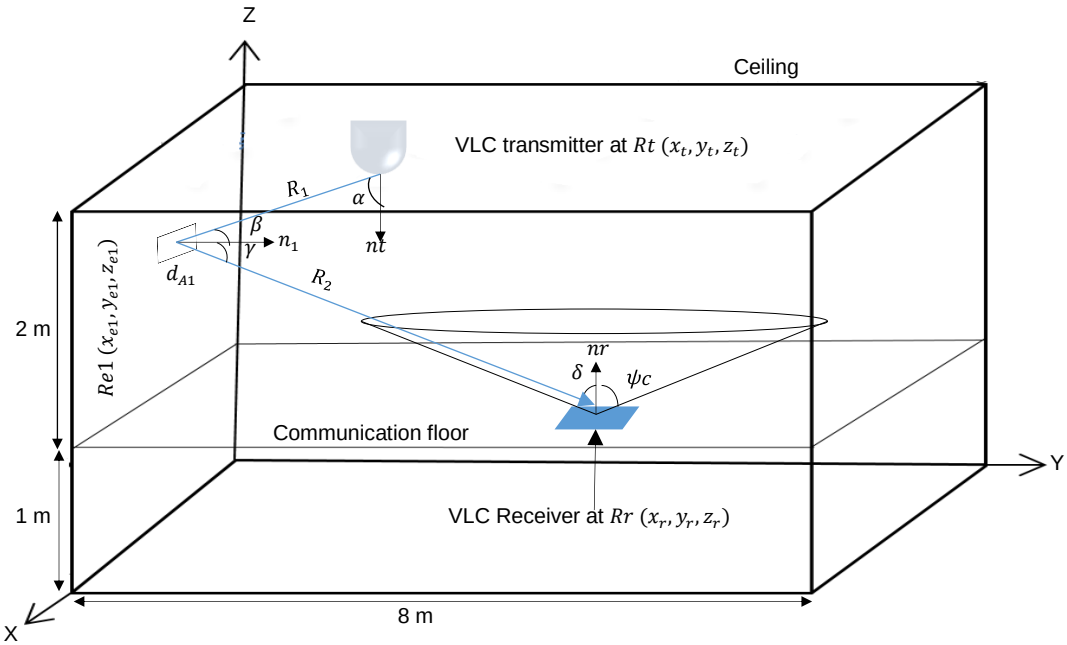

Figure 3-4: Ray tracing for first order reflection.

The reflective element turns into a secondary small transmitter where its retransmitted optical power is determined by its reflection coefficient and the

received optical power from the transmitter. The four angles in Equation (3.9) can be computed as:

$$\left\{\begin{array}{l} \alpha = \cos^{-1}\left(\frac{\widehat{n_t}.(Re1 - Rt)}{R_1}\right), \beta = \cos^{-1}\left(\frac{\widehat{n_1}.(Rt - Re1)}{R_1}\right) \\ \gamma = \cos^{-1}\left(\frac{\widehat{n_1}.(Rr - Re1)}{R_2}\right) and\ \ \delta = \cos^{-1}\left(\frac{\widehat{n_r}.(Re1 - Rr)}{R_2}\right) \end{array}\right\} \quad (3.10)$$

here $\widehat{n_1}$ is the normal of the reflective element 1 at location $Re1$.

3.3.1.3 Analysis of the second order reflection

Broadening the reflection to additional surfaces and utilising the Lambertian model once more, the second order reflection is computed in three stages:

1- Calculation of the amount of incident optical power to the reflective element from the transmitter, which is similar to the approach that used to calculate the LOS optical received power.
2- Calculation of the amount of the incident optical power to the second reflective element from the first reflective element.
3- Calculation of the reflected power emitted from the second reflective element to the receiver.

The second order reflections can be obtained by using the same evaluation method of the first order reflections. As depicted in Figure. 3.5, considering first order reflection computations, the received optical by the second order reflections (P_{2nd}) can be given as:

$$P_{2nd} = \left\{\begin{array}{ll} \frac{(n+1)(n_e+1)^2}{8\pi^3 R_1^2 R_2^2 R_3^2} \times P_s \times d_{A1} \times d_{A2} \times \rho_1 \times \rho_2 \times cos^n(\alpha) \times & \\ cos(\beta) \times cos^{ne}(\alpha 1) \times cos(\beta 1) \times cos^{ne}(\alpha 2) \times \cos(\delta) \times A_r\,, & 0 \le \delta \le \psi c \\ 0, & \delta > \ \psi c \end{array}\right.$$

(3.11)

where R_1 is the distance between the transmitter and the first reflective element, R_2 is the distance between the first reflective element and the second reflective element, R_3 is the distance between the receiver and the second reflective element. d_{A1} is the area of the first refractive element and d_{A2} is the area of the second refractive element. The reflection coefficient of the first refractive element and the reflection coefficient of the second refractive element are ρ_1 and ρ_2, respectively. α is the angle between the normal of the transmitter and the irradiance ray, β is the angle between the normal of the reflective element 1 and the incident light from the transmitter, $\alpha 1$ is the angle between the first reflective element's normal and the reflected ray to the second refractive element, $\beta 1$ is The angle between the first reflecting ray and the normal of the second reflective element, $\alpha 2$ is the angle between the second reflected ray and the normal of the second reflective element and δ is the angle between the normal of the receiver and the second reflected ray.

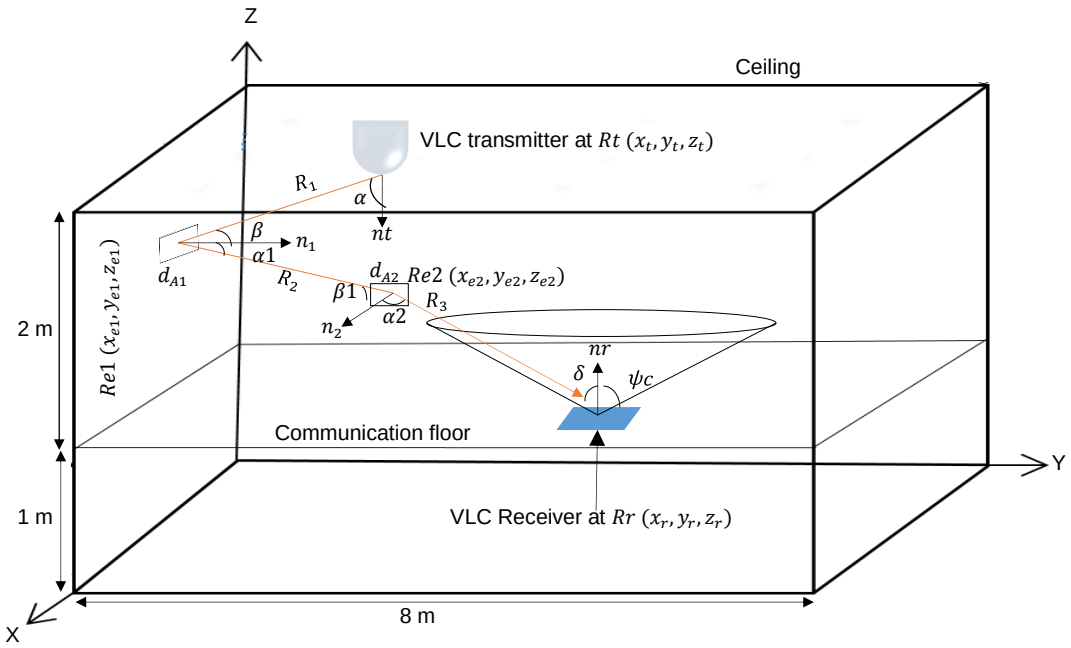

Figure 3-5 .: Ray tracing for second order reflection.

Six angles are required for the second order reflection. These angles can be obtained in a similar way to the direct path and the first order reflection by tracing the ray from the transmitter to the receiver as:

$$\left\{\begin{array}{c} \alpha = \cos^{-1}\left(\frac{\widehat{n_t}.(Re1 - Rt)}{R_1}\right), \beta = \cos^{-1}\left(\frac{\widehat{n_1}.(Rt - Re1)}{R_1}\right), \\ \alpha 1 = \cos^{-1}\left(\frac{\widehat{n_1}.(Re2 - Re1)}{R_2}\right), \beta 1 = \cos^{-1}\left(\frac{\widehat{n_2}.(Re1 - Re2)}{R_2}\right), \\ \alpha 2 = \cos^{-1}\left(\frac{\widehat{n_2}.(Rr - Re1)}{R_3}\right) \; and \; \delta = \cos^{-1}\left(\frac{\widehat{n_r}.(Re2 - Rr)}{R_3}\right) \end{array}\right\} \quad (3.12)$$

here $\widehat{n_2}$ is the normal of the second reflecting element at $Re2$.

3.4 Impulse Response

The impulse response of the practical VLC system is continuous, but the room reflective surfaces (walls, ceiling and floor) were subdivided into discrete elements by the simulator. Therefore, to reduce the effect of the discretization, time was subdivided into bins of width Δt, grouping the power received within each bin into a single received power. Based on the empirical results, a good choice for the bin width is the time light takes to travel between neighbouring elements [93]. Thus, the time bin (Δt) can be given as [93], [38]:

$$\Delta t \leq \frac{\sqrt{d_A}}{C} \quad (3.13)$$

where d_A is the reflection element area and C is the speed of light. Light rays received within similar time intervals are assembled and stored for a particular transmitter-receiver position on the communication floor. An exact histogram of the practical impulse response can be achieved when d_A approaches zero. It should be noted that reduction of d_A results in improved resolution in impulse response assessment. However, this leads to an increase in the computation time. Thus, the reflective element size (d_A) has to be selected to keep the computation time within acceptable limits [97], [98], [99]. The indoor channel of the VLC system can be completely analysed via its impulse response $h(t)$. A number of parameters may be calculated from the impulse response such as delay spread, path loss and SNR.

3.5 Delay Spread

Due to non-directed transmission, indoor VLC systems are subject to multipath dispersion, which causes pulse spread in time. Delay spread is a good measure of signal pulse spread due to the temporal dispersion of the incoming signal. The delay spread of an impulse response is given by [91]:

$$D = \sqrt{\frac{\sum (t_i - \mu)^2 \, P_{ri}^2}{\sum P_{ri}^2}} \tag{3.14}$$

where t_i is the delay time associated with the received optical power P_{ri}, and μ is the mean delay given by:

$$\mu = \frac{\sum t_i \, P_{ri}^2}{\sum P_{ri}^2} \tag{3.15}$$

In this thesis, for every location, the delay spread is computed as the impulse response is calculated. In practice the delay spread may change for a given transmitter and receiver location if the reflecting elements in the room move, for example people entering and leaving and fans rotating. These effects are not considered here and have not been quantified by other researchers to the best of our knowledge.

3.6 Calculations of Signal to Noise Ratio (SNR)

The performance of the VLC system is best evaluated using the SNR, which provides due consideration to the noise and signal spread (eye opening). The bit error rate *(BER*) is expressed as [12]:

$$BER = Q\left(\sqrt{SNR}\right) \tag{3.16}$$

where Q is the Gaussian function and can be given as:

$$Q(x) = \frac{1}{2} \, erfc\left(\sqrt{x/2}\right) \tag{3.17}$$

wher erfc is the complementary error function. The function has the value *x* = 6 at BER of 10^{-9}. Hence, SNR =36 (15.6 dB) is needed for a 10^{-9} BER. In OOK, the SNR associated with the received signal can be calculated by considering

P_{s1} and P_{s2} (the powers associated to logic 1 and 0 respectively). These powers (P_{s1} and P_{s2}) determine the eye opening at the sample instant, thus ISI. The SNR is given by [100], [101], [102]:

$$SNR = \left(\frac{R(P_{s1} - P_{s0})}{\sigma t}\right)^2 \tag{3.18}$$

where R is the responsivity of the photodetector and σt is the standard deviation of the total noise. The total noise can be classified into three components and can be given as [101]:

$$\sigma t = \sqrt{\sigma_{bn}^2 + \sigma_s^2 + \sigma_{pr}^2} \tag{3.19}$$

where σ_{bn} is the background shot noise component, σ_s is the shot noise component associated with the received signal and σ_{pr} is the preamplifier noise component.

In this thesis, two schemes are considered to process the electrical signal from different branches of the angle diversity receiver and the imaging receiver: selection combining (SC) and maximum ratio combing (MRC). In the SC, the receiver just selects the branch with the largest SNR among the branches. The SC SNR is given by:

$$SNR_{SC} = max_k \left(\frac{R(P_{s1k} - P_{s0k})}{\sigma t}\right)^2 \ , 1 \leq k \ \leq J \tag{3.20}$$

where J represents the total number of detectors/pixels used in receiver. Unlike the SC method, the MRC makes use of all detectors/pixels. All output signals from the detectors/pixels are combined through an adder circuit. Each input to the circuit is weighed in proportion to the SNR of the relevant branch so as to maximise the output SNR. The MRC SNR is given as [103]:

$$SNR_{MRC} = \sum_{i=1}^{J} \left(\frac{R^2(P_{s1i} - P_{s0i})^2}{\sigma ti^2}\right) \tag{3.21}$$

This SNR analysis will be used throughout the thesis to evaluate the performance of the VLC system.

3.7 Simulation Package

For the purpose of evaluating the performance of the VLC system under the impact of the multipath propagation and the user mobility, the channel impulse response of the VLC system has to be evaluated. A simulation tool was used in this thesis that is similar to the one developed by Barry et al. [93]. The simulation tool was used to produce the impulse response, path loss and 3 dB channel bandwidth and to calculate the delay spread and the SNR. A MATLAB program was used to simulate and calculate the results in this thesis.

Simulations were run in a typical rectangular room that was unfurnished, with dimensions of 4 m width, 8 m length and 3 m height. The walls and ceiling were segmented into small reflective elements. The reflective elements were treated as small secondary emitters that diffuse the received signal in the shape of a Lambertian pattern, with a reflectivity of 0.8 for walls and ceiling and 0.3 for the floor and Lambertian emission order (n) of 1 [5], [37]. The accuracy of the received impulse response profile evaluated is controlled by the size of the reflective elements (dA). Thus, to keep computations within a reasonable time, a 5 cm × 5 cm size was chosen for the surface element in the first reflections and 20 cm × 20 cm size for second reflections [104]. In this thesis, up to second order reflections were considered in modelling the indoor VLC channel, as second order reflections have a great impact on the system performance at the high data rate. In addition, references [95] and [96] found that most of the received optical power is within the first and second order reflections as when it goes beyond the second order signals are highly attenuated. Therefore, reflections up to the second order are considered in this thesis.

In this chapter, the VLC system in conjunction with a wide field of view receiver (W-FOV), an angle diversity receiver (ADR) and an imaging receiver, which is presented in detailed in [96], [75], [73], is studied and evaluated under constraining of multipath propagation and mobility. This VLC system with the three types of the receivers used for comparison purposes in order to evaluate the novel configurations proposed in this thesis in later chapters. In addition, we compared the results of our simulator in the case of the traditional VLC

system that presented in [94], [105] (see Appendix A). Besides that, the author has verified his simulator against the results of the basic IROW systems such as a conventional diffuse system (CDS), line strip multi-beam system (LSMS) and beam clustering method (BCM) [91], [93], [102] [106], [107]. A very good match was observed between the results of the author's simulator and other researchers' work (see Appendix A). This gives confidence in the capability of the author's simulator to assess new VLC systems.

3.8 Simulation Results

The purpose of our simulator was to assess the capability of the VLC system under the influence of multipath dispersion and user mobility. In this section, the simulator was used to assess the VLC system in conjunction with the W-FOV, the ADR and the imaging receiver. The results of the simulation are reported in the form of the impulse response, delay spread and SNR.

An empty room that has neither doors nor windows used for the analysis as shown in Figure 3.6. The dimensions of the room are 4 m × 8 m × 3 m (width × length × height) with reflection coefficients of 0.3 for the floor and 0.8 for the ceiling and walls. Walls, ceiling and floor were modelled as Lambertian reflectors. The room was divided into a number of equal square-shaped surface elements and each surface element was treated as Lambertian source with n = 1. To keep computations within a reasonable time, a 5 cm × 5 cm size was chosen for the surface element in the first reflections and 20 cm × 20 cm size for second reflections Up to second-order reflections were considered in the simulation. In the simulation, eight RGB-LDs light units were used for illumination, and were installed on the ceiling (along the *x*-*y* axis) of the room (3 m above the floor), which ensures the ISO and European illumination requirements were met [108]. Each RGB-LDs light unit had 9 RGB-LDs (3 × 3) with a separation of 3 cm. The transmitted optical power from each RGB LD was 2 W. The coordinates of the RGB LDs-light units were (1 m, 1 m, 3 m), (1 m, 3 m, 3 m), (1 m, 5 m, 3 m), (1 m, 7 m, 3 m), (3 m, 1 m, 3 m), (3 m, 3 m, 3 m), (3 m, 5 m, 3 m), and (3 m, 7 m, 3 m), as shown in Figure 3.6. In the

analysis, the optical receiver was placed 1 m above the floor, which represents the communication floor as shown Figure 3.6.

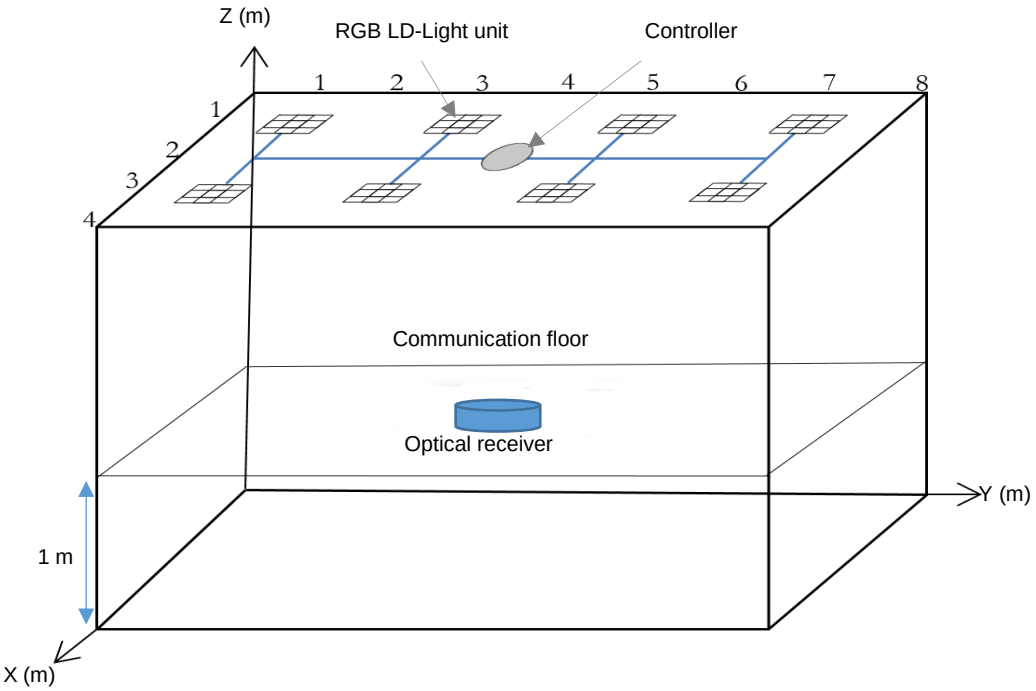

Figure 3-6 : VLC system room.

3.8.1 VLC system with single wide FOV receiver

The single photodetector receiver was used with FOV = 90^{o} and photosensitive area of 1 cm^{2} with a responsivity of 0.4 A/W. The wide FOV receiver is the most basic receiver configuration and has been widely investigated. Figure 3.7 shows the impulse responses of the VLC system with the wide FOV when the optical receiver was located at the room center (2 m, 4 m, 1 m), which represent the weakest location on the communication floor as the distance between the transmitters and the receivers becomes maximum at this location.

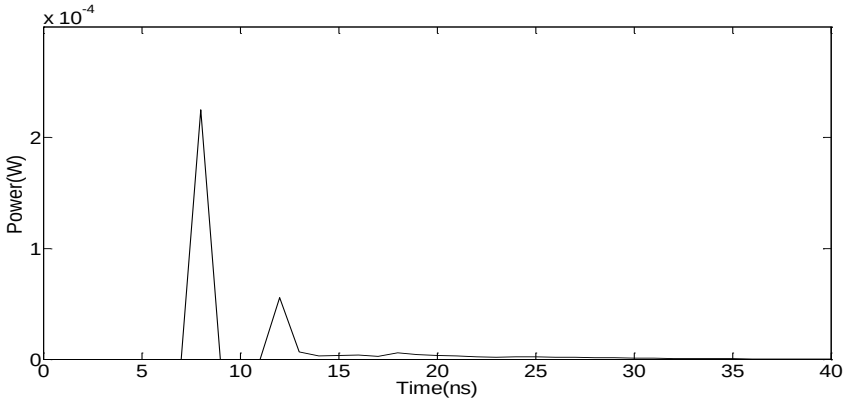

Figure 3-7 ': Impulse response of the VLC system with the wide FOV receiver when the optical receiver was located at room centre (2 m, 4 m, 1 m).

Figure 3.8 presents the VLC system delay spread associated with the wide FOV. The results were obtained when the mobile user was moving along the y-axis and at x = 1 m and x = 2m.

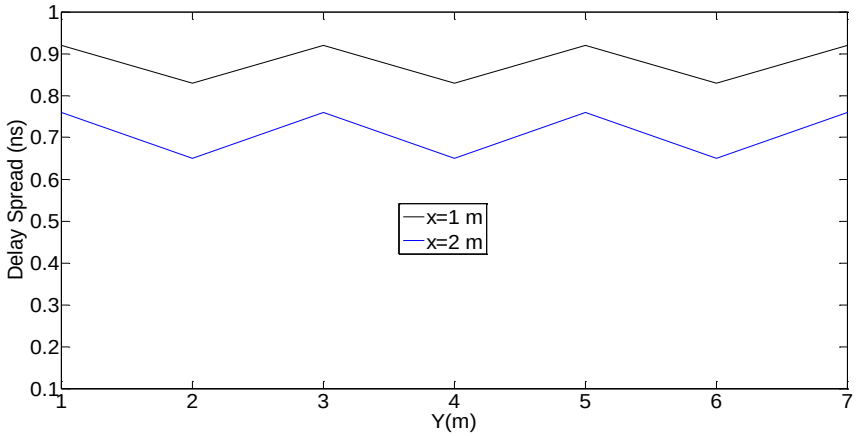

Figure 3-8: Delay spread of the VLC system with the wide FOV when the mobile user was moving along the y-axis and at x = 1 m and x = 2 m.

The SNR of the VLC system with the wide FOV receiver is shown in Figure 3.9. The results were obtained when the mobile user was moving along the y-axis and at x = 1 m and x = 2 m and when the system was operating at a data rate 50 Mb/s.

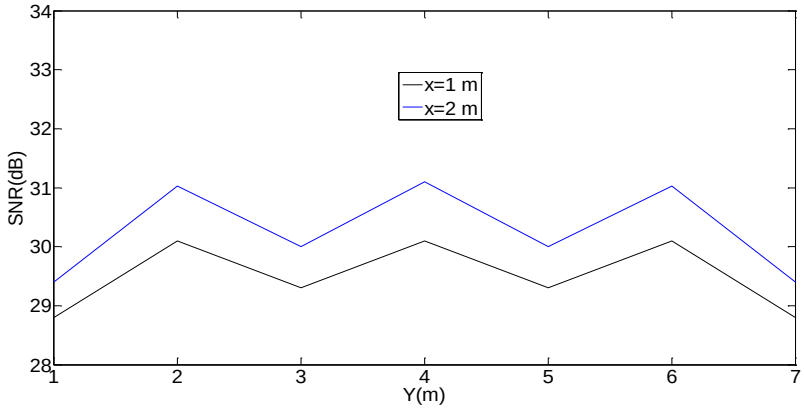

Figure 3-9 : SNR of the VLC system associated with the wide FOV when the mobile user was moving along the y-axis and at x = 1 m and x = 2m and when the system was operating at 50 Mb/s.

3.8.2 VLC system with the ADR

The ADR is a group of narrow FOV detectors pointed in different directions as shown in Figure 3.10. The ADR consists of three branches with

photodetectors that have a responsivity of 0.4 A/W each. The ADR uses a photodetector area of 4 mm^2. The ADR was always placed on the communication floor. The direction of each branch in the ADR is defined by two angles: the azimuth angle (*Az*) and the elevation angle (*El*). The *Az* of the three detectors were set at 0º, 180º and 0º, and the El for the three branches were fixed at 90º, 60º and 60º. The corresponding FOVs were fixed to 30º, 25º and 25º. The photocurrents received in each branch can be amplified separately and can be processed using different methods, such as selection combining (SC), equal gain combining (EGC) or maximum ratio combining (MRC) [91]. The MRC approach was used to obtain the result of the VLC system with the ADR.

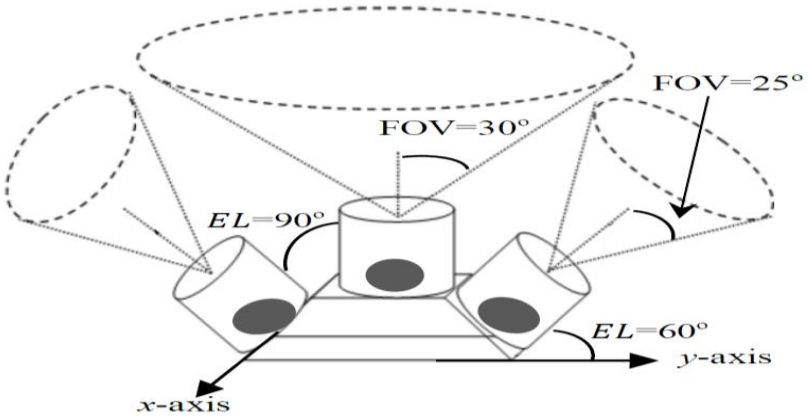

Figure 3-10 : Configuration of the ADR.

Figure 3.11 shows the impulse responses of the VLC system with the ADR when the optical receiver was located at the room center (2 m, 4 m, 1 m), which represent the weakest location on the communication floor as the distance between the transmitters and the receivers becomes maximum at this location.

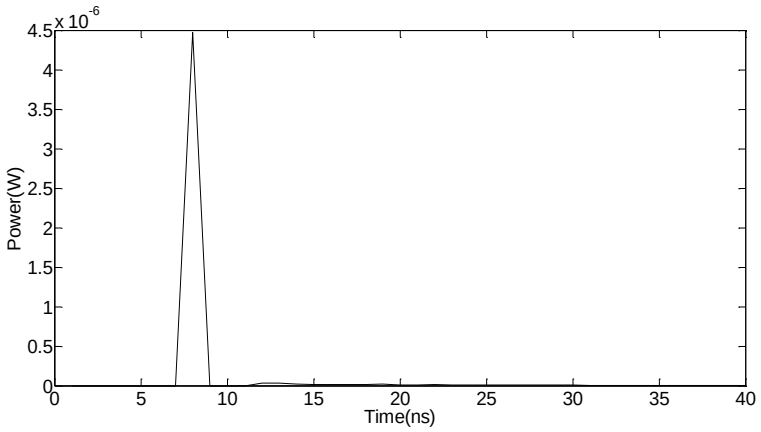

Figure 3-11 : Impulse response of the VLC system with the ADR when the optical receiver was located at the room centre.

Figure 3.12 shows the VLC system delay spread associated with the ADR. The results were obtained when the mobile user was moving along the y-axis and at x = 1 m and x = 2m.

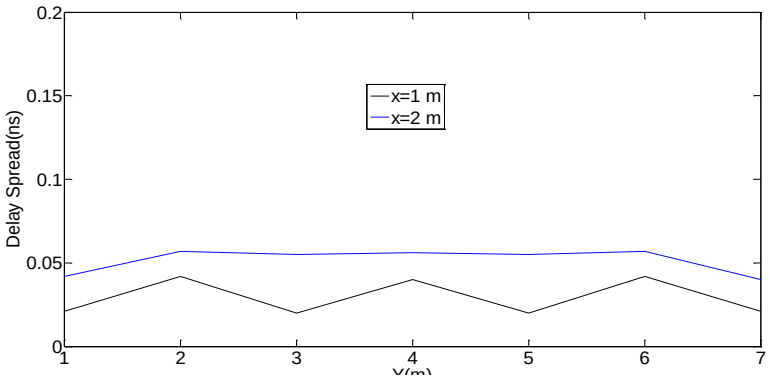

Figure 3-12 : Delay spread of the VLC system with the ADR when the mobile user was moving along the y-axis and at x = 1 m and x = 2 m.

The SNR of the VLC system with the ADR is shown in Figure 3.13. The results were obtained when the mobile user was moving along the y-axis and at x = 1 m and x = 2 m and when the system was operating at a data rate 50 Mb/s.

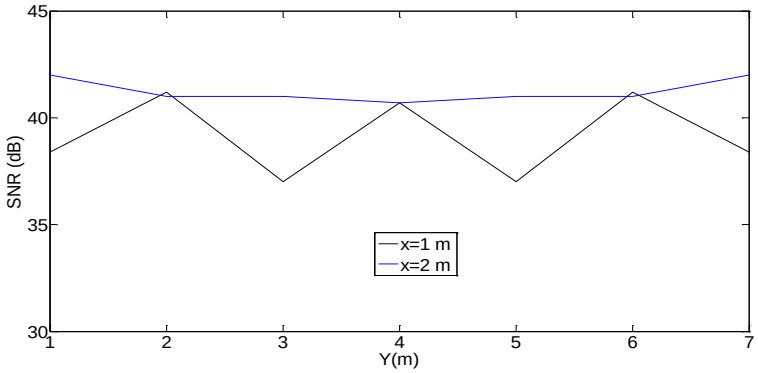

Figure 3-13 : SNR of the VLC system associated with the wide FOV when the mobile user was moving along the y-axis and at x = 1 m and x = 2m and when the system was operating at 50 Mb/s.

3.8.3 VLC system with imaging receiver

In the imaging receiver, all photodetectors were laid out in a single detector segmented into *J* equal-sized rectangular-shaped elements with no gaps between them. The area of each pixel was equal to the area of the photodetector divided by the number of pixels. The imaging receiver has 50 pixels. A lens was used as a concentrator to collect and concentrate the light

from a large area down to a smaller detector area as shown in Figure 3.14. The lens used was that in [103]. The entrance area of the concentrator was $A = \frac{9\pi}{4}$ cm^2 with exit area $A' = \frac{Asin^2(\psi)}{N^2}$, where N is the refractive index (N = 1.7) and ψ is the acceptance angle of the concentrator (ψ < 90^o). The acceptance angle of the concentrated (ψ) was chosen as 65^o so that the imaging receiver viewed the whole ceiling when it was located at the centre of the room. In addition, the size of the detector array was selected equal to the exit area of the concentrator. Therefore, the photosensitive area of the detector used in this work was 2 cm^2 (1 cm along the *x*-axis and 2 cm along the *y*-axis) and the area of each pixel was 4 mm^2. Each pixel in the imaging receiver could amplify the photocurrents received separately (Figure 3.14). The SC approach was used to obtain the result of the VLC system with the imaging receiver.

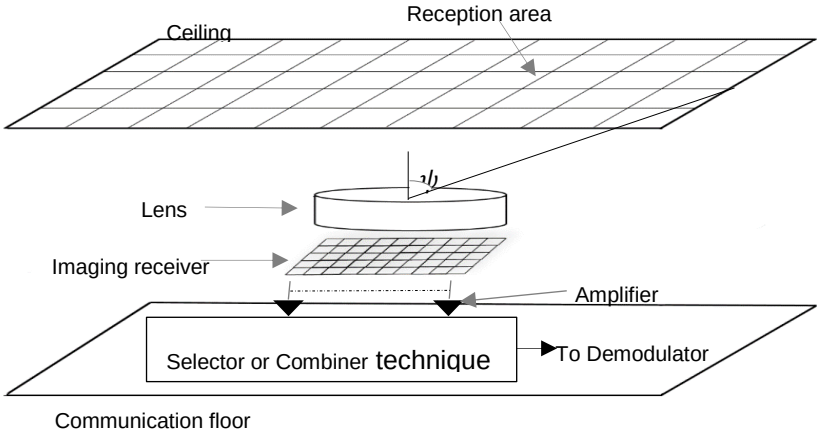

Figure 3-14 : Imaging receiver physical structure.

The impulse responses of the VLC system with the imaging receiver at the centre of the room, (2 m, 4 m, 1 m), which represents the worst case scenario (maximum path loss and minimum between the transmitters and the receiver), is depicted in Figure 3.15.

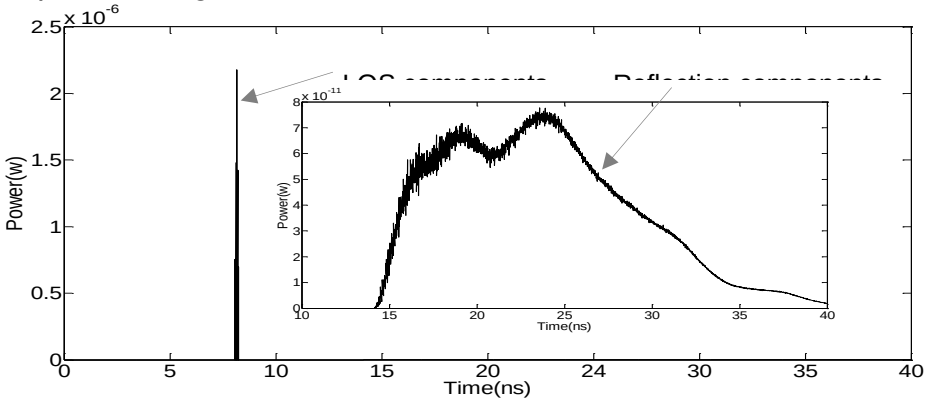

Figure 3-15 : Impulse response of the VLC system with the imaging receiver at the room centre.

Figure 3.16 shows the delay spread of the VLC system with the imaging receiver when the receiver moves along the *y*-axis and at x = 1 m and *x* = 2 m.

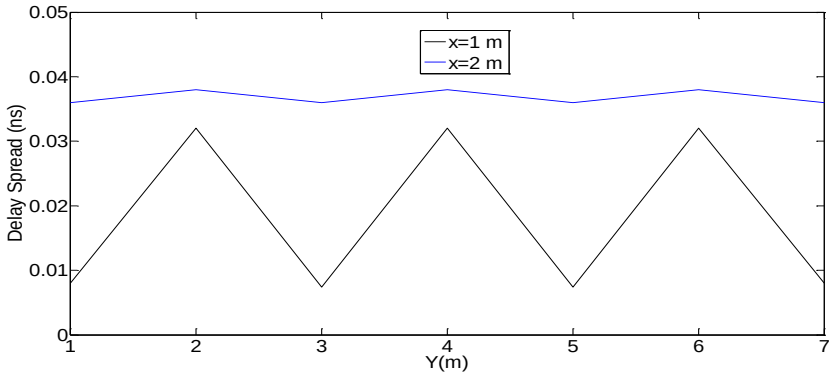

Figure 3-16 : Delay spread of the VLC system with the imaging receiver when the mobile user was moving along the y-axis and at x = 1 m and x = 2 m.

The SNR of the VLC system with the imaging receiver is shown in Figure 3.17. The results were obtained when the mobile user was moving along the y-axis and at x = 1 m and x = 2 m and when the system was operating at a data rate 30 Mb/s.

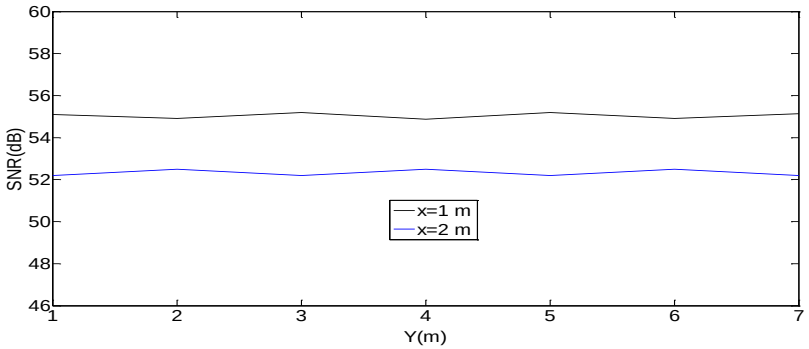

Figure 3-17 : SNR of the VLC system associated with the imaging receiver when the mobile user was moving along the y-axis and at x = 1 m and x = 2m and when the system was operating at 30 Mb/s.

3.9 Simulation Setup for the Proposed VLC Systems

3.9.1 Rooms setup

Two room configurations were used in the analysis. An empty room that has neither doors nor windows and a realistic room that has a door, windows, bookshelves and physical partitions as shown in Figure 3.18 (a) and (b), respectively. The dimensions of the empty room and the realistic room were 4 m × 8 m × 3 m (width × length × height) with reflection coefficients of 0.3 for

the floor and 0.8 for the ceiling and walls [5]. The realistic room, which represented a small office, has a door, three large windows, bookshelves, furniture, chairs, desks, tables and mini cubicle offices as shown in Figure 3.18 (b). The reflection coefficients of the door and three windows were set to zero, which means that they reflect no signals.

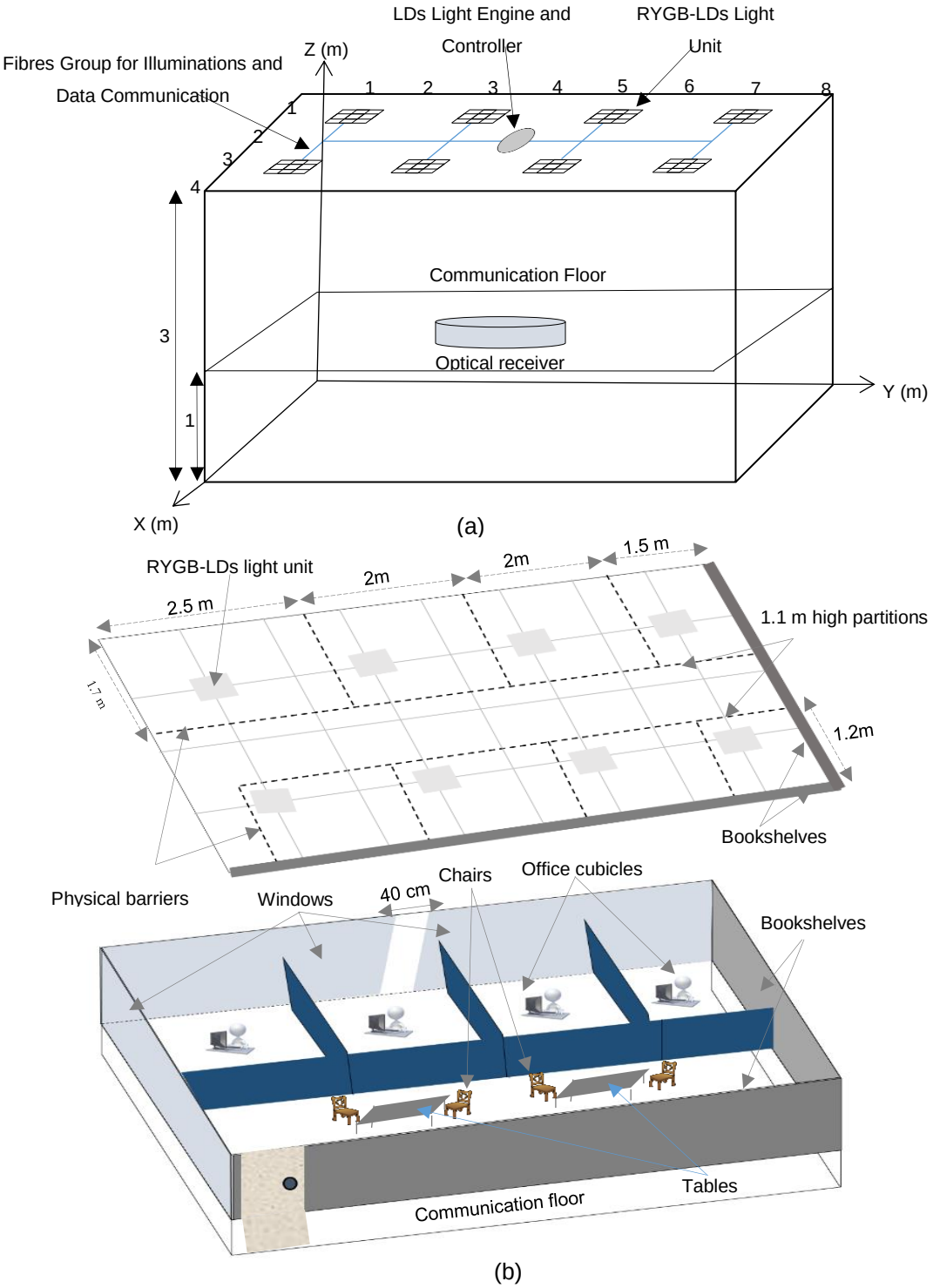

Figure 3.18:: An empty room and (b) a realistic room.

The two walls (x = 4 m and y = 8 m) in the realistic room are covered with bookshelves and filling cabinets (see Figure 3.18 (b)) and have a 0.4 reflectivity [109]. The mini cubicle office partitions were assumed to either absorb or block the signal. Furthermore, the reflection coefficients of the desks, chairs and tables inside realisitc room were set to 0.3 (similar to the roof). The physical partitions and low reflective objects in the realisitc room created shadowing, which leads to increased complexity in the realistic room. The walls, ceiling and floor were modelled as Lambertian reflectors, where experimental measurements have shown that plaster walls are roughly Lambertian reflectors [5]. A ray tracing algorithm was used to model the reflections; thus, the empty room and the realistic room were divided into a number of equal square-shaped surface elements with an area of d_A and reflection coefficient of ρ. Each surface element was treated as Lambertian source with n = 1, where n is the Lambertain emission order. To obtain results with high resolution, the size of the surface element should be very small, but the computation time increases exponentially. Thus, to keep computations within a reasonable time, a 5 cm × 5 cm size was chosen for the surface element in the first order reflections and 20 cm × 20 cm size for second order reflections [69], [110].

3.9.2 Laser diodes illumination system design

In this thesis, LDs were used rather than LEDs to achieve multi-gigabit data rates while employing a simple modulation technique (OOK). LDs are proposed to replace LEDs because of more efficiency in illumination and communication [35]. In addition, LDs have linear characteristics compared with LEDs (the input current behaves linear with the light output as shown in Figure 3.19) [111].

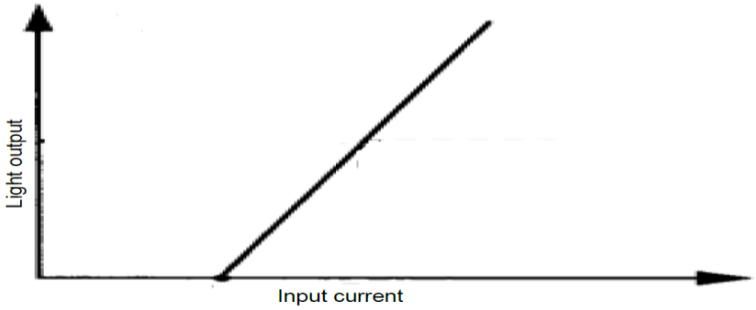

Figure 3.19: Output Characteristic of the LD [111].

Recent research has shown that LDs are much brighter than LEDs and have output powers (several watts) more than LEDs, which leads to high lumen output [112]. A prototype from Sandia lab showed that by using four colour laser sources it could provide a practical white light illumination source [113]. In their experiment, four laser diodes were used (red, green, yellow and blue) to generate white light that was similar to that from other light sources, such as incandescent lights and white LEDs. Lasers were not expected to be ideal light sources because of their extremely narrow line-width and extremely narrow spot size. However, the results from using four-colour laser sources have shown experimentally that the colour rendering quality of the white light is good, and this paved the way for serious consideration of the use of lasers in solid state lighting [113]. One of the main potential issues associated with using laser lighting is that lasers can be dangerous to human eyes. Therefore, it should be noted that while the original sources indeed have laser source properties (colours red, green, yellow and blue), once they have been combined (using chromatic beam-combiners) and had the beam scattered and diffused to reduce speckle then produce white light [114], [115].

We used the same specifications of the red, yellow, green and blue (RYGB) LDs that were used in [113]. Figure 3.20 shows the architecture of the LD light units, where the light from four lasers (i.e., RYGB) is combined using beam combiners, then passes through multiple ground glass diffusers to reduce speckle before illuminating the room.

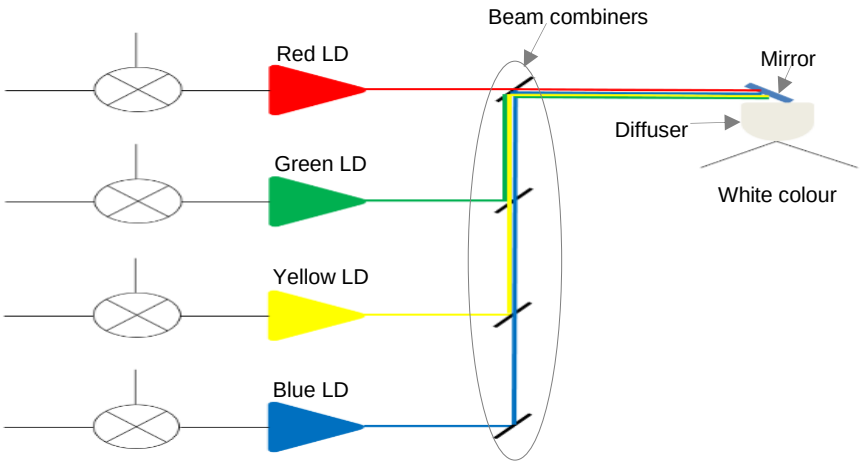

Figure 3.20: Architecture of RYGB-LD white light.

In our simulation, many RYGB LDs-light units were used for illumination and were installed on the ceiling (along the *x-y* axis) of the room (3 m above the floor). In addition, the RYGB LDs-light units were distributed on the ceiling to achieve an acceptable illumination level in the room, which ensures the ISO and European illumination requirements were met [108]. Each RYGB LDs-light unit had many RYGB LDs (3 × 3). Due to using a diffuser, the output of the RYGB LD was assumed to have a Lambertian radiation pattern. Therefore, the LOS illumination can be obtained at a point (x, y) as [94], [96]:

$$E_{LOS} = \frac{I\,(0)\; cos^{n}(\theta)\cos(\Upsilon)}{R_1^2} \tag{3.22}$$

where $I(0)$ is the centre luminous intensity of the LD, θ is the irradiance angle, R_1 is the distance between the LD and any point in the floor, Υ is the angle of incidence and n is the Lambertion emission order as defend in [12]:

$$n = -\frac{ln(2)}{ln\left(cos\left(\Phi_{\frac{1}{2}}\right)\right)} \tag{3.23}$$

where $\Phi_{\frac{1}{2}}$ is the semi angle at half power of the LD. The first reflection of the illumination can be given as below [75]:

$$E_{1^{st}} = \frac{I(0)cos^{n}(\theta)\cos(\Upsilon)\cos(\alpha)\cos(\varphi)\,d_{A1}\,\rho_1}{2\pi^2 R_1^2 R_2^2} \tag{3.24}$$

where R_1 is the distance between the LD and the surface element, R_2 is the distance from the surface element to the floor, d_{A1} is the size of the surface element in the first reflection, ρ_1 is the reflection coefficient in the first reflection, α is the irradiance angle for the surface element and φ is the incidence angle for the surface elements. Consequently, the second reflection of the illumination can be expressed as [75]:

$$E_{2^{nd}} = \frac{I(0)cos^{n}(\theta)\cos(\Upsilon)\cos(\alpha)\cos(\varphi)\cos(\Phi)\cos(\beta)\;d_{A1}\,d_{A2}\,\rho_1\,\rho_2}{2\pi^2 R_1^2 R_2^2 R_3^2} \tag{3.25}$$

where R_1 is the distance between the LD and the first surface element, R_2 is the distance from the first surface element to the second surface element, R_3 is the distance between the second surface element and the floor, d_{A2} is the size

of the surface element in the second reflection, ρ_2 is the reflection coefficient in the second reflection, Φ is the irradiance angle for the second surface element and β is the incidence angle for the second surface elements. Thus, the illumination level at any point in the floor is equal to the summation of the E_{LOS}, $E_{1^{st}}$ and $E_{2^{nd}}$.

3.10 Summary

The performance of the indoor VLC system can be evaluated by modelling the indoor VLC channel. This chapter has provided the propagation model that is used in this thesis. The ray tracing algorithm, calculations and received optical power were explained and evaluated. The simulation was done with the use of Matlab. In this chapter, the traditional VLC system was studied and evaluated. In addition, the results of the IROW were verified as can be seen in Appendix A. A very good match was observed between the results of the author's simulation and other researchers' work. This gives confidence in the capability of the author's simulator to assess new VLC systems.

4. Computer Generated Holograms for High Data Rate Indoor VLC System

4.1 Introduction

In the indoor VLC systems, many transmitters (LEDs or LDs) with broad beams are employed to obtain an acceptable level of lighting in a given room. Thus, the channel in indoor VLC systems includes many LOS components that arrive at an optical receiver with different delays, and consequently induce ISI at a high data rate. In addition, multipath propagation results in optical signals reaching an optical receiver through reflections from reflective surfaces of a room leading to pulse spreading and significant ISI. In this chapter, we propose, design and evaluate three indoor VLC systems based on computer generated holograms (CGHs). Each transmitter is followed by the CGH, and this CGH is utilized to direct part of the total power from the best transmitter and focus it to a specific area on the communication floor. This leads to reduction in ISI and increasing in the received optical power, which leads to higher data rates with a reliable connection.

CGHs are widely used in optical wireless communication systems. In IR systems, the CGHs has been used to optimize the distribution of the diffusing spots, which leads to improving the received optical power [95], [116], [76], [117]. In VLC systems, the CGHs has been utilized to direct a part of the total optical power of the best transmitter and direct it to a specific area on the communication floor, which leads to improve the performance of the system and increase the data rate [77], [78], [79]. More enhancement in the performance of the optical wireless communication systems can be obtained with optical beam steering technique. In the optical beam steering technique, the optical power is directed to the location of the optical receiver. This leads to improve the received optical power and increase the data rates. Optical wireless energy transmission using optical beam steering and beam forming

with a spatial light modulator (SLM) has demonstrated in [118], [119]. They focused light on the desired target using optical beam steering and beam forming to transfer optical wireless energy. An indoor optical wireless communications link was designed and demonstrated to carry of a 400 Gb/s by using optical beam steering [120]. The beam steering technique can be used as a solution to reduce the impact of the mobility and the orientation of the optical receiver [121]. In [77] and [78] the CGHs was used to generate one beam and steer it to the optical receiver and this leads to achieve a data rate of 20 Gb/s and 25 Gb/s, respectively.

In this chapter, three systems based on the CGHs are proposed in this chapter, which are single beam static CGH-VLC system, static CGH-VLC system and adaptive CGH-VLC system. In the first system (single beam static CGH-VLC system), the CGH is used to produce one fixed broad beam from the best light unit and focus it to a specific area on the communication floor. In the second system (static CGH-VLC system), the CGH generates 100 beams (all these beams carry same data) from the best transmitter and directs these beams to an area of 2 m × 2 m on the communication floor. In the third system (adaptive CGH-VLC system), the CGH is used to generate eight beams from the best transmitter and steer these beams to the receiver's location. In addition, each one of these eight beams carries a different data stream. Whereas in the first and the second systems a single photodetector is used (added simplicity), an imaging receiver is used in the third one to obtain spatial multiplexing. We consider the lighting constraints where illumination should be at acceptable level and consider diffusing reflections (up to second order) to find the maximum data rate that can be offered by each system. Moreover, due to the fact that each beam in the adaptive CGH-VLC system conveys a different data stream, co-channel interference (CCI) between beams is taken into account. We evaluate our proposed systems in two different indoor environments: an empty room and a realistic room using simple OOK modulation.

4.2 Simulation Setup

4.2.1 Rooms setup

In this Chapter, we used two rooms an empty room (room A) and a realistic room (room B) and we used the ray tracing algorithm to model the indoor channel of VLC systems as described in Chapter 3.

In this Chapter, eight RYGB LDs-light units were used for illumination and were installed on the ceiling (along the *x-y* axis) of the room (3 m above the floor) as shown in Figures 4.1 (a) and (b). In addition, the coordinates of the RYGB-LDs light units were (1 m, 1 m, 3 m), (1 m, 3 m, 3 m), (1 m, 5 m, 3 m), (1 m, 7 m, 3 m), (3 m, 1 m, 3 m), (3 m, 3 m, 3 m), (3 m, 5 m, 3 m), and (3 m, 7 m, 3 m) to achieve an acceptable illumination level in the room, which is not less than 300 lx.

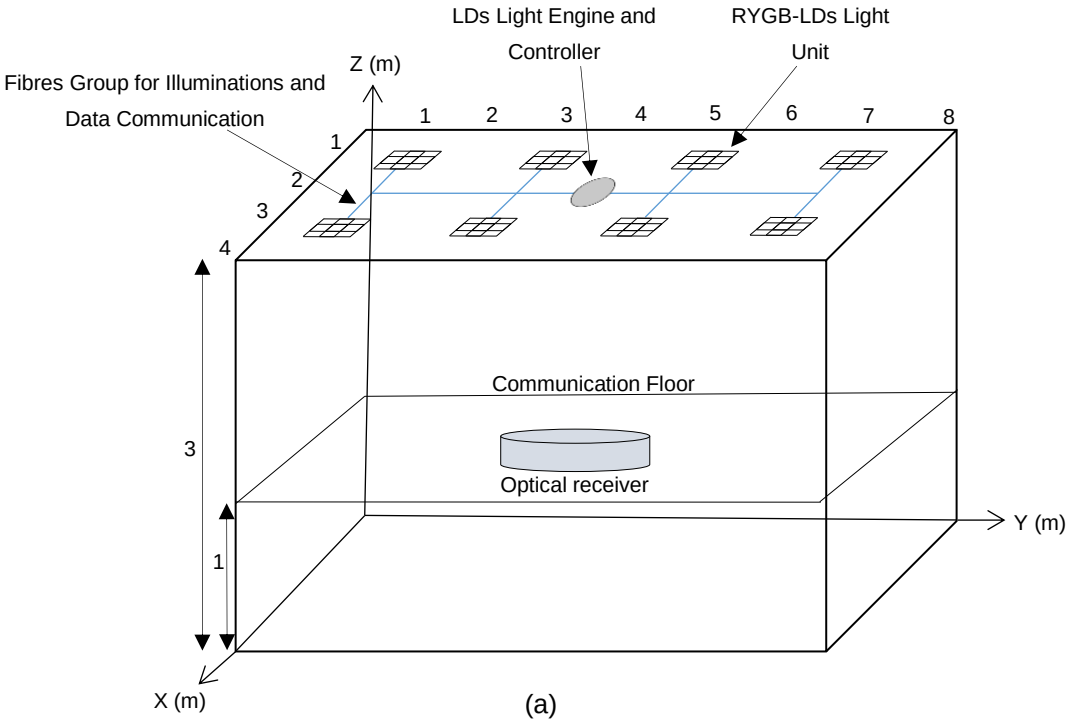

(a)

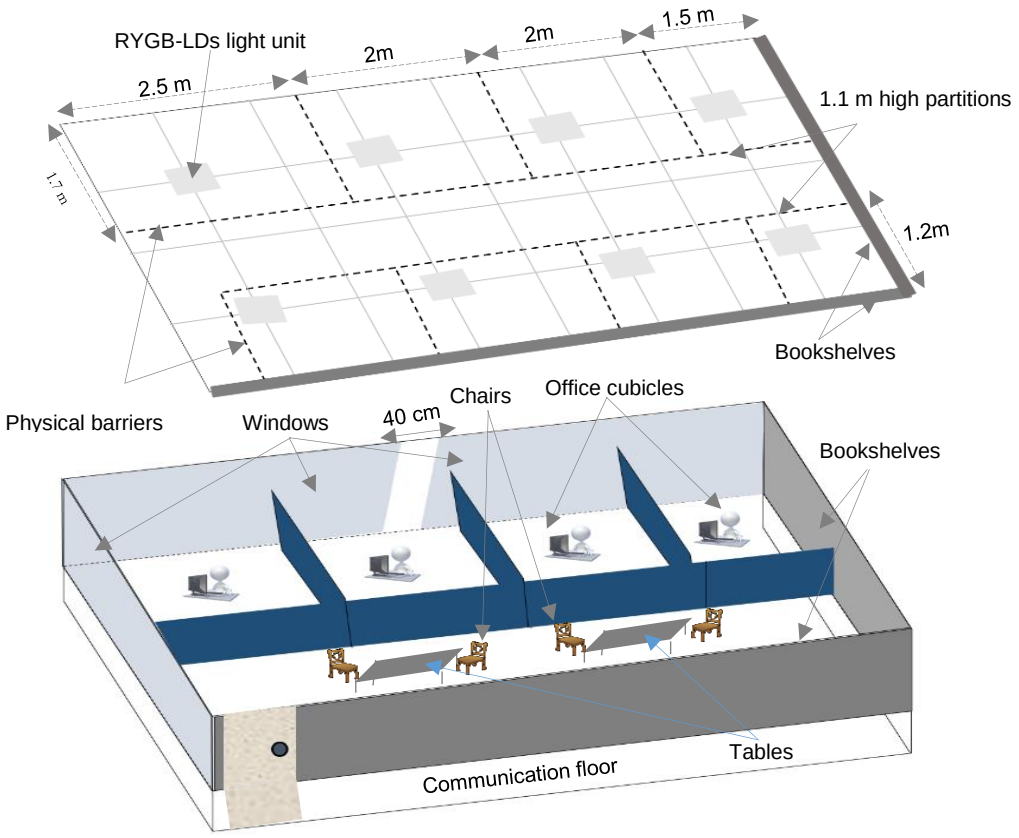

(b)

Figure 4.1: An empty room (room A) and (b) a realistic room (room B).

4.2.1 Receivers configuration

Two receivers were used in this chapter: a single photodetector receiver and an imaging receiver. The single photodetector receiver was used with single beam static CGH-VLC system and static CGH-VLC system, which is the most basic receiver configuration and has been widely investigated. The photosensitive area of the single photodetector was chosen to be 0.5 mm^2 to decrease the internal capacitance of the photodetector and enable the photodetector to operate at high data rates while collecting significant optical power as shown in the results section.

The speed of the photodetector is a measure of how fast the generated carriers are extracted to an external circuit as output current. This expresses as rise time or cut-off frequency. Two factors are effect on the rise time, which are time constant and carrier transient time. The time constant depends on the

internal capacitor of the photodetector. This capacitor is proportional to the photosensitive area of the photodetector and can be reduced by reduce the area of the photodetector. The carrier transient time is the time required to the carriers travel in the depletion layer. This time depends on the width of the depletion layer and can be reduced by short the distance travelled by the carriers or increase the reverse voltage of the photodetector. In this thesis, we neglected the carrier transient time. This is due to the carrier transient time is very small compared with the time constant and we used a photodetector has depletion layer with small width [122].

For a silicon photodetector, the bandwidth of the single photodetector receiver given as [122]:

$$BW = \frac{1}{2\,\pi\,R_l\,C_d} \tag{4.1}$$

where R_l is the load resistor and C_d is the photodetector's capacitance which is proportional to the photosensitive area of the photodetector and can be given as [123]:

$$C_d = \frac{\varepsilon_0\,\varepsilon_r\,A}{w} \tag{4.2}$$

where A is the photodetector's area and w is the detector thickness (w = 100 μm). A value of R_l equal to 50 Ω leads to matching between the photodetector and the preamplifier [122]. Thus, the maximum band width of this photodetector is ~ 6.18 GHz, which can receive data at rates up to 8.83 Gb/s since the bandwidth needed is 0.7 times the bit rate for OOK modulation [100]. To reduce the multipath dispersion and pulse spread, a narrow FOV should be selected. However, this FOV should be chosen to ensure that the photodetector views at least one RYGB LDs-light unit at any location on the communication floor of the room. Therefore, the FOV of the single photodetector was selected to be equal to 40^{o}, which ensures that the receiver will see at least one RYGB LDs-light unit when it is placed at the room centre (2 m, 4 m, 1 m) as the distance between the transmitters and the receiver become maximum at this location.

An imaging receiver was used in the adaptive CGH-VLC system rather than the single receiver to achieve spatial multiplexing. The main advantages of using an imaging receiver are: 1) one concentrator is used for all photodetectors, which reduces the size and the cost of the receiver and 2) the ability to realize a large number of pixels in a single planner array of photodetectors [103]. In addition, the imaging receiver in the VLC system mitigates the delay spread because each pixel in the imaging receiver receives a limited range of rays (each pixel has a narrow FOV), which leads to an increase in the channel bandwidth and increase in the SNR [124]. In the imaging receiver, all photodetectors were laid out as a single detector segmented into *J* equal-sized rectangular-shaped elements with no gaps between them. Therefore, the signal fell on no more than four pixels [107]. Thus, the area of each pixel was equal to the area of the photodetector divided by the number of pixels. The imaging receiver has 288 (12 × 24) pixels. In addition, the lens was used as a concentrator to collect and concentrate the light from a large area down to a smaller detector area as shown in Figure 4.2. In our analysis, we employed the lens that was used in [103]. The diameter of the entrance aperture of the lens is equal to 3 cm; thus, the entrance area of the lens was $A = \frac{9\pi}{4}$ cm^2 with exit area $A' = \frac{Asin^2(\psi)}{N^2}$, where N is the refractive index (N = 1.7) and ψ is the acceptance angle of the lens (ψ < 90^o).

The transmission factor of the imaging concentrator is given by [103], [125], [126]:

$$T_c(\delta) = -0.1982\delta^2 + 0.0425\delta + 0.8778 \quad (4.3)$$

where δ is the incidence angle measured in radians. The acceptance angle of the concentrator (ψ) was chosen as 65^o so that the imaging receiver viewed the whole ceiling when it was located at the centre of the room. In addition, the size of the detector array was selected equal to the exit area of the concentrator. Therefore, the photosensitive area of the detector used in this work was 2 cm^2 (1 cm along the *x*-axis and 2 cm along the *y*-axis) and the area of each pixel was 0.69 mm^2. Each pixel in the imaging receiver could amplify the photocurrents received separately (see Figure 4.2), thus different methods can be used for processing, such as select the best (SB), equal gain combining

(EGC) or maximum ratio combining (MRC) techniques [116], [103]. In our analysis, the single photodetector and the imaging receiver were placed 1 m above the floor, which represents the communication floor as shown in Figure 4.1 (a).

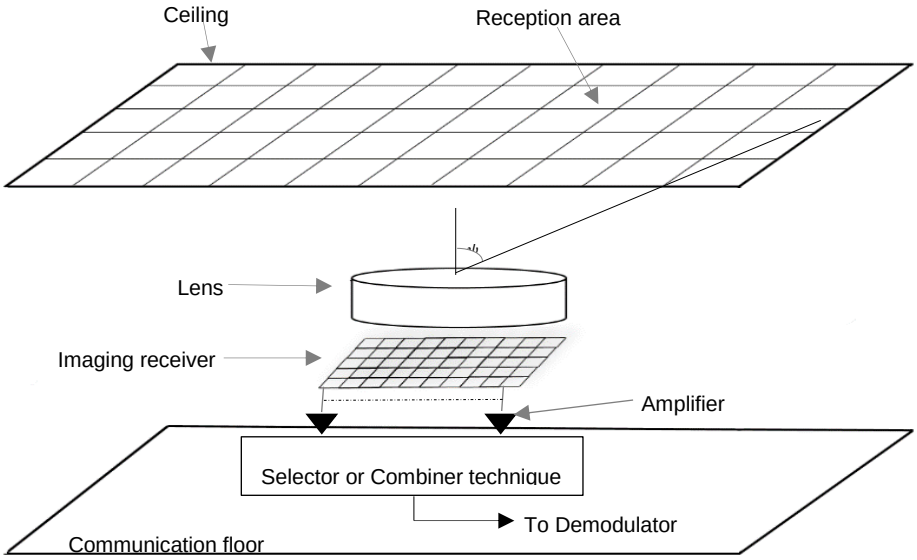

Figure 4.2: Imaging receiver physical structure.

The imaging receiver could see the whole ceiling when it was located at the room center; thus, the ceiling was divided into small divisions called reception areas, as shown in Figure 4.2. In our design, the ceiling was divided into 288 reception areas, and each reception area was cast onto a single pixel. The reception area was found (when the receiver was at the room center) based on the reception angles along the *x*-axis (α_x) and *y*-axis (α_y) directions with respect to the receiver's normal vector, see Figure 4.3.

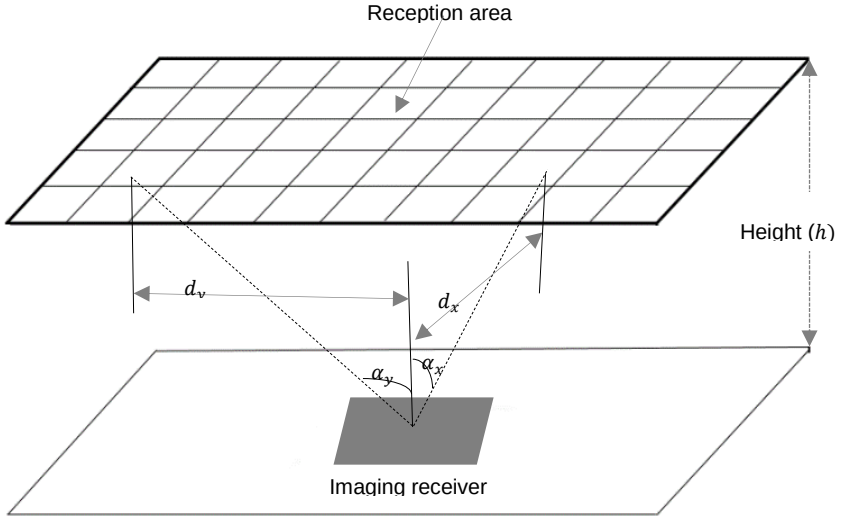

Figure 4.3: Reception areas associated with the pixels when the imaging receiver is located at the room centre (2 m, 4 m, 1 m).

The reception angles can be calculated as [127]:

$$\alpha_x = tan^{-1}\left(\frac{d_x}{h}\right) \text{ and } \alpha_y = tan^{-1}\left(\frac{d_y}{h}\right) \tag{4.4}$$

where d_x is the x-axis horizontal separation, d_y is the y-axis horizontal separation and h is the reception area height as shown in Figure 4.3. When the imaging receiver is located at the room center, all reception areas are located on the ceiling. However, when the imaging receiver moves along the *x*-axis and/or *y*-axis, some of the reception areas on the ceiling start to appear on the walls. Figure 4.4 shows that some of the reception areas start to appear on X-Z wall and Y-Z wall when the receiver is located at the room corner (1 m, 1 m, 1 m). Thus, when the receiver starts moving the new reception areas should be calculated with respect to the height of the center of the reception areas above the communication floor on the X-Z wall (Z_x) or on the Y-Z wall (Z_y) (see Figure 4.4) as [75]:

$$Z_x = \frac{X_r}{\tan(\alpha_x)} \text{ and } Z_y = \frac{Y_r}{\tan(\alpha_y)} \tag{4.5}$$

where X_r is the horizontal separation distance between the imaging receiver and the Y-Z wall and Y_r is the horizontal separation distance between the imaging receiver and the X-Z wall as shown in Figure 4.5.

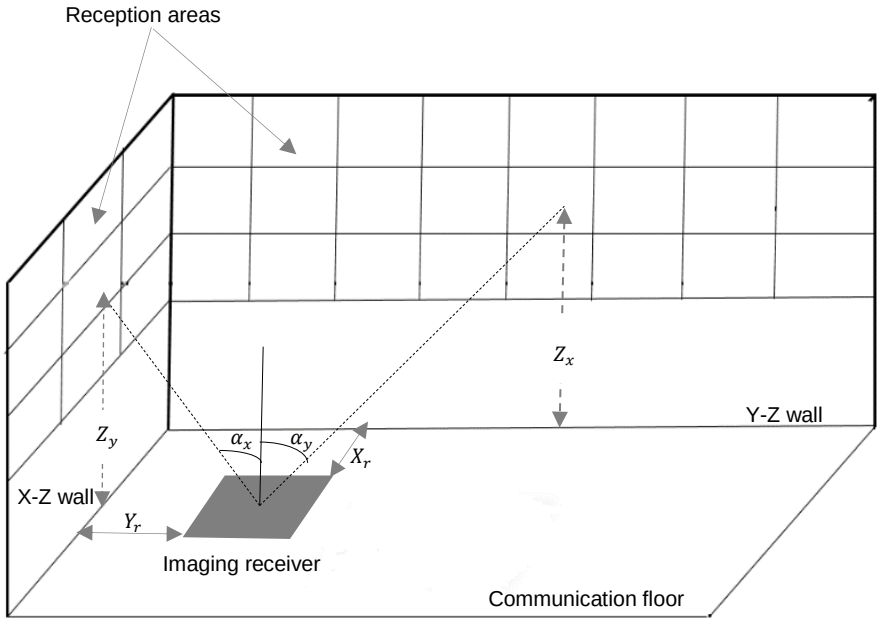

Figure 4.4: Reception areas associated with the pixels when the imaging receiver is located at the room corner (1 m, 1 m, 1 m).

Based on the area of the pixel, the maximum bandwidth of each pixel of the imaging receiver is ~ 4.48 GHz, which supports data rates up to 6.35 Gb/s.

4.3 CGH Design for Indoor VLC System

In VLC systems, many light units, which are spatially separated, are installed in a room ceiling to obtain the required illumination level. However, for a data communication, this means that many LOS components reach the optical receiver with different times of arrival, which leads to ISI at high data rates. Therefore, just one RYGB LDs-light unit is used to transmit a data for a given receiver position. This is the unit that has the best SNR for the given optical receiver location. However, this leads to decrease in the received optical power. Thus, each RYGB LDs light unit was followed by a CGH, which is an optical device that can be used to modulate the phase and the amplitude of the light on each pixel [119]. The CGH is utilized to direct part of the total power of the best RYGB LDs-light unit and focus it on a specific area on the communication floor of the room. In addition, use of the CGH leads to a reduction in multipath propagation.

The CGH can produce spots with any prescribed amplitude and phase distribution. Computing the CGH means the calculation of the complex transmittance of the CGH as given [109]:

$$H(u,v) = A(u,v)e^{j\Phi(u,v)} \tag{4.6}$$

here $A(u,v)$ is the amplitude distribution of the hologram, $\Phi(u,v)$ is the hologram's phase distribution and (u,v) are coordinates in frequency space. The CGH has the ability to modulate the amplitude and/or the phase of an incoming wavefront. The CGH is used to direct a part of the total power of the best light unit and focus it into a specific area. Thus, the hologram used modulates only the phase of the incoming wavefront, which makes the transmittance amplitude equal to unity. Diffraction theory is used to compute the distribution of the beams and this is encoded into a hologram [128] in which the phase of each pixel in the CGH will be optimized to obtain the desired far-field pattern. The hologram $H(u,v)$ is in the frequency domain and the location

of each pixel in the hologram is defined by the frequency coordinates u and v whereas the observed diffraction pattern (reconstruction far field pattern in the communication floor) is in the spatial domain. Therefore, there are two domains, the CGH domain and the far-field pattern domain, and a Fourier transform is used to establish the relationship between them as [129], [130]:

$$h(x,y) = \iint H(u,v)\, e^{-j2\pi(ux+vy)}\, dx\, dy \tag{4.7}$$

The hologram has an $M \times N$ array of rectangular cells and each cell has a size of R × S with complex transmittance value H_{kl}: $-M/2\ k \leq M/2$ and $-N/2\ \ l \leq N/2$ [109]. Consequently, the diffraction pattern is given as [129], [130]:

$$h(x,y) = RS\ sinc\left(R_x, S_y\right) \sum_{k=-\frac{M}{2}}^{\frac{M}{2}-1} \sum_{l=-\frac{N}{2}}^{\frac{N}{2}-1} H_{kl}\ e^{j2\pi(Rxk+Syl)} \tag{4.8}$$

Due to the finite resolution of the output device, the cost function (CF) was defined as the difference between the desired far-field pattern and the actual output pattern. Simulated annealing algorithm was used to optimize the output of the CGH where the phase of the CGH gradually changed to obtain the desired far-field pattern [131]. The distribution of the pattern in the far field is $f(x,y) = |f(x,y)|\, e^{j\Phi(x,y)}$. The target of the design is to obtain the distribution of the CGH $g(v,u)$ that generates a reconstruction $g(x,y)$ as close as possible to the desired distribution $f(x,y)$. The CF is a mean square error that corresponding to the difference between the normalized desired object energy $f''(x,y)$ and the scaled reconstruction energy of the kth iteration $g''(x,y)$ as [77]:

$$CF_k = \sqrt{\sum_{i=1}^{M}\sum_{j=1}^{N}(|f''(x,y)|^2 - |g''(x,y)|^2)^2} \tag{4.9}$$

4.4 Design of CGH-VLC Systems

4.4.1 Single beam static CGH-VLC system design

Only one RYGB LDs-light unit is utilized to transmit the data. Thus, select the best algorithm (SBA) was used to select the best (RYGB LDs-light unit) transmitter, which gives an optimum link between the transmitter and the receiver. The SBA can be used to find the optimum link according to the following steps:

1. The controller gives an ID to each RYGB LDs-light unit.
2. The controller activates one of the RYGB LDs-light units to send a pilot signal.
3. SNR is calculated at the receiver side.
4. The user transceiver sends (using an IR beam) a low data rate control feedback signal to inform the controller of the SNR associated with the first RYGB LDs-light unit. The design of IR uplink has been investigated in [132].
5. Repeat steps 2 to 4 for other RYGB LDs-light units.
6. The RYGB LDs-light unit that yields the best SNR is chosen by the controller.
7. The controller activates a silent mode for the remaining seven transmitters and keeps the best RYGB LDs-light unit ‘ON’ (in the communications sense) to send the information signal.

The SNR of each RYGB LDs-light unit relies on the distance between the RYGB LDs-light unit and the optical receiver. Thus, in some locations, two or more RYGB LDs-light units may have the same SNR. In this case, the controller selects one of them and discards the others. In addition, due to switching ON the RYGB LDs-light units individually, there was no interference between the signals transmitted from the RYGB LDs-light units. Thus, the SNR of each RYGB LDs-light unit was obtained without CCI.

In the single beam static CGH-VLC system, we used a static CGH in which the CGH generates one wide fixed beam without steering it towards the optical receiver. Therefore, the size of the beam should be selected to cover all possible locations of the optical receiver on the communication floor and the

amount of power used by this beam should not affect the illumination level. Although selecting a beam with a small size offers high received optical power, this leads to reduce the coverage area of the CGH and restrict the mobility of the user. On the other hand, a beam with a large size leads to increase the coverage area of the CGH, but this offers low received optical power. Thus, the optimum size of the beam should be selected. Due to the distribution of the RYGB LDs-light units on the ceiling of the room, the communication floor of the room was divided into eight small areas with an area of 2 m × 2 m each as shown in Figure 4.5. One RYGB LDs-light unit transmits the data for the given receiver location. The single beam static CGH generates one beam and focuses it on this small area (see Figure 4.5).

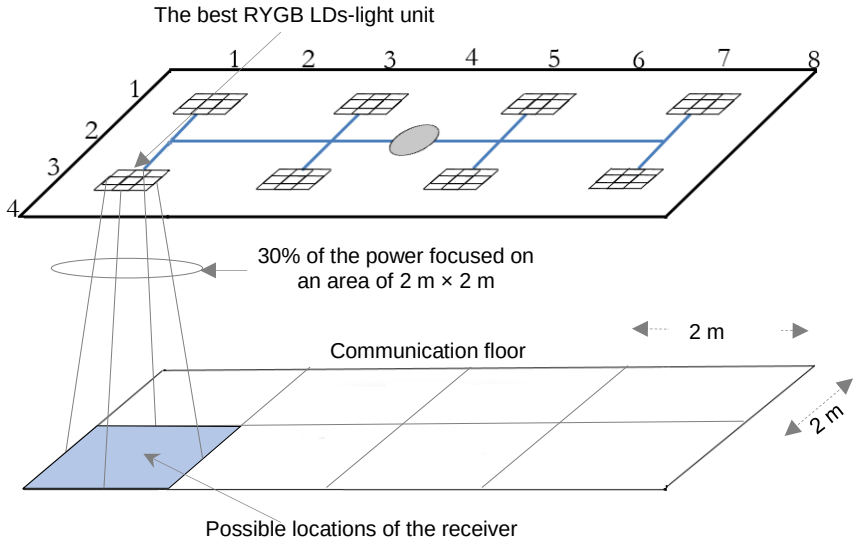

Figure 4.5: Size of the beam of the single beam statistic CGH-VLC system.

The illumination level in the room considered. Thus, to calculate the amount power that will be taken from the best light unit by the CGH without impact on the acceptable illumination level in the room, we investigated different values such as 20%, 30% and 40% of the total power of the best light unit, and we examined these values with considering the best light unit is located at one of the room' corners (i.e. the optical receiver placed at 1 m, 1 m, 1 m) as the lowest illumination occurs at the corners of the room. The results showed that 30% of the total power of the best light unit can be focused on the communication floor with a size of 2 m × 2 m without reducing the

illumination under the sufficient level (i.e. 300 lx [108]). Figure 4.6 illustrates the distribution of the illumination level on the communication floor of the room. It can be seen that without generate the beam the minimum lighting value is equal to 338 lx, which achieve the sufficient illumination in the room (i.e. more than 300 lx) while the minimum lighting levels when using 20%, 30% and 40% of the total power of the best light unit (i.e. the best light unit is the one that located at 1 m, 1 m, 1 m) are equal to 314 lx, 302 lx and 286 lx respectively. Thus, 30% of the total power of the best light unit is selected to keep the illumination at an acceptable level.

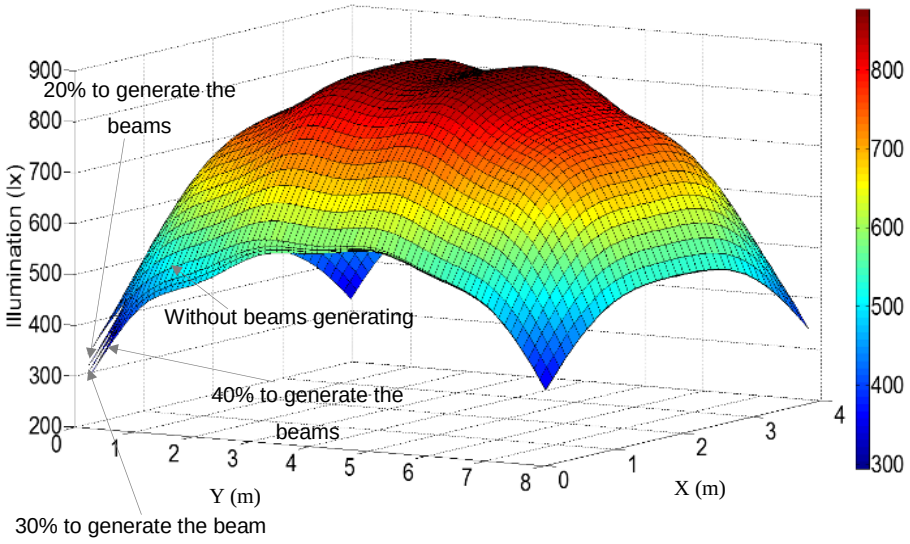

Figure 4.6: The distribution of illumination of the single beam static CGH-VLC system on the communication floor.

4.4.2 Static CGH-VLC system design

More enhancement in the performance of the indoor CGH-VLC system can be obtained when using the CGH to generate multiple beams and direct them to the receiver location. In the static CGH-VLC system, the CGH generates multiple fixed beams without beam steering towards the optical receiver. Therefore, the size and the number of the beams should be selected to cover all possible locations of the receiver on the communication floor and the amount of power used by these beams and their spatial organization should not affect the illumination level. The static CGH generates 100 (10 × 10) beams and focuses them on an area of 2 m × 2 m, where the receiver is placed as shown in Figure 4.7. The size of each beam should be selected to

increase the received optical power and improve the user mobility. For example, if the size of the beam is 20 cm, this will cover an area of 2 m × 2 m (2 m × 2 m/ 20 cm × 20 cm = 100). However, this will leave gaps between adjacent beams. Thus, a beam diameter of 30 cm is used to eliminate the gaps between adjacent beams. However, some of the beams (beams near to the walls) will hit the walls and increase diffusing reflections. It should be noted that all the beams generated by the static CGH carry the same data. In addition, the single photodetector was used with this system.

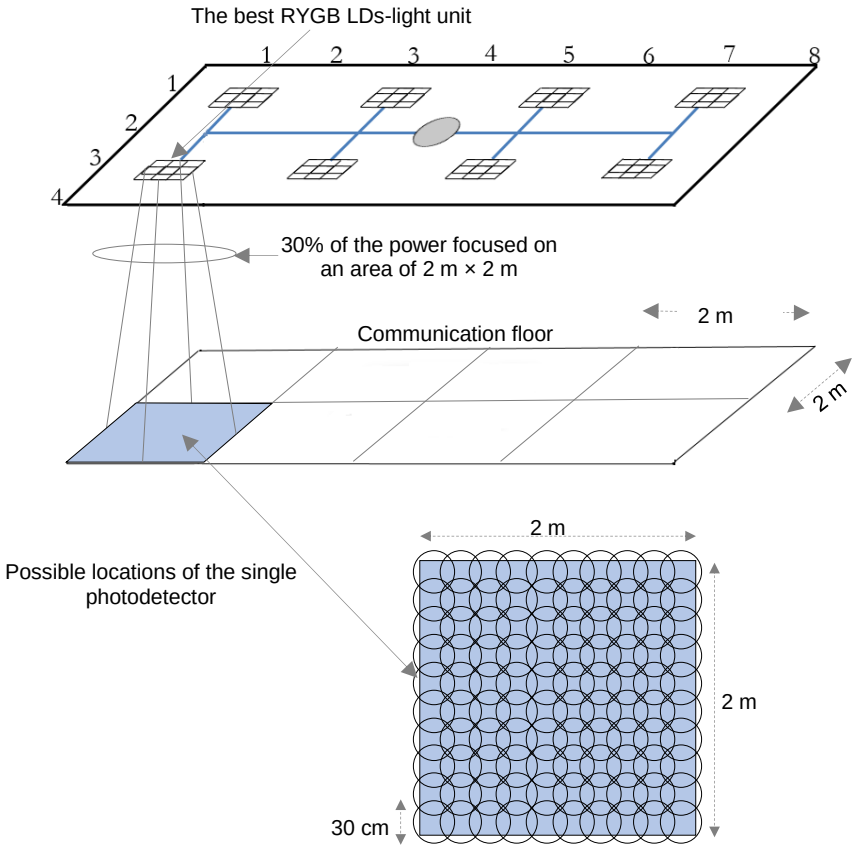

Figure 4.7: Configuration of the static CGH-VLC system.

In this system, we used the same algorithm that was presented in the single beam static CGH-VLC system to find the best transmitter.

4.4.3 Design of an adaptive CGH-VLC system

Although more complex, additional enhancements (such as increasing the received optical power and reduce the effect of ISI) in the indoor VLC system

can be obtained by steering multiple beams of light from the best RYGB LDs-light unit towards the optical receiver. Thus, in the adaptive CGH-VLC system, the CGH was used to generate multiple beams from the best RYGB LDs-light unit and direct these beams to the optical receiver (see Figure 4.8); hence, the exact location of the optical receiver should be obtained. We used the imaging receiver with the adaptive CGH-VLC system, which enables each beam from each RYGB LD in the best RYGB LDs-light unit to carry a different data stream, received by a different pixel. The effect of the CCI was taken into account in this system. The number of the optimum beams that should be generated by the CGH at a specific data rate will be explained later. Due to directing all beams towards the optical receiver, the CGH used only 20% of the total power from each RYGB LD in the best RYGB LDs-light unit to generate the beams. The 20% value was selected to ensure that the illumination level stayed at an acceptable level. The following algorithms were used to design the adaptive CGH-VLC system:

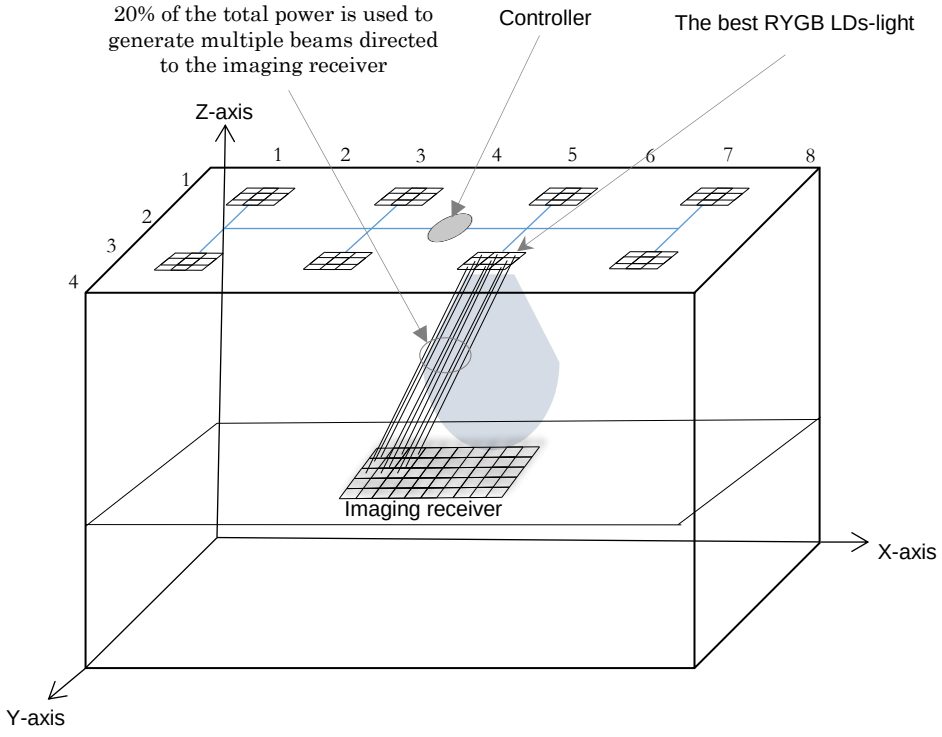

Figure 4.8: Configuration of the adaptive CGH-VLC system.

4.4.3.1 Select the best algorithm (SBA)

In this system, we used the same algorithm that was presented in the single beam static CGH-VLC system to find the best transmitter. However, here the SNR is estimated at each pixel of the imaging receiver and the controller selects the number of the pixel (the best pixel) that gives the best SNR at each step.

4.4.3.2 Position identification algorithm (PIA)

A PIA algorithm was introduced to identify the location of the optical receiver. Each RYGB LDs-light unit can find the location of the receiver via searching the area underneath it (2 m × 2 m), which reduces the time to find the receiver's location. The RYGB LDs-light unit that was chosen in the SBA initially produces a single beam using the CGH and scans it along a number of possible locations in its small area (2 m × 2 m) of the room to find the receiver location. The CGH can be used to change the intensity and the direction of the light beams adaptively, with low complexity [117]. Thus, the best RYGB LDs-light unit followed by the CGH can be used to find the receiver's location by generating a directional beam to scan possible locations of the receiver in the small area (2 m × 2 m). The locations of the generated beam can be altered by changing the transmission angles of the CGH along the *x*-axis (θ_x) and along the *y*-axis (θ_y) with respect to the transmitter's normal vector. We used a divide and conquer (D&C) algorithm to find the receiver's location. In this algorithm, the possible location areas were divided into four sub-divided areas, and in each area, the CGH produced a single beam and scanned it with a step angle (θ_{step}) along the *x*-axis and *y*-axis in the sub-divided area. The sub-divided area that had the best SNR was chosen as the new possible location area, and it was divided into another four sub-divisions. Eight iterations were carried out to find the exact location of the receiver. The PIA determined the receiver location according to the following steps:

1. Set up the initial parameters of the CGH in the best RYGB LDs-light unit to define the boundary scan of the small area (2 m × 2 m). These parameters were the transmission angles along the *x*-axis ($\theta_{x\text{-}start}$ to $\theta_{x\text{-}}$

$_{end}$) and the transmission angles along the *y*-axis ($\theta_{y\text{-}start}$ to $\theta_{y\text{-}end}$) with respect to the transmitter's normal vector. The transmission angles in the *xy*-axes are configured to vary between -26.6^o and 26.6^o, which covers the area of 2 m × 2 m along the *xy*-axes.

2. The scan area (2 m × 2 m) was divided into four sub-areas (quadrants) for the first iteration. The boundary angles associated with the first quadrant were $\theta_{x\text{-}start}$ to 0 and $\theta_{y\text{-}start}$ to 0; the second quadrant angles were $\theta_{x\text{-}start}$ to 0 and 0 to $\theta_{y\text{-}end}$; the third quadrant angles were 0 to $\theta_{x\text{-}end}$ and $\theta_{y\text{-}start}$ to 0 and the fourth quadrant angles were 0 to $\theta_{x\text{-}end}$ and 0 to $\theta_{y\text{-}end}$.
3. A single beam was generated and moved with a step size of 100 cm to scan the four quadrants.
4. The SNR was estimated at each step and the user transceiver sent a control feedback signal at a low data rate to inform the controller of the SNR associated with each step.
5. The controller compares the SNRs recorded with the associated transmission angles θ_x and θ_y that gave the maximum SNR.
6. The controller configured the parameters of the best quadrant for the next iteration and reduce the step size of the beam by a factor of two.
7. It repeats steps 4 to 6.
8. The iterations stop if the step size ≤ 1 cm.
9. The controller assigns the optimum location with coordinates (*x*, *y*, *z*) to the transmitter.

It should be noted that in the SBA and PIA, the CGH generated one beam to select the best RYGB LDs-light unit and to find the exact location of the optical receiver. Thus, the calculations of the above algorithms were based on the SNR.

The controller connecting all RYGB LDs-light units is used to accomplish the connection between transmitters and the optical receiver. Thus, it is proposed that the optical receiver re-evaluates its performance periodically at 1s intervals as a speed of 1 m/s is assumed of indoor pedestrians. Hence, if the performance changes compared to the previous state, the optical receiver informs the controller via the feedback signal to update the RYGB LDs-light

unit according to the SBA and PIA. If the time required to determine the value of each SNR in the SBA and PIA is equal to 1 ms, then the SBA training time is equal to 8 ms (8 RYGB LDs-light units × 1 ms) and the PIA requires 32 ms (8 iterations × 4 quadrants × 1 ms). Therefore, the adaptive CGH-VLC system can achieve 100% of the specified data rate when stationary and 96% in the case of a mobile user (i.e. 40 Gb/s for a stationary user and 38.4 Gb/s for a mobile user). It should be noted that users in an indoor environment, such as the one considered, are typically nomadic and therefore spend most of the time in one location, and as such achieve an average data rate near the maximum data rate supported.

4.4.3.3 Multiple beams generation technique

Once the exact location of the receiver is found by PIA, the CGH algorithm generates the optimum number of beams that achieves a strong communication link between the transmitter and the receiver. It should be noted that due to the fact that each RYGB LDs-light unit has 9 RYGB LDs, the optimum number of beams generated varies from one to nine as each beam carries a different data stream. Later we will find the optimum number of beams by considering CCI. As an example, a desired far-field image pattern is shown in Figure 4.9. To realize this far field pattern, the phase distribution of the CGH was gradually optimized by the simulated annealing algorithm (see Figure 4.10). Figure 4.10 illustrates three snapshots (iteration 1, 15 and 100) of the phase distribution of the hologram and the image of the far-field pattern. It can be seen that by increasing the number of iterations, the desired far-field image is improved. This is due to the error (cost function) reduction through the simulated annealing algorithm as shown in Figure 4.11. It should be noted that the optimization process is carried out before communication starts.

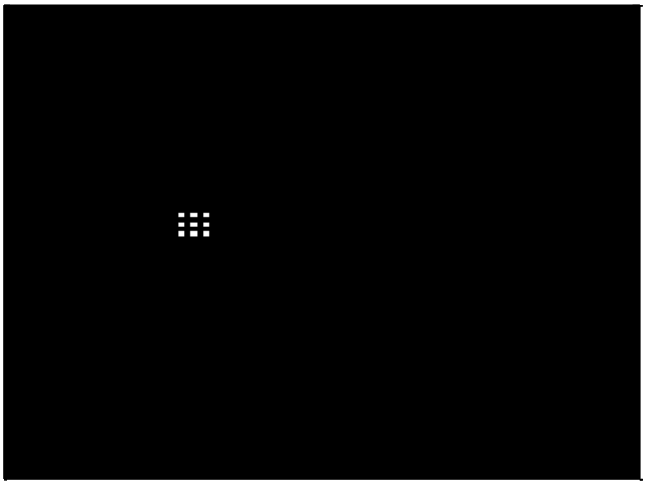

Figure 4.9: Desired beams in the far-field.

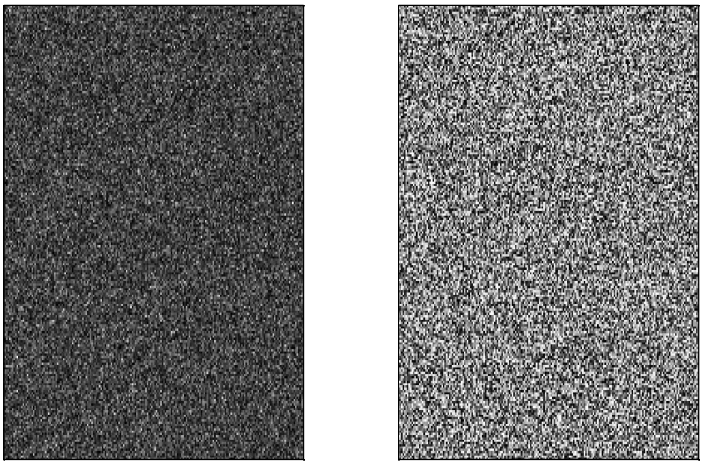

Iteration 1

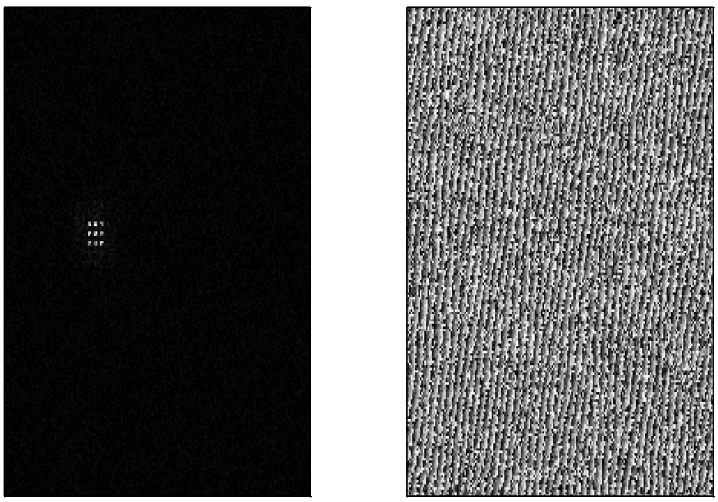

Iteration 15

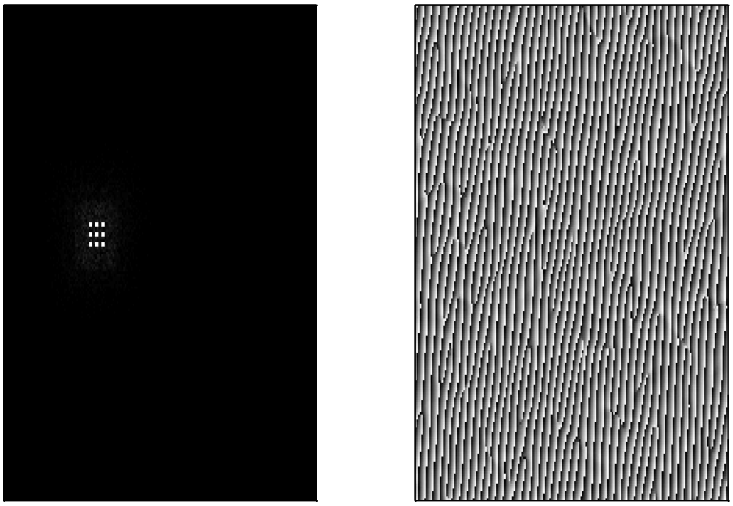

Iteration 100

Figure 4-10: Phase distribution of the CGH (right hand) and the actual output pattern (left hand).

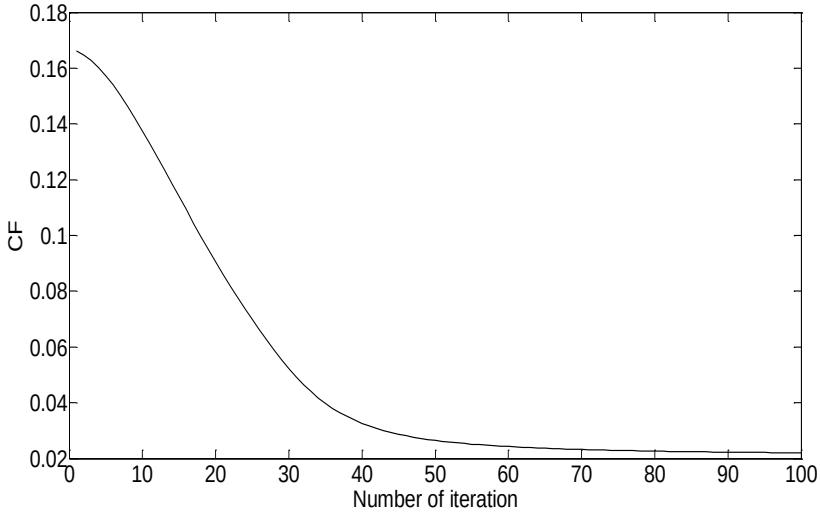

Figure 4-11 CF versus number of iterations.

To find the optimum number of beams that to be generated by the CGH, we assume the bit error rate (BER) of each beam does not exceed 10^{-9}. In the adaptive CGH-VLC system, the CCI between beams was taken into account; hence, increasing the number of beams generated leads to increase in the CCI which degrades the system performance as each beam carries a different data. For OOK modulation, the BER can be given as [12]:

$$BER = Q\left(\sqrt{SINR}\right) \tag{4.10}$$

where $Q(x) = \frac{\int_x^\infty e^{-z^2/2}}{\sqrt{2\pi}}$ and $SINR$ is the signal to interference plus noise ratio. By considering ISI, the $SINR$ is expressed as [103], [102]:

$$SINR = \frac{R^2(P_{s1} - P_{s0})^2}{\sigma t^2 + \sum_i^k (RP_i)^2} \tag{4.11}$$

where R is the photodetector's responsivity (0.4 A/W), (P_{s1}) is the received power associated with logic 1, (P_{s0}) is the received power associated with logic 0, σt is the total noise associated with the received signal, P_i is the interference power from the other beams and k is the number of beams. The total noise can be classified into three components and can be given as [126], [133]:

$$\sigma t = \sqrt{\sigma_{bn}^2 + \sigma_s^2 + \sigma_{pr}^2} \tag{4.12}$$

where σ_{bn} is the background shot noise component, σ_s is the shot noise component associated with the received signal and σ_{pr} is the preamplifier noise component. We consider the effect of the three components of the noise.

To obtain the optimum number of beams that can be generated with BER not exceeding $10^{-9,}$ we placed the imaging receiver at the room centre (2 m, 4 m, 1 m) as the distance between the transmitters and the receiver is maximum at this location. We assumed the first beam generated is the desired beam and the other beams are the interfering beams. The $SINR$ and the BER were calculated for the desired beam at a data rate of 5 Gb/s with an increase in the number of interfering beams. In this work, the effect of reflections is considered. Hence, by increasing the number of beams, this leads to increase in the level of CCI due to reflections and degrades the performance of each beam. The results are shown in Table 4.1. As each RYGB LDs-light unit has 9 RYGB LDs, the CGH was utilized to generate up to 9 beams, and each beam carries a different data stream at the same data rate. It can be noted that the performance of the desired beam degrades when the number of the interfering beams is increased and this is attributed to the increase in the level of the CCI. As shown in Table 4.1, the optimum number of the beams is equal to 8, which gives BER not exceeding 10^{-9} given our system set up and parameters. Thus,

the maximum data rate of our adaptive CGH-VLC system is 40 Gb/s (8 beams × 5 Gb/s). To find the pixels that received the data from each beam, each beam is given an ID. In the simulation, we set up a threshold in terms of $SINR$. Any pixel has $SINR$ less than 15.6 dB (BER more than 10^{-9}) was excluded. Hence, just the outputs of pixels that received data streams from beams enter to parallel to serial converter to obtain the data.

Table 4.1: Effect of the number of beams on the link performance.

Number of beams	SINR	BER
1	20.05	Error free
2	19.65	Error free
3	19.11	Error free
4	18.46	Error free
5	17.74	6.44×10^{-15}
6	16.98	8.29×10^{-13}
7	16.21	5.21×10^{-11}
8	15.63	0.75×10^{-9}
9	14.13	1.88×10^{-7}

One of the main benefits of the imaging receiver is that each pixel can be treated as a single separate photodetector with narrow FOV, which can amplify the photocurrents received separately. Moreover, the imaging receiver has the ability to distinguish between signals that have a different incidence angle. This is due to the imaging receiver ability to perform angular-spatial mapping (each pixel has a very small acceptance angle), which means each received signal is focused onto a different pixel depending on the incidence angle of this signal as shown in Figure 4.12 [134]. Therefore, the multiple beams were spatially separated by the CGH to give each beam a different incidence angle and each beam is received by a particular pixel (see Figure 4.12). The lens has an entrance aperture with a diameter equal to 3 cm. Therefore, the separation between beams was adjusted based on this diameter. A requirement in our proposed system is the presence of an LOS component between the transmitter and the receiver. It should be noted that the key benefit of the adaptive CGH-VLC system over the other two systems is that all beams

generated by the CGH are focused to the optical receiver. This leads to enhance 3-dB channel bandwidth, reduce path loss and increase received optical power. In addition, the adaptive CGH-VLC system tracks the optical receiver whenever the location of the optical receiver changes. The complexity in the design of the adaptive CGH-VLC system will be at the transmitter side. This is due to adding an extra device (i.e. the adaptive CGH) at the transmitter to find the receiver location and generated the beams. Therefore, the down link transmitters in the ceiling can be a quite bulky and expensive.

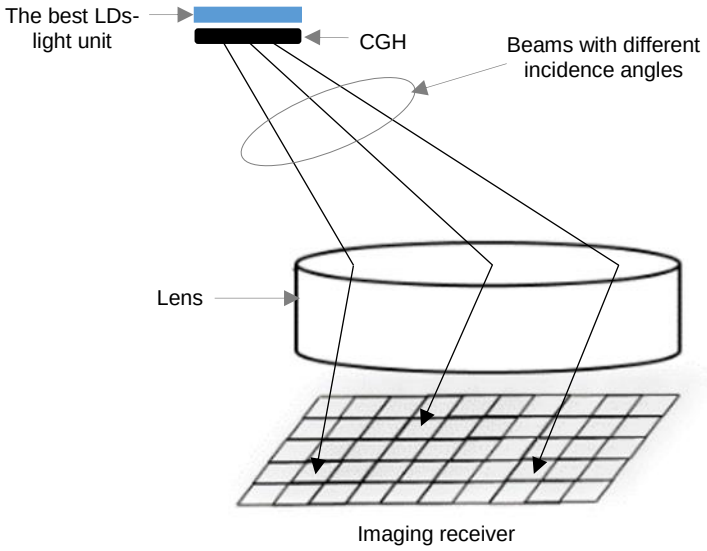

Figure 4-12: Imaging optical receiver with angular spatial mapping.

4.5 Simulation Results

The performance of the proposed systems in an empty room (room A) and a realistic room (room B) was evaluated. In this work, we used approach in [93] to produce the impulse response and hence determine the path loss, 3 dB channel bandwidth, the delay spread, SNR and SINR. A MATLAB program was used to obtain the results in this thesis. The proposed systems were investigated in many locations on the communication floor of the rooms. Table 4.2 gives the simulation parameters that were used in this chapter.

Table 4.2: Simulation parameters.

Parameters	Configurations
Rooms	
Length	8 m
Width	4 m
Height	3 m
ρ-xz Wall	0.8
ρ-yz Wall	0.8
ρ-xz op. Wall	0.8
ρ-yz op. Wall	0.8
ρ-Floor	0.3
ρ-Windows	0
ρ-Bookshelves	0.4
Bounces	1 2
Number of elements	32000 2000
d_A	5 cm × 5 cm 20 cm×20 cm
Lambertian emission order (n)	1
Sime-angle at half power	60°
Transmitters	
Number of transmitters	8
Number of RYGB LDs per unit	9 (3 × 3)
RYGB LDs interval	0.03 m
Transmitted Optical power/RYGB LD	1.9 W
Centre luminous intensity	162 cd
Lambertian emission order (n)	0.65
Sime-angle at half power	70°
Receivers	
Single photodetector	
Area of the photodetector	0.5 mm^2
FOV	40°
Responsivity	0.4 A/W
Receiver's bandwidth	6.18 GHz
Imaging receiver	
Concentrator entrance area	$\frac{9\pi}{4}$ cm^2
Concentrator refractive index	1.7
Concentrator acceptance angle	65°
Receiver's area	2 cm^2
Number of pixels	288
Pixel's area	0.69 mm^2
Responsivity	0.4 A/W
Receiver's bandwidth	4.48 Hz

4.5.1 Single beam static CGH-VLC system results

The single beam static CGH-VLC system was evaluated when the optical receiver was moving along the *x*-axis and *y*-axis in a step of 1 m. Due to the symmetry of room A, the results were obtained along the *y*-axis and along *x* = 1 m and *x* = 2 m whereas the results were obtained along the *y*-axis and along *x* = 1 m, *x* = 2 m and *x* = 3 m for room B. For comparison purposes, we introduced results of a traditional VLC system (without using the CGH), and

for the both system, one transmitter was used to send the data. In this system, we considered the single photodetector as an optical receiver.

The delay spread of the traditional indoor VLC system and the single beam static CGH-VLC system in room A is illustrated in Figure 4.13. The results show that using the CGH for the indoor VLC system leads to reduce the delay spread and consequently reduced ISI at the a high data rate. As shown in Figure 4.13, the maximum value of the delay spread was 0.27 ns for the VLC system without using the CGH whereas was 0.09 ns for the VLC system using the CGH. This reduction in the delay spread attributed to the 30% of the total power of the best transmitter directed to an area of 2 m × 2 m on the communication floor. This leads to increase in the received optical power associated with the LOS components and decrease in the effect of reflections from walls and ceiling of the room.

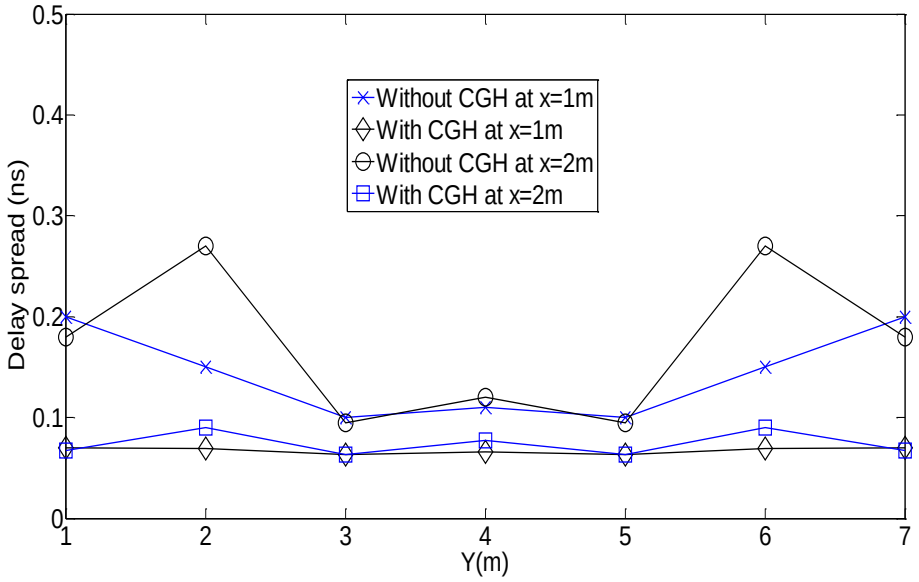

Figure 4.13: Delay spread of the traditional indoor VLC system and the single beam static CGH-VLC system in room A along x = 1 m and x = 2 m.

Table 4.3 shows the 3 dB channel bandwidth of the traditional indoor VLC system and the single beam static CGH-VLC system when the optical receiver was moving along the *y*-axis at x = 1 m and x = 2 m on the communication floor of room A. It can be seen that the single beam static CGH-VLC system provides a larger bandwidth compared to the traditional indoor VLC system. The minimum 3 dB channel bandwidth of the traditional indoor VLC system

was 0.17 GHz. In contrast, the minimum 3 dB channel bandwidth of the single beam static CGH-VLC system was 0.52 GHz. Thus, the maximum data rate that could be supported by the traditional indoor VLC system's channel was 0.24 GHz while the maximum data rate that could be supported by the single beam static CGH-VLC system's channel was 0.74 GHz. This is due to the 3 dB channel bandwidth needed is 0.7 times the bit rate [99].

Table 4.3: 3 dB channel bandwidth of the traditional indoor VLC system and the single beam static CGH-VLC system in room A along x = 1 m and x = 2 m.

3 dB channel bandwidth (GHz)					
Receiver locations (m)	Traditional indoor VLC system	Single beam static CGH-VLC system	Receiver locations (m)	Traditional indoor VLC system	Single beam static CGH-VLC system
1, 1, 1	1.25	2.86	2, 1, 1	1.38	2.98
1, 2, 1	1.75	2.89	2, 2, 1	1.21	2.2
1, 3, 1	2.1	3.1	2, 3, 1	2.3	3.17
1, 4, 1	1.9	3.03	2, 4, 1	1.67	2.6
1, 5, 1	2.1	3.1	2, 5, 1	2.3	3.17
1, 6, 1	1.75	2.89	2, 6, 1	1.21	2.2
1, 7, 1	1.25	2.86	2, 7, 1	1.38	2.98

To study the effect of obstacles on our proposed system the analysis was extended to the realistic room (room B). In the realistic room, we took into account the effects of signal blockage, due to mini cubicles, a door, windows, furniture, multipath propagation and mobility (see Figure 4.1 (b)). Due to the asymmetry of the realistic room, results were obtained when the mobile user was moving along the *y*-axis on the lines x = 1 m, x = 2 m and x = 3 m.

Figure 4.14 shows the received optical power gain due to using CGH when the mobile receiver moved along the *y*-axis and at x = 1 m, x = 2 m, and x = 3 m in a step of 1 m in room B. This gain can be expressed as:

$$Power\ gain\ (dB) = Pr_{CGH}(dB) - Pr(dB) \tag{4.13}$$

where $Pr_{CGH}(dB)$ is the received optical power of the single beam static CGH-VLC system and $Pr(dB)$ is the received optical power of the traditional indoor VLC system. It can be seen that due to the use of the fixed CGH, the minimum gain in optical received power was equal to 3 dB, 2.2 dB and 2.8 dB along the

x = 1 m, x = 2 m and x = 3 m, respectively. Thus, by using the fixed CGH, the quality of the connection improves without increasing the transmitted power.

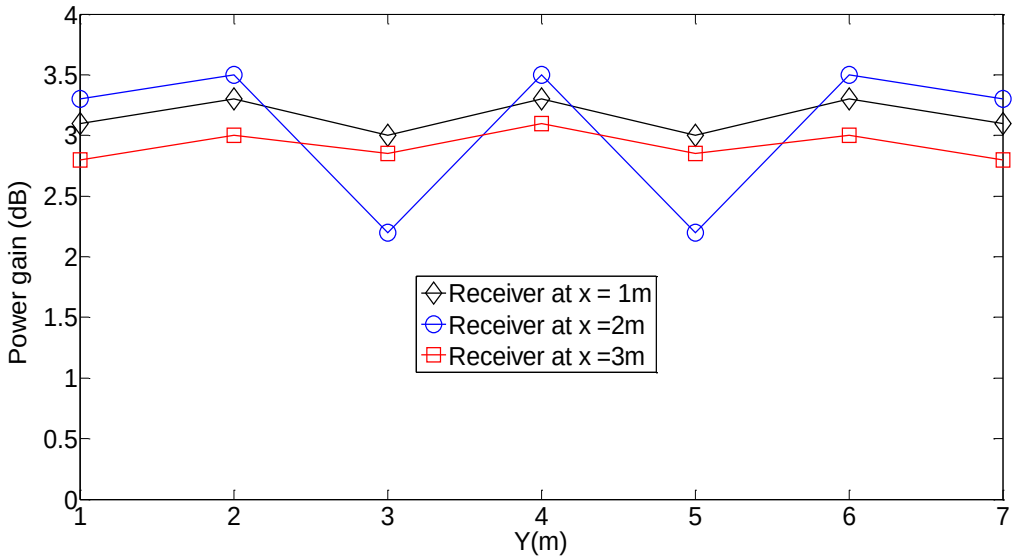

Figure 4-14: Optical power gain when the receiver moving along the y-axis and at x = 1 m, x = 2 m and x = 3 m in room B.

4.5.2 Static CGH-VLC system results

We investigated the performance of the static CGH-VLC system in two different environments with the presence of diffusing reflections (up to second order) and mobility. In this system, we considered the single photodetector as an optical receiver and the results were obtained in terms of delay spread and SNR. It should be noted that just one RYGB LDs-light unit (the best RYGB LDs-light unit) was used to transmit the data and the static CGH that followed this transmitter was utilized to generate multiple beams (100 beams) on an area of 2 m × 2 m.

Figure 4.15 shows the cumulative distribution function (CDF) of the delay spread of the static CGH-VLC system when the single photodetector was randomly located (500 random locations) on the communication floor of room A and room B. It can be seen that the value of the delay spread is less than 0.05 ns for almost 91% of the total locations of the single photodetector in room A. On the other hand, 90% of the total locations of the single photodetector on the communication floor of room B has delay spread less than 0.0012 ns. This is due to two walls (x = 0 and y = 0) in room B which have

windows with reflection coefficient equal to zero. In addition, two walls (wall *x* = 4 and wall *y* = 8) of room B are covered by bookshelves, which have reflection coefficients equal to 0.4. This leads to a reduction in the effect of the reflection components and consequently decrease the delay spread compared to room A.

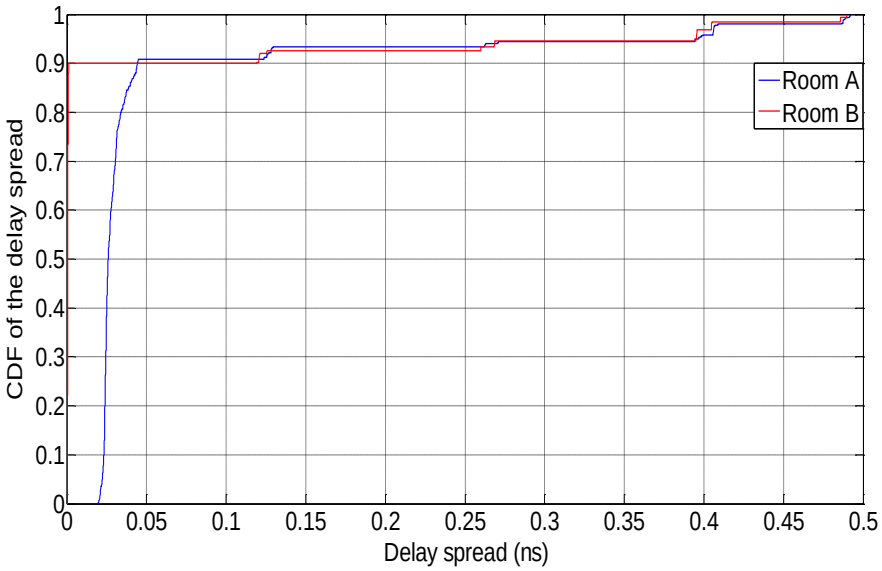

Figure 4-15: CDF of the delay spread of the static CGH-VLC system when the single photodetector was randomly placed in room A and in room B.

The CDF of the SNR for the static CGH-VLC system when the single photodetector is placed randomly on the communication floor of room A and room B is illustrated in Figure 4.16. The SNR was obtained when the system operated at a data rate equal to 8 Gb/s. As seen in Figure 4.16, at 80% of the locations, the static CGH-VLC system achieved a data rate of 8 Gb/s with SNR more than 15.6 dB (BER less than 10^{-9}). This system achieved an SNR between 13 dB and 15.6 dB at 20% of the total locations in room A and room B, with the 15.6 dB SNR supporting a data rate of 8 Gb/s at BER of 10^{-9}. For the 20% of locations with BER less than 10^{-9}, forward error correction codes can be used to reduce the BER to 10^{-9}.

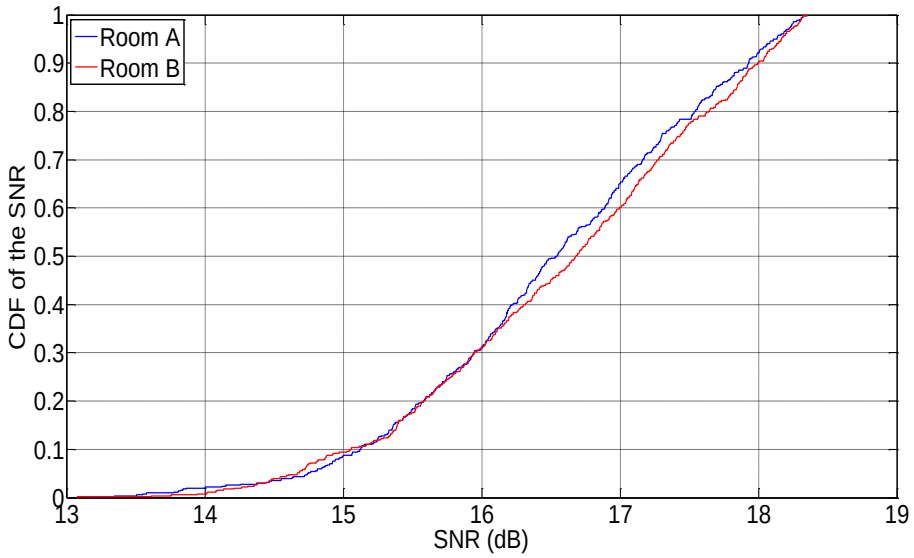

Figure 4-16: CDF of the SNR of the static CGH-VLC system when the system operates at 8 Gb/s and the single photodetector was randomly located in room A and in room B.

4.5.3 Performance evaluation of the adaptive CGH-VLC system

In the adaptive CGH-VLC system, each beam carries a different data stream at a rate of 5 Gb/s and the optimum number of beams that achieve a good communication link between the transmitter and the optical receiver (i.e. BER = 10^{-9} for each beam) was equal to eight, which enables the system to work at data rate of 40 Gb/s (8 beams × 5 Gb/s). Moreover, the results were displayed for one beam because of all beams have similar performance. In this system, we considered the imaging receiver as an optical receiver.

It should be noted that just 20% of the total power of each RYGB LD in the best RYGB LDs-light unit was used to generate the beams in this system. To ensure that the illumination level stayed at an acceptable level in the room, Figure 4.17 shows the distribution of the illumination in the room when the best RYGB LDs-light unit for communication was one of the light units at the room corner (the coordinates of the unit were 1 m, 7 m, 3 m), as the room corner has the lowest illumination level. As can be seen in Figure 4.17, the illumination level achieved the minimum requirement for the illumination (i.e. 300 lx [108]).

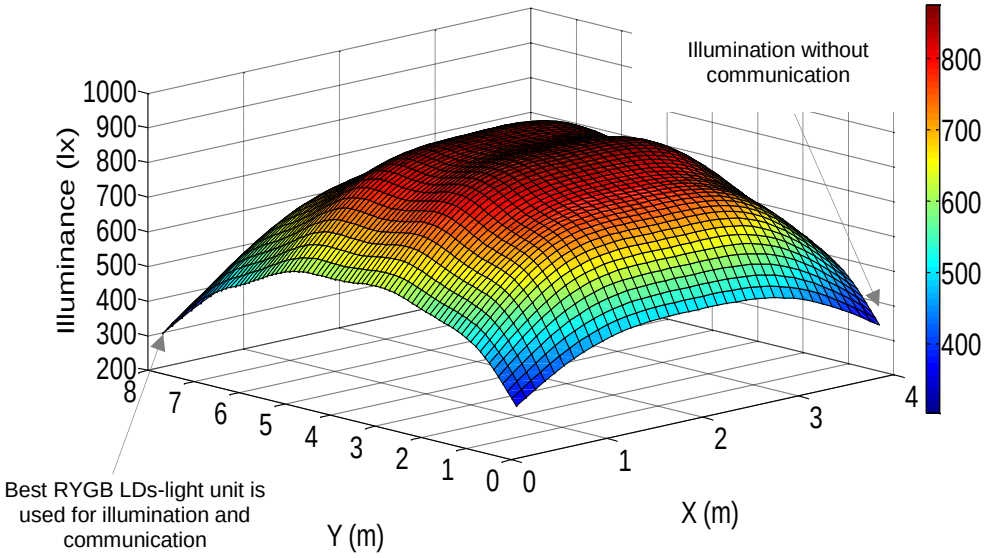

Figure 4-17: Distribution of the illumination of the adaptive CGH-VLC system on the communication floor; minimum illumination 303 lx and maximum illumination 874 lx.

4.5.3.1 Optical path loss

Optical path loss is used to measure the attenuation of the transmitted beams, attributed to propagation in the free space and reflection components. Thus, the path loss is one of the main components that can help explain the VLC system's performance. The path loss (PL) is given as [135]:

$$PL(dB) = -10log_{10}\left(\int_{-\infty}^{\infty} h(t)dt\right) \tag{4.14}$$

where $h(t)$ is the impulse response.

Figure 4.18 illustrates the path loss of the adaptive CGH-VLC system (path loss of one beam) when the imaging receiver was located at *x* = 1 m and *x* = 2 m along the *y*-axis on the communication floor of room A. It can be seen that the lowest values of the path loss accrued when the receiver was placed near to the best RYGB LDs-light unit. Thus, the path loss along *x* = 1 m is better than *x* = 2 m since the receiver is close to the transmitters.

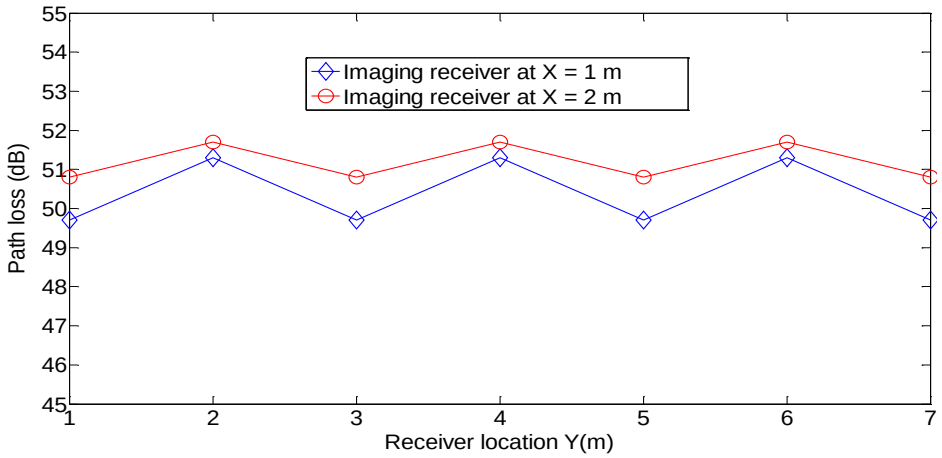

Figure 4-18: Path loss of the adaptive CGH-VLC system at different locations along the y-axis and at x = 1 m and x = 2 m in room A.

4.5.3.2 Delay spread evaluation

Figure 4.19 shows the delay spread of one beam of the adaptive CGH-VLC system at different locations of the imaging receiver along *x* = 1 m and *x* = 2 m. It can be seen that the worst case (the highest delay spread) for the proposed system was when the imaging receiver was located at the room edges. This is due to the delay spread being affected by the received power and delay time of the ray. Thus, the receiver is far from the walls *y* = 8 and *y* = 0, which means that the rays in the first and second reflections travel long distances at these locations. While, the best case for the delay spread (the lowest delay spread) for the designed system was when the imaging receiver was placed at the room center, due to the symmetry of room A and the optical receiver being close to all reflective surfaces of room A.

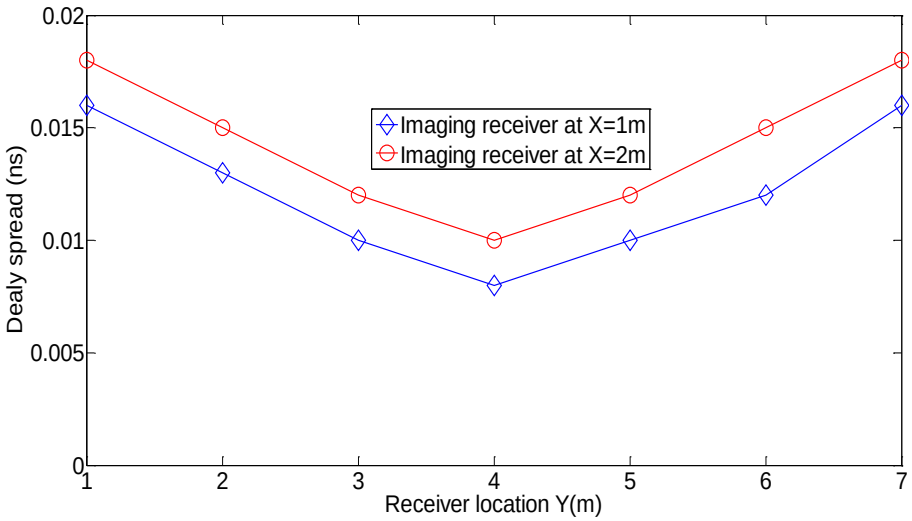

Figure 4.19: Delay spread of one beam of the adaptive CGH-VLC system at different locations along the y-axis and at x = 1 m and x = 2 m in room A.

4.5.3.3 3dB Channel bandwidth

The 3 dB channel bandwidth is an important factor in VLC systems, which is used to measure the ability of the VLC channel to support at a certain data rate. Figure 4.20 shows the 3 dB channel bandwidth when the imaging receiver was located at different places of room A along the *y*-axis and at *x* = 1 m and *x* = 2 m. It can be seen that at all given locations of the imaging receiver on the communication floor of room A, the lowest 3 dB channel bandwidth of each produced beam in the best RYGB LDs-light unit was more than 5 GHz. Therefore, a high data rate (5 Gb/s) can be transmitted through each beam without ISI given that typically the bandwidth needed is 0.7 times the bit rate [99].

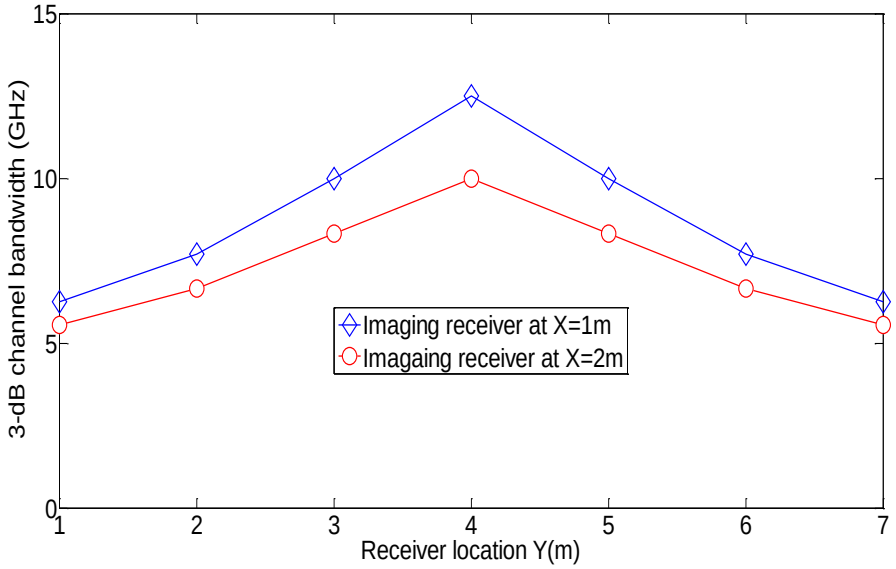

Figure 4-20: The 3 dB channel bandwidth of one beam of the adaptive CGH-VLC system at different locations of the imaging receiver along the y-axis and at x = 1 m and x = 2 m in room A.

4.5.3.4 SINR of the adaptive CGH-VLC system

Figure 4.21 depicts the SINR of the adaptive CGH-VLC system when the imaging receiver is placed at a different location along the *y*-axis at *x* = 1 m and *x* = 2 m in room A. The SINR was obtained when each beam operated at 5 Gb/s. In this system, each beam from each RYGB LD in the best transmitter sends a different data stream at 5 Gb/s. It can be seen that at all proposed locations of the imaging receiver in room A, the value of the SINR of the beam offered a strong communication link at a high data rate of 5 Gb/s. Thus, the

adaptive CGH-VLC system has the ability to achieve a high data rate of 40 Gb/s (8 beams × 5 Gb/s) with BER not exceeding 10^{-9}. Note that to get a data rate with BER not exceeding 10^{-9}, the SINR should not be less than 15.6 dB. Therefore, at some locations of the imaging receiver on the communication floor of room A (when the imaging receiver was located underneath of the best RYGB LDs-light unit) the data rate can be increased beyond 40 Gb/s. This is due to the high SINR (SINR = 17.3 dB) achieved at these locations.

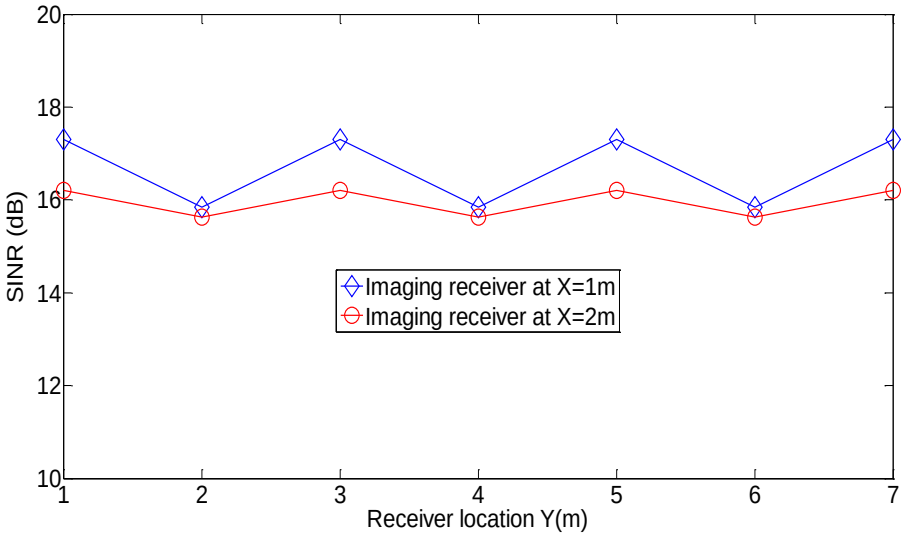

Figure 4-21: SINR of one beam of the adaptive CGH-VLC system at different locations of the imaging receiver along the y-axis and at x = 1 m and x = 2 m in room A when each beam operates at a data rate of 5 Gb/s.

4.5.3.5 Effect of blockage and shadowing on adaptive CGH-VLC system

To evaluate the effect of obstacles on the adaptive CGH-VLC system, the analysis was extended to the realistic room (room B). Due to the asymmetry of the realistic room, the imaging receiver was considered at different locations along the *y*-axis on the lines x = 1 m, x = 2 m and x = 3 m.

Figure 4.22 shows the impulse responses of one beam that was generated from the best RYGB LDs-light unit in two different room environments A and B when the imaging receiver was located at (2 m, 4 m, 1 m). As mentioned previously, LOS components have a great impact on VLC systems. Therefore, the performance of the adaptive CGH-VLC system was evaluated at all locations of the communication floor in room B, and it was found that our

proposed system has the ability to establish LOS components at all locations. Thus, the LOS components of the proposed system in both room scenarios are equal, as shown in Figure 4.22. On the other hand, the power collected from the reflection components (reflection components produced from the 80% of the total power of the best RYGB LDs-light unit) at the receiver side in room B were lower compared with room A, and this is due to several reasons. Firstly, in room B rays are prevented from reaching the imaging receiver by the physical partitions. Moreover, two walls (x = 0 and y = 0) in room B have windows that have a reflection coefficient of zero, which means that no signal will be reflected from them. In addition, in room B, two walls (x = 4 and y = 8) were covered with bookshelves with a reflectivity of 0.4, and consequently, the power reflected from these walls is reduced.

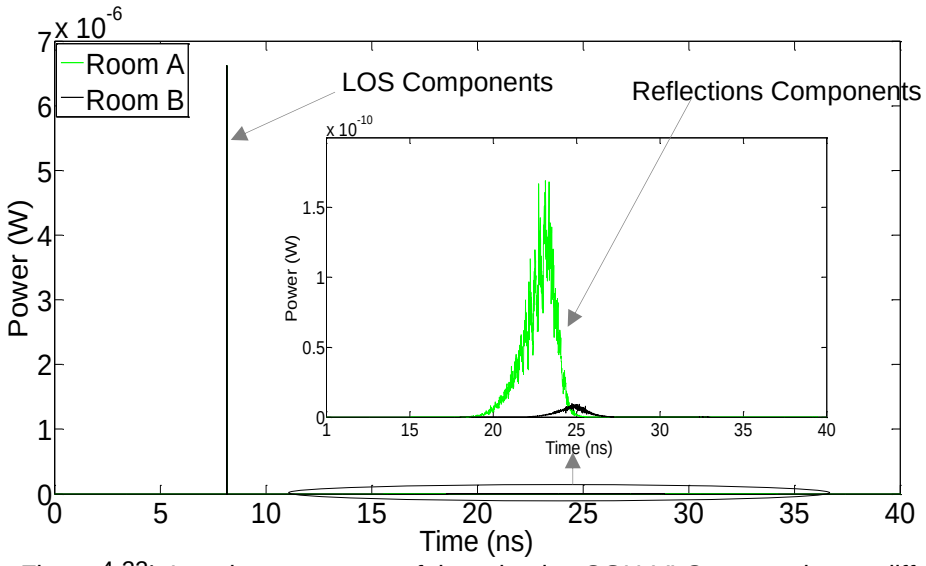

Figure 4-22: Impulse responses of the adaptive CGH-VLC system in two different environments when the imaging receiver is located at the centre (2 m, 4 m, 1 m) of room A and room B.

The path loss distribution of the adaptive CGH-VLC system in room B when the imaging receiver was placed along the y-axis at x = 1 m, x = 2 m and x = 3 m are illustrated in Figure 4.23. It can be noted that the maximum path loss occurred when the imaging receiver was located along x = 2 m, and this is because of the distribution of the RYGB LDs-light units on the ceiling, which increases the distance to the maximum between the transmitters and the optical receiver along x = 2 m. As can be seen, when the imaging receiver is investigated along x = 3 m, the path loss was better (slightly lower) compared

with that along x = 1 m. This is because along x = 3 m the closest walls (wall x = 4 and wall y = 8) to the optical receiver is covered by bookshelves with reflection coefficients of 0.4 while when the optical receiver was placed along x = 1 m, the closest walls (x = 0 and y = 0) has windows, which have zero reflection coefficients.

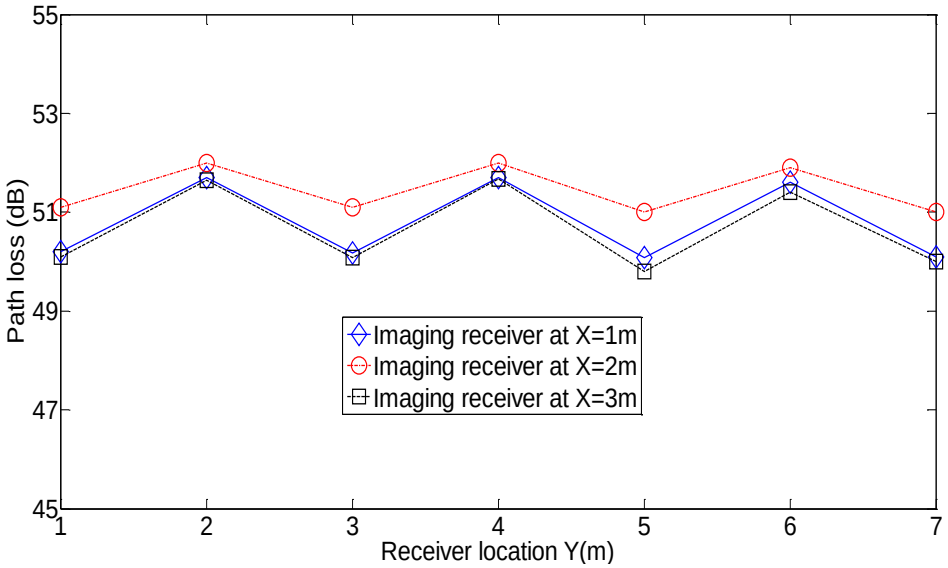

Figure 4-23: Path loss of one beam of the adaptive CGH-VLC system in room B when the imaging receiver was placed along the y-axis and at x = 1 m, x = 2 m and x = 3 m.

Figure 4.24 shows the SINR of the adaptive CGH-VLC system in the realistic room for different locations of the imaging receiver along the y-axis at x = 1 m, x = 2 m and x = 3 m. The lowest values of the SINR occurred when the receiver was located along the y-axis at x = 2 m. The SINR of the system when the optical receiver was located along the y-axis at x = 1 m and x = 3 m are comparable as shown in Figure 4.24. However, the SINR along x = 1 m is slightly higher than the SINR along x = 3 m. This is due to the presence of the windows, which have zero reflection coefficients, when the imaging receiver was placed along x = 1 m, while the bookshelves, which have 0.4 reflection coefficient, are close to the receiver when it was located along x = 3 m. Consequently, along x = 1 m the reflection components are minimal, which leads to enhanced system performance.

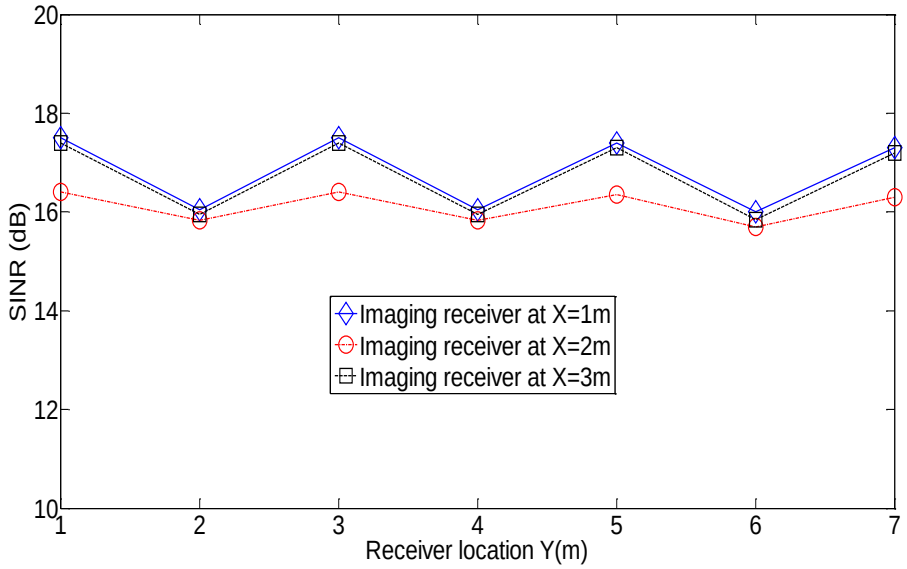

Figure 4-24: SINR of one beam of the adaptive CGH-VLC system in room B when the imaging receiver was placed along the y-axis and at x = 1 m, x = 2 m and x = 3 m when each beam operates at a data rate of 5 Gb/s.

The BER of one beam of the adaptive CGH-VLC system when the imaging receiver was located at different locations on the communication floor of room B along the *y*-axis at x = 1 m, x = 2 m and x = 3 m and when each beam carried a data rate of 5 Gb/s are given in Table 4.4. It can be seen that the maximum value of the BER of the proposed system is 3×10^{-10}, which can achieve a high data rate (5 Gb/s for each beam) with a strong communication link.

It should be noted that the CGH redirects the generated beams to the optical receiver whenever the location of the receiver changes. As seen in Table 4.4, the BER is lower when the optical receiver moves along x = 1 m and x = 3 m compared with x = 2 m. This is due to the fact that along x = 2 m, the distance between the transmitters and the optical receiver are higher compared with the distances when the imaging receiver moves along x = 1 m and x = 3 m, which leads to a reduced received optical power and consequently increased BER along x = 2 m. Furthermore, the BER can change despite beam steering when the position of the imaging receiver is changed if the beams are broad and are not fully collected by the receiver pixel.

Table 4.4: The BER of the one beam of the CGH-VLC system in room b when the receiver is located at x = 1, x = 2 and x = 3.

Receiver locations along x = 1 m	BER	Receiver locations along x = 2 m	BER	Receiver locations along x = 3 m	BER
1, 1, 1	4×10^{-14}	2, 1, 1	2×10^{-11}	3, 1, 1	7×10^{-14}
1, 2, 1	2×10^{-10}	2, 2, 1	3×10^{-10}	3, 2, 1	2×10^{-10}
1, 3, 1	4×10^{-14}	2, 3, 1	2×10^{-11}	3, 3, 1	7×10^{-14}
1, 4, 1	2×10^{-10}	2, 4, 1	3×10^{-10}	3, 4, 1	2×10^{-10}
1, 5, 1	4×10^{-14}	2, 5, 1	2×10^{-11}	3, 5, 1	7×10^{-14}
1, 6, 1	2×10^{-10}	2, 6, 1	3×10^{-10}	3, 6, 1	2×10^{-10}
1, 7, 1	4×10^{-14}	2, 7, 1	2×10^{-11}	3, 7, 1	7×10^{-14}

4.6 Summary

Three indoor VLC systems based on a CGH were presented in this chapter, a single beam static CGH-VLC system, a static CGH-VLC system and an adaptive CGH-VLC system. The CGH is used to direct a part of the total power of the best RYGB LDs-light unit, generate beam(s) and focus these beam(s) on a specific area on the communication floor of the room.

In the single beam static CGH-VLC system, the CGH is utilized to direct 30% of the total power of the best transmitter, to generate single broad beam and to direct this beams on an area of 2 m × 2 m on the communication floor. The 30% was selected to ensure that the illumination stayed at the level required by standards. The single beam static CGH-VLC system had the ability to decrease the delay spread of the traditional VLC system (VLC system without using the CGH) and improve the 3 dB channel bandwidth.

In the static CGH-VLC system, the CGH is utilized to direct 30% of the total power of the best transmitter, to generate 100 beams and to direct these beams on an area of 2 m × 2 m. All generated beams transmitted the same data. The static CGH-VLC system was able to achieve a data rate of 8 Gb/s while using a single photodetector and considering the influence of the reflections (up to second order) and mobility of the optical receiver.

In the adaptive CGH-VLC system, the CGH was used to direct 20% of the total power of the best RYGB LDs-light unit, generate eight beams (optimum number of beams dictated by CCI) and steer these beams to the imaging receiver. Each generated beam conveyed a different data stream at a rate of

5 Gb/s. The CCI between beams was taken into account in this system as the beams conveyed different data streams. The adaptive CGH-VLC system offered a data rate of 40 Gb/s (8 beams × 5 Gb/s) with BER not going below 10^{-9}.

5. Subcarrier Multiplexing Tones for Parallel Data Transmission in Indoor Visible Light Communication Systems

5.1 Introduction

Many transmitters (LEDs or LDs) are used in indoor VLC systems to ensure a sufficient level of illumination in the indoor environment. This makes multiple input multiple output (MIMO) very attractive technique for indoor VLC systems to enhance the achievable data rate. In chapter four, we introduced the CGH for indoor VLS system to improve the system performance (increase the 3-dB channel bandwidth and increase the data rate). However, adding an extra device (i.e. the adaptive CGH) at the transmitter increasing the complexity to design the VLC system, which makes the down link transmitter in the ceiling a quite bulky and expensive.

This chapter presents an indoor VLC system in conjunction with an imaging receiver with parallel data transmission (spatial multiplexing) to reduce the effects of ISI. To distinguish between light units (transmitters) and to match the light units used to convey the data with the pixels of the imaging receiver, we propose the use of subcarrier multiplexing (SCM) tones. Each light unit transmission is multiplexed with a unique tone. At the receiver, a SCM tone decision system is utilized to measure the power level of each SCM tone and consequently associated each pixel with a light unit. In addition, the level of CCI between light units is estimated using the SCM tones. Our proposed VLC system is examined in two indoor environments with tacking into account reflective components (the first order and the second order reflections). The results show that the VLC system has the ability to achieve an aggregate data rate of 8 Gb/s with a BER equal to 10^{-6} for each light unit, using simple OOK.

MIMO techniques have been investigated widely in indoor VLC systems. An indoor VLC MIMO system with imaging receiver and non-imaging receiver was considered in [52]. It was shown that based on the location of the receiver, a lens located at a good place between the transmitters and the receivers can de-correlate the matrix of the MIMO channel. The work in [136] described spatial modulation in a MIMO indoor VLC system. It showed that interference between transmitters can be avoided by activating just one transmitter at any time. An indoor VLC system based on 4 × 9 MIMO was shown to achieve a data rate of 1 Gb/s over 1 m, where the equalizer was implemented in both the receiver and the transmitter to extend the bandwidth of the system [137]. A 50 Mb/s data rate was achieved experimentally over a distance of 2 m for an indoor 4 × 4 MIMO VLC system [138]. Advanced receivers were proposed to reduce the correlation between the VLC-MIMO channels in [139], [140], [141].

In this chapter, the VLC system uses parallel data transmission in conjunction with an imaging receiver. Each pixel of the imaging receiver is considered as a single photodetector that has a narrow FOV. To distinguish between the light units, the transmission from each light unit was multiplexed with a unique SCM tone. These unmodulated tones are used at the beginning of the communication to set up the connection between the light units and the optical receiver. The SCM tones were used to calculate the level of crosstalk between wavelength division multiplexing (WDM) channels [142] and were utilized for indoor VLC system positioning systems [143]. Here, the SCM tones were used to give an ID to each light unit (transmitter), to help find the light units that have a good channel for high data rate transmission and match these light units with pixel(s) of the imaging receiver. The SCM tones were also used to calculate the CCI level at each pixel of the imaging receiver. To our best knowledge, this is the first time that SCM tones have been suggested to support parallel data transmission in an indoor VLC system. To achieve a good link between the optical receiver and the transmitters, each light unit sends a different data stream with a target bit error rate (BER) = 10^{-6}. Based on ISI and the level of CCI, each light unit sends a different data stream at a different data rate.

The reminder of this chapter is organized as follows: The setup of the rooms, configurations of the RYGB LDs-light units and the configurations of the receiver are described in Section 5.2. Section 5.3 presents the proposed system's design. Results of the simulation of the system in the proposed rooms are shown in Section 5.4 and summary are given in Section 5.5.

5.2 Simulation Setup

To evaluate the performance of our proposed system, we used two rooms that are shown in Figure 5.1 (a) and (b). In addition, we used the ray tracing algorithm to modal the indoor channel of the VLC systems in a similar way to that depicted in Chapter 3.

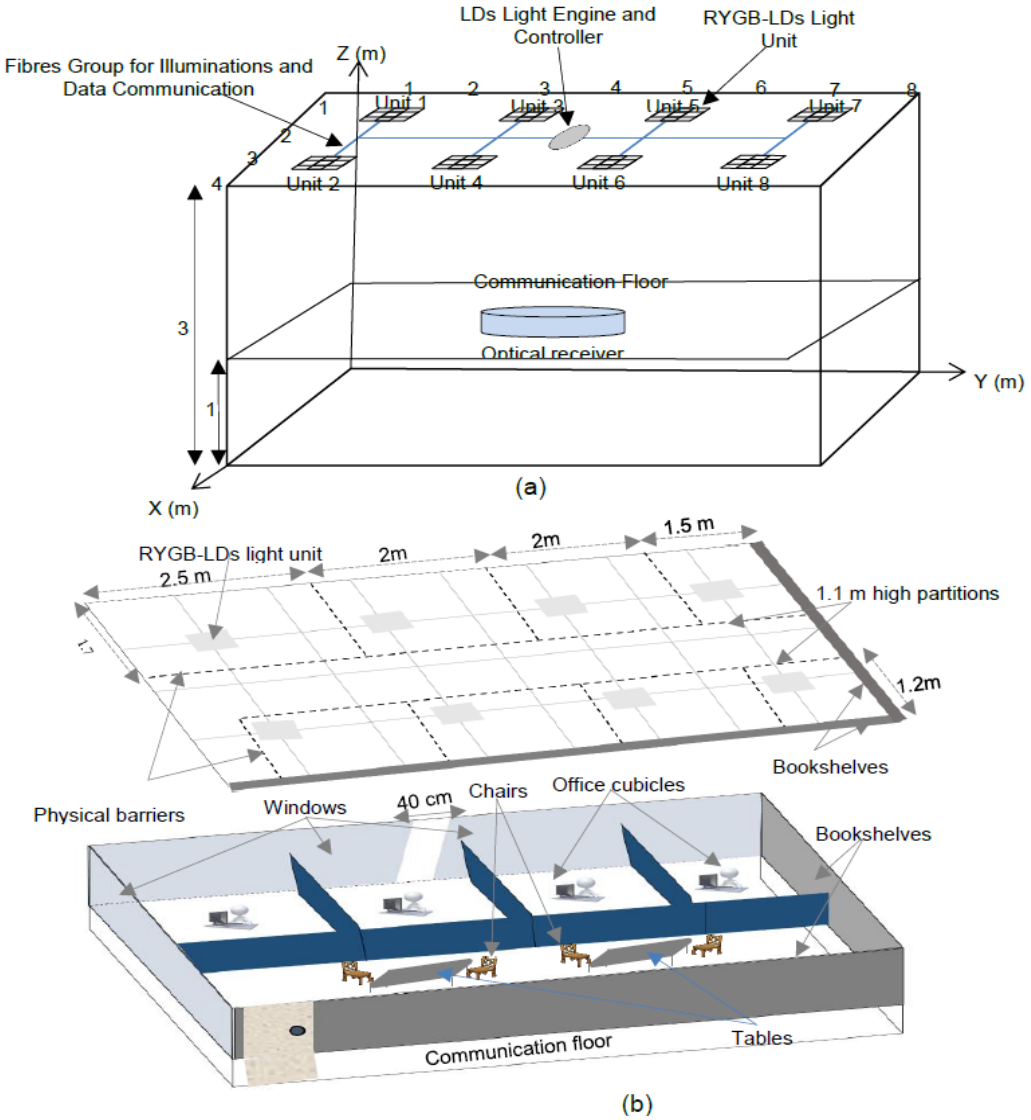

Figure 5.1: VLC system rooms (a) an empty room (Room A) and (b) a realistic room which has a door, three large glass windows a number of rectangular-shaped cubicles with surfaces parallel to the room walls (Room B).

5.3 Design of Proposed VLC system

In our proposed rooms, the RYGB LDs-light units (transmitters) were spatially separated to obtain a suitable illumination level. Moreover, each pixel of the imaging receiver was treated as a separate single photodetector receiver with a narrow FOV. Thus, each transmitter was viewed by different pixel(s) of the imaging receiver and each transmitter was utilized to send a different data stream at a different data rate.

The SCM tones are used to:

1. Identify each light unit.
2. Determine the RYGB LDs-light units that can be used to transmit data (active light units).
3. Find the pixels that viewed these light units.
4. Calculate the level of CCI between the light units.

The performance of each transmitter was evaluated based on the level of CCI and ISI due to the diffuse components (up to second order).

5.3.1 Distinguishing the RYGB LDs-light units

To distinguish the RYGB LDs-light units, each unit is given an ID. A preamble code or a packet header can be used to identify RYGB LDs-light units. The preamble code and the packet header are sequences of bits that can be added to the data frame of each RYGB LDs-light unit to distinguish them. For example, eight RYGB LDs-light units were used in our proposed rooms; hence, a sequence of three bits (000 - 111) may be assumed to identify each RYGB LDs-light unit. However, any error in decoding these sequence of bits used to identify each RYGB LDs-light unit would lead to a wrong decision at the receiver and the loss of the data since the data is transmitted through the RYGB LDs-light units in parallel. Errors may occur in the header or preamble due to the RYGB LDs-light units emitting signals for broad coverage; hence, the ISI of the diffuse channel may cause an error when decoding the header and the preamble. In addition, intensity modulation with direct detection (IM/DD) are used in our VLC system, which means that each pixel

of the imaging receiver responds in this case to all signals that are conveyed from all RYGB LDs-light units; thus, the CCI at the receiver can lead to an increase in the probability of error when decoding the header and the preamble.

Here, we propose SCM tones to identify each RYGB LDs-light unit, where these unmodulated tones are not affected by the channel dispersion [142]. Each RYGB LDs-light unit is multiplexed with a unique tone signal, which enables the receiver to easily distinguish the RYGB LDs-light units. A unique SCM tone (f_1 – f_8) was multiplexed into each RYGB LDs-light unit as can be seen in Figure 5.2. It should be noted that the identification tones were used at the beginning of the communication to set up the connection between the light units and the imaging receiver (to find the RYGB LDs-light units that had good channel conditions with the optical receiver, to match these light units with the pixels of the imaging receiver and to find the level of the CCI) as will be explained further. The serial data were divided among only the RYGB LDs-light units that had a reliable connection with the imaging receiver (i.e., high channel dc gain, low level of CCI and low ISI); hence, the other RYGB LDs-light units were used for lighting only (no data transmitted through these units). In addition, each of the RYGB LDs-light units that was utilized to convey data, sent a different data stream at a different data rate while maintaining a target BER = 10^{-6}.

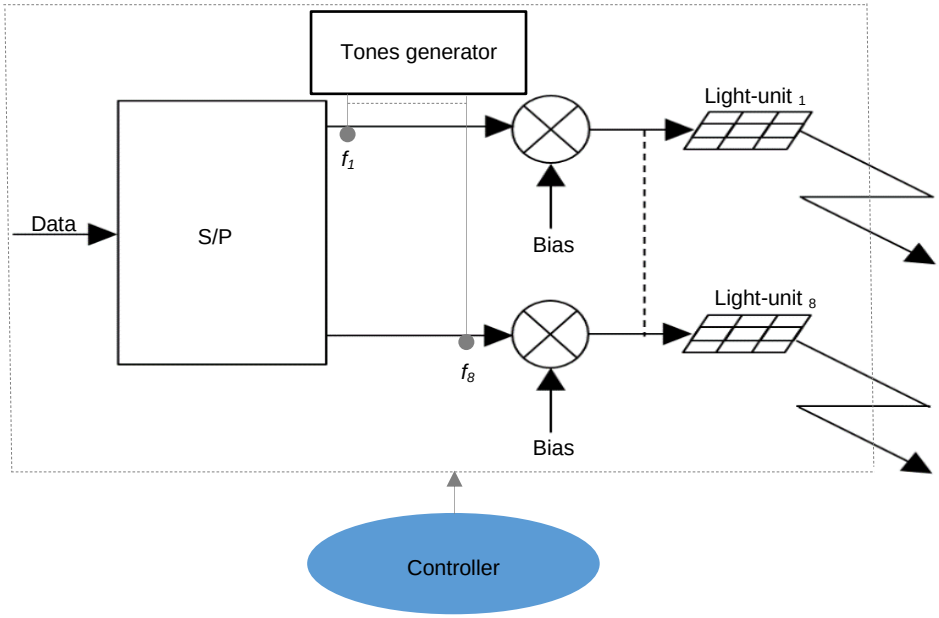

(a)

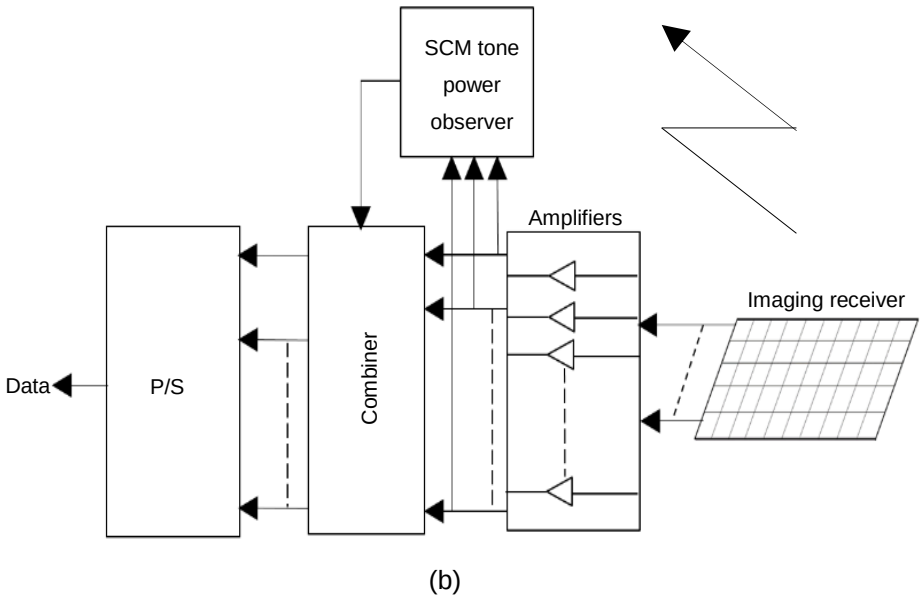

(b)

Figure 5-2: Structure of the VLC system (a) transmitter and (b) receiver front-end.

To find the RYGB LDs-light units that have a strong connection (units able to send a high data rate with a reliable connection; i.e. low BER) with the optical receiver, the controller arranges for the light units to send only the identification tones (no data transmission). At the receiver, the SCM tone identification system (see Figure 5.2) was used to bandpass filter the received power due to each tone at each imaging receiver's pixel. The input current to RYGB LDs when including *mth* SCM tone is given as:

$$I_m(t) = I_{bais} + A_m sin(w_m t) \tag{5.1}$$

where I_{bais} is the bias current, $w_m = 2\pi f_m$, f_m is the SCM tone frequency and A_m is the amplitude of the SCM tone. The received optical power (Pr_n) of any SCM tone at the *nth* pixel of the imaging receiver due to *mth* light unit is given as:

$$Pr_n = \sum_{k=1}^{s} P_{LOS}^{k} + \sum_{i=1}^{l} P_{1st}^{i} + \sum_{d=1}^{y} P_{2nd}^{d} \tag{5.2}$$

where P_{LOS}, P_{1st} and P_{2nd} are the received optical power from the *mth* RYGB light unit due to the LOS components, the first order reflection components

and the second order reflection components, respectively, s is the number of rays due to LOS components, l is the rays number due to the first order reflection components and y is the number of rays due to the second order reflection components. Calculations of P_{LOS}, P_{1st} and P_{2nd} can be found in [109] and [93]. In this work, the H matrix is formed by the received optical power (Pr) of each SCM tones at each pixel of the imaging receiver as:

$$H = \begin{bmatrix} Pr_{11} & \cdots & Pr_{1M} \\ \vdots & \ddots & \vdots \\ Pr_{N1} & \cdots & Pr_{NM} \end{bmatrix} \tag{5.3}$$

where N is the number of pixels and M is the number of transmitters.

It should be noticed that the channel frequency response of indoor VLC systems shows low pass characteristic in the electrical domain [144]. To ensure that the range of the frequencies that is given to the SCM tones is located near to the DC where the attenuation of the channel is low, we calculated the 3-dB channel bandwidth of the channel frequency response of the indoor VLC system. In our system, however, each RYGB light unit has a different channel frequency response as each RYGB light unit sends a different data stream. Therefore, we calculated the 3-dB channel bandwidth of each light unit when the optical receiver was placed at the centre of room A (2 m, 4 m, 1 m) as the imaging receiver sees all light units and the distances between the light units and the optical receiver become maximum at this location. The channel frequency response of each RYGB light unit is given as:

$$H(f_m) = \int_0^\infty h_m(t) e^{-j2\pi f_m t}\, dt \tag{5.4}$$

here $h(t)$ is the indoor channel's impulse response in the time domain (we obtained the $h\,(t)$ similar to that in [93] for each RYGB light unit).

Table 5.1 shows the 3-dB channel bandwidth of each RYGB light unit when the optical receiver was placed at the centre of room A. It can be seen that RYGB light units 1, 2, 7 and 8 have the same 3-dB channel bandwidth and RYGB light units 3, 4, 5 and 6 have similar 3-dB channel bandwidth also, and this is attributed to the symmetry of room A. As seen in Table 5.1, the

lowest 3-dB channel bandwidth is 1.93 GHz. Therefore, the range of the frequencies chosen for the SCM tones were 500 MHz to 920 MHz with a guard interval of 60 MHz, which also enables to use of low electronic components.

Table 5.1: 3-db channel bandwidth of RYGB light units when the optical receiver was located at the centre of room A.

RYGB light units	Unit 1	Unit 2	Unit 3	Unit 4	Unit 5	Unit 6	Unit 7	Unit 8
3-dB channel bandwidth (GHz)	1.93	1.93	5.37	5.37	5.37	5.37	1.93	1.93

Each pixel of the imaging receiver receives optical power from all light units (either due to LOS components or due to reflection components). Accordingly, eight bandpass filters (BPFs), which have centre frequencies equal to the frequencies of the SCM tones, are used in the SCM tone identification system to separate the SCM tones at each pixel of the imaging receiver as shown in Figure 5.3. It should be noted that the SCM tone identification system is used at the beginning of the communication to set up the connection between the light units and the optical receiver. Therefore, during just this monitoring time the received signals from light units enter the BPFs. The output of each BPF is either a desired SCM tone (the SCM tone that has LOS component with the imaging receiver) plus noise or an undesired SCM tone (the SCM tone that has no LOS component with the imaging receiver) plus noise. Therefore, to decide the output of the BPF, an optimum threshold should be obtained.

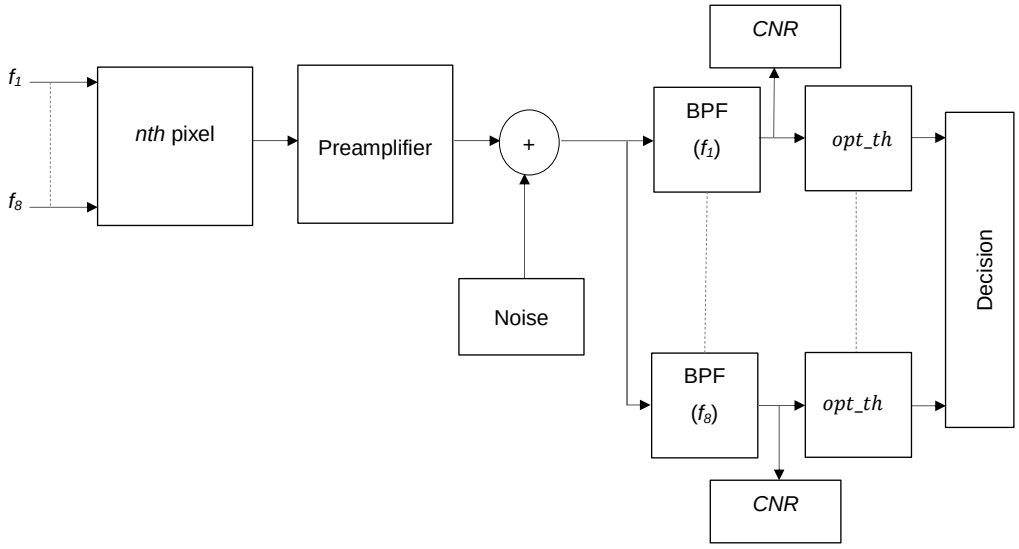

Figure 5-3: Architecture of the SCM tone identification system.

To identify the output electrical current (z) of each BPF, we hypothesize two situations:

Hypothesis 1 ($H1$): z = undesired SCM tone plus noise (b + n).

Hypothesis 2 ($H2$): z = desired SCM tone plus noise (a + n).

The total noise (n) that is seen by each SCM tone is white Gaussian zero mean, with total standard deviation σ_t. It is generated by shot noise due to the background light, signal shot niose and preamplifier thermal niose. The total standard deviation of the noise (σ_t) can thus be written as [101]:

$$\sigma_t = \sqrt{\sigma_{bn}^2 + \sigma_s^2 + \sigma_{pr}^2} \tag{5.5}$$

where σ_{bn} is the ambient shot noise, σ_s is the shot noise related with the SCM tone and σ_{pr} is the pre-amplifier thermal noise. The background light shot niose (σ_{bn}) is given as:

$$\sigma_{bn} = \sqrt{2qAI_{bn}BW_{BPF}} \tag{5.6}$$

here q is the charge of the electron, I_{bn} is the background photocurrent, which is induced due to the light from the sky and background light sources (I_{bn}= 10^{-3} A/cm^2) [5], and BW_{BPF} is the bandwidth of the BPF, which was selected to be equal to 4 MHz (following BER optimisation using the results in this section),

to reduce the noise seen by each SCM tone. The shot noise induced by the SCM tones is expressed as [145]:

$$\sigma_s = \sqrt{2qRPr_n BW_{BPF}} \tag{5.7}$$

In this section, the p-i-n FET receiver designed in [146] was used. The input noise current for this receiver is equal to 4.5 pA/$\sqrt{Hz}$.

The values of a and b (the electrical currents of the desired SCM tone and the undesired SCM tone) depend on the distance between the optical receiver and the light units. Thus, a and b are random variables whose distribution we determined experimentally by considering 1000 random locations of the optical receiver randomly (1000 locations) on the communication floor of room A. Due to the symmetry of room A, we considered light unit 1 as the desired transmitter and light unit 2 as the interfering source. At each place of the receiver, we obtained the electrical current of a and b generated by the desired SCM tone and the undesired SCM tone. Figure 5.4 and Figure 5.5 show the histogram and the curve fitting of the desired SCM tone and the undesired SCM tone, respectively.

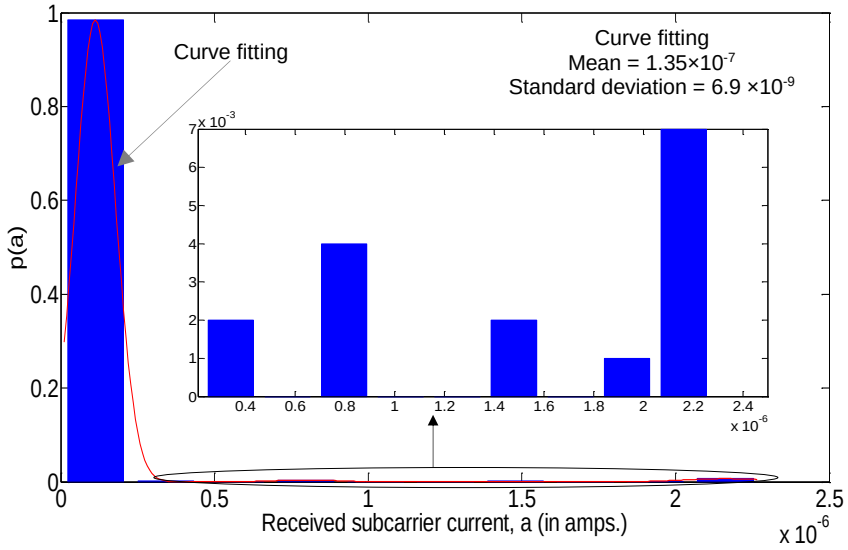

Figure 5-4: Histogram and the curve fitting of the desired SCM tone.

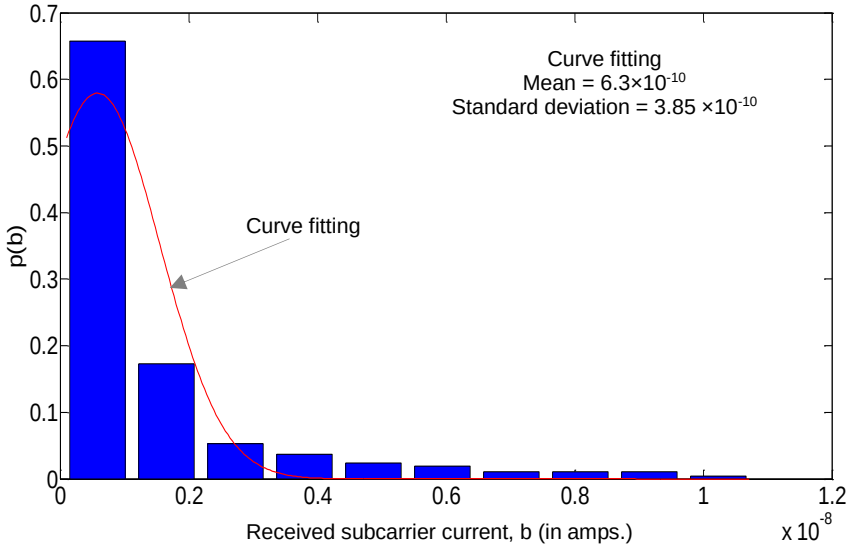

Figure 5-5: : Histogram and the curve fitting of the undesired SCM tone.

From the curve fitting, the normalized probability density functions (pdfs) of a $(p(a))$ and b $(p(b))$ are given as:

$$p(a) = \frac{1}{\sqrt{2\pi}\,\sigma_{ds}} e^{-\left(\frac{a-m_{ds}}{\sqrt{2}\sigma_{ds}}\right)^2} \tag{5.8}$$

and

$$p(b) = \frac{1}{\sqrt{2\pi}\,\sigma_{us}} e^{-\left(\frac{b-m_{us}}{\sqrt{2}\sigma_{us}}\right)^2} \tag{5.9}$$

where we assumed a Gaussian distribution for the received power which is reasonable given the multiple reflecting surfaces and the observed results. Here, m_{ds} and σ_{ds} are the mean value and the standard deviation of the desired SCM tone, respectively and m_{us} and σ_{us} are the mean value and the standard deviation of the undesired SCM tone, respectively.

We can write the pdf's of z given hypotheses $H1$ and $H2$, respectively. Under hypothesis $H1$, z is the convolution of the noise pdf and the undesired SCM tone pdf and is given as:

$$fz(z|H1) = p(b) \otimes p(n) \tag{5.10}$$

After solving the above equation, $fz(z|H1)$ can be written as:

$$fz(z|H1) = \frac{1}{\sqrt{2\pi({\sigma_{us}}^2 + {\sigma_t}^2)}} e^{-\left(\frac{z-m_{us}}{\sqrt{2({\sigma_{us}}^2+{\sigma_t}^2)}}\right)^2} \tag{5.11}$$

Under hypothesis $H2$, z is the convolution of the noise pdf and the desired SCM tone pdf and is given as:

$$fz(z|H2) = \frac{1}{\sqrt{2\pi({\sigma_{ds}}^2 + {\sigma_t}^2)}} e^{-\left(\frac{z-m_{ds}}{\sqrt{2({\sigma_{ds}}^2+{\sigma_t}^2)}}\right)^2} \tag{5.12}$$

Detailed derivation of the convolution is presented in Appendix B. Applying likelihood ratio to equations (5.11) and (5.12) [147], we get:

$$\frac{fz(z|H2)}{fz(z|H1)} \underset{H1}{\overset{H2}{\gtrless}} 1 = \frac{\frac{1}{\sqrt{2\pi({\sigma_{ds}}^2 + {\sigma_t}^2)}} e^{-\left(\frac{z-m_{ds}}{\sqrt{2({\sigma_{ds}}^2+{\sigma_t}^2)}}\right)^2}}{\frac{1}{\sqrt{2\pi({\sigma_{us}}^2 + {\sigma_t}^2)}} e^{-\left(\frac{z-m_{us}}{\sqrt{2({\sigma_{us}}^2+{\sigma_t}^2)}}\right)^2}} \underset{H1}{\overset{H2}{\gtrless}} 1 \tag{5.13}$$

Solving equation (5.13) we get:

$$\begin{aligned} z &\underset{H1}{\overset{H2}{\gtrless}} \frac{1}{{\sigma_{ds}}^2 - {\sigma_{us}}^2}\left(m_{us}({\sigma_{ds}}^2 + {\sigma_t}^2) - m_{ds}({\sigma_{us}}^2 + {\sigma_t}^2) \right. \\ &+ \left. \sqrt{\begin{pmatrix} {\sigma_{ds}}^2{\sigma_{us}}^4 + {\sigma_t}^4{\sigma_{us}}^2 + {\sigma_t}^2{\sigma_{us}}^4 \\ -{\sigma_{ds}}^4{\sigma_t}^2 - {\sigma_{ds}}^4{\sigma_{us}}^2 - {\sigma_{ds}}^2{\sigma_t}^4 \end{pmatrix} \ln\left(\frac{{\sigma_{us}}^2 + {\sigma_t}^2}{{\sigma_{ds}}^2 + {\sigma_t}^2}\right) + \\ (m_{ds} - m_{us})^2({\sigma_t}^2{\sigma_{ds}}^2 + {\sigma_{ds}}^2{\sigma_{us}}^2 + {\sigma_t}^4 + {\sigma_t}^2{\sigma_{us}}^2) \end{pmatrix}} \right) \\ &= z \underset{H1}{\overset{H2}{\gtrless}} opt\_th \end{aligned} \tag{5.14}$$

Detailed derivation of the optimum threshold is presented in Appendix B. It should be noted that when the σ_{ds}, σ_{us} and m_{us} are very small compared with m_{ds}, the optimum threshold (opt_th) ~ $\frac{m_{ds}}{2}$. Figure 5.6 shows the relationship between σ_{ds} and z using (5.14). As can be seen in Figure 5.6, the optimum threshold ~ $\frac{m_{ds}}{2}$ when $\sigma_{ds} < 10^{-9}$.

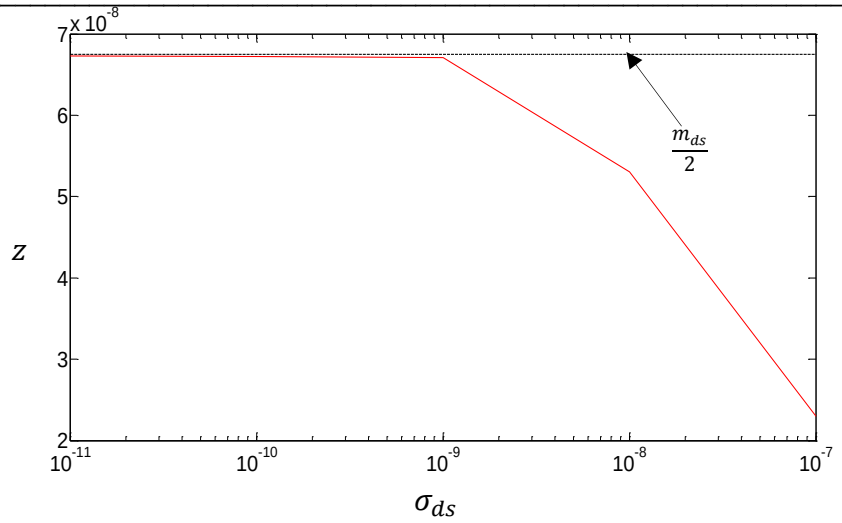

Figure 5-6: Relationship between the standard deviation of the desired SCM tone ($\boldsymbol{\sigma_{ds}}$) and the optimum threshold (opt_th).

It should be noted that the standard deviation of the desired SCM tone (σ_{ds}) depends on the size of the proposed rooms, light units' distribution, distance between transmitters and the receiver and the FOV of the receiver. Thus, changing these parameters changes the optimum threshold value.

The probability of detection of the desired SCM tone, which is the probability of correct decision of the desired SCM tone ($Pcds$) is given as:

$$Pcds = \int_{opt\_th}^{\infty} fz(z|H2)dz$$
$$= \int_{opt\_th}^{\infty} \frac{1}{\sqrt{2\pi({\sigma_{ds}}^2 + {\sigma_t}^2)}} e^{-\left(\frac{z-m_{ds}}{\sqrt{2({\sigma_{ds}}^2+{\sigma_t}^2)}}\right)^2} dz \quad (5.15)$$

Consequently, the probability of detection of the undesired SCM tone, which is the probability of false alarm of the undesired SCM ($Pfus$) tone (i.e. the undesired SCM tone considered as the desired SCM tone) is given as:

$$Pfus = \int_{opt_{th}}^{\infty} fz(z|H1)dz = \frac{1}{\sqrt{2\pi({\sigma_{us}}^2 + {\sigma_t}^2)}} e^{-\left(\frac{z-m_{us}}{\sqrt{2({\sigma_{us}}^2+{\sigma_t}^2)}}\right)^2} dz \qquad (5.16)$$

Hence, the probability of not assigning the undesired SCM tone to a user, which is the probability of the correct decision in the undesired SCM tone ($Pcus$) is:

$$Pcus = 1 - Pfus \qquad (5.17)$$

The overall probability of the SCM identification system to make a correct decision (Pcd) is:

$$Pcd = Pcds\ (Pcus)^{M-1} \qquad (5.18)$$

Consequently, the probability of being wrong in the decision (Pwd) is $1 - Pcd$. In our system, and for the given set of parameters in the analysis, Pwd is 1.45 × 10^{-10}, which can be ignored as each RYGB light unit sends data with a target BER = 10^{-6}. Therefore, our SCM identification system is able to associate each pixel(s) of the imaging receiver with a light unit at a low "association probability of error, Pwd".

We next use the SCM tones as a simple mechanism to estimate the CCI in our system. The CCI level is defined as the total received power at the nth pixel, except for the received optical power of the desired signal (SCM tone here). For example, if the desired tone is f_m (identification tone of mth light unit), the electrical power of this tone ($S_{n,m}$) and the level of CCI due to the other tones at *nth* pixel of the imaging receiver can be given as:

$$S_{n,m} = \frac{\left(R\ Pr_{n,m}\right)^2}{2} \text{ and } I_{n,k} = \sum_{\substack{k=1 \\ k \neq m}}^{M} \frac{\left(R\ Pr_{n,k}\right)^2}{2}, \tag{5.19}$$

$n \in [1, 2 \ldots . N],\ \ m \in [1, 2 \ldots . M]$

The carrier to noise (CNR) ratio of the *mth* tone at the *nth* pixel of the imaging receiver is given as:

$$CNR_{n,m} = \frac{(R\ Pr_{nm})^2}{2\ {\sigma_t}^2} \tag{5.20}$$

A few pixels of the imaging receiver are used to receive the parallel data. In addition, based on the channel condition of each RYGB light unit with the optical receiver, not all RYGB light units were used to transmit the data. Therefore, to exclude the unwanted pixels (pixels that collected very low optical power from the RYGB light units) and to find the RYGB light unit that has the ability to send data, we set up a threshold level for each pixel. We defined the factor CNR/I as the threshold level:

$$\left(\frac{CNR}{I}\right)_{n,m} = \frac{(R\ Pr_{nm})^2}{2({\sigma_t}^2 + I)} \tag{5.21}$$

Hence, if any RYGB LDs-light unit has CNR/I > 13.6 dB (BER = 10^{-6}) at any pixel of the imaging receiver, the optical receiver informs the controller to consider this light unit to transmit data, else switch OFF this RYGB LDs-light unit illumination only. The feedback signal can be a low data rate infrared channel such as the one; we considered [130]. In addition, if this RYGB light unit is used for data communication, the SCM tone identification system informs the combiner (see Figure 5.2) of the pixel(s) that viewed this RYGB LDs-light unit. Accordingly, the combiner selects the pixel(s) of the imaging receiver that have a good connection with the light units and excludes the other pixels. The signal to interference to noise ratio (SINR) was used to evaluate the performance of the data channels. Thus, the 13.6 dB was chosen, which gives BER = 10^{-6} for OOK modulation.

5.3.2 Performance analysis of the proposed VLC system

To calculate the maximum data rate that can be sent through each light unit of the active RYGB LDs-light units, the ISI due to multipath dispersion of the data signal should be obtained. The delay spread (D) associated with a given impulse response can be given as [148]:

$$D = \sqrt{\frac{\sum (t_i - \mu)^2 \, P_{ri}^2}{\sum P_{ri}^2}} \tag{5.22}$$

here t_i, P_{ri} and μ are the delay time, the received optical power and the mean delay, respectively. The mean delay is given as:

$$\mu = \frac{\sum t_i \, P_{ri}^2}{\sum P_{ri}^2} \tag{5.23}$$

When using the OOK technique, the relationship between the BER and the $SINR$ is given as [127]:

$$BER = Q\left(\sqrt{SINR}\right) \tag{5.24}$$

here $Q(x) = \frac{\int_x^\infty e^{-z^2/2} \, dz}{\sqrt{2\pi}}$. The $SINR$ can be expressed as [127], [149]:

$$SINR = \frac{R^2 (P_{s1} - P_{s0})^2}{{\sigma_{dt}}^2 + I} \tag{5.25}$$

where P_{s1} and P_{s0} are the received powers of logic 1, and logic 0, respectively and σ_{dt} is the total noise related with the received data. It should be noted that to calculate σ_{dt}, we considered the receiver bandwidth, which is 4 GHz. The received power related with logic 1, (P_{s1}) and logic 0 (P_{s0}) can determined from the transmitted signal and the channel impulse response. In some locations of the optical receiver, more than one pixels views the same light unit. In this case, an MRC scheme was used to calculate the $SINR$ as:

$$SINR_{MRC} = \sum_{i=1}^{J} \left(\frac{R^2 (P_{s1i} - P_{s0i})^2}{{\sigma_{dti}}^2 + I_i} \right) \tag{5.26}$$

here J is the number of pixels that see the same light unit.

5.4 Simulation Results

The performance of our VLC system in room A (empty room) and the room B (realistic room) was assessed. A simulation tool similar to the one we reported in [77], [76], [150], [151], [152] was used. A MATLAB program is utilized to get the results in this paper. The performance of our VLC system was examined at many places on rooms' communication floor. For room A, the results were obtained when the mobile user moved at x = 1 m and x = 2 m and along the y-axis. This is attributed to the symmetry of room A. For room B, however, the results were evaluated at x = 1 m, x = 2 m and x = 3 m and along the y-axis. Table 5.2 shows the simulation parameters that were used in this chapter.

Table 5.2: Simulation parameters.

Parameters	Configurations	
Rooms		
Room's length (x)	8 m	
Room's width (y)	4 m	
Room's height (z)	3 m	
ρ-xz Wall	0.8	
ρ-yz Wall	0.8	
ρ-xz op. Wall	0.8	
ρ-yz op. Wall	0.8	
ρ-Floor	0.3	
ρ-Windows	0	
ρ-Bookshelves	0.4	
Number of Bounces	1	2
Surface elements' number	32000	2000
d_A	5 cm × 5 cm	20 cm × 20 cm
Lambertian emission order (n)	1	
Semi-angle	60°	
Light units		
Number of transmitters	8	
Places (x, y, z) m	(1, 1, 3), (1, 3, 3), (1, 5, 3), (1, 7, 3), (3, 1, 3), (3, 3, 3), (3, 5, 3), (3, 7, 3)	
RYGB LDs per unit	9 (3 × 3)	
Interval between RYGB LDs	0.03 m	
Optical power/RYGB LD	1.9 W	
Centre luminous intensity	162 cd	
Lambertian emission order (n)	0.65	
Semi-angle	70°	
Receiver		
Number of receivers	1	
Concentrator entrance area	$\frac{9\pi}{4}$ cm^2	
Concentrator refractive index	1.7	
Concentrator acceptance angle	65°	
Receiver's area	2 cm^2	
Number of pixels	288	
Pixel's area	0.694 mm^2	
Responsivity	0.4 A/W	
Receiver's bandwidth	4 GHz	

The RYGB LDs-light units delay spread when the optical receiver was located along the *y*-axis and at x = 1 m and x = 2 m in room A is shown in Table 5.3. It is worthy o know that the delay spread is affected by the delay time and the optical received power of the rays (see equation 5.22). Thus, at each place of the imaging receiver, the RYGB LDs-light units near the receiver have delay spread lower than the further one as shown in Table 5.3.

Table 5.3: Delay spread of each RYGB LDs-light unit when the imaging receiver was placed at many locations in room A.

RYGB LDs-Light units	**Delay spread (ns)**													
	Receiver locations (m)							**Receiver locations (m)**						
	1,1,1	**1,2,1**	**1,3,1**	**1,4,1**	**1,5,1**	**1,6,1**	**1,7,1**	**2,1,1**	**2,2,1**	**2,3,1**	**2,4,1**	**2,5,1**	**2,6,1**	**2,7,1**
Transmitter 1	0.021	0.027	0.054	0.4	0.7	4.2	4.4	0.05	0.053	0.41	0.52	3.1	3.1	3.2
Transmitter 2	0.063	1.65	1.9	2.8	4.4	4.8	5.1	0.051	0.052	0.4	0.52	1.03	2.9	3.3
Transmitter 3	0.05	0.028	0.022	0.035	0.05	0.08	0.4	0.41	0.05	0.03	0.031	0.49	0.08	1.2
Transmitter 4	1.57	2.11	0.04	2.1	1.7	1.8	2.1	0.41	0.05	0.03	0.031	0.47	0.081	1.3
Transmitter 5	0.3	0.08	0.051	0.033	0.021	0.028	0.05	1.2	0.08	0.5	0.031	0.029	0.05	0.41
Transmitter 6	2.1	1.8	1.6	2.2	0.04	2	1.6	1.3	0.081	0.48	0.031	0.03	0.05	0.4
Transmitter 7	4.5	4.1	0.6	2.8	0.053	0.027	0.021	3.1	2.9	1.06	0.51	0.3	0.05	0.048
Transmitter 8	5.2	4.8	4.5	0.39	2.1	1.7	0.06	3.2	2.9	1.06	0.52	0.41	0.049	0.045

Table 5.4 shows the active RYGB LDs-light units that were utilized to convey the data and the maximum data rate of each active unit (data rate that can be transmitted with SINR = 13.6 dB, BER = 10^{-6}) when the optical receiver was placed at the corner (1 m, 1 m, 1 m) and the centre (2 m, 4 m 1 m) of room A. It should be noted that the performance of each active light unit was obtained based on the channel dc gain, level of CCI due to other light units, and ISI due to diffusing reflections. As can be seen, three RYGB LDs-light units (unit 1, unit 2 and unit 3) were used to carry the data when the optical receiver was located at the corner of room A, whereas four units (unit 3, unit 4, unit 5 and unit 6) were utilized to send the data when the receiver was placed at the centre of room A. This is related to the poor performance of other light units (light units that were used for lighting only). In other words, the levels of the CCI and the ISI were high for these light units. In addition, it can be seen that when the optical receiver was placed at the room center, all active units

sent a different data stream at the same rate, and this is attributed to the symmetry of room A (see Figure 5.1 (a)).

Table 5.4: Active RYGB LDs-light units conveying data when the receiver was located at (1 m, 1 m, 1 m) and at (2 m, 4 m 1 m) in room A.

Receiver is located at room corner (1 m, 1 m, 1 m)			**Receiver is located at room center (2 m, 4 m, 1 m)**		
RYGB LDs-light units	**Status**	**Data rate (Gb/s)**	**RYGB LDs-light units**	**Status**	**Data rate (Gb/s)**
Transmitter 1	ON	4	Transmitter 1	OFF	-
Transmitter 2	ON	2.4	Transmitter 2	OFF	-
Transmitter 3	ON	1.75	Transmitter 3	ON	2.42
Transmitter 4	OFF	-	Transmitter 4	ON	2.42
Transmitter 5	OFF	-	Transmitter 5	ON	2.42
Transmitter 6	OFF	-	Transmitter 6	ON	2.42
Transmitter 7	OFF	-	Transmitter 7	OFF	-
Transmitter 8	OFF	-	Transmitter 8	OFF	-

Figure 5.7 illustrates the aggregate data rate of our VLC system when the receiver is placed at many positions on the communication floor of room A at x = 1 m and x = 2 m and along the y-axis. The aggregate data rate was obtained at BER = 10^{-6} (SINR = 13.6 dB) for the received data for each active RYGB LDs-light unit. As can be seen, the minimum aggregate data rate (8.05 Gb/s) was achieved when the optical receiver is placed at the corner of room A (1 m, 1 m, 1 m). This is due to some of light units being out of the FOV of the imaging receiver at this place. The maximum aggregate data rate (8.95 Gb/s) was obtained when the optical receiver was positioned at the room centre (2 m, 4 m, 1 m), and this is attributed to the imaging receiver being able to view more transmitters with good performance (low CCI level and low ISI) at this location. The maximum data rate transmitted through each active RYGB LDs-light unit not exceed the data rate supported by each the pixel of the imaging receiver.

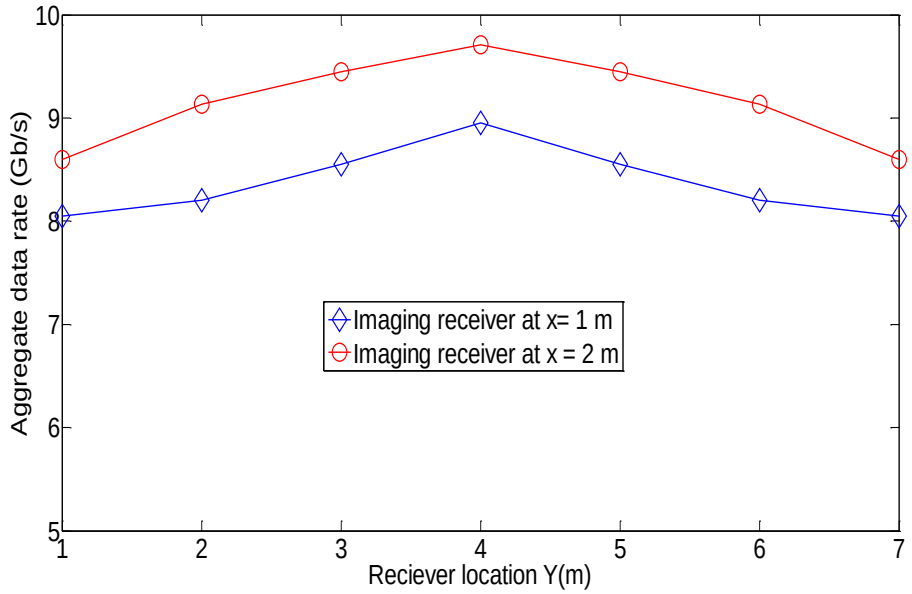

Figure 5-7: An aggregate data rate of the proposed indoor system at different locations of the optical receiver in room A with BER = 10-6 (SINR = 13.6 dB).

In order to consider the obstacles effect on our proposed VLC system, we extended the analysis to room B (the realistic room). In room B, we account for the effects of signal blockage, due to small cubicles, a door, windows, and furniture and multipath propagation (see Figure 5.1 (b)). Due to the asymmetry of room B, the mobile receiver was considered to be at different places on lines x = 1 m, x = 2 m and x = 3 m along the y-axis.

The aggregate data rates of the system when the mobile receiver is located at many places along the y-axis at x = 1 m, x = 2 m and x = 3 m in room B are shown in Figure 5.8. In general, the performance of the system was better when the mobile receiver moved along x = 2 m. This is because of the optical receiver viewing more light units along the x = 2 m when compared with x = 1 m and x = 3 m. As can be seen, the aggregate data rate along x = 1 m was better than the aggregate data rate along x = 3 m. As along x = 1 m, the nearest walls (x = 0 and y = 0) to the receiver are windows, which have zero reflection coefficients; whereas, along x = 3 m, the nearest walls (wall x = 4 m and wall y = 8 m) to the receiver are covered by bookshelves, which have reflection coefficients of 0.4. Therefore, the CCI level and ISI due to reflection components were higher along x = 3 m compared with x = 1 m, which led to a decrease in the aggregate data rate along x = 3 m.

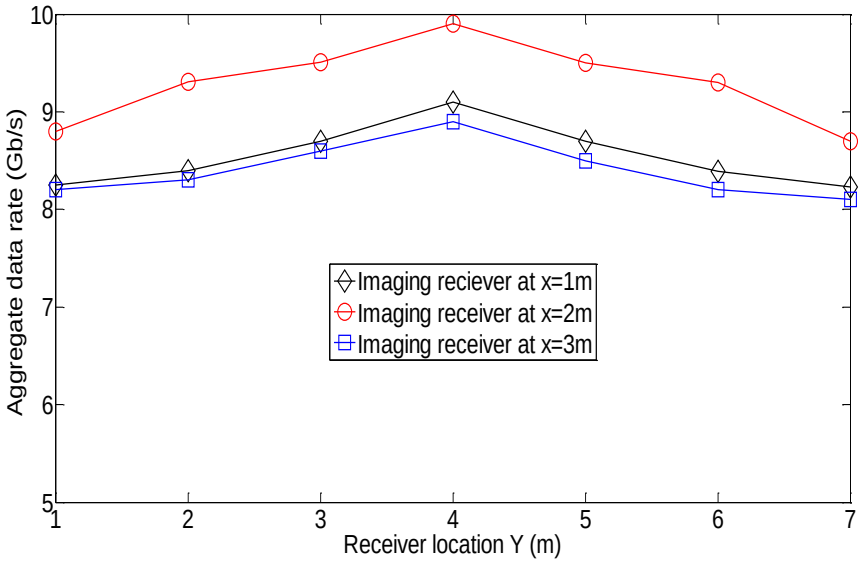

Figure 5-8: Aggregate data rate of the proposed indoor VLC system at different locations of the optical receiver in room B with BER = 10^{-6} (SINR = 13.6 dB).

5.5 Summary

In this chapter, we introduced an indoor VLC system that can offer a data rate of 8 Gb/s with BER = 10^{-6} (SINR = 13.6 dB) when using simple OOK modulation. The system used parallel data transmission sent from multiple RYGB LDs-light units, which are installed on the room's ceiling to get a suitable level of lighting. An imaging receiver was used in this work to benefit from spatial multiplexing and to mitigate the effect of the ISI. SCM tones were proposed in this chapter to identify each RYGB LDs-light unit and to find the pixel(s) that received the signals from these light units. Additionally, these tones were used to calculate the CCI level between the transmitters. Based on the performance (CCI level and ISI) of each RYGB LDs-light unit, serial data were divided (only) between the light units that were able to send a high data rate with a strong connection. Our proposed system was investigated in two different rooms (empty and realistic rooms) with considering the effect of the CCI and diffusing reflections (up to second order).

6. WDM for High Data Rate Indoor VLC Systems

6.1 Introduction

Due to using RYGB LDs as sources of illumination and data communication, each colour of the RYGB LDs can be used to carry a different data. Thus, in this chapter we used wavelength division multiplexing (WDM) to achieve a high data rate for indoor VLC systems. We proposed two VLC systems based on WDM: a single user VLC system and a multiuser VLC system.

In the single user VLC system, an imaging diversity receiver (IMDR) is used as an optical receiver. Based on the location of the IMDR, each colour of the RYGB LDs sends a different data stream at a different rate. Each pixel of the IMDR is covered by a specific colour optical filter. In this chapter, a multispectral colour filter array (MCFA) is assumed to design the pattern of the array colour filters of the IMDR.

WDM has been widely investigated in indoor VLC systems. A data rate of 2.3 Gb/s was demonstrated over a distance of 30 cm by using WDM with orthogonal frequency division multiplexing (OFDM) [63]. A three colours LED based WDM-VLC system was investigated with carrier-less amplitude and phase (CAP) modulation and adaptive equalization to achieve an aggregate data rate of 4.5 Gb/s. This data rate was obtained over 1.5 m with bit error rate (BER) of 3.8×10^{-3}, and consideration was given to use forward error correction (FEC) codes [64]. Commercial multicolour (RYGB) LEDs were used with discrete multi-tone (DMT) modulation to achieve an offline aggregate data rate of 5.6 Gb/s at BER = 3.8×10^{-3} [65]. A four channel WDM system with CAP modulation and hybrid post-equalizer was investigated experimentally obtaining a data rate of 8 Gb/s with BER = 3.8×10^{-3} [66]. A VLC system based WDM was reported using commercial red LEDs, custom green LEDs and micro LEDs. It achieved a data rate of 11.28 Gb/s over 1.5 m [67].

Resource allocation is one of the challenges that face VLC systems to realise high data rate multiuser. This is due to use of many transmitters in VLC systems to obtain an acceptable illumination level that meets the lighting demands. The overlap in coverage between the multiple transmitters is therefore very high [153]. Furthermore, the communication area (size of the cell) in VLC systems changes based on the illumination level provided, which means that the multiple VLC transmitters in the room are usually treated as one source of information/transmitter [154]. In addition, IM/DD are the most preferred modulation technique in VLC systems. Therefore, transmitting many signals through overlapping multiple transmitters increases interference from undesired transmitters [153]. Thus, we propose the SCM tones, which are unmodulated signals, to identify each light unit, to find the optimum light unit for each user and to calculate the level of the CCI. SCM tones studied in indoor optical wireless communication systems for a range of applications [142], [143], [155]. In [142], the SCM tones were utilized to find the crosstalk level between WDM channels while in [143], the SCM tones were utilized to design an indoor VLC positioning system. The work [155] introduced SCM tones for parallel data transmission in an indoor VLC system where the SCM tones were utilized to match each light unit with the pixel(s) of an imaging receiver as well as to calculate the CCI level. At the beginning of the connection, one colour of the RYGB LDs light unit (green colour here) sends the SCM tones to set up the connection between the light units and the users (to find the optimum light unit for each user). After identifying the optimum light unit for each user, data is transmitted in parallel through RYGB LDs. We used WDM in multiuser VLC system to attain a high data rate for each user. To evaluate the performance of the multiuser VLC system, we proposed two types of receivers: an array of non-imaging receivers (NI-R) and an array of non-imaging angle diversity receivers (NI-ADR).

Many approaches have been proposed to provide multi-user communication in VLC systems. One of these is to use multiple input single output (MISO) and multiple input multiple output (MIMO) techniques with zero-forcing (ZF) precoding schemes to reduce the effects of co-channel interference (CCI) between transmitters [156], [157], [158]. Other approached utilize multiple access dimensions to support multi-user communication in VLC

systems. The methods investigated include code division multiple access (CDMA) [159], non-orthogonal multiple access (NOMA) [160], [161] and expurgated pulse position modulation (EPPM) [161]. A range of resource allocation methods were also developed for multi-user communication in VLC systems [162], [163], [152].

In this chapter, the effects of multipath propagation and mobility on the performance of the single user VLC system are taken into account. The results showed that our proposed system achieved an aggregate data rate of 10 Gb/s with BER = 10^{-6} by using a simple OOK. In addition, the effect of the CCI on the performance of the multiuser VLC system is considered. The results showed that the multiuser VLC system has the ability to serve many users simultaneously with a good communication link.

6.2 Room Configuration

Figure 6.1 shows the assumed room that was used to build the simulation for the single user VLC system and the multiuser VLC system. We used an empty room that has neither doors nor windows similar to the one that presented in Chapter 5. We also used the ray tracing algorithm to simulate the indoor channel of the VLC system in a similar way to that directed in Chapter 3.

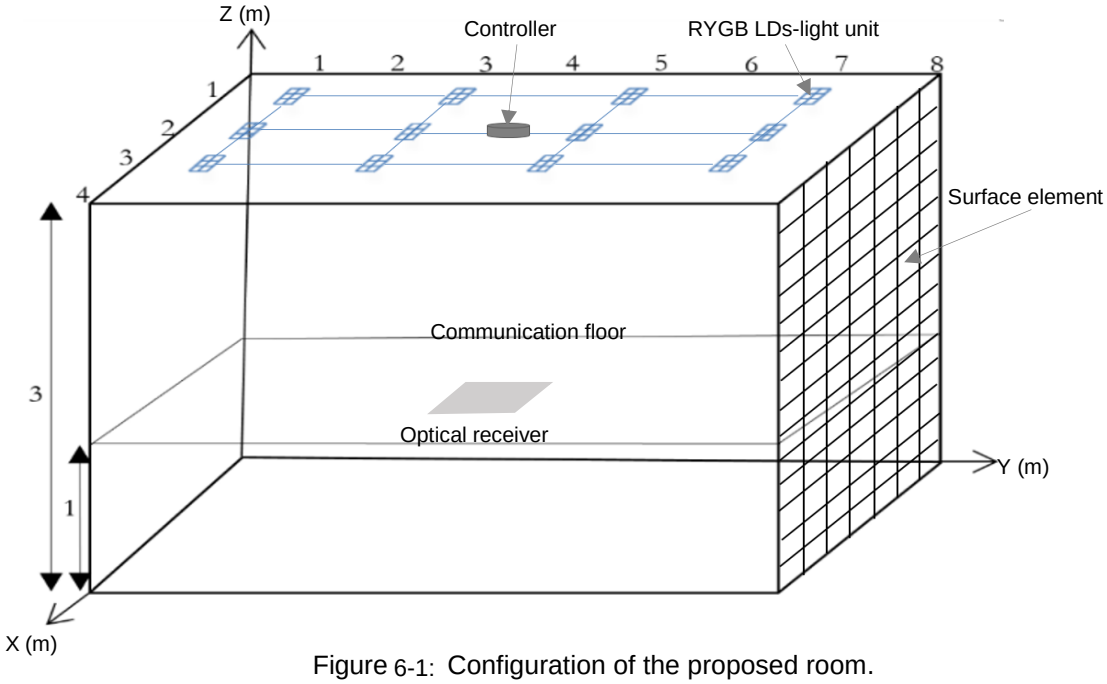

Figure 6-1: Configuration of the proposed room.

In this Chapter, twelve RYGB LDs-light units were installed on the ceiling (see Figure 6.1) to achieve acceptable lighting level inside the room which met the ISO and European illumination requirements [108], which is not less than 300 lx at any location on the communication floor of the room (see Figure 6.2). Each RYGB LDs-light unit has 6 RYGB LDs (2 × 3) with a separation of 2 cm. The coordinates of the RYGB-LDs light units were (1 m, 1 m, 3 m), (1 m, 3 m, 3 m), (1 m, 5 m, 3 m), (1 m, 7 m, 3 m), (2 m, 1 m, 3 m), (2 m, 3 m, 3 m), (2 m, 5 m, 3 m), (2 m, 7 m, 3 m), (3 m, 1 m, 3 m), (3 m, 3 m, 3 m), (3 m, 5 m, 3 m) and (3 m, 7 m, 3 m) as shown in Figure 6.1.

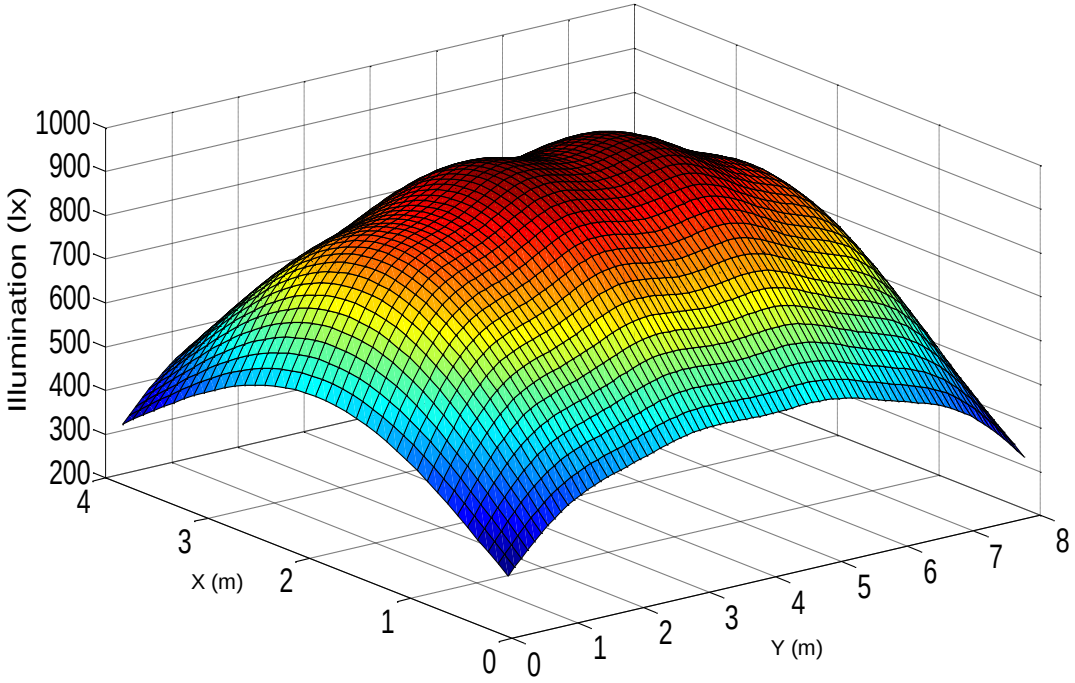

Figure 6-2: The distribution of illumination on the communication floor.

6.3 Design of the Single User VLC System

In the single user VLC system, each colour of the RYGB LDs transmits a different data stream as shown in Figure 6.3.

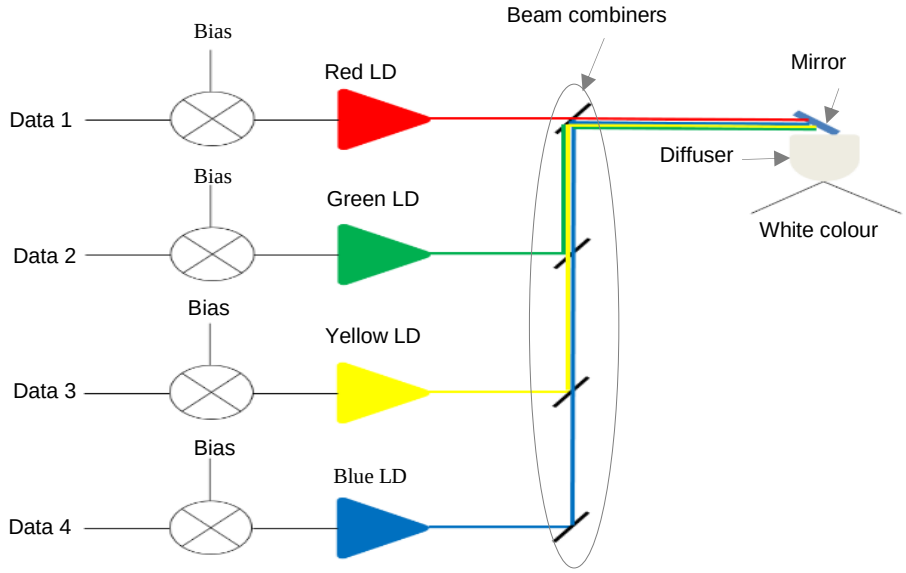

Figure 6-3: Configuration of the RYGB LDs for the single VLC system.

The IMDR is proposed for the single user VLC system as an optical receiver. The IMDR is a combination of imaging receiver and diversity receiver [150]. Many advantages can be obtained when the IMDR is used compared with a single photodetector. These benefits are: 1) a large number of photodetectors will be shared with one concentrator, 2) each pixel has small FOV, which leads to receiving a limited range of light rays; hence, decreasing the effect of ISI and 3) each pixel is treated as a single photodetector able to receive an optical signal and convert it to an electrical signal [103], [126]. In this system, we proposed IMDR that has three photodetector faces as shown in Figure 6.4. Each side of the IMDR has two-dimensional pixels array segmented into *J* equal-sized rectangular-shaped pixels with no gaps between them as shown in Figure 6.4. Therefore, under most situations, the optical signal will fall on up to four pixels. Besides that, the area of each pixel in each photodetector side of the IMDR is equal to the area of that photodetector divided by the number of the pixels. Each side of the IMDR was oriented to a different direction. To find the direction of each side in the IMDR, two angles were used: azimuth (*Az*) and elevation (*El*). The *Az* is the photodetector's angle alignment. It was fixed at 0^{o} for the side facing up and 90^{o} and 270^{o} for each of the other sides of the IMDR. Whereas the *El* of the IMDR face up was fixed at 90^{o}, the *El* of the two sides were chosen to be 30^{o}. Each face of the IMDR has a lens (see Figure 6.4), which is used as a concentrator to project

and concentrate the incident light from a large area down to the smaller detector area. In this system, for the analysis of the IMDR, we used the lens that was used in [103]. This lens has an entrance aperture diameter equal to 3 cm, which gives an entrance area equal to $A = \frac{9\pi}{4}$ cm^2 and an exit area equal to $A' = \frac{Asin^2(\psi)}{N^2}$, where N is the refractive index and ψ is the acceptance angle of the lens (ψ < 90^o). The acceptance angle (ψ) of the lens was set at 65^o for the side facing up and 40^o for each of the other sides of the IMDR as shown in Figure 6.4. It should be noted that all three lenses that were used in the IMDR have the same entrance area. Moreover, the area of each face of the IMDR was selected to be equal to its lens's exit area. Thus, the photosensitive area of the IMDR face up is 2 cm^2 and the photosensitive area of each side of the IMDR is 1 cm^2. In addition, the side that faces up of the IMDR has 288 pixels (12 × 24), while each side of the IMDR has 144 pixels (12 × 12).

The IMDR characteristics (*Az*, *El* and FOV) were chosen follows. For the IMDR side that faces up, the values of the *Az*, *El* and FOV were selected to enable it to see the whole ceiling when the IMDR is located at the centre of the room, hence; it receives power from all RYGB LDs-light units installed on the ceiling. However, when the IMDR is placed at the corner of the room, some of the pixels of the IMDR that faces up will see the walls and consequently, some of the RYGB LDs-light units will be out of the view of the side of the IMDR that faces up. Therefore, the values of the *Az*, *El*, and FOV of each side of the IMDR were chosen to enable the IMDR to see some of the RYGB LDs-light units that cannot be seen by the side of the IMDR that faces up when the IMDR starts to move to the room corner.

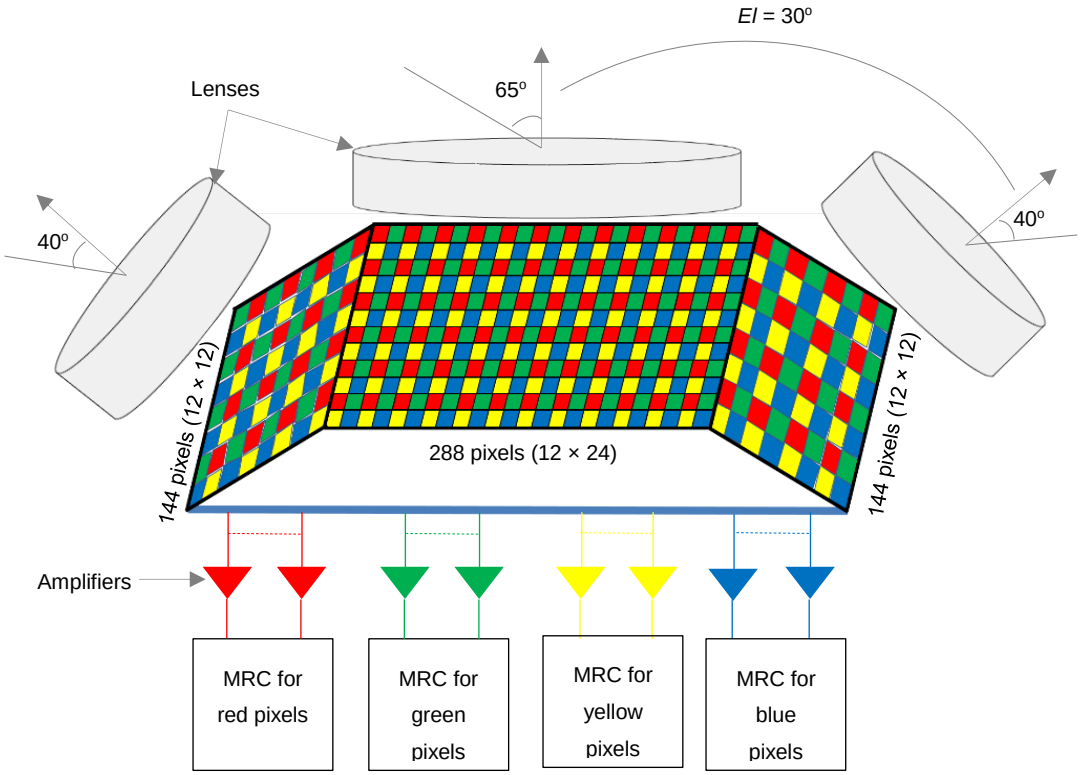

Figure 6-4: Structure of the IMDR receiver.

Each pixel of the IMDR was covered by a colour optical filter, hence; each pixel senses a specific colour. Due to the use of a large number of pixels in each face of the IMDR, MCFA was used. It offers many benefits like low cost and robustness against interference [164], [165]. Due to the data being carried on four channels (four colours, RYGB), we used four colour bands in the MCFA as shown in Figure 6.4. Each group of four adjacent pixels of each side in the IMDR was covered by the four colour bands of the MCFA as shown in Figure 6.4. This is due to the fact that the shape of the pixel of the IMDR is rectangular, hence; the optical signal will fall on no more than four pixels, which consequently ensures that the IMDR will always receive data from all colours at all possible locations of the IMDR on the communication floor of the room. In addition, this distribution of the MCFA was selected to ensure that the IMDR will receive data from all channels at all possible locations in our proposed room. It should be noted that the transmission factor of the filters was assumed to be equal to 1. Additionally, in the IMDR, each pixel amplifies the received signal separately, thus; several possible diversity schemes could be considered: SB, EGC and MRC. MRC (which produces the best results among

the three schemes) was used for each group of pixels that have the same colour filter in the IMDR as shown in Figure 6.4. In our analysis, the IMDR was located 1 m above the floor, which represents the communication floor as shown in Figure 6.1.

6.4 Simulation Results of the Single User VLC System

We investigated the performance of the single VLC system in an empty room. In this system, we used a simulation tool similar to that in [93]. The simulation tool was used to obtain the impulse response and consequently, derive the SNR and calculate the BER. In this system, a MATLAB program was used to obtain the results. To ensure that the system will achieve the certain data rate at all possible locations of the receiver on the communication floor of the room, the results were obtained when the receiver moves along the *x*-axis and the *y*-axis in steps of 0.5 m. However, due to the symmetry of the room, the performance was investigated when the receiver moved along the *y*-axis and at x = 0.5 m, x = 1 m, x = 1.5 m and x = 2 m. In addition, the effect of the diffuse reflections (reflections up to second order), which degrade the performance of the indoor VLC system, was taken into account in this system. In order to obtain a high data rate for an indoor VLC system, the SNR should be high. In the single user VLC system, the OOK modulation was used. The MRC schem was used for each group of pixels that was covered by the same colour.

Figure 6.5 (a), Figure 6.5 (b), Figure 6.5 (c) and Figure 6.5 (d) shows the data rate of the VLC system when the IMDR moved in a step of 0.5 m along the *y*-axis and at x = 0.5 m, x = 1 m, x = 1.5 m and x = 2 m. It should be noted that the data rate of each colour (channel) was obtained when the BER = 10^{-6} (SNR = 13.6 dB). It can be seen that the minimum aggregate data rate of the proposed system was equal to 10.18 Gb/s when the IMDR was located at the corner of the room (0.5 m, 0.5 m, 1m). However, the aggregate data rate increased slightly when the IMDR moved to the room centre because the IMDR exposed to more transmitters when it moves to the room centre. It is worthy of mention that many factors affected the achieved data rate of our

proposed system such as how many transmitters were seen by the IMDR at its location. In addition, another factor is the distance between the IMDR and the transmitters that were seen by the IMDR. Besides that, the ISI between logic 1 and logic 0 was considered in this system; hence, the power received due to reflection components varied with the IMDR locations. Thus, at some locations of the IMDR (typically when the IMDR was located near to the walls of the room) the received power from the reflection components (first and second reflections) is high, which affects the performance of the systems at high data rates. As can be seen from Figure 6.5, the data rate of each channel fluctuated when the IMDR moved on the communication floor of the room. This is due to each group of pixels that has the same colour filters seeing a different number of transmitters at each location of the IMDR.

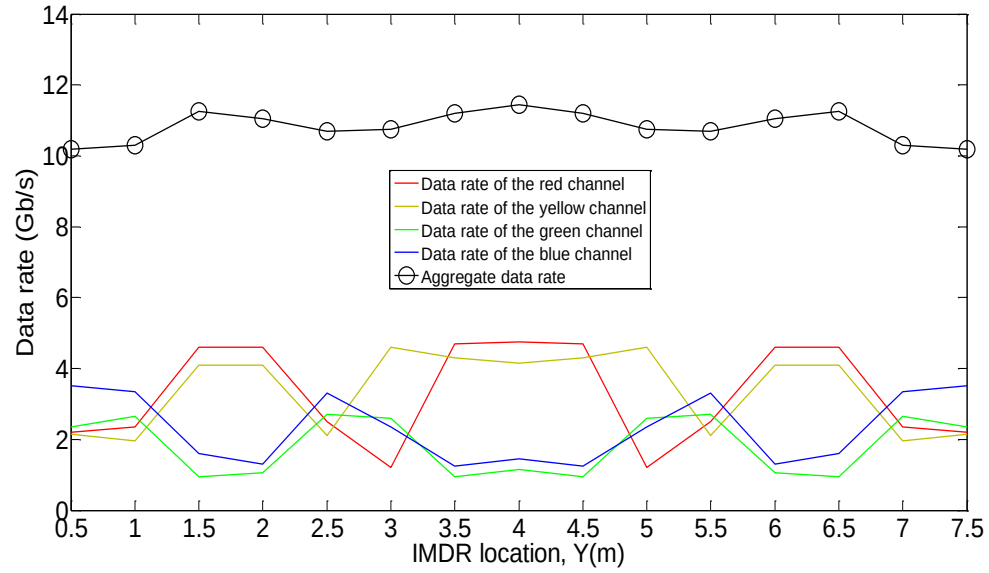

(a)

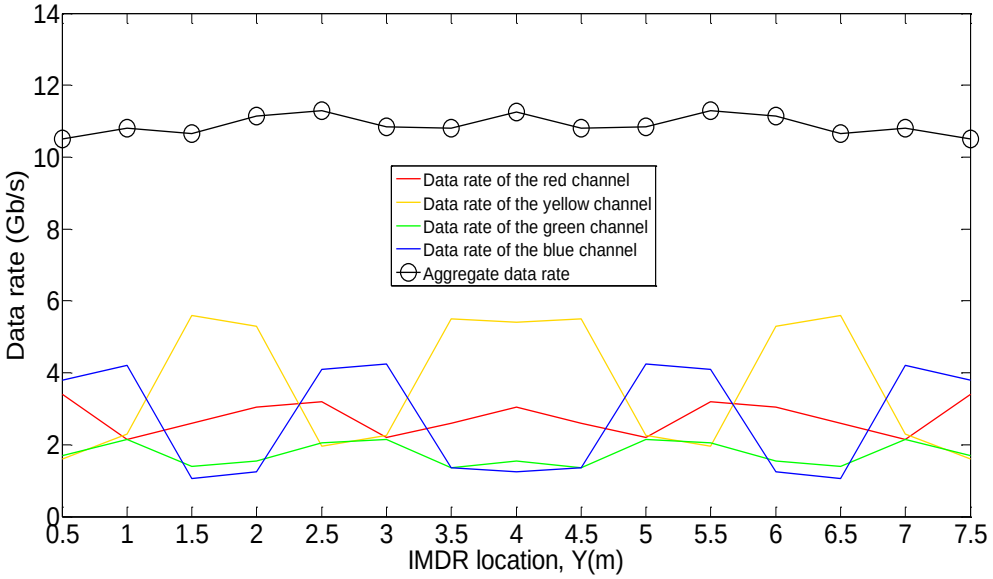

(b)

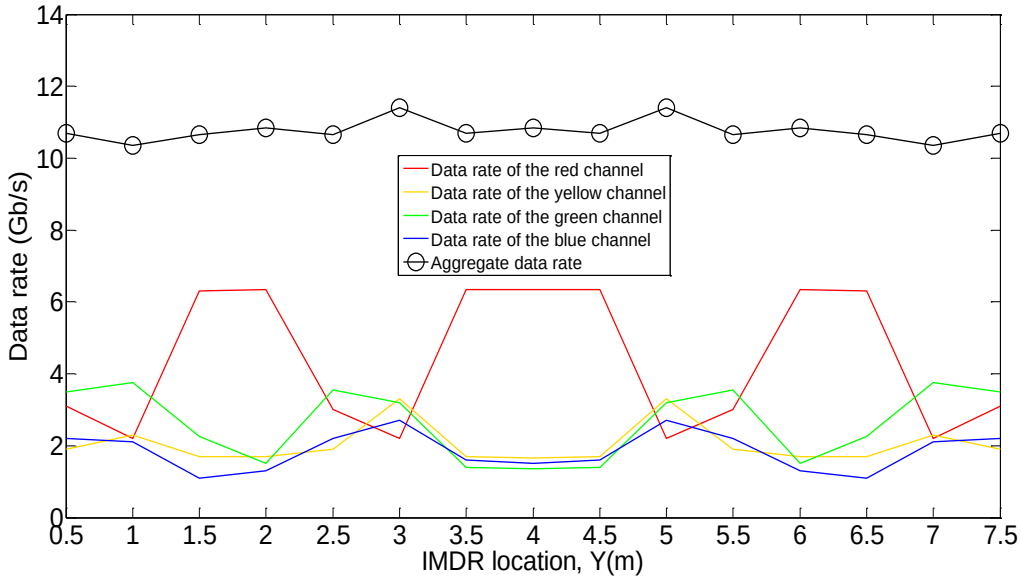

(c)

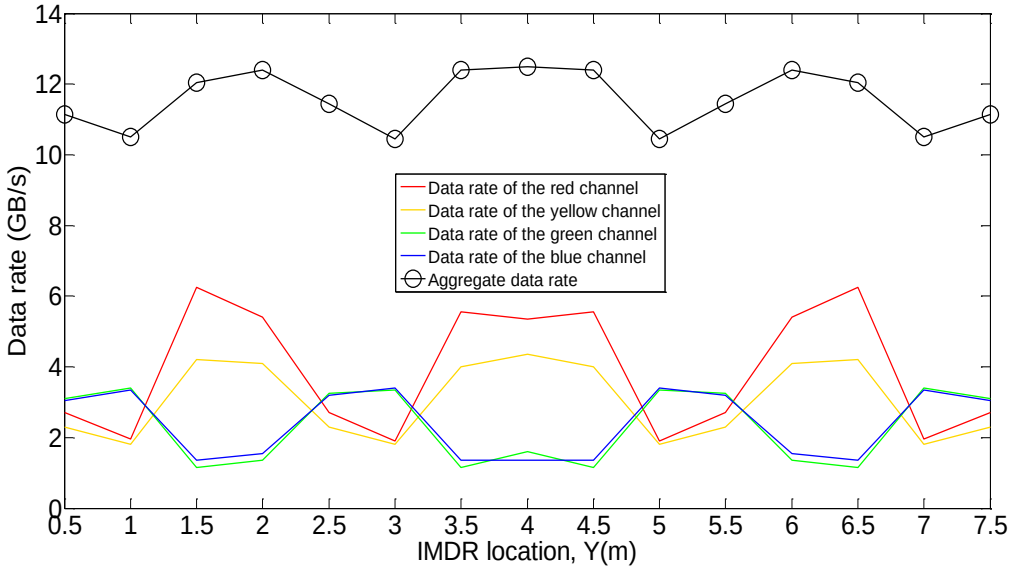

(d)

Figure 6-5: Achieved data rate when the IMDR moves along y-axis and at (a) x = 0.5 m, (b) x = 1 m, (c) x = 1.5 m and (d) x = 2 m (SNR = 13.6 dB and BER = 10^{-6}).

6.5 Design of the Multiuser User VLC System

In this section, we used WDM in conjunction with SCM tones to obtian a high data rate multi-user indoor VLC system where the spatial domain and the relatively high directivity of optical signals are also exploited by assigning a light unit to each user. We used SCM tones to recognise each light unit, to find the best light unit for each user and to calculate the level of the CCI. At the beginning of the connection, one colour of the RYGB LDs light unit (green

colour here) sends the SCM tones to set up the connection between the light units and the users. After identifying the optimum light unit for each user, the data is transmitted in parallel through RYGB LDs. Figure 6.6 shows the configuration of the RYGB LDs for multiuser VLC system.

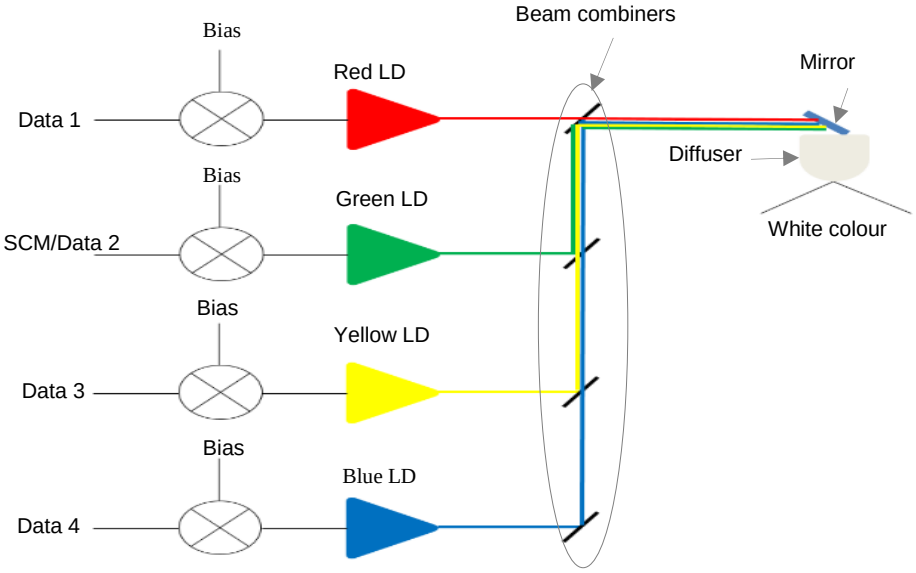

Figure 6-6: RYGB LDs configuration for the multiuser VLC system.

6.5.1 Multiuser VLC system's receivers design

Two types of receivers are proposed in the multiuser VLC system: the NI-R and the NI-ADR receivers as shown in Figure 6.7 (a) and Figure 6.7 (b). In the NI-R, an array (2 × 2) of photodetectors is used. Each photodetector has an area equal to 6.25 mm^2 and a FOV of 40^o. The area of each photodetector in the NI-R is selected to enable each photodetector to work at a high data rate while gathering a significant optical power. Calculations of the bandwidth of the photodetector can be found in [79]. The FOV of each photodetector is chosen to ensure that the NI-R sees at least one light unit at any location of the optical receiver on the communication floor. As shown in Figure 6.7 (a), each photodetector is covered with a different optical filter. Hence, each photodetector responds to a specific wavelength. Due to the use of four colours LDs as sources of illumination and data communication, four colours optical filters (red, yellow, green and blue) are used as shown in Figure 6.7 (a). The green colour is used to send the SCM tones at the beginning of the connection, although any other colour can be used. Thus, at the beginning of

the connection, the output of the green photodetector enters to the SCM tone identification system to set up the connection. When each user is assigned to its optimum light unit, the output of the green colour enters to the parallel to serial (P/S) converter, as this colour is then used to send a data stream as shown in Figure 6.7 (a).

To reduce the effect of CCI and the multipath reflections on the performance of our proposed system, the NI-ADR is introduced. This NI-ADR has seven faces (1 – 7) and each face consists of an array of four photodetectors (2 × 2) with an area of 4 mm^2 for each photodetector as shown in Figure 6.7 (b). Each photodetector is covered by a different optical filter and consequently, each photodetector senses a different wavelength. To determine the orientation of each branch in the NI-ADR, two angles are used: azimuth (A_z) and elevation (El). The El angle of the first face is selected to be equal to 90º, while the other six branches are given an El of 50º. The A_z angle is defined as the orientation of the branch's angle. The A_z angles of the seven faces are fixed at 0º, 0º, 60º, 120º, 180º, 240º and 300º. In addition, the FOV of each photodetector is selected to be 20º. It should be noted that the parameters of the NI-ADR (A_z, El and FOV) are chosen to ensure that the NI-ADR is able to see at least one transmitter at any location of the optical receiver on the communication floor of the room following an optimisation similar to that in [98]. Each photodetector in each face of the NI-ADR amplifies the received signal separately; therefore, many possible diversity schemes can be used: SB scheme, EGC scheme and MRC scheme. We used SB for the photodetectors that covered by the same colour filters as shown in Figure 6.7 (b).

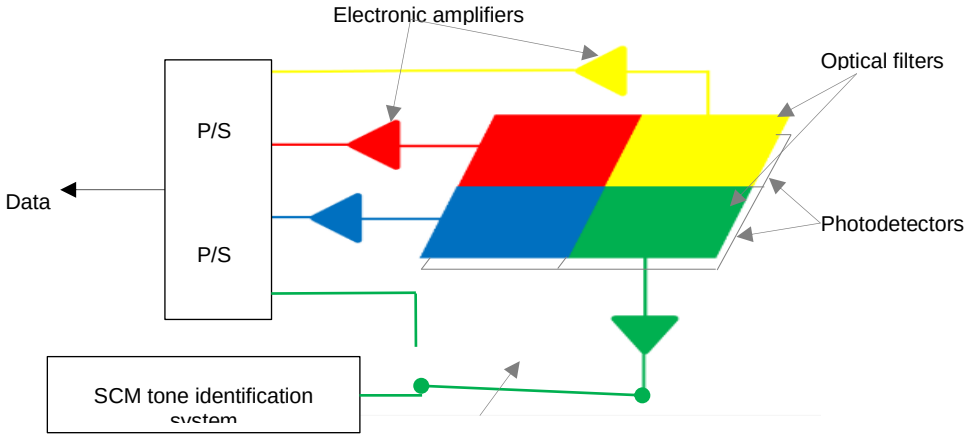

(a)

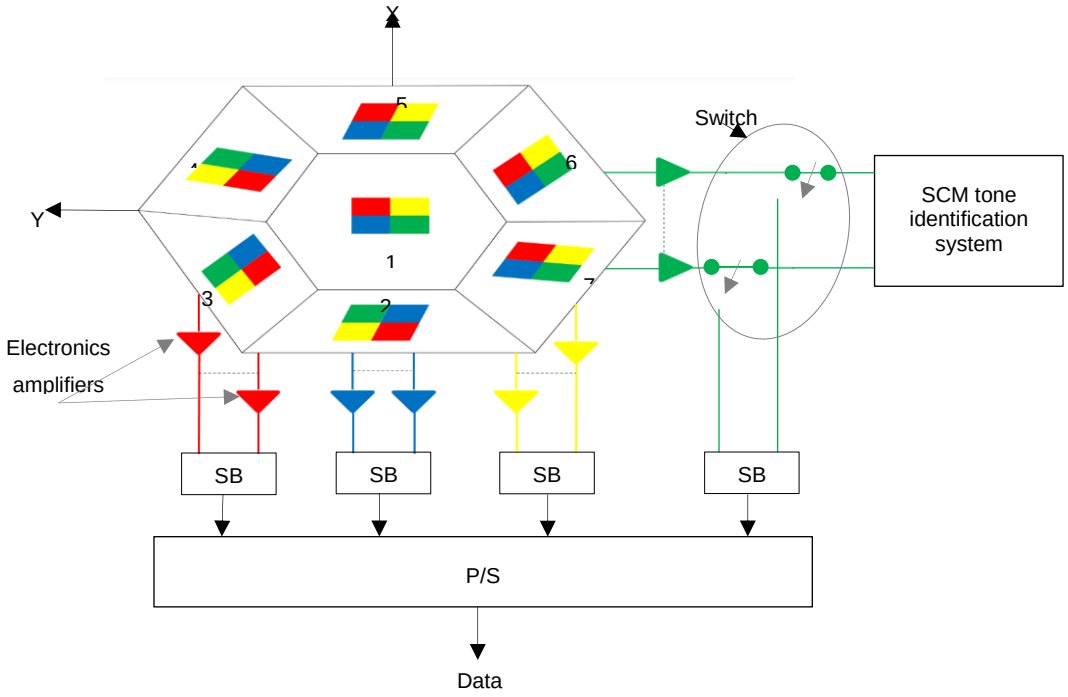

(b)

Figure 6-7: Multiuser VLC system's receiver structures: (a) NI-R configuration and (b) NI-ADR configuration.

Table 6.1 summaries the parameters of the transmitters and receivers.

Table 6.1: Parameters of the transmitters and receivers of the multiuser VLC system.

Parameters	Configurations
Transmitters (RYGB LDs-light units)	
Number of transmitters	12
Transmitters/light units locations(x, y, z) m	(1, 1, 3), (1, 3, 3), (1, 5, 3),(1, 7, 3), (2, 1, 3), (2, 3, 3), (2, 5, 3), (2, 7, 3), (3, 1, 3), (3, 3, 3), (3, 5, 3), (3, 7, 3)
Number of RYGB LDs per unit	6 (2 × 3)
RYGB LDs interval	0.02 m
Optical power of R LD	0.8 W
Optical power of Y LD	0.5 W
Optical power of G LD	0.3 W
Optical power of B LD	0.3 W
Total centre luminous intensity	162 cd
Lambertian emission order (n)	0.65
Semi-angle at half power	70°
NI-R	
Number of photodetectors	4
FOV of each photodetector	40°
Elevation of each photodetector	90°
Azimuth of each photodetector	0°
Photodetector's area	6.25 mm^2
Photodetector's responsivity (red)	0.4
Photodetector's responsivity (yellow)	0.35
Photodetector's responsivity (green)	0.3
Photodetector's responsivity (blue)	0.2
Receiver's bandwidth	0.5 GHz
NI-ADR	
Number of branches	7
Number of photodetectors/branch	4
FOV of each photodetector	20°
Elevation of each branch	90°, 50°, 50°, 50°, 50°, 50°, 50°
Azimuth of each branch	0°, 0°, 60°, 120°, 180°, 240° 300°
Photodetector's area	4 mm^2
Receiver's bandwidth	0.75 Hz

6.5.2 System description

In the multi-user scenario, interference happens when multiple signals from the interfering light units land on the optical receiver. The interference is occurred due to either LOS components and/or non-line-of-sight (NLOS) components. The optical receiver of each user is connected with all light units through the SCM tones. Thus, the output of the photodetectors that covered by the green filters enter to twelve bandpass filters (BPFs) as shown in Figure 6.8. These BPFs have center frequencies equal to the frequencies of the SCM tones.

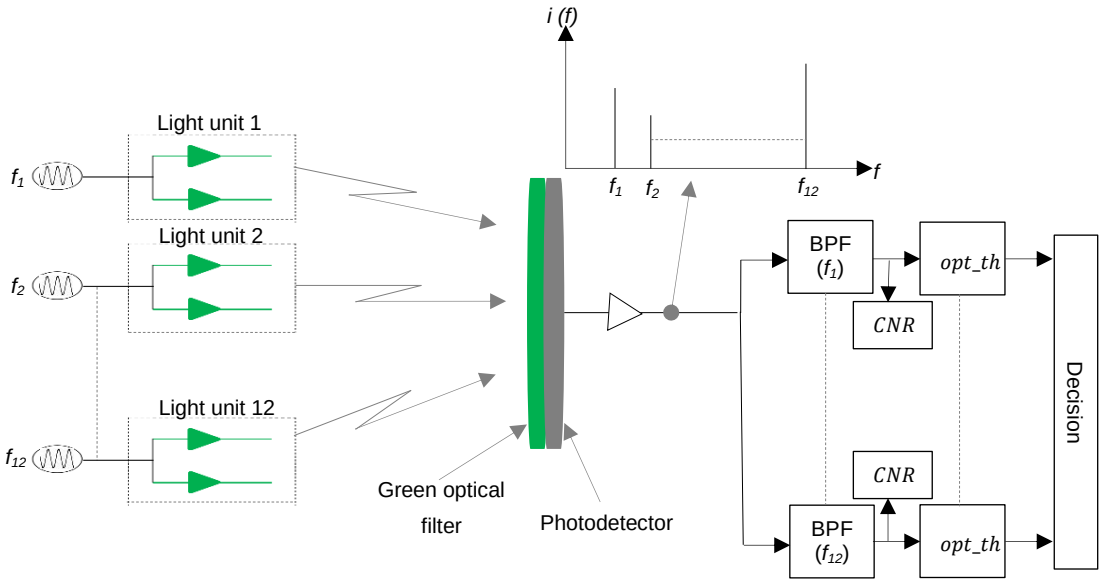

Figure 6-8: : Calculating the CCI level using SCM tones.

The indoor channel frequency response of VLC systems has low pass characteristic in the electrical domain [144]. Thus, the range of the frequencies assigned to the SCM tones should be selected near to the DC where the channel has low attenuation. We obtained the 3-dB channel bandwidth of the NI-R and the NI-ADR when the mobile user moved in steps of 1 m along the *y*-axis and at x = 0.5 m and x = 1.5 m as shown in Figure 6.9. We considered locations at x = 0.5 m and at x = 1.5 and along the *y*-axis as the user moves near to the wall (at x = 0.5 m) and moves between light units not underneath them (at x = 1.5 m) where ISI is high. It can be seen that the minimum 3-dB channel bandwidth is associated with the NI-R, and is 1.23 GHz. Therefore, the frequency range selected for the 12 SCM tones was 500 MHz to 1160 MHz

with a guard of 60 MHz. The bandwidth of each BPF was selected equal to 4 MHz, which reduces the noise that seen by each SCM tone, and allows for SCM oscillator drift and BPF tolerances [142].

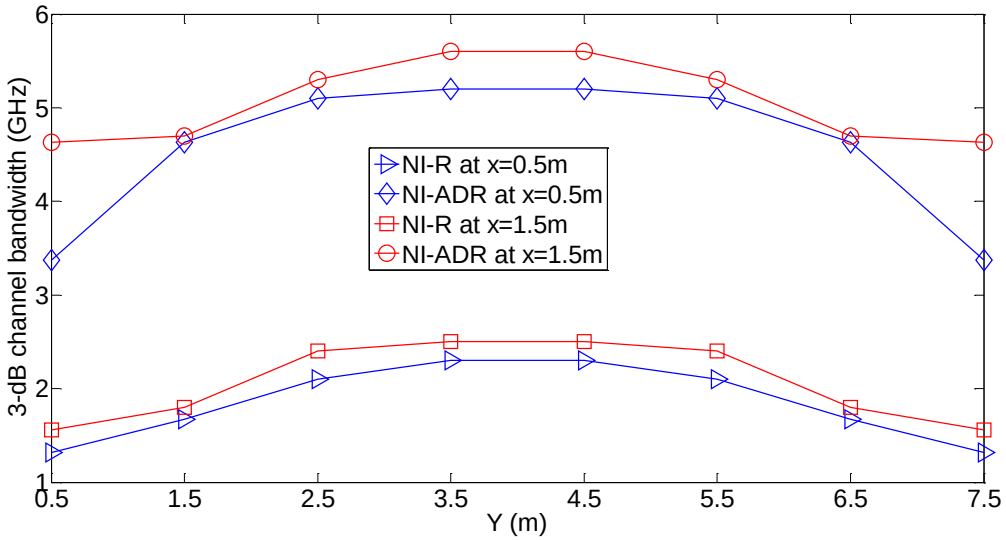

Figure 6-9: The 3-dB channel bandwidth of the NI-R and the NI-ADR when the mobile user moved along the y-axis and at x = 0.5 m and x = 1.5 m.

6.5.2.1 Transmitters allocation

A controller connected to all light units (see Figure 6.1) is used to manage the light units and the users. Each user is assigned one light unit for data transmission and the other light units (the light units assigned to other users) are considered as interfering light units. Thus, based on the channel conditions between the transmitters and the receivers, each user is allocated the light unit that has a good channel (high optical received power and low level of CCI). To find the optimum light unit that gives a reliable connection to each user, the SCM tone identification system at each receiver is used to calculate the received power of each SCM tone.

The SCM tones are separated in frequency; thus, there is no interference between the SCM tones. Therefore, the output of each BPF (see Figure 6.8) is a SCM tone plus noise. Hence, to match each user with its closest light unit (the light unit that offers the highest optical power), an optimum threshold should be set. When the NI-Rs are used, in some user locations, more than one light units (up to four light units) have LOS components with the users and this is attributed to the wide FOV of the NI-R and the distribution of the light

units. In this case, the ability of the SCM tone identification system to match each user with its closest light unit should be evaluated.

We defined three cases based on the location of a user. In case one, a user has LOS components with one light unit and has just NLOS components with the other light units. In case two, a user has LOS components with two light units and has just NLOS components with the other light units. In case three, a user has LOS components with three or four light units and has just NLOS components with the other light units. In addition, we defined the probability of not allocating the closest light unit to each user as the probability of a wrong decision. Thus, in case one, the probability of wrong decision is the probability of a user being assigned a light unit that has no LOS components with it. While in case two, the probability of the wrong decision is the probability of assigning the second closest light unit to a user, in case three, the probability of a wrong decision is the probability of assigning the second, the third or the fourth nearest light unit to a user. Here, we will evaluate the probability of wrong decision for case two only. This is due to the fact that in case two, the probability of allocating the second nearest light uint to a user is higher than the probability of assigning a light unit that has no LOS components with a user (case one) and higher than the probability of assigning the third or the fourth closest light unit to a user (case three). This is because we consider the received power of each light unit to decide which light unit offers the highest power.

In case two, the output of each BPF (see Figure 6.8) is the SCM tone transmitted from the closest light unit (desired SCM tone) to a user plus noise, the SCM tone transmitted from the second nearest light unit (undesired SCM tone) to a user plus noise or the SCM tone that reaches the user through only NLOS components plus noise, which can be ignored (case one). An optimum threshold should be obtained to decide the output of each the BPF.

To classify the electrical current (z) the output of each BPF, we hypothesize two states [155]. Under hypothesis 1 ($H1$), the electrical current (z) is the undesired SCM tone plus noise (b + n), while under hypothesis 2 ($H2$), z is the desired SCM tone plus noise (a + n).

The total noise (n) that is seen by each SCM tone is white Gaussian zero mean.

The values of the desired SCM tone electrical current (a) and the undesired SCM tone electrical current (b) depend on the distance between the optical receiver and the light units. Therefore, a and b are random variables and their distributions were obtained through simulation of the indoor channel. The simulations considered 1000 random positions of the receiver on the communication floor to determine the distribution of a and b. At each position of the receiver, the values of a and b were calculated. Figure 6.10 and Figure 6.11 show the histogram and the curve fitting of the a and b parameters, respectively.

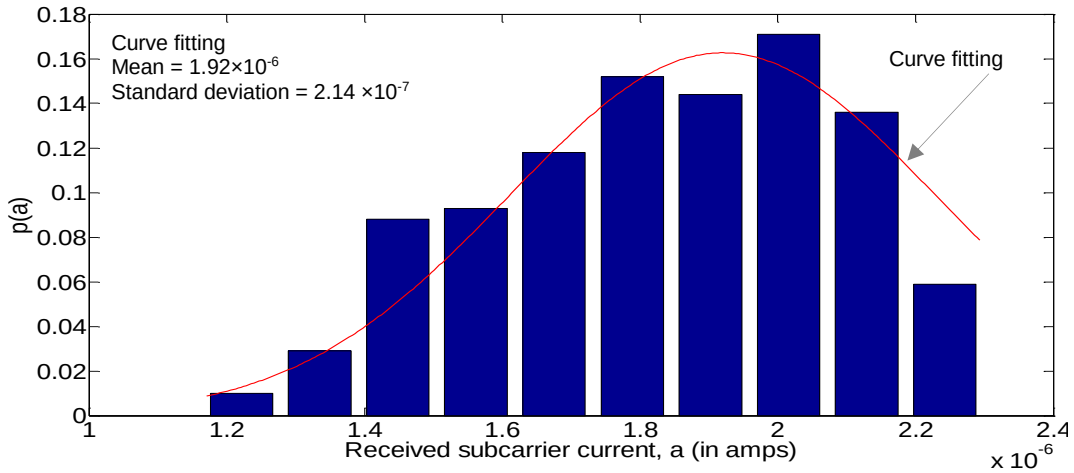

Figure 6-10: Histogram and curve fitting of the desired SCM tone received electrical current.

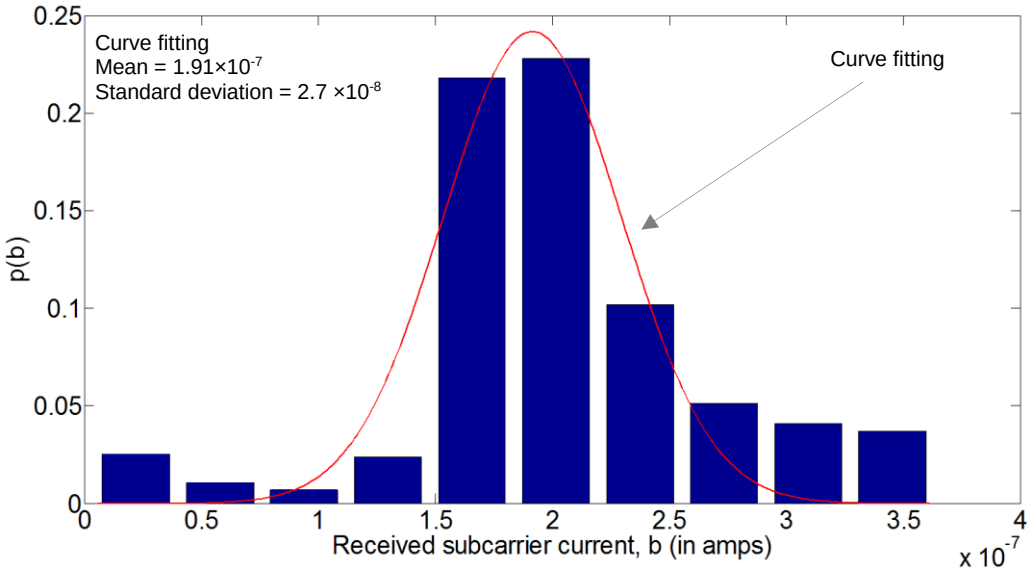

Figure 6-11: Histogram and curve fitting of the undesired SCM tone received electrical current.

From the curve fitting, the normalized probability density functions (pdfs) of a ($p(a)$) and b ($p(b)$) are written as:

$$p(a) = \frac{1}{\sqrt{2\pi}\,\sigma_{ds}} e^{-\left(\frac{a-m_{ds}}{\sqrt{2}\sigma_{ds}}\right)^2} \tag{6.1}$$

and

$$p(b) = \frac{1}{\sqrt{2\pi}\,\sigma_{us}} e^{-\left(\frac{b-m_{us}}{\sqrt{2}\sigma_{us}}\right)^2} \tag{6.2}$$

where we presumed a Gaussian distribution for the received power which is reasonable given the multiple locations (giving rise to multiple angles and distances), the multiple reflecting surfaces and the observed results. Here, σ_{ds} and m_{ds} are the standard deviation and the mean value of a, respectively and σ_{us} and m_{us} are the standard deviation and the mean value of b, respectively.

The pdfs of z given $H1$ and $H2$ can be written as follows: under $H1$, z is the convolution of the undesired SCM tone pdf and the noise pdf:

$$fz(z|H1) = p(b) \otimes p(n) \tag{6.3}$$

Solving equation (6.3) $fz(z|H1)$ can be written as:

$$fz(z|H1) = \frac{1}{\sqrt{2\pi({\sigma_{us}}^2 + {\sigma_t}^2)}} e^{-\left(\frac{z-m_{us}}{\sqrt{2({\sigma_{us}}^2+{\sigma_t}^2)}}\right)^2} \tag{6.4}$$

Under $H2$, z is the convolution of the desired SCM tone pdf and the noise pdf, which is given as:

$$fz(z|H2) = \frac{1}{\sqrt{2\pi({\sigma_{ds}}^2 + {\sigma_t}^2)}} e^{-\left(\frac{z-m_{ds}}{\sqrt{2({\sigma_{ds}}^2+{\sigma_t}^2)}}\right)^2} \tag{6.5}$$

Applying likelihood ratio to equations (6.4) and (6.5), we get:

$$\frac{fz(z|H2)}{fz(z|H1)} \underset{H1}{\overset{H2}{\gtrless}} 1 = \frac{\frac{1}{\sqrt{2\pi({\sigma_{ds}}^2 + {\sigma_t}^2)}} e^{-\left(\frac{z-m_{ds}}{\sqrt{2({\sigma_{ds}}^2+{\sigma_t}^2)}}\right)^2}}{\frac{1}{\sqrt{2\pi({\sigma_{us}}^2 + {\sigma_t}^2)}} e^{-\left(\frac{z-m_{us}}{\sqrt{2({\sigma_{us}}^2+{\sigma_t}^2)}}\right)^2}} \underset{H1}{\overset{H2}{\gtrless}} 1 \tag{6.6}$$

Solving equation (6.6) we get:

$$z \underset{H1}{\overset{H2}{\gtrless}} \frac{1}{{\sigma_{ds}}^2-{\sigma_{us}}^2}\left(m_{us}({\sigma_{ds}}^2+{\sigma_t}^2)-m_{ds}({\sigma_{us}}^2+{\sigma_t}^2)+ \sqrt{\begin{pmatrix}{\sigma_{ds}}^2{\sigma_{us}}^4+{\sigma_t}^4{\sigma_{us}}^2+{\sigma_t}^2{\sigma_{us}}^4 \\ -{\sigma_{ds}}^4{\sigma_t}^2-{\sigma_{ds}}^4{\sigma_{us}}^2-{\sigma_{ds}}^2{\sigma_t}^4\end{pmatrix}\ln\left(\frac{{\sigma_{us}}^2+{\sigma_t}^2}{{\sigma_{ds}}^2+{\sigma_t}^2}\right)+ (m_{ds}-m_{us})^2({\sigma_t}^2{\sigma_{ds}}^2+{\sigma_{ds}}^2{\sigma_{us}}^2+{\sigma_t}^4+{\sigma_t}^2{\sigma_{us}}^2)}\right) = z \underset{H1}{\overset{H2}{\gtrless}} opt\_th \quad (6.7)$$

If m_{ds} is very large compared with σ_{ds}, σ_{us} and m_{us}, the optimum threshold (opt_th) ~ $\frac{m_{ds}}{2}$ as expected. The probability of correct detection of the desired SCM tone, which is the probability of a correct decision on the desired SCM tone ($Pcds$) is:

$$Pcds = \int_{opt\_th}^{\infty} fz(z|H2)dz = \int_{opt\_th}^{\infty} \frac{1}{\sqrt{2\pi({\sigma_{ds}}^2+{\sigma_t}^2)}} e^{-\left(\frac{z-m_{ds}}{\sqrt{2({\sigma_{ds}}^2+{\sigma_t}^2)}}\right)^2} dz \quad (6.8)$$

The probability of correct detection of the undesired SCM tone, which is the probability of a false alarm in the undesired SCM tone ($Pfus$) (i.e. the undesired SCM tone is considered as the desired SCM tone) is:

$$Pfus = \int_{opt_{th}}^{\infty} fz(z|H1)dz = \frac{1}{\sqrt{2\pi({\sigma_{us}}^2+{\sigma_t}^2)}} e^{-\left(\frac{z-m_{us}}{\sqrt{2({\sigma_{us}}^2+{\sigma_t}^2)}}\right)^2} dz \quad (6.9)$$

Consequently, the probability of not allocating the undesired SCM tone to a user, which is the probability of correct decision in the undesired SCM tone ($Pcus$) is:

$$Pcus = 1 - Pfus \quad (6.10)$$

Thus, the overall probability of the SCM identification system makes a correct dissection (Pcd) is:

$$Pcd = Pcds\ (Pcus)^{M-1} \quad (6.11)$$

where M is the number of the light units. Consequently, the probability of making wrong decision in the SCM identification system is Pwd is $1 - Pcd$. In our system, and for the given set of parameters in this paper, Pwd is 1.2×10^{-12}, which shows that the SCM tone identification system has the ability to

match each user to its nearest light unit with high accuracy. Due to the distribution of the light units on the ceiling of the room, in some user locations, two or four light units may have the same distances to a user. In this case, any one of these light units can be considered as the nearest one to a user.

When NI-ADRs are used instead of NI-Rs, each photodetector covered by the green filter in each face of the NI-ADR is treated separately to find the nearest light unit to each user. However, the FOV of each photodetector is 20º, which means no more than one light unit (the light unit that has LOS components with the photodetector) can be seen by each face. This is similar to case one in the NI-R, which means that the probability of wrong decision is lower than 10^{-12} for the NI-ADR.

By calculating the CNR of each SCM tone at each user, through an IR signal, the optical receiver of each user informs the controller the CNR associated with each SCM tone. Each user is allocated one light unit. For each user, the controller sorts the light units in descending order (each user has a different descending order of the light units starting with the light unit that has the highest (CNR) and ending with the light unit that has the lowest (CNR)). The controller allocates one light unit, the light unit that has the highest CNR, to each user to transmit the data. It should be noted that we used the design of the IR uplink presented in [130]. In addition, to prevent interference in the uplink, each user is given a time slot to send the feedback information to the controller. The electrical power of a SCM tone (S) at a user is given as:

$$S = \left(\frac{R_g \, Pr}{2}\right)^2 \tag{6.12}$$

here R_g is the photodetector's responsivity for the green spectrum and Pr is the received optical (green) power. Consequently, CNR of any SCM tone at any user is given as:

$$CNR_{n,m} = \frac{\left(R_g \, Pr\right)^2}{2 \, {\sigma_t}^2} \tag{6.13}$$

Due to the fact that the SCM tones are unmodulated tones and have unique frequencies, there is no interference between these SCM tones at any optical receiver. Therefore, the CCI level is defined as the total received power at *nth*

receiver, except for the received power of the desired SCM tone. For example, if the desired tone of mth transmitter is f_m, the level of the CCI at *nth* user (I_n) due to the other SCM tones are given as:

$$I_n = \sum_{\substack{k=1 \\ k \neq m}}^{Ma} \left(\frac{R_g \, Pr_{n,k}}{2}\right)^2, \quad n \in [1, 2 \dots N], \quad m \in [1, 2 \dots Ma] \tag{6.14}$$

where Ma is the number of active light units (the light units assigned to users to send data) and N is the number of receivers (in our system, $N = Ma$).

The closest light unit to a user offers a higher optical power than the other light units. However, the user connected to the nearest light unit may experience poor channel performance (i.e., high level of CCI). Thus, for the NI-Rs, when two users are located near to each other, the NI-Rs of the two users view the same light units. This leads to high CCI level at these users. In this case, we choose to give the priority to the stationary receiver (no data will be transmitted to the mobile user). On the other hand, for the NI-ADR, the controller assigns the best light unit to the stationary user and the second best light unit to the mobile user. This is due to the NI-ADR construction where there are many faces and each face is directed to a different direction, which enables NI-ADR to see many light units from a different direction.

6.5.2.2 Performance analysis of the data channels

To find the data rate that can be provided from each active light unit (the light units allocated to users), we consider that each light unit sends data with BER = 10^{-6}, which gives a reliable connection between transmitters and receivers. The relationship between the BER and signal to interference to noise ($SINR$) ratio of the OOK modulation is given as [12]:

$$BER = Q\left(\sqrt{SINR}\right) \tag{6.15}$$

where $Q(x) = \frac{\int_x^\infty e^{-z^2/2} \, dz}{\sqrt{2\pi}}$. The $SINR$ can be expressed as [94], [103]:

$$SINR = \frac{R^2 (P_{s1} - P_{s0})^2}{{\sigma_{td}}^2 + I} \tag{6.16}$$

where (P_{s1}) is the received optical power associated with logic 1, (P_{s0}) is the received optical power associated with logic 0 and σ_{td} is the standard deviation of the total noise associated with the received data. To calculate σ_{td}, we considered the receiver bandwidth while we considered the bandwidth of the BPF to obtain σ_t. All photodetectors in the NI-R and in each face of the NI-ADR views the same area. Hence, the amount of the CCI level that was calculated from the green channel (SCM tone) is used to calculate the level of the CCI of the signal channels. In addition, each photodetector was covered by a specific optical filter. Thus, the level of the CCI on the data channels can be obtained from the CCI level of the SCM tones as:

$$I_{red} = \left(\frac{R_r}{R_g}\right)^2 \left(\frac{Pt_r}{Pt_g}\right) I_{green} \quad , \quad I_{yellow} \left(\frac{R_y}{R_g}\right)^2 \left(\frac{Pt_y}{Pt_g}\right) I_{green} \quad \text{and} \quad I_{blue} \left(\frac{R_b}{R_g}\right)^2 \left(\frac{Pt_b}{Pt_g}\right) I_{green} \tag{6.17}$$

where R_r, R_y and R_b are responsivity of the photodetector for the red, yellow and blue colours and Pt_r, Pt_g, Pt_y and Pt_b are the red, green, yellow and blue optical transmitted power. Consequently, the $SINR$ of each data channel is written as:

$$SINR_{red} = \frac{R_r^2 (P_{s1} - P_{s0})^2}{{\sigma_{td}}^2 + \left(\frac{R_r}{R_g}\right)^2 \left(\frac{Pt_r}{Pt_g}\right) I_{green}} \tag{6.18}$$

$$SINR_{yellow} = \frac{R_y^2 (P_{s1} - P_{s0})^2}{{\sigma_{td}}^2 + \left(\frac{R_y}{R_g}\right)^2 \left(\frac{Pt_y}{Pt_g}\right) I_{green}} \tag{6.19}$$

$$SINR_{blue} = \frac{R_b^2 (P_{s1} - P_{s0})^2}{{\sigma_{td}}^2 + \left(\frac{R_b}{R_g}\right)^2 \left(\frac{Pt_b}{Pt_g}\right) I_{green}} \tag{6.20}$$

$$SINR_{green} = \frac{R_g^2 (P_{s1} - P_{s0})^2}{{\sigma_{td}}^2 + I_{green}} \tag{6.21}$$

It should be noted that for the data signals, we considered the level of the CCI that comes from the active light units only as other units do not transmit data. Figure 6.12 shows the block diagram of the simulator for the data channels.

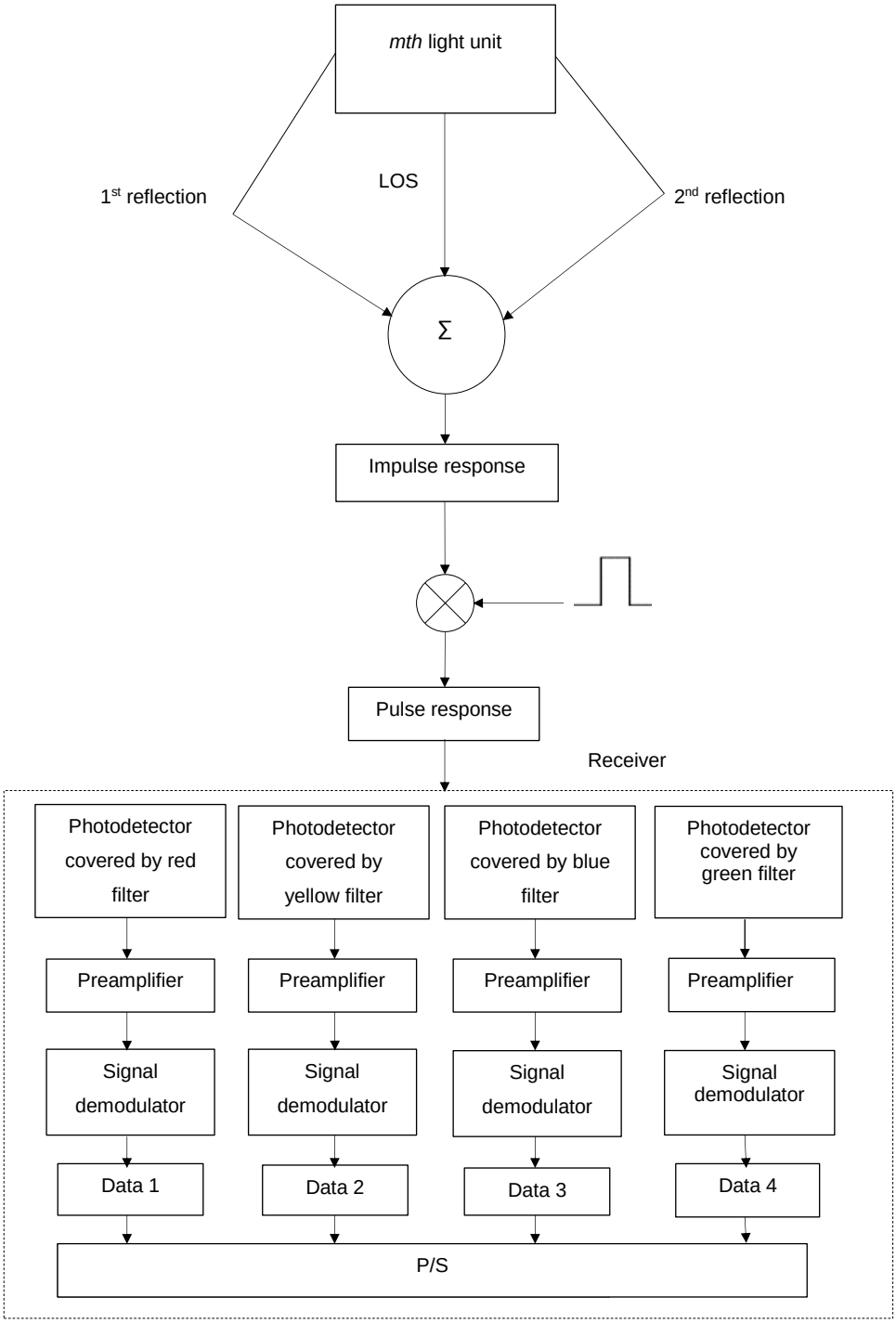

Figure 6-12: Block diagram of the simulator of the data channels.

6.6 Simulation results

Three users (two stationary users and one mobile user) were investigated in four scenarios as shown in Figure 6.13. In the first scenario, one of the stationary users (user 1) was located at (1 m, 1 m, 1 m) while the other

stationary user (user 2) was placed at (1 m, 7 m, 1 m). In the second scenario, user 1 was placed at (1 m, 4 m, 1 m) and user 2 was located at (3 m, 4 m, 1 m). In the third scenario, user 1 and user 2 were located at (2 m, 1 m, 1 m) and (2 m, 7 m, 1 m), respectively while for the fourth scenario, user 1 was placed at (1 m, 1 m, 1 m) and user 2 was placed at (2 m, 4 m, 1 m). The mobile user (user 3) moved in steps of 1 m along the *y*-axis and at x = 0.5 m and x = 1.5 m in all scenarios. The four scenarios were selected out of many cases based on many criteria such as separation distance between the optical receivers, the effect of the mobility on the performance and the weakest points on the communication floor (the largest distances between the transmitters and the receivers).

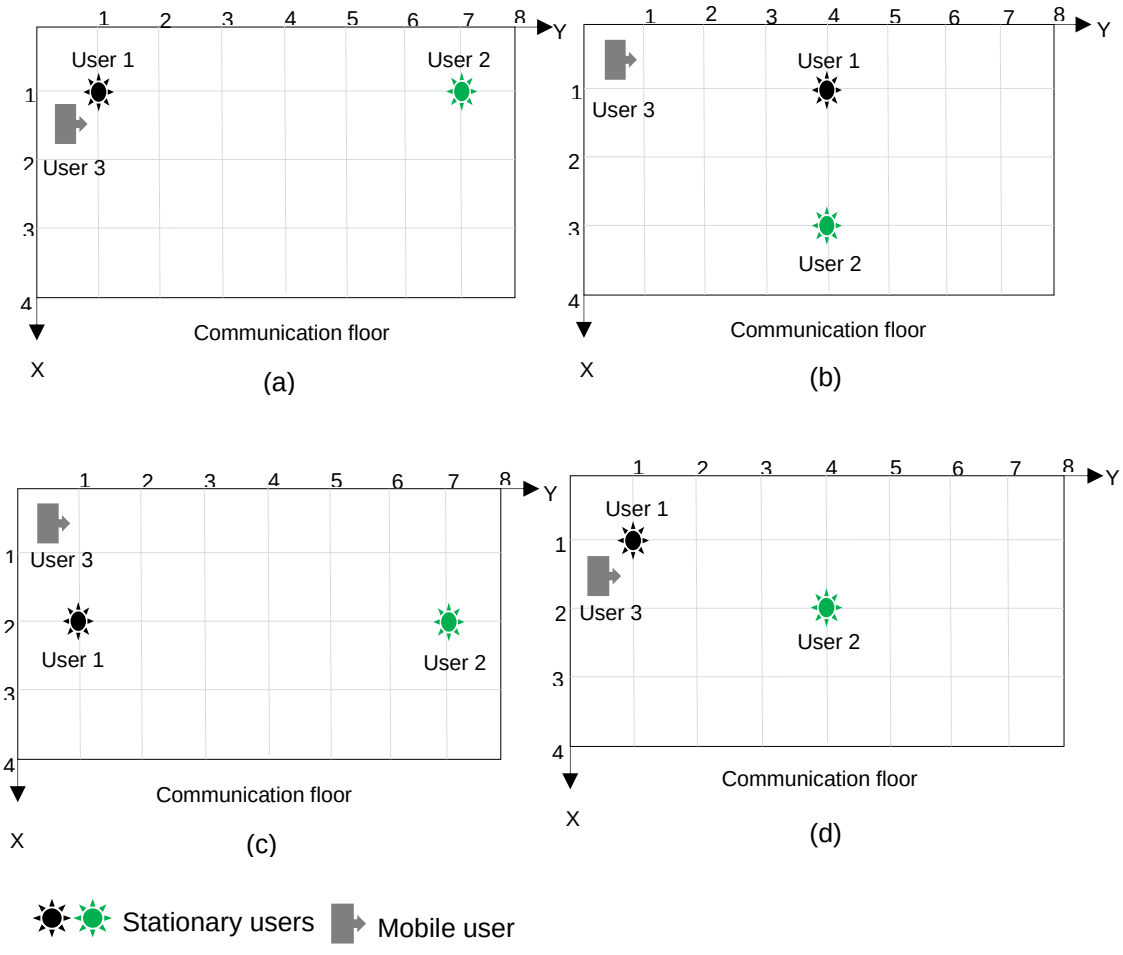

Figure 6-13: Receivers location on the communication floor: (a) scenario 1, (b) scenario 2, (c) scenario 3 and (d) scenario 4.

Figure 6.14 and Figure 6.15 show the aggregate data rate of the NI-R and the NI-ADR for the three users under the four different scenarios. The results were obtained when the mobile user (user 3) moves along the *y*-axis and at *x* = 0.5 m and *x* = 1.5 m. It should be noted that the maximum data rate of each data channel from each assigned light unit for each user was obtained when the BER = 10^{-6} (SINR = 13.6 dB). The maximum achieved data rate of each data channel depends on many factors. These are 1) the distance between the user and its allocated light unit, 2) the level of CCI at the user and 3) the diffuse reflections, which introduce ISI. When two users are located at the same location, the priority is given to the stationary user (the controller assigns the best light unit to the stationary user). Thus, for the NI-R, when the mobile user is near to one of the stationary users, the achieved data rate of the mobile user was almost equal to zero at BER = 10^{-6} as shown in Figure 6.14 and Figure 6.15. This is due to the high level of CCI compared to its signal channel. In this case, the controller assigns light units to just the stationary users. On the other hand, by using the NI-ADR, better performance was achieved as the NI-ADR has many faces and each face is directed to a different area, which enables it to view many light units at its location. Thus, two users can be served when they are located at the same place by using the NI-ADR as shown in Figure 6.14 and Figure 6.15. In addition, the achieved data rate of the NI-ADR was better than the data rate of the NI-R. This is attributed to the small FOV (20^{o}) of each photodetector at each branch of the NI-ADR, which means that the number of rays due to first and second reflections that were captured by each photodetector in each branch is small compared with that of the NI-R. This leads to a reduction in the level of the CCI and consequently increase in the data rate.

It should be noted that the 3-dB channel bandwidth of each system using a given colour (see Figure 6.9) is higher than the obtained data rate of each channel for NI-R and NI-ADR. The full channel bandwidth could not be exploited due to the limited transmit power available. High power per colour may be used to increase the data rate, but this affects the illumination. In addition, our system can support up to 12 users (as we installed 12 light units in the ceiling of the room) in the room if each user is given all four colours in

the light unit. However, the system can support up to 36 users in the room if each user is given one colour from its optimum light unit. In this case the, it is helpful if the users are distributed uniformly in the room with appropriate distances between them. Adding more users to the systems increases the aggregate data rate of the system. However, this degrades the per-user data rate due to interference.

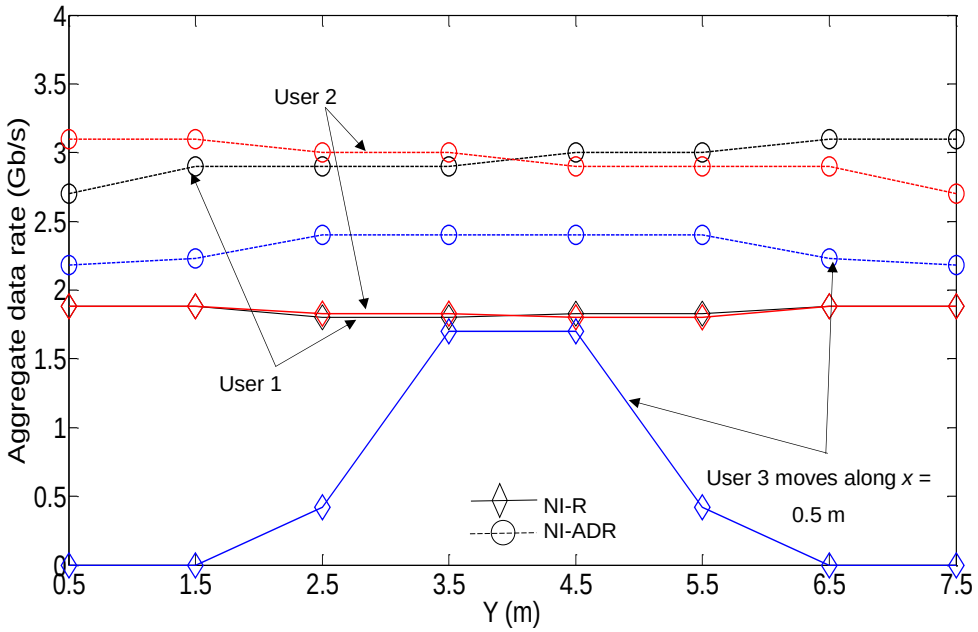

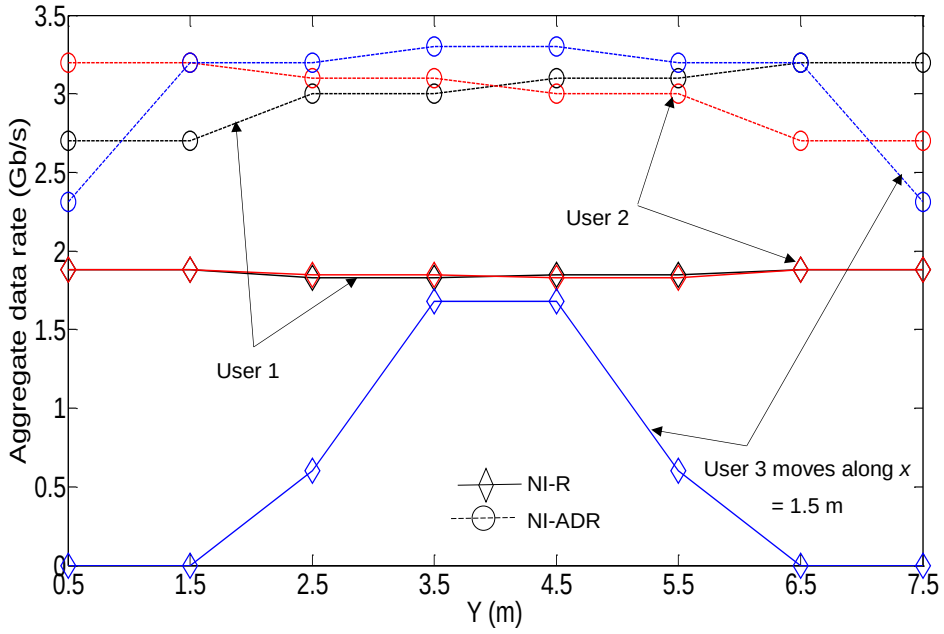

(a)

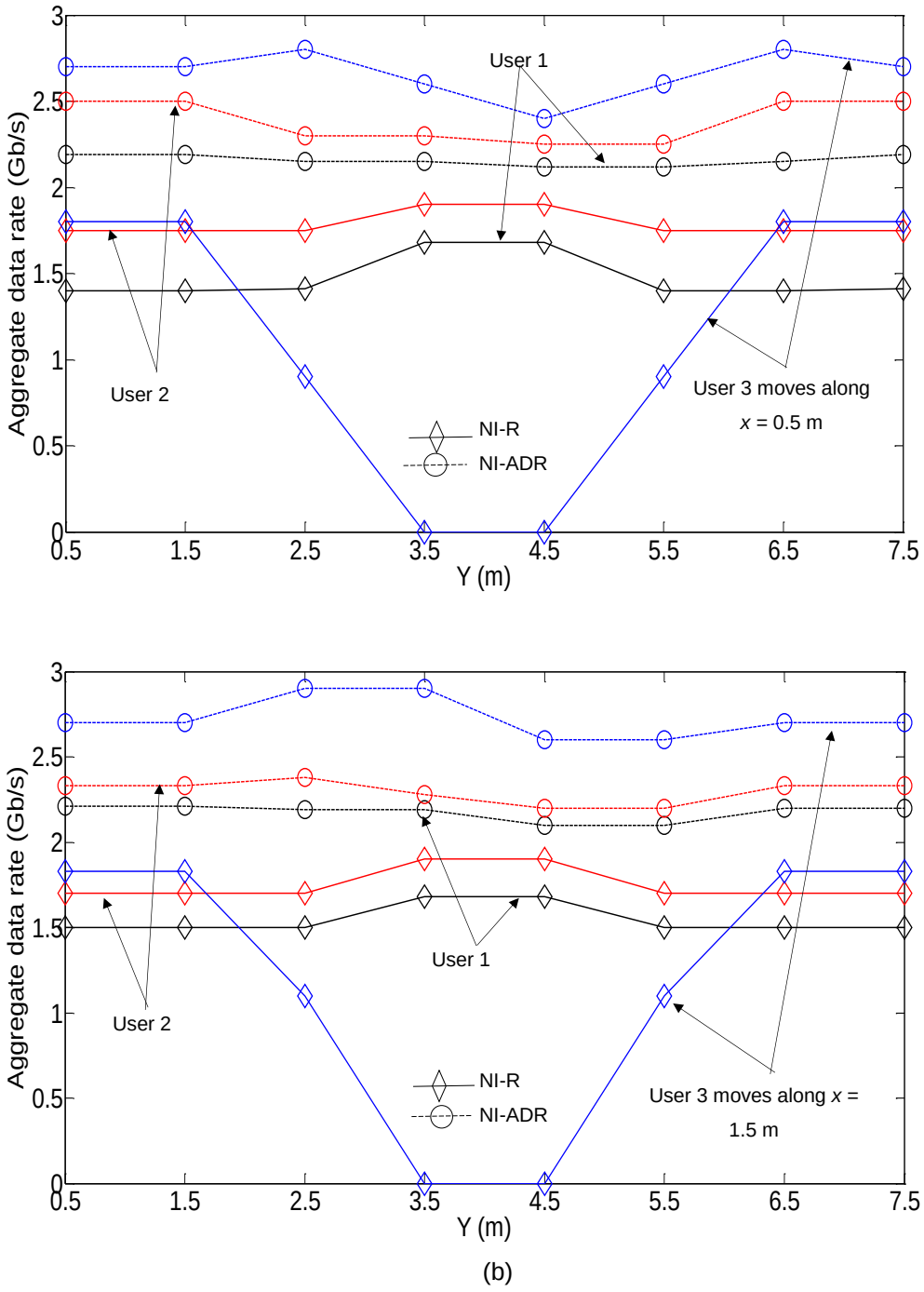

Figure 6-14: Aggregate data rate of the NI-R and the NI-ADR for the three users when the mobile user moves along x = 0.5 m and x = 1.5 m along the y-axis and under: (a) scenario 1 and (b) scenario 2.

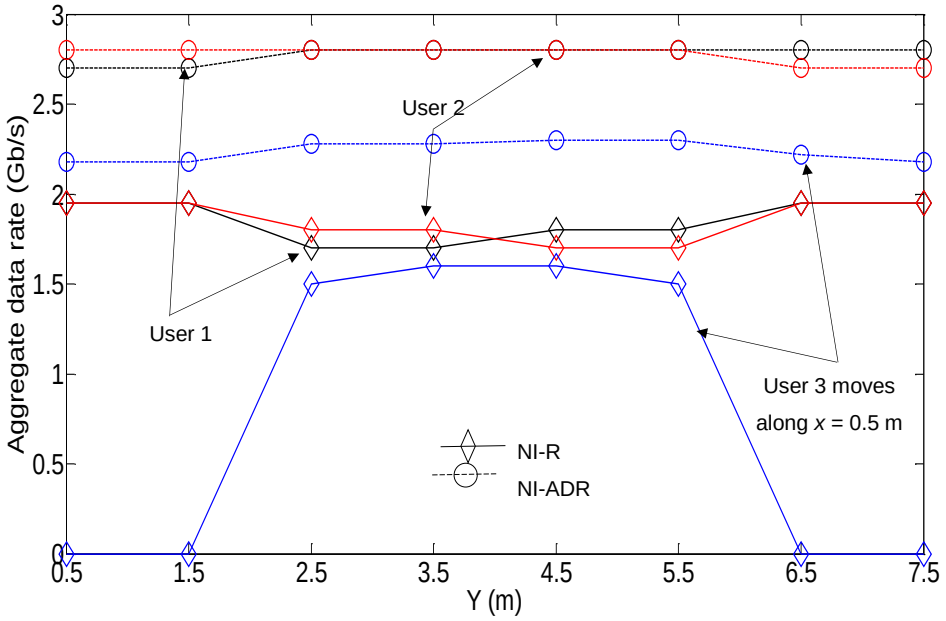
Aggregate data rate (Gb/s)
Y (m)
User 1
User 2
User 3 moves
along x = 0.5 m
NI-R
NI-ADR

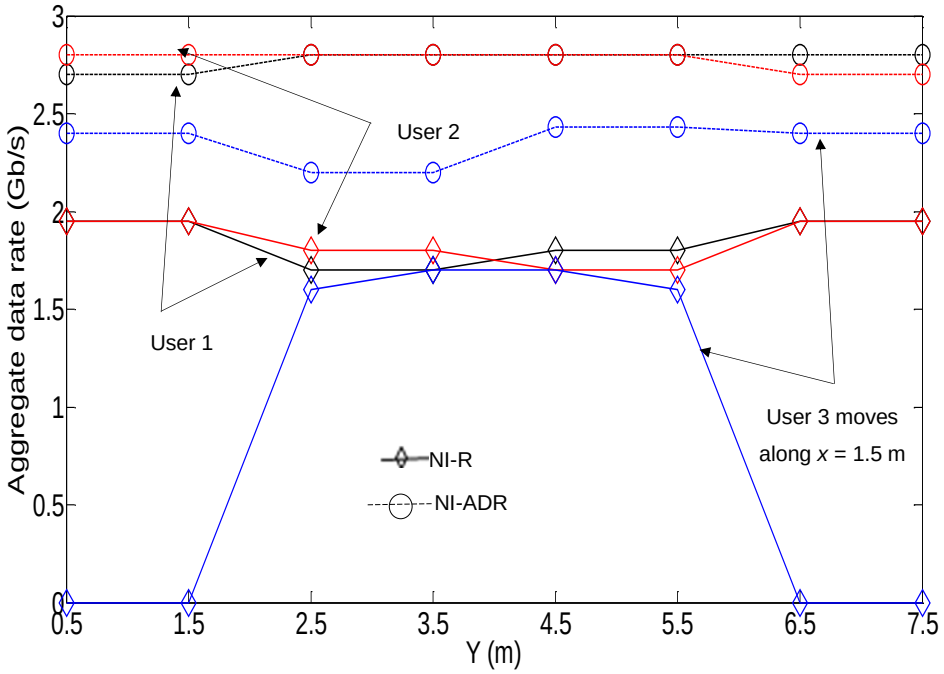
Aggregate data rate (Gb/s)
Y (m)
User 1
User 2
User 3 moves
along x = 1.5 m
NI-R
NI-ADR

(a)

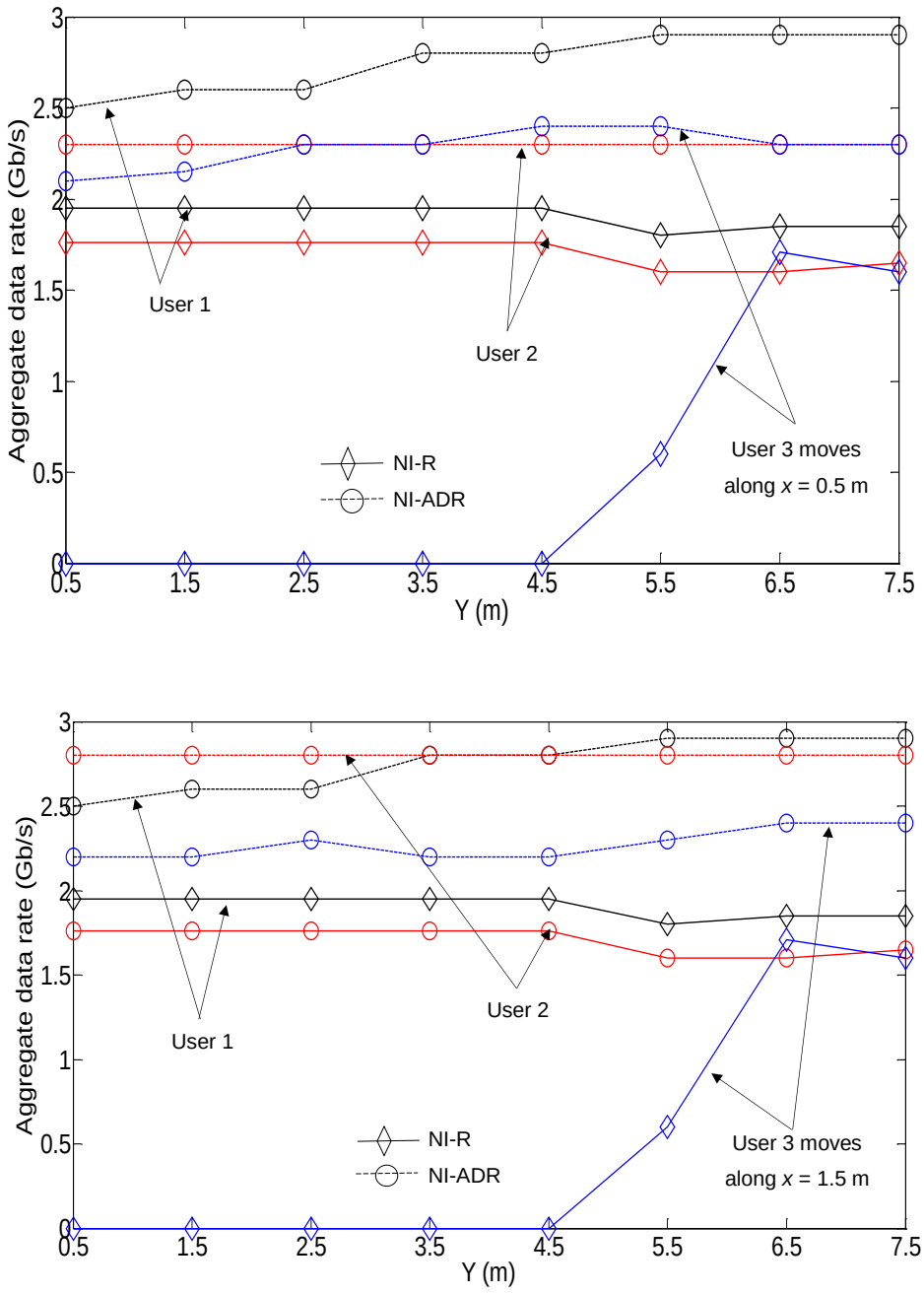

(b)

Figure 6-15: Aggregate data rate of the NI-R and the NI-ADR for the three users when the mobile user moves along x = 0.5 m and x = 1.5 m along the y-axis and under: (a) scenario 3 and (b) scenario 4.

6.7 Summary

In this chapter, a single user VLC system based on WDM that can offer a data rate of 10 Gb/s over the entire proposed room with BER = 10^{-6} and using OOK as a modulation technique was introduced. This WDM system was realised by using RYGB LDs as transmitters and an IMDR as an optical receiver. Each pixel of the IMDR was covered by a specific colour filter, which allowed it to sense a particular colour. Due to using a large number of pixels in the IMDR, we used the MCFA to design the pattern of the array colour filters of each side of the IMDR. In addition, MCFA that has four bands (colours) was used in this work and this is attributed to the use of four colours (RYGB) LD as a transmitter. The effect of the reflection components and the mobility of the IMDR were taken into account.

We proposed also a multi-user VLC system based on SCM tones and WDM in this chapter. The SCM tones were used to give an ID to each light unit, to find the optimum light unit for each user and to calculate the level of the CCI between the light units. The performance of our proposed system was evaluated in an empty room with three users (two stationary users and one mobile user) under four different scenarios. We investigated the performance of the proposed system with two types of receivers (NI-R and NI-ADR) in the presence of CCI, diffuse reflections and mobility. The results showed that when using the NI-R, the distances between users should be considered to avoid high CCI between the users. However, the NI-ADR eliminates this limitation in the NI-R. In addition, a higher data rate was obtained when the NI-ADR was used compared with the NI-R. This is attributed to the small FOV of the NI-ADR, which limits the number of captured rays due to first and second reflections and consequently reduces the effect of the CCI and diffuse reflections induced ISI.

7. Multi-branch Transmitter for Indoor Visible Light Communication Systems

7.1 Introduction

One of the main aims of indoor visible light communication (VLC) systems is to deliver a high data rate services in a single user scenario and in multiuser scenarios. A key obstacle is the ability of the indoor VLC channel to support high data rates in the scenarios of interest. This is due to transmitters in VLC systems are used for lighting and then for data communication, which means many transmitters with wide beams must be employed to attain the required lighting level in the indoor environments. This results multipath propagation and makes the indoor VLC channel acts as a low pass filter. Supporting multiuser in VLC systems is another challenge that needs to be tackled. In indoor VLC systems, the lighting level should meet the illumination demands, which means that the overlap between multiple transmitters is very high [153]. In addition, due to the use of intensity modulation and direct detection (IM/DD) in the VLC system, transmission of many signals through overlapping multiple transmitters saturates the receiver terminal (photodetector) with the desired signal and interference signals from interfering transmitters [153] since the photodetector will respond to all the transmitted signals. In VLC systems, the communication area (size and the shape of the cell) varies based on the direction and level of the illumination provided, which means that multiple transmitters are treated as one transmitter [154]. One of the suggestions to improve the 3 dB channel bandwidth is using computer generated holograms (CGHs) as showed in chapter four. The CGHs were used to direct the beam of the light units to the optical receiver, which improved the 3 dB channel bandwidth and enhanced the performance of the VLC system [79], [78]. However, using CGHs increases the complexity of the VLC system's design.

One of the main benefits of the indoor VLC systems is that the shape, the direction, the intensity and the width of the beam of the luminaires (transmitters) can be controlled to obtain an acceptable level of lighting in the indoor environment [121]. By controlling one or all these parameters of the luminaires, the channel of the indoor VLC systems can be improved to support a high data rate and support multi-user scenario. Thus, we used a multi-branch transmitter (MBT) as a solution to improve the indoor channel of the VLC and supporting multi-user scenario. The MBT has many transmitter branches (TBs) and each one directed to a specific area. Due to reducing the semi angle of each TB, this leads to reduce the effect of multipath propagations and improve the received optical power.

MBT has widely studied in indoor VLC systems. Space division multiple access (SDMA) was realised by using MBT to serve many users simultaneously [166], [167]. It was shown that increasing the number of TBs leads to improve the performance of the VLC system. However, the effect of the diffuse reflections was not considered in [166], [167]. In [168], the MBT was used to split the area of the communication into small areas (attocells) to mitigate the interference between users. However, perfect channel knowledge was supposed between the transmitter and the receiver in [168]. Due to the directivity of the MTB, MTB was used to estimate an accurate position of the receiver [169], [170]. MTB was used to assign a group of LEDs for users [171]. It was shown that using multi-element receivers with MTB can improve the performance of the VLC systems [171].

In this chapter, we first evaluate the performance of the MBT with a single user VLC system. In this case, we obtained the delay spread, 3-dB channel bandwidth and SNR of the user, which are the important factors that measure the performance of the communication in VLC systems. We evaluated the performance of this system with two types of receivers: W-FOV receiver and ADR. We considered the effect of multipath propagation, mobility and illumination constraint in our system. The results show that this system can provide a data rate of 4 Gb/s and 10 Gb/s when using wide FOV receiver and ADR, respectively.

Secondly, we used the MBT with WDM and SCM tones to realise a high data rate multiuser indoor VLC system. Each TB can be used to send different data; therefore, many users can be served simultaneously. One of the main challenges in multiuser indoor VLC systems is to allocate the optimum transmitter for each user. Thus, we introduced SCM tones, which are unmodulated tones, to assign the best TB for each user. In addition, these SCM tones are utilized to calculate the CCI between luminaires and to maintain the handover during the mobility of the users. Four colours laser diodes (RYGB LDs) are used as sources of illumination and data communication. One colour of these four colour is used to convey the SCM tones at the beginning of the connection to set up the connection. When the connection is set up the data will be transformed in parallel through the RYGB LDs. We used WDM to increase the data rate of each user. The multiuser VLC system is investigated with the NI-ADR. The effect of the CCI, mobility, diffuse reflection (up to second order) components and lighting constraints (acceptable illumination level in the room) are considered in this system.

The rest of this paper is organised as follows: Section 7.2 describes the simulation setup. Section 7.3 describes the structure of the MBT. Evaluation of the performance of the MBT with a single user VLC system is given in Section 7.4. The MBT for the multiuser VLC system is described in Section 7.5. Finally, conclusions are given in Section 7.6.

7.2 Simulation Set-up

A simulation was developed in an empty room as shown in Figure 7.1. In this Chapter, we used the ray tracing algorithm to model the indoor channel of the VLC systems in the similar way to that presented in Chapter 3.

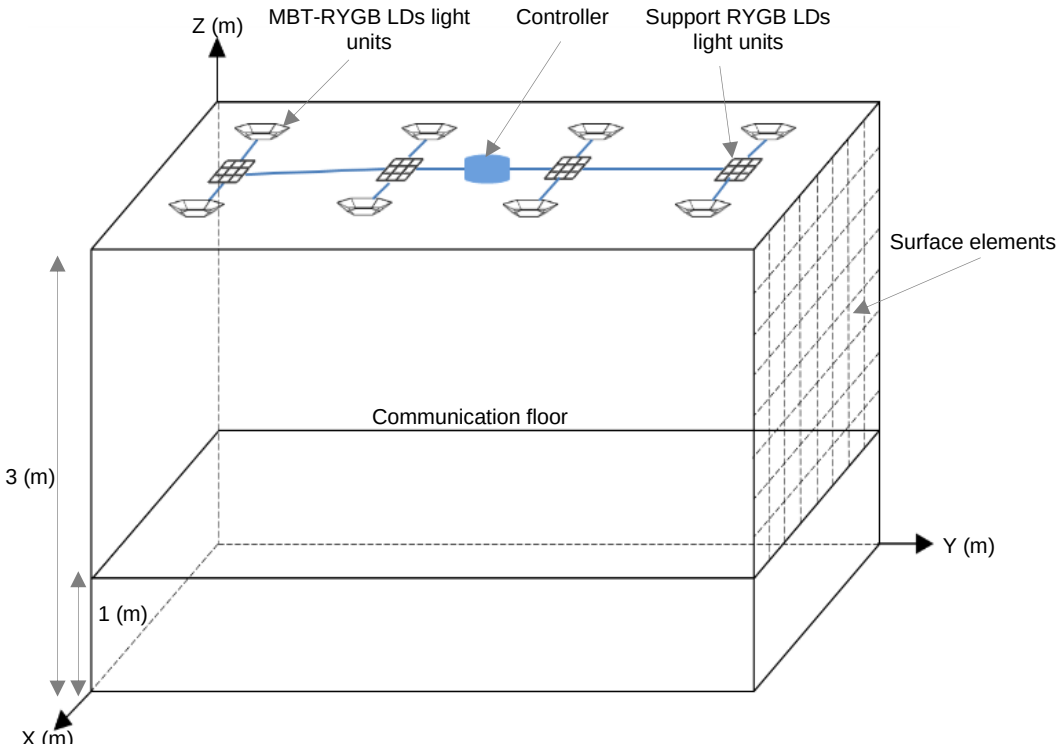

Figure 7-1: VLC room system configuration.

RYGB LDs were used as sources of illumination and data communication. For the single user VLC system, the four colours of the LDs were utilized to send the same data rate while for the multi user indoor VLC system, each colour of the RYGB LDs was used to send a different data as shown in Figure 7.2 (a) and 7.2 (b), respectively. In addition, for the multiuser VLC system, the green colour of the RYGB LDs was used to convey the SCM tones (see Figure 7.2 (b)) at the beginning of the connection to set up the connection between the transmitters and the receivers.

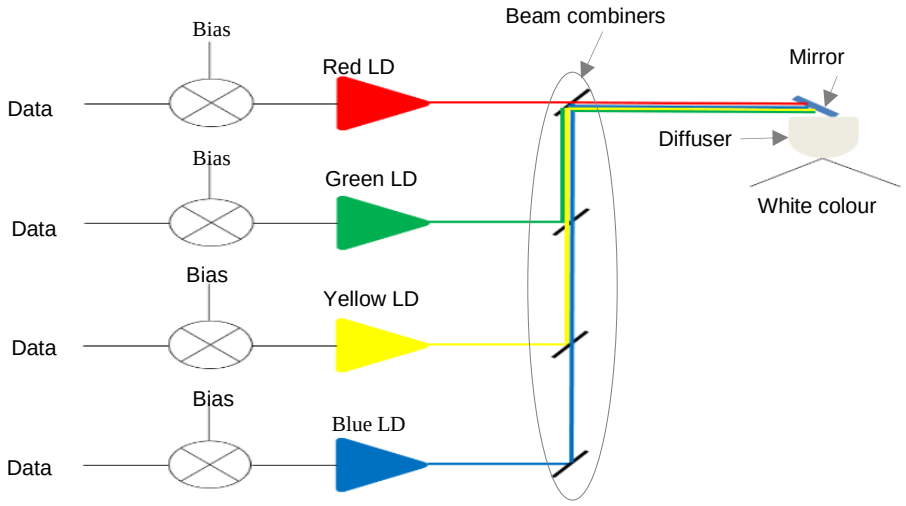

(a)

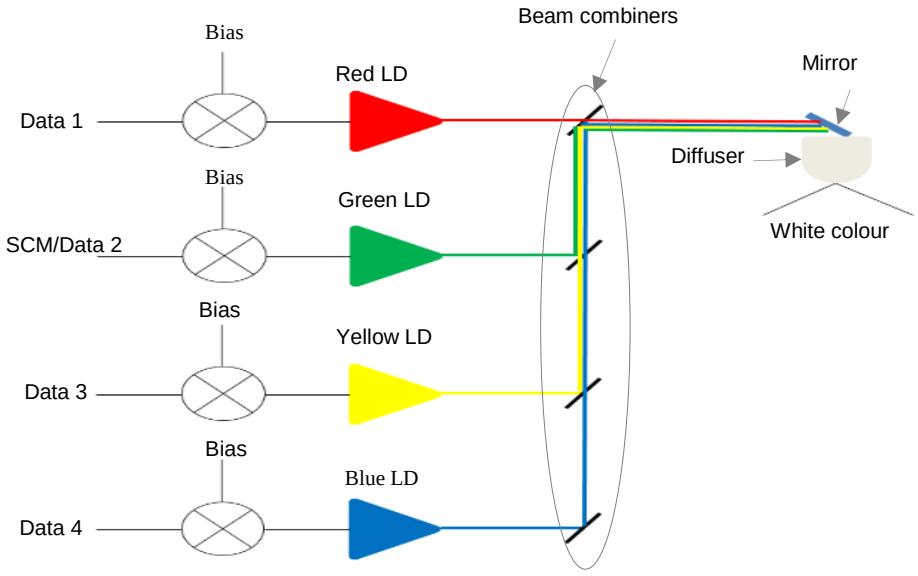

(b)

Figure 7-2: RYGB LDs configuration (a) for the single user VLC system and (b) for the multiuser VLC system.

7.3 MBT Structure

The MBT is a group of TBs in which each TB is oriented to a different direction and covers a small different part of the room, as shown in Figure 7.3. In this work, the MBT has seven TBs (1 to 7), and each TB has two narrow-semi angles white RYGB LDs. The two RYGB LDs were used in each branch to give illumination at the acceptable level in the room, which meets the demanded level of lighting. The coverage area of each TB can be modified by changing the Lambertian emission order (n). The value of n should be selected to reduce the overlap between the TBs and to keep the illumination level at the desired value. In this work, the Lambertion emission order of each RYGB LDs in the TB was 11, which gives the semi angle equal to 20.127º. This leads to overlapping between two adjacent TBs of up to 5.6% and provides an acceptable illumination as shown in Figure 7.3. It should be noted that there is a trade-off between the illumination level and the overlapping percentage. If the percentage of the overlap between the two adjacent TBs equals zero, this leads to gaps between branches and reduces the illumination level in some areas so it is under the recommended value (i.e., 300 lx [108]). On the other hand, a decrease in the value of n leads to an increase in the overlap between the TBs that consequently increases the interference.

Each branch in the MBT has a certain direction that can be defined by two angles: azimuth (A_z) and elevation (El). In this work, the El angle of the first TB was set at 90º, and the other six TBs were given an El of 60º. The A_z angles of the seven TBs were fixed at 0º, 0º, 60º, 120º, 180º, 240º and 300º. The values of the Els and A_{zs} of the MBT were chosen to give sufficient illumination and to achieve a good communication quality between the transmitter and the receiver at all possible locations on the communication floor of the room.

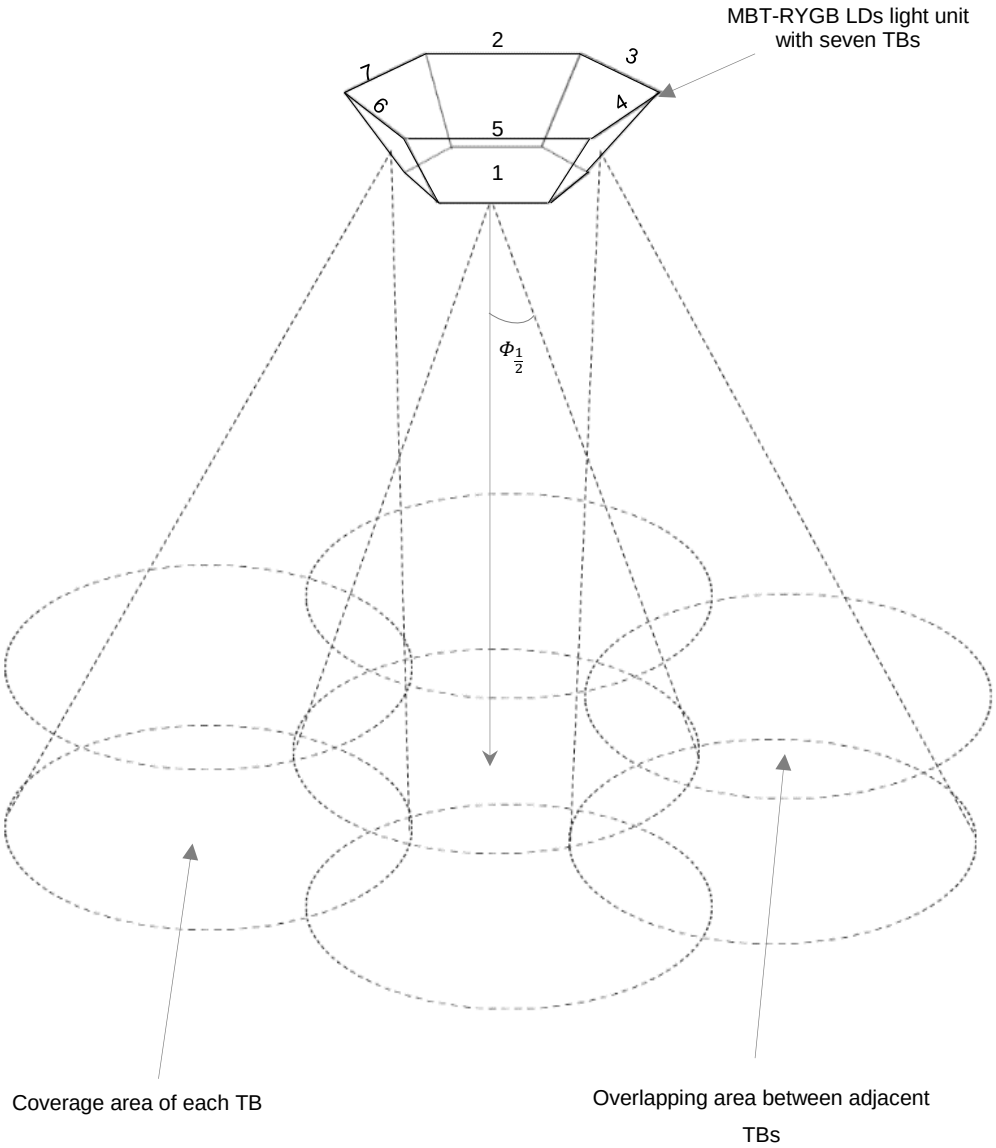

Figure 7-3: Structure of MBT.

To compute the irradiance angle (θ) for any TB, the A_z and El should be taken into account. Therfore, a point P was defined; and located on the

transmitter's normal, 1 m under the transmitter, as shown in Figure 7.4. This point is located in the FOV of the TB and is assumed to have 1 m length from the TB to ease the analysis. Figure 7.4 also depicts the transmitted light from a TB to the receiver. By using geomatrical analysis, θ can be given as:

$$\theta = cos^{-1}\left(\frac{|\overrightarrow{PT_x}|^2 + |\overrightarrow{R_xT_x}|^2 - |\overrightarrow{PR_x}|^2}{2\,|\overrightarrow{PT_x}|\,|\overrightarrow{R_xT_x}|}\right) \tag{7.1}$$

where:

$$|\overrightarrow{R_xT_x}|^2 = (x_r - x_t)^2 + (y_r - y_t)^2 + (z_r - z_t)^2 \tag{7.2}$$

$$|\overrightarrow{PT_x}|^2 = 1 + d^2 \tag{7.3}$$

and

$$|\overrightarrow{PR_x}|^2 = \left(x_p - x_r\right)^2 + \left(y_p - y_r\right)^2 + \left(z_p - z_r\right)^2 \tag{7.4}$$

From Figure 7.4, we also can calculate the:

$$El = tan^{-1}\left(\frac{1}{d}\right) \tag{7.5}$$

$$x_p = x_t + \frac{cos(A_z)}{tan(El)} \tag{7.6}$$

$$y_p = y_t + \frac{sin(A_z)}{tan(El)} \tag{7.7}$$

and

$$z_p = z_t - 1 \tag{7.8}$$

By substituting (7.6) – (7.8) in (7.4), PR_x can be rewritten as:

$$|\overrightarrow{PR_x}|^2 = \left(\left(x_t + \frac{cos(A_z)}{tan(El)}\right) - x_r\right)^2 + \left(\left(y_t + \frac{sin(A_z)}{tan(El)}\right) - y_r\right)^2 + \left((z_t - 1) - z_r\right)^2 \tag{7.9}$$

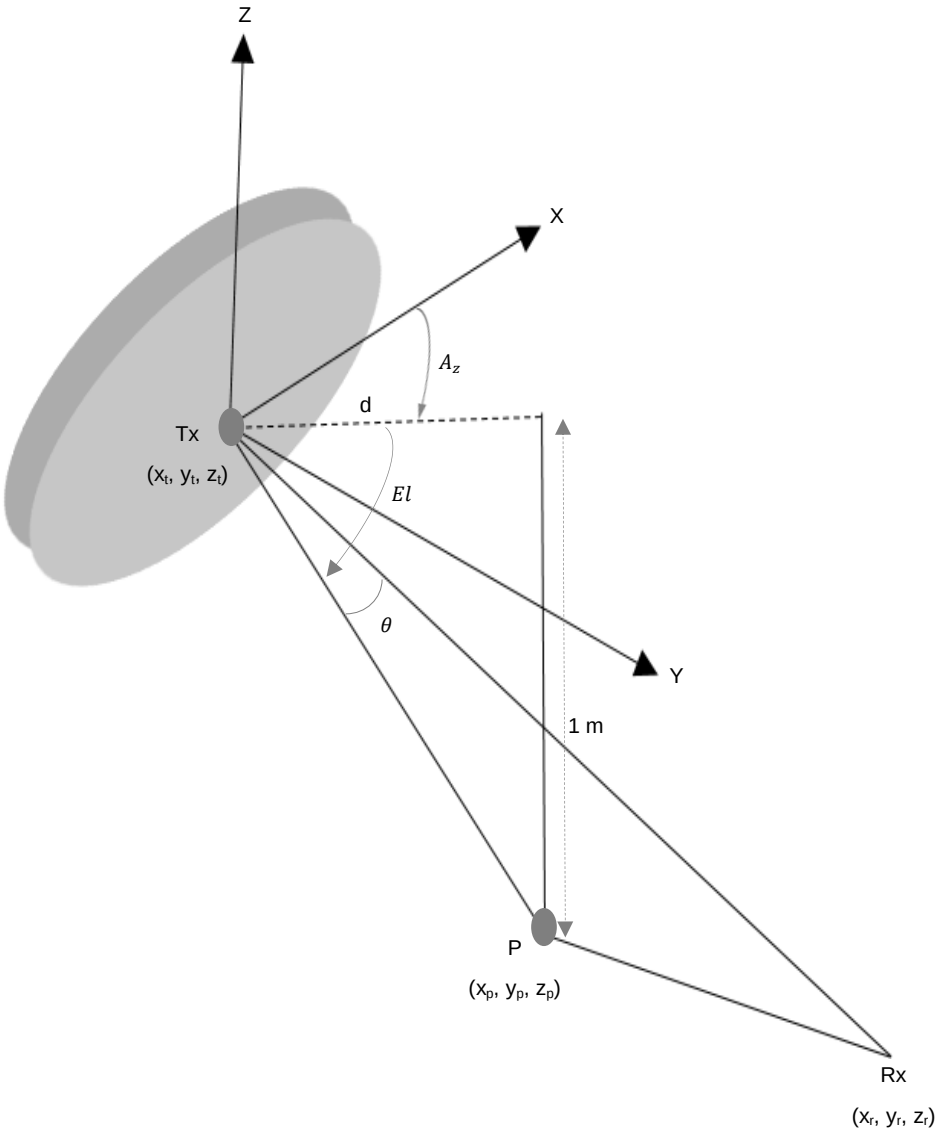

Figure 7-4: Elevation and azimuth analysis for the MBT.

Eight MBT-RYGB LDs light units were installed on the ceiling and used for illumination and data communication. Each MBT-RYGB LDs light unit had seven branches and each branch had two RYGB LDs. However, due to the narrow FOV of each branch in the MBT, the illumination level of lighting that is recommended by the ISO and European standards cannot be maintained (i.e., illumination will be lower than 300 lx) [108] as shown in Figure 7.5 (a). Therefore, additional RYGB LDs light units (four support RYGB LDs light units) were added to enhance the illumination level (see Figure 7.1). These support RYGB LDs light units were used for illumination only, and each unit had 3 × 3 RYGB LDs. Hence, the required illumination level in the room was achieved as shown in Figure 7.5 (b). It should be noted that an increase in the number of MBT-RYGB LDs light units and/or the number of RYGB LDs in each branch of the MBT-RYGB LDs light units could not help achieve the target illumination level (i.e., 300 lx). Therefore, the support RYGB LDs light units were added to enhance the illumination level (these support light units can be either LDs or LEDs as they are not used for communication).

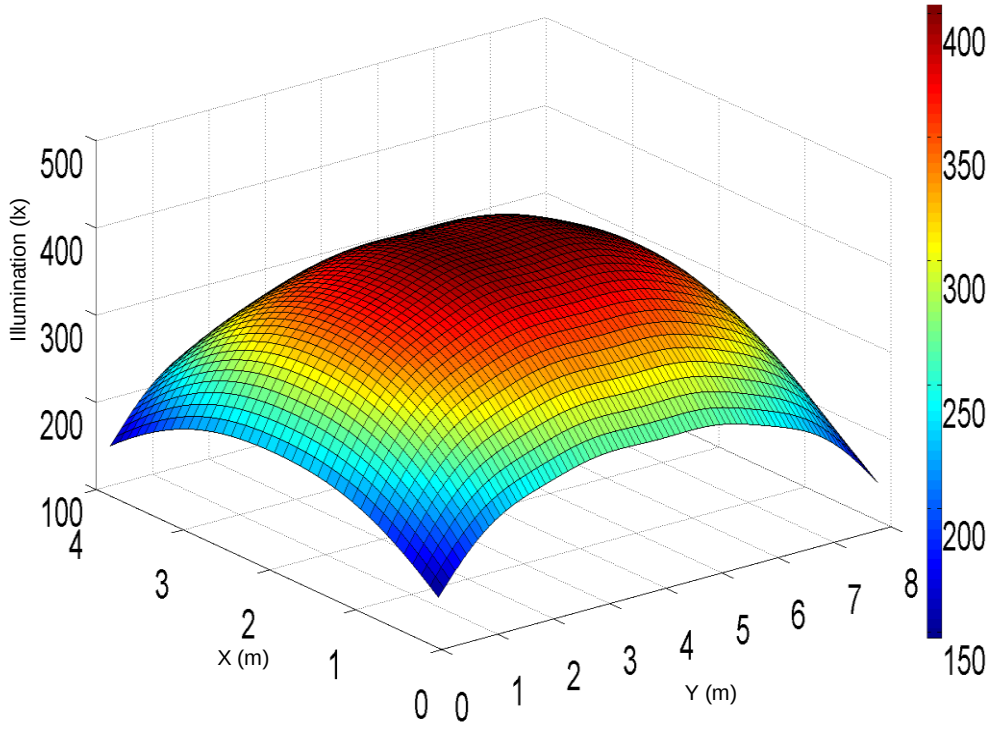

(a)

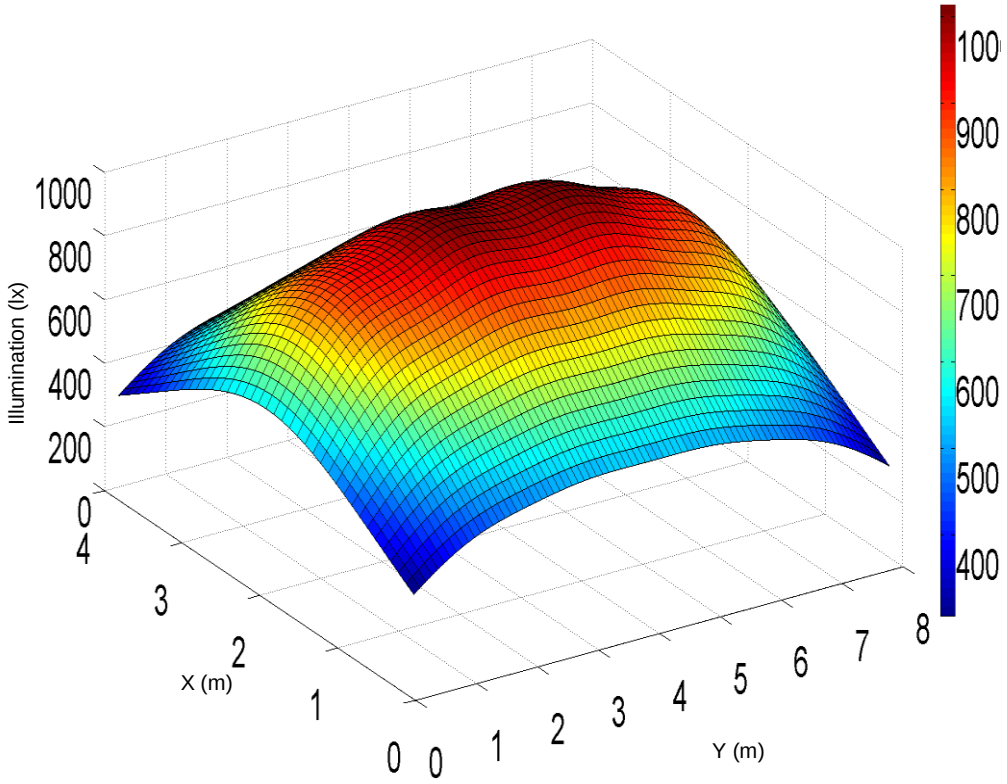

(b)

Figure 7-5: Distribution of illumination at communication floor: (a) without support RYGB LD light units (minimum illumination 107 lx and maximum illumination 403 lx) and (b) with support RYGB LD light units (minimum illumination 305 lx and maximum illumination 1012 lx).

The room and light units parameters are shown in Table 7.1.

Table 7.1: Simulation parameters

Parameters	Configurations	
Room		
Length	8 m	
Width	4 m	
Height	3 m	
ρ-xz Wall	0.8	
ρ-yz Wall	0.8	
ρ-xz op. Wall	0.8	
ρ-yz op. Wall	0.8	
ρ-Floor	0.3	
Bounces	1	2
Number of elements	32000	2000
d_A	5 cm × 5 cm	20 cm × 20 cm
Lambertian emission order (n)	1	
Support RYGB LDs light units		
Number of units	4	
Locations (*x, y, z*) m	(2, 1, 3), (2, 3, 3), (2, 5, 3), (2, 7, 3)	
Number of RYGB-LDs/ unit	9 (3 × 3)	
Elevation	90^o	
Azimuth	0^o	
Transmitted optical power/RYGB LDs	1.9 W	
Centre luminous intensity/RYGB LDs	162 cd	
Lambertian emission order (n)	0.65	
MBT- RYGB LDs light units		
Number of units	8	
Number of TBs/unit	7	
Locations(*x, y, z*) m	(1, 1, 3), (1, 3, 3), (1, 5, 3), (1, 7, 3), (3, 1, 3), (3, 3, 3), (3, 5, 3), (3, 7, 3)	
Elevation/TB	90^o, 60^o, 60^o, 60^o, 60^o, 60^o, 60^o	
Azimuth/TB	0^o, 0^o, 60^o, 120^o, 180^o, 240^o 300^o	
Transmitted optical power/RYGB LDs	1.9 W	
Centre luminous intensity/RYGB LDs	162 cd	
Lambertian emission order (n)	11	

7.4 Evaluation of the Performance of the MBT for a Single User VLC System.

In this section, we report the performance of the MBT for the single user VLC system. Two receivers were used in this section: W-FOV receiver and ADR. The W-FOV receiver has a responsivity of 0.4 A/W and FOV of 40^o to enable it to view at least one transmitter at any location on the communication floor. In addition, the area of the W-FOV receiver was selected to be 1 mm^2, which enables the W-FOV receiver to work at a high data rate up to 4.4 Gb/s [79]. The ADR is a group of narrow FOV detectors directed in different directions. In this work, the ADR consisted of seven detector branches (1-7) with photodetectors that have a responsivity of 0.4 A/W. Two angles were used to define the direction of each branch in the ADR: A_z and El. The El angle of the first detector was set at 90^o, whereas the other six detectors were given

an El of 60°. The A_z angle is the orientation of the detector's angle, and the A_z angles of the seven detectors were fixed at 0°, 0°, 60°, 120°, 180°, 240° and 300°. The FOV of each branch was 20°. In the ADR, each photodetector has an active area 0.4 mm^2. Each detector ofin the ADR amplifies the received signal separately; thus, several possible diversity schemes could be considered: SB, EGC and MRC. In the single user VLC system, we used SB scheme to obtain the the results. The W-FOV receiver and each photodetector in the ADR employed a compound parabolic concentrator (CPC) that was introduced in [12]. This CPC has an acceptance angle (ψ) of less than 90° and gain ($g(\psi)$) [12]:

$$g(\psi) = \begin{cases} \dfrac{N^2}{sin^2\psi}, 0 \le \psi \le \Upsilon \\ 0, \quad \psi \ge \Upsilon \end{cases} \tag{7.10}$$

where N is the refractive index and Υ is the incidence angle.

To obtain the result of the MBT for the single user VLC system, we used a simulation tool that was similar to the one developed by Barry *et al* [93]. The simulation tool was used to produce the impulse response and to calculate the delay spread and SNR. The effect of the mobility and reflections on the system performance were taken into account. The results were obtained when the mobile user moved along x = 0.5 m and x = 2 m, which represents the worst-cases as the ISI is high at x = 0.5 m and the distance between the MBT-RYGB LDs light units and the mobile user being at a maximum at x = 2 m. At each location of the mobile user, one TB is allocated for the optical receiver. Thus, select the best TB algorithm is used to assign the mobile user best TB. Select the best TB algorithm can be obtained following these steps:

1. Each TB is assigned an ID by the controller.
2. The controller gives an order to turn on the TBs individually.
3. At the receiver, the SNR of each TB is calculated.

4. The receiver informs the controller the SNR associated with each TB by sending a feedback signal (using an infrared, IR) at a low data rate. The design of IR uplink has been investigated in [152].
5. The controller selects the TB that achieves the highest SNR.
6. The controller deactivates data communication in the other TBs.

It should be noted that in some optical receiver locations, two or more TBs can achieve the same SNR, due to room symmetry. Therefore, in this case, the controller chooses one TB and ignore the other(s). It is worthy to know that the transmitted data is modulated by the two RYGB LDs in each TB for the single user VLC system.

7.4.1 Impulse response

The impulse responses of the W-FOV receiver and the ADR when the mobile user was at (0.5 m, 0.5 m, 1 m), which represents the worst-case as the ISI is high at this location, shown in Figure 7.6 (a) and Figure 7.6 (b), respectively. Despite the area of the W-FOV is larger than the area of the ADR, the LOS received power at the ADR was high compared to the LOS received power at the W-FOV receiver. This difference in the LOS received power between the two types of receivers (W-FOV receiver and ADR) is due to the difference in the gain of the CPCs that were used in the ADR and W-FOV receiver. In addition, it can be seen that the impulse response of the ADR (see Figure 7.6 (b)) was better than that of the W-FOV receiver (see Figure 7.6 (a)) in terms of signal spread, which reduced the delay spread and improved the 3 dB channel bandwidth. This was due to the FOV for each branch of the ADR being lower than that in the W-FOV, which limited the number of rays captured by the ADR.

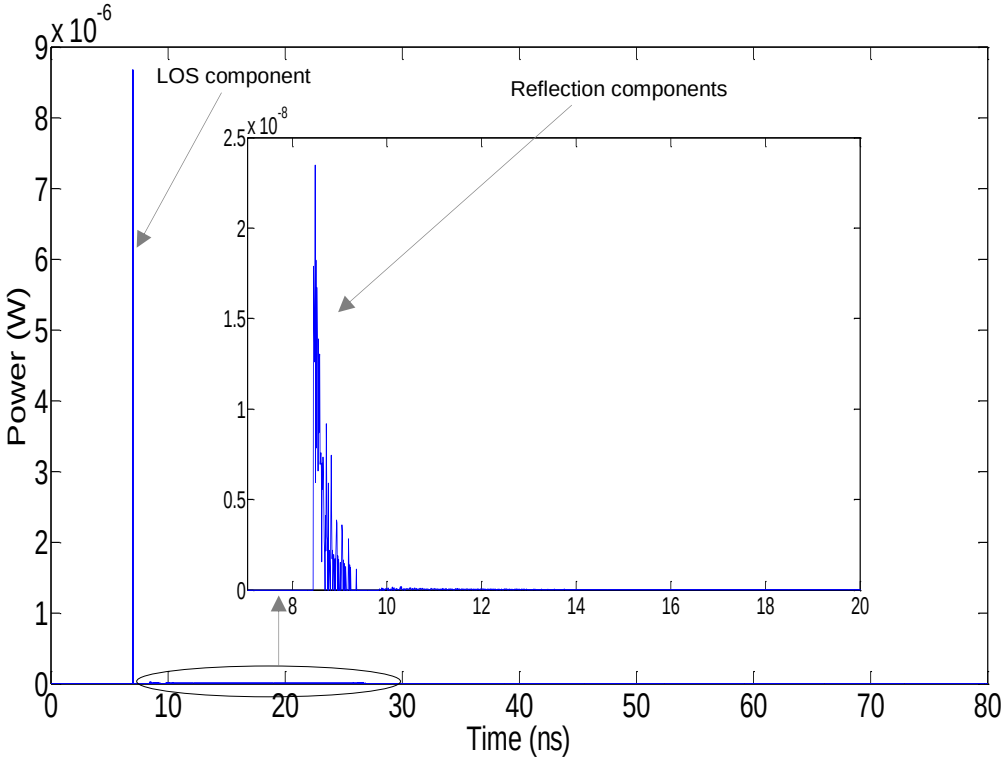

(a)

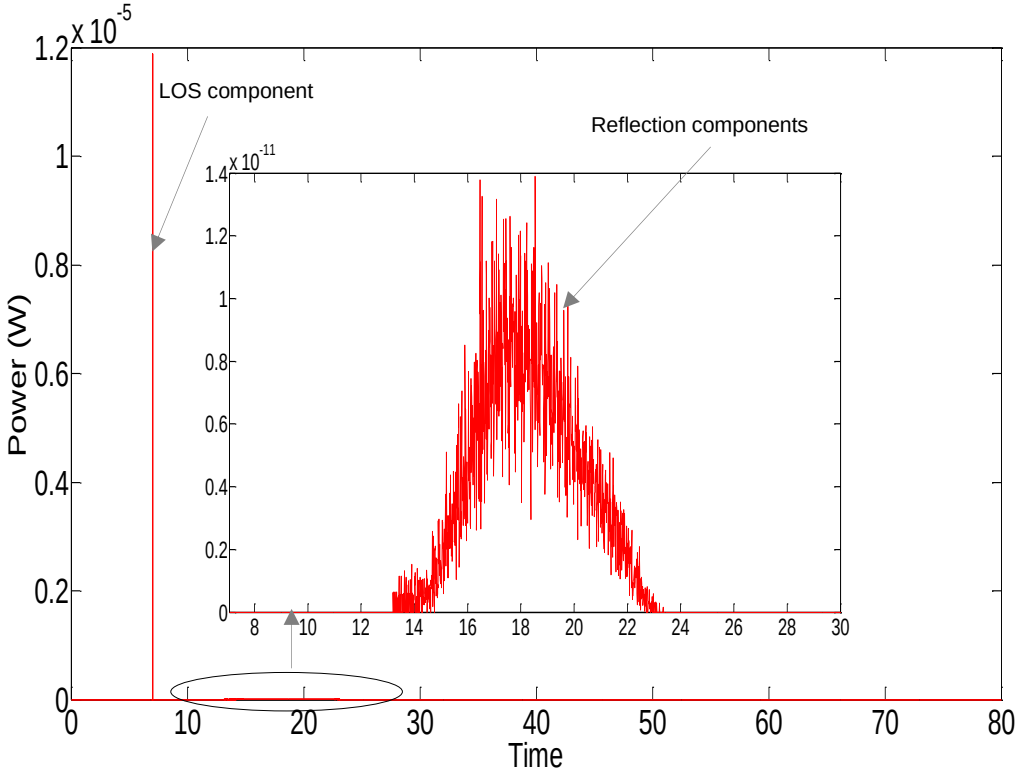

(b)

Figure 7-6: Impulse responses when the mobile user is located at (0.5 m, 0.5 m, 1 m): (a) W-FOV receiver and (b) ADR.

7.4.2 Delay spread evaluation and 3-dB channel bandwidth

Figure 7.7 illustrates the delay spread of the W-FOV receiver and the ADR when the mobile user moves along the *y*-axis over the communication floor at x = 0.5 m and at x = 2 m. It should be noted that the delay spread is affected by the received power, therefore; reduction in collected power from the reflection components leads to a reduction in delay spread. Thus, it can be seen that the delay spread when the W-FOV receiver was used was worse than when the ADR was used along x = 0.5 m. This is attributed to the large FOV of the W-FOV receiver, which means the number of rays that were captured by the W-FOV receiver is large compared with that of the ADR. However, when the mobile user moves at x = 2 m, the ADR offers better performance over the W-FOV at (2 m, 0.5 m, 1 m) and (2 m, 7.5 m, 1 m) only. This is due to the W-FOV receiver and the ADR were located far from walls at x = 2 m and the TB that served the mobile user at x = 2 m directed to the communication floor of the room, which means reflections from walls and the ceiling of the room are very low. Thus, the performance of the W-FOV is comparable with that of the ADR. We can conclude that the ADR offers better performance over the W-FOV receiver when the optical receiver is located near to the walls of the room.

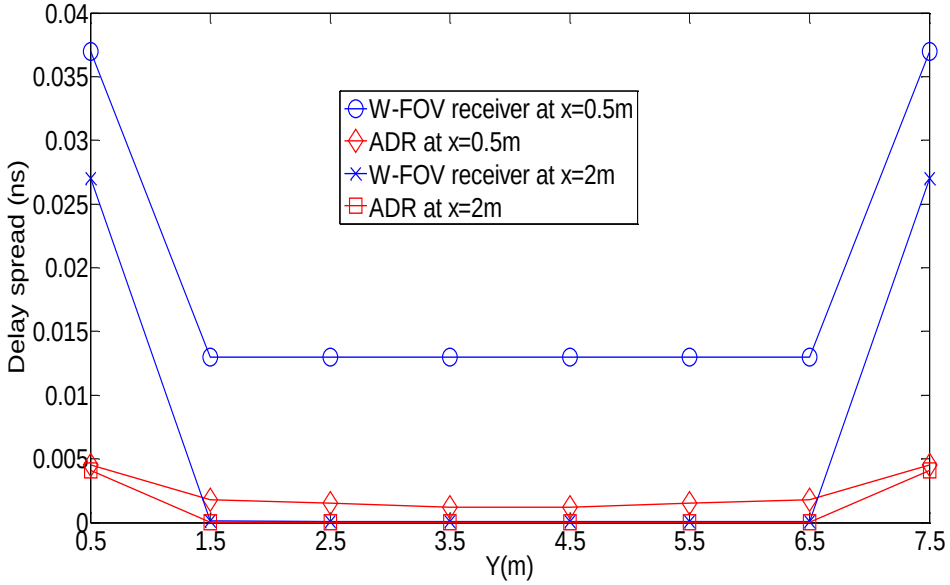

Figure 7-7: Optical receiver delay spread distribution of the W-FOV receiver and ADR when the mobile user moved along y –axis and at x = 0.5 m and x = 2 m

The 3 dB channel bandwidth is a significant factor in the VLC system that is used to measure the ability of the VLC channel to support at a certain data rate. Table 7.2 illustrates the 3-dB channel bandwidth of the mobile user along the *y*-axis and at x = 0.5 m and x = 2 m with two types of receivers (W-FOV and ADR). In general, the ADR provides bandwidth larger than that of the W-FOV receiver. This is due to the ADR reducing the effect of the reflection components due to the narrow FOV of each photodetector, which significantly reduces the delay spread and increases the bandwidth. It can be seen that the minimum value of the 3-dB channel bandwidth is 4.5 GHz for the W-FOV receiver and 22.3 GHz for the ADR. These values of the 3-dB channel bandwidth enable the indoor channel of the VLC system to support a high data rates up to 6.4 Gb/s for W-FOV receiver and up to 31.8 Gb/s for ADR without ISI while using a simple modulation technique (OOK). This is attributed to the optimum receiver bandwidth in an optical direct detection system being 0.7 times the bit rate [99]. When the optical receiver is located at the middle of the room (at x = 2 m), the channel of the indoor visible light communication system can be assumed to be flat channel for both receivers. This is due to the reflection components, which make the indoor channel acts as low pass filter, are very low at x = 2 m.

Table 7.2: 3-dB Channel bandwidth of the mobile user along y-axis.

Y(m)	3-dB Channel bandwidth (GHz)			
	Receiver at x = 0.5 m		Receiver at x = 2 m	
	W-FOV	ADR	W-FOV	ADR
0.5	4.5	22.3	6.17	24.4
1.5	7.7	55.6	Flat channel	Flat channel
2.5	7.7	56.1	Flat channel	Flat channel
3.5	7.7	56	Flat channel	Flat channel
4.5	7.7	56	Flat channel	Flat channel
5.5	7.7	56	Flat channel	Flat channel
6.5	7.7	56	Flat channel	Flat channel
7.5	4.5	22.3	6.17	22.4

7.4.3 SNR Evaluation

Figure 7.8 shows the results of the SNR of the two receivers when operating at a bit rate of 4 Gb/s. Our system's SNR was obtained when the mobile user moved along the *y*-axis and x = 0.5 m and x = 2 m. It can be seen that the lowest value of the SNR achieved by the W-FOV receiver was 13.2 dB when the mobile user was placed at (0.5 m, 0.5 m, 1 m). This means that the W-FOV receiver provides a good communication link at a data rate of 4 Gb/s. A significant improvement was achieved in the SNR at a data rate of 4 Gb/s when the ADR was used instead of the W-FOV receiver along x = 0.5 m. This improvement in the SNR due to the narrow FOV of each branch in the ADR that leads to a reduction in the reflection components. However, the performance of the W-FOV is comparable to that of the ADR when the optical receiver was located at the centre of the room (i.e. along x = 2 m) as can be seen in Figure 7.8. This is due to the W-FOV receiver and the ADR were placed far from walls of the room at x = 2 m. In addition, the TB that served the mobile user at x = 2 m is directed to the communication floor of the room, which means reflections from walls and the ceiling of the room are very low. Thus, both receivers can offer a good performance at a data rate of 4 Gb/s in the center of the room.

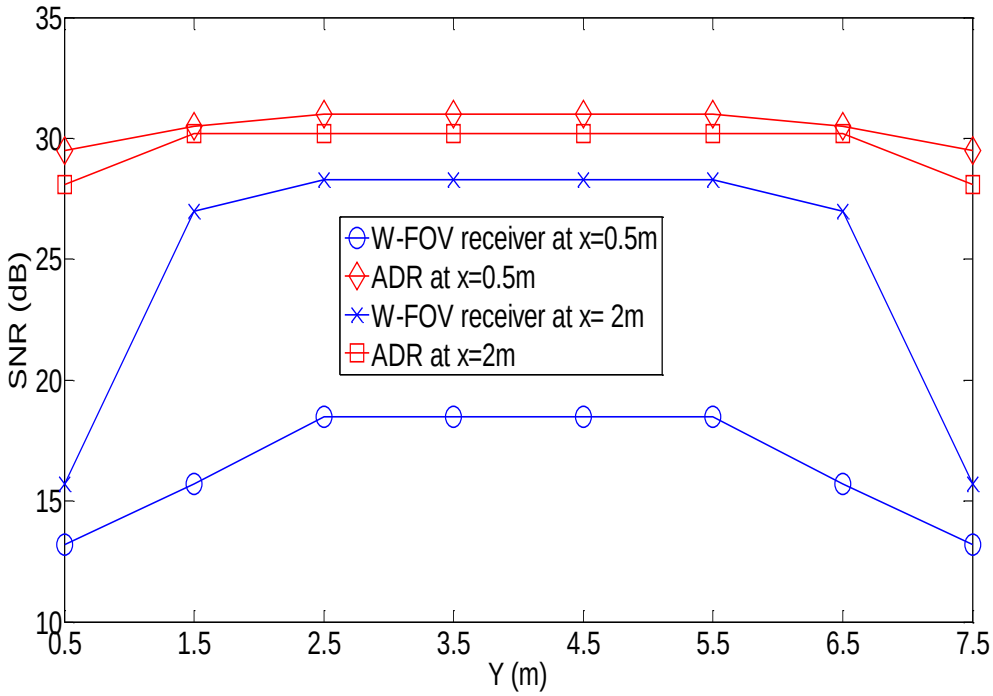

Figure 7-8: SNR of the W-FOV receiver and the ADR when operating at 4 Gb/s at x = 0.5 m and at x = 2 m along the y-axis.

Figure 7.9 illustrates the mobile user SNR of the ADR when the system operates at a data rate of 10 Gb/s. We only present the results of the ADR at a data rate of 10 Gb/s. This is due to the 3-dB channel bandwidth produced by the W-FOV receiver (see Table 7.2) not being able to transfer a high data rate of 10 Gb/s when the optical receiver was located at the corner of the room (at (0.5 m, 0.5 m, 1m) and at (0.5 m, 7.5 m, 1 m)). In addition, the photodetector area of the W-FOV receiver is 1 mm^2, which enable it to work at a data rate up 4.4 Gb/s. We emphasise that the performance of the W-FOV receiver is comparable to the ADR when the optical receiver is located far from the walls of the room where the reflections components are very low. It can be seen that the lowest SNR is 14.2 dB when the ADR operated at a data rate of 10 Gb/s, which gives a BER of 1.5×10^{-7}.

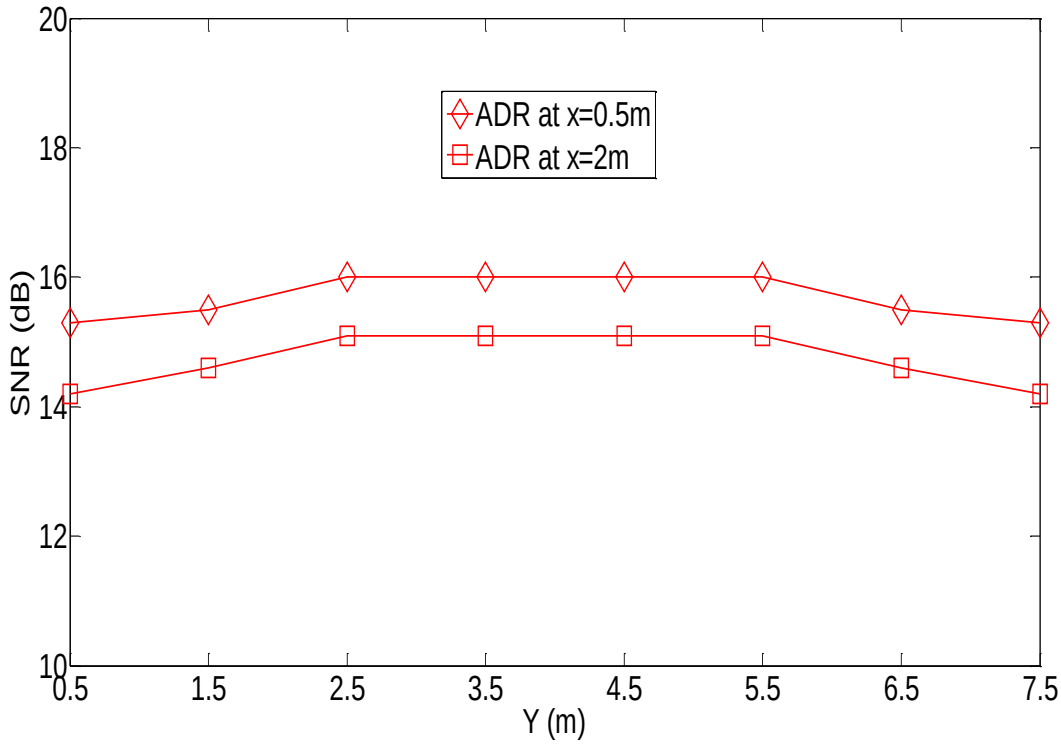

Figure 7-9: SNR of the ADR operating at 10 Gb/s, at x = 0.5 m and at x = 2 m along the y-axis.

7.5 MBT for Multiuser Indoor VLC System.

Due to direct each TB to a specific location on the communication floor of the room, many users can be served simultaneously. In addition, we used RYGB LDs as luminaires; hence, WDM can be used to enable each TB serves

up to four users at the same time. Allocating an optimum transmitter for each user in multiuser indoor VLC system is one of the main challenges that need to be tackled. In this section, we proposed SCM tones to assign a TB for each user.

Each user is connected with the TB that offers good channel conditions (high optical power and low level of CCI). These SCM tones are unmodulated signals and were used to identify each TB, allocate the best TB for each user, calculate the CCI between the TBs and managing the handover during the user mobility. The green colour of the RYGB LDs is used to convey the SCM tones at the beginning of the connection to set up the connection between TBs and users although any colour can be used for this purpose. Once the connection is set up, the data will be transmitted through the four colours of the RYGB LDs.

We used NI-ADR that shown in Figure 7.10 as an optical receiver for the multiuser VLC system. This NI-ADR has seven faces (1-7) and each face has an array of four photodetectors (2 × 2). Each photodetector has an area of 0.5 mm^2, which enable it to work at a data rate up to 8.8 Gb/s [79]. Due to using WDM, each photodetector in each branch of the NI-ADR was covered by a different optical filter. Four WDM channels are used; hence, four optical filters (red, yellow, green and blue) are utilized as shown in Figure 7.10. Thus, each photodetector responds to a specific wavelength. The El angle of the first face was set at 90^o, whereas the other six branches were given an El of 60^o. The A_z angles of the seven faces were fixed at 0^o, 0^o, 60^o, 120^o, 180^o, 240^o and 300^o. The FOV of each photodetector in each face was set to 20^o. The characteristics of the ADR (A_{zs}, Els and FOVs) were chosen to enable the NI-ADR sees at least one transmitter at any location of the optical receiver on the communication floor. We used SB scheme for the photodetectors that covered by the same colour filters as shown in Figure 7.10.

As mentioned, the green channel is utilized to convey the SCM tones for setting up the transmission between users and transmitters, which means a data is not transmitted at the beginning of the connection. Therefore, the outputs of green photodetectors of each user entered to SCM tone

identification system to find the optimum TB for each user as can be seen in Figure 7.10.

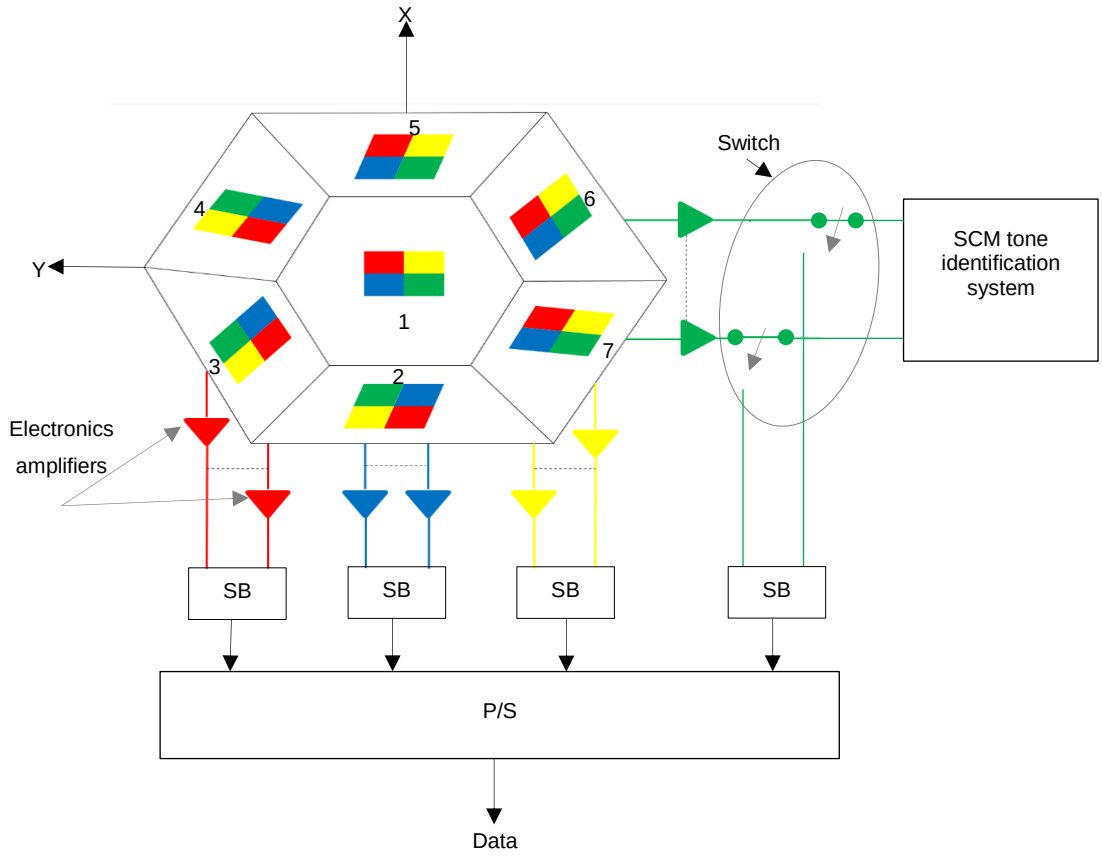

Figure 7-10: NI-ADR configuration.

The SCM tone identification system is utilized to match each user with a TB that offers a good communication link without needing to know the location of the user. In addition, these SCM tones are utilized to obtain the CCI level at each user. The output of the photodetectors that covered by the green filters enters to SCM tone identification system that shown in Figure 7.11. Each TB is given a unique frequency. At the receiver, the output of the green photodetectors enters into bandpass filters (BPFs). These BPFs have centre frequencies equal to the frequencies of the SCM tones. The range of the frequencies given to the SCM tones should be chosen near to the DC of the indoor channel frequency response where the channel has low attenuation. From Table 7.2, we can see the minimum 3-dB channel bandwidth is 4.5 GHz. Thus, the frequency range chosen for SCM tones was 500 MHz to 3.8 GHz

with a guard of 60 MHz. In addition, the bandwidth of the BPF was chosen to be 4 MHz, which reduces the noise that seen by each SCM tone, and allows for SCM oscillator drift and BPF tolerances. Due to each TB was given a unique SCM tone, the output of the BPFs is a SCM tone plus noise. Based on the analyses that have been done in chapter 5 and chapter 6, the SCM tone identification system has the ability to allocate each user to its closest TB with a probability of error not more than 10^{-11}.

As seen in Figure 7.1, the controller is used to manage the connection between transmitters and users. At receiver side of each user, the carrier to noise (CNR) ratio of each SCM tone is calculated. The optical receiver of each user informs the controller the value of CNR associated with each SCM tone. Hence, the controller sorts the TBs in descending order (each user has a different descending order of TBs starting with the TB that has the highest (CNR) and ending with the TB that has the lowest (CNR)). Therefore, the controller allocates each user the TB that yields highest CNR from its group. For uplink transmission, we used the IR uplink design that proposed in [130]. In addition, each user was assigned a time slot to send the feedback information to the controller, which prevent interference in the uplink. The CNR of any SCM tone at any user is given as:

$$CNR = \frac{\left(R_g\, Pr\right)^2}{2\,{\sigma_{ts}}^2} \tag{7.11}$$

here R_g is the photodetector's responsivity for the green spectrum, Pr is the received optical (green) power and σ_{ts} is the total standard deviation of the noise that seen by each SCM tone. It should be noted that to calculate σ_{ts}, we considered the bandwidth of the BPF.

The SCM tones are used also to calculate the CCI level. However, no interference occurs between these SCM tones as shown in Figure 7.11. Thus, we defined the CCI level at any user, as the total received power of all SCM tones except the one that was allocated to the user. For instance, if the

allocated tone of mth TB is f_m, the CCI level at *nth* user (I_n) due to the other SCM tones can be given as:

$$I_n = \sum_{\substack{k=1 \\ k \neq m}}^{Ma} \left(\frac{R_g \, Pr_{n,k}}{2}\right)^2, \quad n \in [1, 2 \dots N], \quad m \in [1, 2 \dots Ma] \tag{7.12}$$

where Ma is the number of active TBs (the TBs assigned to other users to send a data) and N is the number of users.

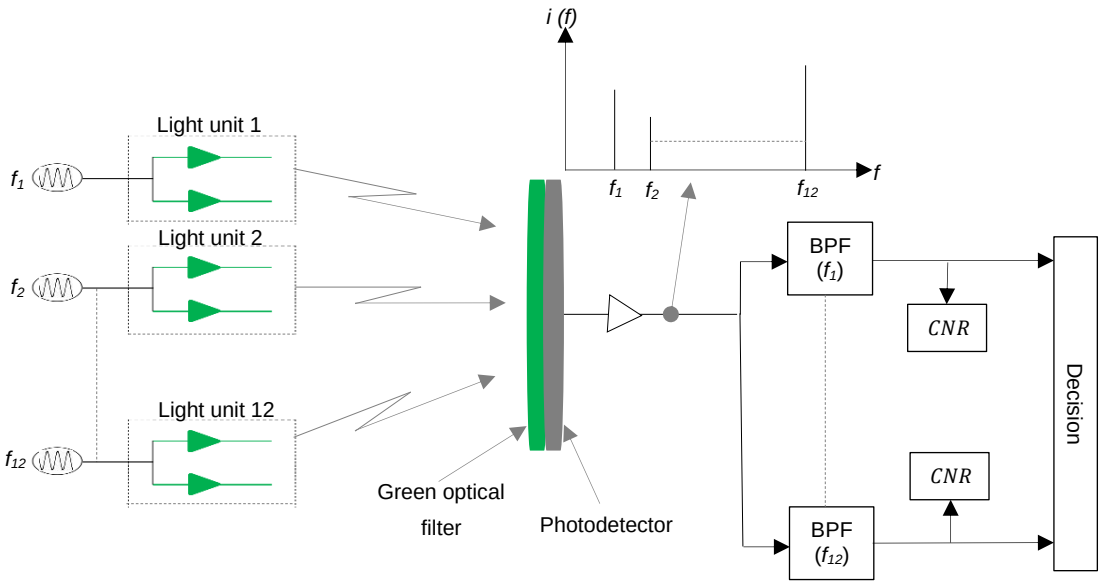

Figure 7-11: Structure of the SCM tone identification system.

Once the controller assigns a TB for each user, the data will be transmitted through the four channels of the RYGB LDs. In this system, we consider the effect of CCI interference. Thus, signal to interference to noise ($SINR$) ratio is used to evaluate the performance of this system. In general, The $SINR$ of the *nth* user is given as [94], [103]:

$$SINR_n = \frac{R^2 (P_{s1} - P_{s0})_n^{\,2}}{{\sigma_t}^2 + I_n} \tag{7.13}$$

It should be noted that we used the green channel to estimate the level of the CCI. For each user, we obtained the CCI level of other channels from the green channel. Each colour of the RYGB LDs has a different transmitted optical power (to obtain an acceptable white colour [113]). In addition, each photodetector in each face of the NI-ADR sees the same area and each photodetector has a specific optical filter that has a different responsivity. Thus, the CCI level of the data channels of the *nth* user (I_n) can be obtained from the CCI level that calculated from SCM tones as:

$$I_{red} = \left(\frac{R_r}{R_g}\right)^2 \left(\frac{Pt_r}{Pt_g}\right) I_{green} \quad , \quad I_{yellow} \left(\frac{R_y}{R_g}\right)^2 \left(\frac{Pt_y}{Pt_g}\right) I_{green} \text{ and } I_{blue} \left(\frac{R_b}{R_g}\right)^2 \left(\frac{Pt_b}{Pt_g}\right) I_{green} \tag{7.14}$$

here R_r, R_y and R_b are responsivity of the photodetector for the red, yellow and blue colours, respectively and Pt_r, Pt_g, Pt_y and Pt_b are the red, green, yellow and blue optical transmitted power, respectively. Hence, the $SINR$ of each data channel at any user is written as:

$$SINR_{red} = \frac{R_r^2 (P_{s1} - P_{s0})^2}{{\sigma_t}^2 + \left(\frac{R_r}{R_g}\right)^2 \left(\frac{Pt_r}{Pt_g}\right) I_{green}} \tag{7.15}$$

$$SINR_{yellow} = \frac{R_y^2 (P_{s1} - P_{s0})^2}{{\sigma_t}^2 + \left(\frac{R_y}{R_g}\right)^2 \left(\frac{Pt_y}{Pt_g}\right) I_{green}} \tag{7.16}$$

$$SINR_{blue} = \frac{R_b^2 (P_{s1} - P_{s0})^2}{{\sigma_t}^2 + \left(\frac{R_b}{R_g}\right)^2 \left(\frac{Pt_b}{Pt_g}\right) I_{green}} \tag{7.17}$$

$$SINR_{green} = \frac{R_g^2 (P_{s1} - P_{s0})^2}{{\sigma_t}^2 + I_{green}} \tag{7.18}$$

Table 7.3 gives the simulation parameters that were used in the multiuser VLC system.

Table 7.3: Simulation parameters of the multiuser VLC system.

Parameters	Configurations
Optical power of R LD	0.8 W
Optical power of Y LD	0.5 W
Optical power of G LD	0.3 W
Optical power of B LD	0.3 W
Number of ADR branches	7
Number of photodetectors/branch	4
FOV of each photodetector	20º
Elevation of each branch	90º, 60º, 60º, 60º, 60º, 60º, 60º
Azimuth of each branch	0º, 0º, 60º, 120º, 180º, 240º 300º
Photodetector's area	1 mm^2
Photodetector's responsivity (red)	0.4
Photodetector's responsivity (yellow)	0.35
Photodetector's responsivity (green)	0.3
Photodetector's responsivity (blue)	0.2

Each TB can serve up to four users simultaneously. Therefore, to evaluate the performance of the multiuser VLC system, we obtained the maximum data that can be transmitted from each channel of the user located at (0.5 m, 0.5 m, 1 m) versus an increase in the number of the active users. We considered that each channel carries a maximum data with BER not exceed 10^{-6}, which gives a reliable connection between users and transmitters. We obtained the maximum data for a user located at (0.5 m, 0.5 m, 1 m,) as this location represents the worst case. This is attributed to reflections are high at this location. Hence, we ensured that other users have better or equal performance of this user. In this system, we considered the effect of diffuse reflections and CCI to obtain the performance of the system. It is worthy to mention that each channel has a 3-dB channel bandwidth (22.3 GHz) similar to that mentioned

in Table 7.2 at (0.5 m, 0.5 m, 1 m). The CCI occurs when multiple signals from the interfering TBs land on the optical receiver.

The interference is happened due to either LOS components and/or reflection components. However, we used NI-ADR, which has many faces pointed to a different locations. Thus, the controller can assign two TBs from two different directions when two users are located at the same location as shown in Figure 7.12. Hence, we guaranteed that there is no CCI due to LOS components (just due to reflection components). In addition, when the number of users is large the controller can allocate one or two channel(s) for each user as the TB can serve up to four users at the same time.

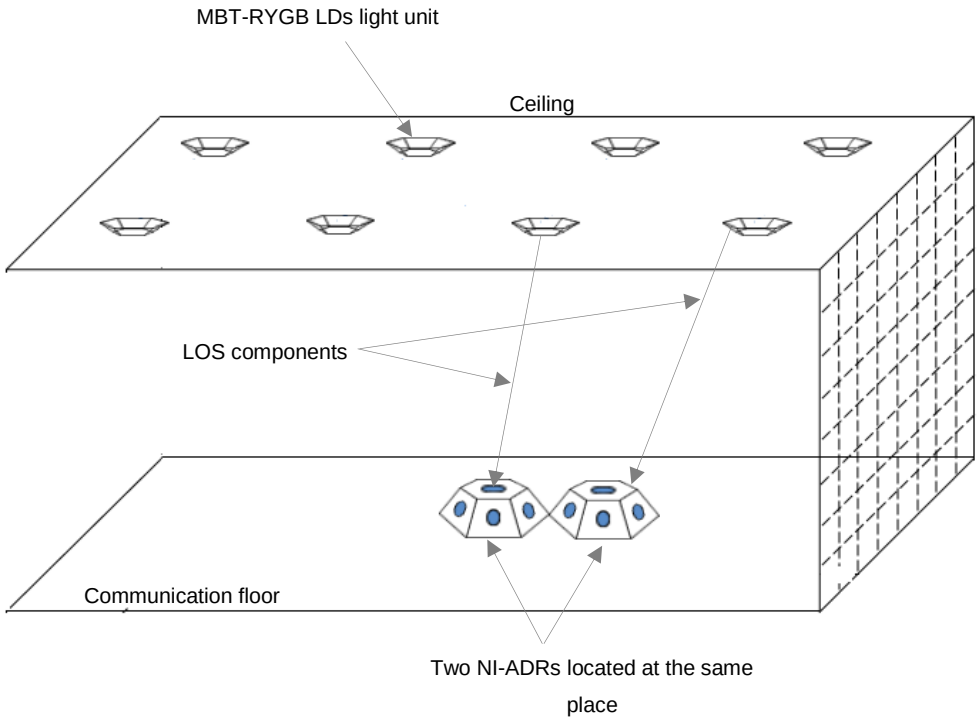

Figure 7-12: Two NI-ADRs located at same place and served by different directions of TBs to prevent interference between LOS components.

Figure 7.13 depicts the influence of the increase in the number of active users on each channel data rate of the user who was located at (0.5 m, 0.5 m 1 m). In addition, the aggregate data rate of the four channels is shown in Figure 7.13. The data rate of each channel was calculated when the BER = 10^{-6} (SINR = 13.6 dB), which gives a reliable link between the transmitter and

the receiver. It should be noted that we obtained the data rate of the user who was placed at (0.5 m, 0.5 m, 1 m) as reflections are high at this location, which leads to high ISI and high CCI. Thus, we guaranteed that all users have a data rate better or similar to that one shown in Figure 7.13 at any location on the communication floor of the room.

As can be seen in Figure 7.13, the red channel offers a higher data rate than the other channels. This is due to the transmitted optical power of the red LD is higher than the other LDs (see Table 7.3). In addition, the responsivity of the red filter is higher than the responsivity of the yellow filter, green filter and blue filter. Due to using MBT as a transmitter and NI-ADR as a receiver, this leads to eliminate interference due to LOS components (CCI happened due to reflections components only). In addition, the limited FOV (FOV = 20^{o}) of each photodetector in each face of the NI-ADR, limited range of rays captured by each photodetector, which leads to a reduction in the effect of the CCI due to the reflection components. Hence, when each TB serves one user, the system can support 56 users with an aggregate data rate not less than 16.3 Gb/s of each user as shown in Figure 7.13.

When each TB serves one optical receiver (i.e. the four channels of the TB are assigned to one optical receiver), the VLC system can support 56 optical receivers with an aggregate data rate per optical receiver not less than 16.3 Gb/s as shown in Figure 7.13. However, each TB can serve up to 4 devices simultaneously (when these devices located inside the coverage area of the TB). Therefore, when each device is given only one channel, our proposed VLC system can support up to 224 devices at a data rate not less than 2.15 Gb/s (the minimum data rate of the blue channel) as can be seen in Figure 7.13. We do not consider the fairness between devices in this work. Thus, the controller assigns one channel for each device in a random way in this case. The aggregate capacity of our proposed VLC systems when fully loaded can be calculated based on the number of the MBT-RYGB LDs light units in the room (eight), the number of TBs per MBT-RYGB LDs light units (seven), the number of colors per TB (four) and the data rate achieved by each colour. Thus, our proposed VLC system can achieve an aggregate data rate of 912.8 Gb/s. Hence, our suggested system may be deployed for indoor

internet of things (IoT) applications as many devices (with a high data rate) can be served in a small area.

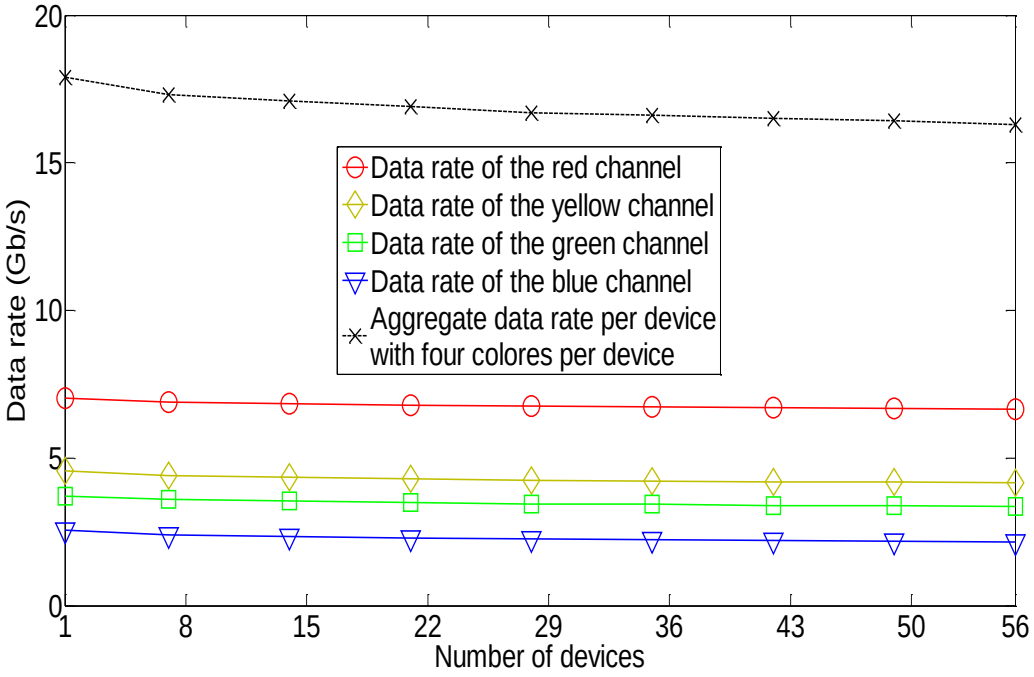

Figure 7-13: Data rate of each channel and aggregate data rate per optical receiver placed at (0.5 m, 0.5 m, 1 m) versus the number of optical receivers.

7.6 Summary

In this chapter, we used a MBT to improve the performance of indoor VLC systems. The MBT had seven TBs and each one of these TBs is directed to a specific location on the room's communication floor. This led to an improvement in the 3dB channel bandwidth of the indoor VLC system and therefore an increase in the received optical power. Two VLC systems were proposed based on MBT: a single user VLC system and a multiuser VLC system. For the single user VLC system, we used a W-FOV receiver and an ADR as optical receivers. The results showed that the single user VLC system offers a data rate of 4 Gb/s and 10 G b/s when using W-FOV receiver and ADR, respectively. The influence of diffuse reflections (up to second order), mobility and lighting constraint were taken into account for the single user VLC system.

In the multiuser VLC system, we proposed SCM tones for resource allocation. Thus, each optical receiver was assigned a TB that offers good performance without the need to know the location of the optical receiver. RYGB LDs were used as luminaires. We, therefore, used WDM to achieve a higher data rate for each optical receiver. In the multiuser VLC system, we proposed NI-ADR as an optical receiver where each photodetector was covered by a specific optical bandpass filter. We considered the effect of the CCI between transmitters in the multiuser VLC system. The results showed that this system can support up to 56 devices when each device was allocated four channels at a data rate not less than 16.3 Gb/s and BER not exceeded 10^{-6}. When each user was allocated one channel, this enabled the TB to serve up to four users simultaneously. Hence, the system can support 224 devices at a data rate not less than 2.15 Gb/s. Therefore, this system may be deployed for indoor IoT applications as many devices (with a high data rate) can be served in a small area.

8. Conclusions and Future Work

8.1 Introduction

This chapter summarises the work that has been achieved and presented in this thesis as well as its findings and original contributions. In addition, it suggests possible directions for future research in the area. Next section presents the contributions of the thesis. Section 8.3 introduces the potential areas that deserve further investigations.

8.2 Conclusions of Research Work

VLC systems have become promising candidates to complement conventional RF systems. This is due to the increasingly saturated RF band and the potential high data rates that can be achieved by VLC systems. A major interest in VLC systems is to understand and tackle the design challenges to achieve multi gigabits per second. These challenges include the low modulation bandwidth of the LEDs, ISI due to multipath propagation and CCI due to multiple transmitters. In addition, resource allocation is one of the main challenges that face VLC systems to achieve a high data rate multi-user. This thesis has presented a range of tools and mathematical models and simulation methods to model the VLC channel link for a single user and multi-user scenarios in different indoor environments. The proposed systems were evaluated in a typical rectangular room with dimensions of 4 m × 8 m × 3 m (width × length × height). The simulation results were carried out through the use of a light ray tracing algorithm where the transmitted VLC signal travels through various paths (LOS, first and second reflections) of different lengths before it reaches to the receiver. The simulations and calculations reported in this thesis were carried out using MATLAB. The performance evaluation of the VLC systems concentrated on the impulse response, delay spread, 3 dB channel bandwidth, SNR and BER.

In this thesis, we used RYGB LDs as source of illumination and data communication instead of LEDs to deal with the low modulation bandwidth of the LEDs. For all systems that presented in this thesis, we considered the effect of the diffuse reflections, mobility and lighting constraints (achieve an acceptable illumination level in the room). In addition, we taken into account the effect of the CCI on the multi-user VLC systems. Besides that, we used OOK modulation for all proposed systems.

Three indoor VLC systems based on a CGH were presented in this work: a single beam static CGH-VLC system, a static CGH-VLC system and an adaptive CGH-VLC system. The CGH is used to direct a part of the total power of the best RYGB LDs-light unit, generate beam(s) and focus these beam(s) on a specific area on the communication floor of the room.

In the single beam static CGH-VLC system, the CGH is utilized to direct 30% of the total power of the best transmitter, to generate single broad beam and to direct this beams on an area of 2 m × 2 m on the communication floor. The 30% was selected to ensure that the illumination stayed at the level required by standards. The single beam static CGH-VLC system had the ability to decrease the delay spread of the traditional VLC system (VLC system without using the CGH) and improve the 3 dB channel bandwidth.

In the static CGH-VLC system, the CGH is utilized to direct 30% of the total power of the best transmitter, to generate 100 beams and to direct these beams on an area of 2 m × 2 m. All generated beams transmitted the same data. The static CGH-VLC system was able to achieve a data rate of 8 Gb/s while using a single photodetector and considering the influence of the reflections (up to second order) and mobility of the optical receiver.

In the adaptive CGH-VLC system, the CGH was used to direct 20% of the total power of the best RYGB LDs-light unit, generate eight beams (optimum number of beams dictated by CCI) and steer these beams to the imaging receiver. Each generated beam conveyed a different data stream at a rate of 5 Gb/s. The CCI between beams was taken into account in this system as the beams conveyed different data streams. The adaptive CGH-VLC system

offered a data rate of 40 Gb/s (8 beams × 5 Gb/s) with BER not going below 10^{-9}.

In this thesis, we introduced an indoor VLC system that can offer a data rate of 8 Gb/s with BER = 10^{-6} (SINR = 13.6 dB) when using simple OOK modulation. The system used parallel data transmission sent from multiple RYGB LDs-light units, which are installed on the room's ceiling to get a suitable level of lighting. An imaging receiver was used in this system to benefit from spatial multiplexing and to mitigate the effect of the ISI. SCM tones were proposed in this system to identify each RYGB LDs-light unit and to find the pixel(s) that received the signals from these light units. Additionally, these tones were used to calculate the CCI level between the transmitters. Based on the performance (CCI level and ISI) of each RYGB LDs-light unit, serial data were divided (only) between the light units that were able to send a high data rate with a strong connection. Our proposed system was investigated in two different rooms (empty and realistic rooms) with considering the effect of the CCI and diffusing reflections (up to second order).

A single user VLC system based on WDM that can offer a data rate of 10 Gb/s over the entire proposed room with BER = 10^{-6} and using OOK as a modulation technique was introduced also in this thesis. This WDM system was realised by using RYGB LDs as transmitters and an IMDR as an optical receiver. Each pixel of the IMDR was covered by a specific colour filter, which allowed it to sense a particular colour. Due to using a large number of pixels in the IMDR, we used the MCFA to design the pattern of the array colour filters of each side of the IMDR. In addition, MCFA that has four bands (colours) was used in this work and this is attributed to the use of four colours (RYGB) LD as a transmitter. The effect of the reflection components and the mobility of the IMDR were taken into account.

We proposed also a multi-user VLC system based on SCM tones and WDM in this thesis. The SCM tones were used to give an ID to each light unit, to find the optimum light unit for each user and to calculate the level of the CCI between the light units. The performance of our proposed system was evaluated in an empty room with three users (two stationary users and one mobile user) under four different scenarios. We investigated the performance

of the proposed system with two types of receivers (NI-R and NI-ADR) in the presence of CCI, diffuse reflections and mobility. The results showed that when using the NI-R, the distances between users should be considered to avoid high CCI between the users. However, the NI-ADR eliminates this limitation in the NI-R. In addition, a higher data rate was obtained when the NI-ADR was used compared with the NI-R. This is attributed to the small FOV of the NI-ADR, which limits the number of captured rays due to first and second reflections and consequently reduces the effect of the CCI and diffuse reflections induced ISI.

We used MBT to enhance the indoor channel of VLC systems in this work. The MBT had seven TBs and each one of these TBs directed to a specific area of the communication floor. This led to improve the 3-dB channel bandwidth of the indoor VLC channel and enhance the received optical power. Two VLC systems proposed based on MBT: a single user VLC system and a multiuser VLC system. For the single user VLC system, we used W-FOV receiver and ADR as optical receivers. The results showed that the single user VLC system could offer a data rate of 4 Gb/s and 10 G b/s when using W-FOV receiver and ADR, respectively. The effect of diffuse reflections (up to second order), mobility and lighting constraint were taken into account for the single user VLC system.

In the multiuser VLC system, we proposed SCM tones for resource allocation. Thus, each user was assigned a TB that offers a good performance without needing to know the location of the user. RYGB LDs were used as luminaires. Hence, we used WDM to realise a high data rate for each user. In the multiuser VLC system, we proposed NI-ADR as an optical receiver in which each photodetector was covered by a specific optical filter. We considered the effect of the CCI between transmitters in the multiuser VLC system. The results showed that this system can support up to 56 users when each user was allocated four channels with a data rate not less than 16.3 Gb/s and BER not exceeded 10^{-6}. When each user was allocated one channel, this enabled the TB to serve up to four users simultaneously. Hence, the system could support 224 users at a data rate not less than 2.15 Gb/s. Therefore, this

system may be deployed for indoor IoT applications as many users with a high data rate can be served in a small area.

8.3 Future Work

The following is a list of potential areas that deserve further investigation and research:

1. Investigate the CGHs for a high data rate multi-user VLC system. The CGHs can be used to generate many beams and direct each beam to a specific direction. Each beam can be utilized to serve one user or up to four users (with using WDM). When these users located at the in the coverage area of the beam.
2. Multicarrier code division multiple access (MC-CDMA) is a transmission scheme that combines the robustness of orthogonal modulation with the flexibility of CDMA schemes. MC-CDMA can be used to provide high data rates for multi user scenarios.
3. In indoor VLC systems, all light units typically emit signals simultaneously, which means the signal from the closest light unit reaches the receiver before signals from distant light units. This causes ISI and degrades the performance of VLC systems. Delay adaptation technique (DAT) can be used to improve the indoor channel of VLC systems. In DAT, signal that has the longest journey is sent first and then the other signals from other light units are sent with different differential delay (Δt). Thus, all signals reach the receiver at the same time. DAT with WDM can be used to obtain a high data rate multi-user VLC system. In this system, the NI-ADR can be used as an optical receive. Thus, each face of the NI-ADR can receive a different data stream from a different transmitter. This leads to increase the aggregate data rate of the user.
4. To further reduce the BER in the proposed VLC systems FEC codes can be used when the VLC systems operate at high data rates.
5. Power adaptation technique (PAT) with genetic algorithm can be used to improve the performance of the VLC systems. Based on the location

of the optical receiver, genetic algorithm can be applied to decide how many light units should be used to serve the user that minimizing the delay spread and maximizing the SNR of the optical receiver.

References

[1] R. W. Burns, *Communications: an international history of the formative years*. IET, 2004.

[2] A. G. Bell, "Upon the production and reproduction of sound by light," *Journal of the Society of Telegraph Engineers,* vol. 9, no. 34, pp. 404-426, 1880.

[3] S. Arnon, J. Barry, G. Karagiannidis, R. Schober, and M. Uysal, *Advanced optical wireless communication systems*. Cambridge university press, 2012.

[4] GreenTouch, Reducing the Net Energy Consumption in Communications Networks by up to 98% by 2020 [online]: "https://s3-us-west-2.amazonaws.com/belllabs-microsite-greentouch/uploads/documents/GreenTouch_Green_Meter_Final_Results_18_June_2015.pdf."

[5] F. R. Gfeller and U. Bapst, "Wireless in-house data communication via diffuse infrared radiation," *Proceedings of the IEEE,* vol. 67, no. 11, pp. 1474-1486, 1979.

[6] G. R. Aiello and G. D. Rogerson, "Ultra-wideband wireless systems," *IEEE microwave magazine,* vol. 4, no. 2, pp. 36-47, 2003.

[7] P. Smulders, "Exploiting the 60 GHz band for local wireless multimedia access: prospects and future directions," *IEEE communications magazine,* vol. 40, no. 1, pp. 140-147, 2002.

[8] M. Tonouchi, "Cutting-edge terahertz technology," *Nature photonics,* vol. 1, no. 2, p. 97, 2007.

[9] T. H. Maiman, "Stimulated optical radiation in ruby," Nature letters, vol.187, no.1, 1960.

[10] K. L. Sterckx, J. M. Elmirghani, and R. A. Cryan, "Pyramidal fly-eye detection antenna for optical wireless systems," 1999.

[11] X. Bao, J. Dai, and X. Zhu, "Visible light communications heterogeneous network (VLC-HetNet): new model and protocols for mobile scenario," *Wireless Networks,* pp. 1-11.

[12] J. M. Kahn and J. R. Barry, "Wireless infrared communications," *Proceedings of the IEEE,* vol. 85, no. 2, pp. 265-298, 1997.

[13] V. N. I. Cisco, "Global Mobile Data Traffic Forecast Update, 2015–2020 White Paper," *Document ID,* vol. 958959758, 2016.

[14] D. Karunatilaka, F. Zafar, V. Kalavally, and R. Parthiban, "LED based indoor visible light communications: State of the art," *Communications Surveys & Tutorials, IEEE,* vol. 17, no. 3, pp. 1649-1678, 2015.

[15] X. Bao, G. Yu, J. Dai, and X. Zhu, "Li-Fi: Light fidelity-a survey," *Wireless Networks,* pp. 1-11, 2015.

[16] H. Haas, L. Yin, Y. Wang, and C. Chen, "What is LiFi?," *Journal of Lightwave Technology,* vol. 34, no. 6, pp. 1533-1544, 2016.

[17] D. O'brien, G. Parry, and P. Stavrinou, "Optical hotspots speed up wireless communication," *Nature Photonics,* vol. 1, no. 5, p. 245, 2007.

[18] G. Yun and M. Kavehrad, "Spot-diffusing and fly-eye receivers for indoor infrared wireless communications," in *Wireless Communications, 1992. Conference Proceedings., 1992 IEEE International Conference on Selected Topics in*, 1992, pp. 262-265: IEEE.

[19] M. D. Audeh and J. M. Kahn, "Performance evaluation of baseband OOK for wireless indoor infrared LAN's operating at 100 Mb/s," *IEEE Transactions on Communications,* vol. 43, no. 6, pp. 2085-2094, 1995.

[20] A. Khalid, G. Cossu, R. Corsini, P. Choudhury, and E. Ciaramella, "1-Gb/s transmission over a phosphorescent white LED by using rate-adaptive discrete multitone modulation," *Photonics Journal, IEEE,* vol. 4, no. 5, pp. 1465-1473, 2012.

[21] T. Cogalan, H. Haas, and E. Panayirci, "Power Control-Based Multi-User Li-Fi Using A Compound Eye Transmitter," in *2015 IEEE Global Communications Conference (GLOBECOM)*, 2015, pp. 1-6: IEEE.

[22] United States Department of Energy. Energy Savings Forecast of Solid-State Lighting in General Illumination Applications.[Online].Available:http://apps1.eere.energy.gov/buildings/publications/pdfs/ssl/energysavingsforecast4.pdf.

[23] H. Elgala, R. Mesleh, and H. Haas, "Indoor optical wireless communication: potential and state-of-the-art," *Communications Magazine, IEEE,* vol. 49, no. 9, pp. 56-62, 2011.

[24] S. H. Lee, S.-Y. Jung, and J. K. Kwon, "Modulation and coding for dimmable visible light communication," *Communications Magazine, IEEE,* vol. 53, no. 2, pp. 136-143, 2015.

[25] J. Luo, L. Fan, and H. Li, "Indoor Positioning Systems Based on Visible Light Communication: State of the Art," *IEEE Communications Surveys & Tutorials,* vol. 19, no. 4, pp. 2871-2893, 2017.

[26] X. Wang *et al.*, "Millimeter wave communication: A comprehensive survey," vol. 20, no. 3, pp. 1616-1653, 2018.

[27] A.-M. Căilean and M. Dimian, "Current challenges for visible light communications usage in vehicle applications: A survey," *IEEE Communications Surveys & Tutorials,* vol. 19, no. 4, pp. 2681-2703, 2017.

[28] A. Street, P. Stavrinou, D. O'brien, and D. Edwards, "Indoor optical wireless systems–a review," *Optical and Quantum Electronics,* vol. 29, no. 3, pp. 349-378, 1997.

[29] M. Kavehrad and S. Jivkova, "Indoor broadband optical wireless communications: optical subsystems designs and their impact on

channel characteristics," *IEEE Wireless Communications,* vol. 10, no. 2, pp. 30-35, 2003.

[30] A. Boucouvalas, "Indoor ambient light noise and its effect on wireless optical links," *IEE Proceedings-Optoelectronics,* vol. 143, no. 6, pp. 334-338, 1996.

[31] J. Elmirghani, H. Chan, and R. Cryan, "Sensitivity evaluation of optical wireless PPM systems utilising PIN-BJT receivers," *IEE Proceedings-Optoelectronics,* vol. 143, no. 6, pp. 355-359, 1996.

[32] S. Arnon, *Visible light communication*. Cambridge University Press, 2015.

[33] J. Hecht, "Changing the lights: Are LEDs ready to become the market standard?," *Optics and Photonics News,* vol. 23, no. 3, pp. 44-50, 2012.

[34] S. Rajbhandari *et al.*, "High-speed integrated visible light communication system: Device constraints and design considerations," *IEEE Journal on Selected Areas in Communications,* vol. 33, no. 9, pp. 1750-1757, 2015.

[35] F. Zafar, M. Bakaul, and R. Parthiban, "Laser-Diode-Based Visible Light Communication: Toward Gigabit Class Communication," *IEEE Communications Magazine,* vol. 55, no. 2, pp. 144-151, 2017.

[36] D. Tsonev, S. Videv, and H. Haas, "Towards a 100 Gb/s visible light wireless access network," *Optics express,* vol. 23, no. 2, pp. 1627-1637, 2015.

[37] K. Lee, H. Park, and J. R. Barry, "Indoor channel characteristics for visible light communications," *IEEE Communications Letters,* vol. 15, no. 2, pp. 217-219, 2011.

[38] J. R. Barry and J. M. Kahn, "Link design for nondirected wireless infrared communications," *Applied optics,* vol. 34, no. 19, pp. 3764-3776, 1995.

[39] E. Sarbazi, M. Uysal, M. Abdallah, and K. Qaraqe, "Indoor channel modelling and characterization for visible light communications," in *Transparent Optical Networks (ICTON), 2014 16th International Conference on*, 2014, pp. 1-4: IEEE.

[40] Z. Ghassemlooy, W. Popoola, and S. Rajbhandari, *Optical wireless communications: system and channel modelling with Matlab®*. CRC press, 2012.

[41] T. Minami, K. Yano, T. Touge, H. Morikawa, and O. Takahashi, "Optical wireless modem for office communication," in *Proceedings of the May 16-19, 1983, national computer conference*, 1983, pp. 721-728: ACM.

[42] D. Tronghop, J. Hwang, S. Jung, Y. Shin, and M. Yoo, "Modeling and analysis of the wireless channel formed by LED angle in visible light communication," in *Information Networking (ICOIN), 2012 International Conference on*, 2012, pp. 354-357: IEEE.

[43] J. P. Savicki and S. P. Morgan, "Hemispherical concentrators and spectral filters for planar sensors in diffuse radiation fields," *Applied optics,* vol. 33, no. 34, pp. 8057-8061, 1994.

[44] K.-P. Ho and J. M. Kahn, "Compound parabolic concentrators for narrowband wireless infrared receivers," *Optical Engineering,* vol. 34, no. 5, pp. 1385-1396, 1995.

[45] A. J. Moreira, R. T. Valadas, and A. de Oliveira Duarte, "Optical interference produced by artificial light," *Wireless Networks,* vol. 3, no. 2, pp. 131-140, 1997.

[46] M. Marhic, M. Kotzin, and A. Van den Heuvel, "Reflectors and immersion lenses for detectors of diffuse radiation," *JOSA,* vol. 72, no. 3, pp. 352-355, 1982.

[47] X. Ning, R. Winston, and J. O'Gallagher, "Dielectric totally internally reflecting concentrators," *Applied optics,* vol. 26, no. 2, pp. 300-305, 1987.

[48] S. H. Younus and J. M. Elmirghani, "WDM for high-speed indoor visible light communication system," in *Transparent Optical Networks (ICTON), 2017 19th International Conference on*, 2017, pp. 1-6: IEEE.

[49] J. M. Senior and M. Y. Jamro, *Optical fiber communications: principles and practice*. Pearson Education, 2009.

[50] S. Arnon, J. Barry, and G. Karagiannidis, *Advanced optical wireless communication systems*. Cambridge university press, 2012.

[51] S. Hranilovic, *Wireless optical communication systems*. Springer Science & Business Media, 2006.

[52] L. Zeng *et al.*, "High data rate multiple input multiple output (MIMO) optical wireless communications using white LED lighting," *Selected Areas in Communications, IEEE Journal on,* vol. 27, no. 9, pp. 1654-1662, 2009.

[53] M. Noshad and M. Brandt-Pearce, "Can visible light communications provide Gb/s service?," *arXiv preprint arXiv:1308.3217,* 2013.

[54] L. Zeng, D. O'Brien, H. Le Minh, K. Lee, D. Jung, and Y. Oh, "Improvement of date rate by using equalization in an indoor visible light communication system," 2008.

[55] H. Le Minh *et al.*, "High-speed visible light communications using multiple-resonant equalization," *Photonics Technology Letters, IEEE,* vol. 20, no. 14, pp. 1243-1245, 2008.

[56] H. Le Minh *et al.*, "80 Mbit/s visible light communications using pre-equalized white LED," in *Optical Communication, 2008. ECOC 2008. 34th European Conference on*, 2008, pp. 1-2: IEEE.

[57] J. Grubor, S. C. J. Lee, K.-D. Langer, T. Koonen, and J. W. Walewski, "Wireless high-speed data transmission with phosphorescent white-light LEDs," *ECOC 2007,* 2007.

[58] A. H. Azhar, T.-A. Tran, and D. O'Brien, "Demonstration of high-speed data transmission using MIMO-OFDM visible light communications," in

GLOBECOM Workshops (GC Wkshps), 2010 IEEE, 2010, pp. 1052-1056: IEEE.

[59] J. Vučić, C. Kottke, S. Nerreter, K.-D. Langer, and J. W. Walewski, "513 Mbit/s visible light communications link based on DMT-modulation of a white LED," *Journal of Lightwave Technology,* vol. 28, no. 24, pp. 3512-3518, 2010.

[60] C. Kottke, J. Hilt, K. Habel, J. Vučić, and K.-D. Langer, "1.25 Gbit/s visible light WDM link based on DMT modulation of a single RGB LED luminary," in *European Conference and Exhibition on Optical Communication*, 2012, p. We. 3. B. 4: Optical Society of America.

[61] G. Cossu, A. M. Khalid, P. Choudhury, R. Corsini, and E. Ciaramella, "2.1 Gbit/s visible optical wireless transmission," in *Optical Communications (ECOC), 2012 38th European Conference and Exhibition on*, 2012, pp. 1-3.

[62] G. Cossu, A. Khalid, P. Choudhury, R. Corsini, and E. Ciaramella, "3.4 Gbit/s visible optical wireless transmission based on RGB LED," *Optics express,* vol. 20, no. 26, pp. B501-B506, 2012.

[63] P. Manousiadis *et al.*, "Demonstration of 2.3 Gb/s RGB White-light VLC using Polymer based Colour-converters and GaN micro-LEDs," in *2015 IEEE Summer Topicals Meeting Series (SUM)*, 2015, pp. 222-223: IEEE.

[64] Y. Wang, X. Huang, L. Tao, J. Shi, and N. Chi, "4.5-Gb/s RGB-LED based WDM visible light communication system employing CAP modulation and RLS based adaptive equalization," *Optics express,* vol. 23, no. 10, pp. 13626-13633, 2015.

[65] G. Cossu, W. Ali, R. Corsini, and E. Ciaramella, "Gigabit-class optical wireless communication system at indoor distances (1.5–4 m)," *Optics express,* vol. 23, no. 12, pp. 15700-15705, 2015.

[66] Y. Wang, L. Tao, X. Huang, J. Shi, and N. Chi, "8-Gb/s RGBY LED-Based WDM VLC System Employing High-Order CAP Modulation and Hybrid Post Equalizer," *IEEE Photonics Journal,* vol. 7, no. 6, pp. 1-7, 2015.

[67] H. Chun *et al.*, "LED Based Wavelength Division Multiplexed 10 Gb/s Visible Light Communications," *Journal of Lightwave Technology,* vol. 34, no. 13, pp. 3047-3052, 2016.

[68] S. Rajagopal, R. D. Roberts, and S.-K. Lim, "IEEE 802.15. 7 visible light communication: modulation schemes and dimming support," *Communications Magazine, IEEE,* vol. 50, no. 3, pp. 72-82, 2012.

[69] A. G. Al-Ghamdi and J. M. Elmirghani, "Performance evaluation of a triangular pyramidal fly-eye diversity detector for optical wireless communications," *IEEE Communications magazine,* vol. 41, no. 3, pp. 80-86, 2003.

[70] G. B. Prince and T. D. Little, "On the performance gains of cooperative transmission concepts in intensity modulated direct detection visible light communication networks," in *Wireless and Mobile*

Communications (ICWMC), 2010 6th International Conference on, 2010, pp. 297-302: IEEE.

[71] T. Borogovac, M. Rahaim, and J. B. Carruthers, "Spotlighting for visible light communications and illumination," in *GLOBECOM Workshops (GC Wkshps), 2010 IEEE*, 2010, pp. 1077-1081: IEEE.

[72] D. Wu, Z. Ghassemlooy, H. Le-Minh, S. Rajbhandari, and L. Chao, "Channel characteristics analysis of diffuse indoor cellular optical wireless communication systems," in *Communications and Photonics Conference and Exhibition, 2011. ACP. Asia*, 2011, pp. 1-6: IEEE.

[73] A. T. Hussein and J. M. Elmirghani, "High-speed indoor visible light communication system employing laser diodes and angle diversity receivers," in *Transparent Optical Networks (ICTON), 2015 17th International Conference on*, 2015, pp. 1-6: IEEE.

[74] Z. Chen, D. Tsonev, and H. Haas, "Improving SINR in indoor cellular visible light communication networks," in *Communications (ICC), 2014 IEEE International Conference on*, 2014, pp. 3383-3388: IEEE.

[75] A. T. Hussein and J. M. H. Elmirghani, "Mobile Multi-Gigabit Visible Light Communication System in Realistic Indoor Environment," *Lightwave Technology, Journal of,* vol. 33, no. 15, pp. 3293-3307, 2015.

[76] M. T. Alresheedi and J. M. Elmirghani, "Performance evaluation of 5 Gbit/s and 10 Gbit/s mobile optical wireless systems employing beam angle and power adaptation with diversity receivers," *IEEE Journal on Selected Areas in Communications,* vol. 29, no. 6, pp. 1328-1340, 2011.

[77] A. Hussein, M. Alresheedi, and J. Elmirghani, "20 Gbps Mobile Indoor Visible Light Communication System Employing Beam Steering and Computer Generated Holograms," 2015.

[78] A. T. Hussein, M. T. Alresheedi, and J. M. Elmirghani, "Fast and efficient adaptation techniques for visible light communication systems," *Journal of Optical Communications and Networking,* vol. 8, no. 6, pp. 382-397, 2016.

[79] S. H. Younus, A. T. Hussein, M. Thameralresheedi, and J. M. Elmirghani, "CGH for Indoor Visible Light Communication System," *IEEE Access,* vol. 5, pp. 24988-25004, 2017.

[80] J. R. Barry, J. M. Kahn, E. A. Lee, and D. G. Messerschmitt, "High-speed nondirective optical communication for wireless networks," *IEEE Network,* vol. 5, no. 6, pp. 44-54, 1991.

[81] A. Street, P. Stavrinou, D. Edwards, and G. Parry, "Optical preamplifier designs for IR-LAN applications," in *Optical Free Space Communication Links, IEE Colloquium on*, 1996, pp. 8/1-8/6: IET.

[82] H. Burchardt, N. Serafimovski, D. Tsonev, S. Videv, and H. Haas, "VLC: Beyond point-to-point communication," *Communications Magazine, IEEE,* vol. 52, no. 7, pp. 98-105, 2014.

[83] C. Singh, J. John, Y. Singh, and K. Tripathi, "A review of indoor optical wireless systems," *IETE Technical review,* vol. 19, no. 1-2, pp. 3-17, 2002.

[84] K. Wong, T. O'Farrell, and M. Kiatweerasakul, "The performance of optical wireless OOK, 2-PPM and spread spectrum under the effects of multipath dispersion and artificial light interference," *International Journal of Communication Systems,* vol. 13, no. 7-8, pp. 551-576, 2000.

[85] R. Cryan, R. Unwin, and J. Elmirghani, "Optical fibre digital pulse position modulation," *Analogue Optical Fibre Communications,* no. 32, p. 139, 1995.

[86] M. Nakajima and S. Haruyama, "New indoor navigation system for visually impaired people using visible light communication," *EURASIP Journal on Wireless Communications and Networking,* vol. 2013, no. 1, p. 37, 2013.

[87] S.-Y. Jung, S. Hann, and C.-S. Park, "TDOA-based optical wireless indoor localization using LED ceiling lamps," *IEEE Transactions on Consumer Electronics,* vol. 57, no. 4, 2011.

[88] W. Zhang and M. Kavehrad, "Comparison of VLC-based indoor positioning techniques," in *Broadband Access Communication Technologies VII*, 2013, vol. 8645, p. 86450M: International Society for Optics and Photonics.

[89] H. B. C. Wook, S. Haruyama, and M. Nakagawa, "Visible light communication with LED traffic lights using 2-dimensional image sensor," *IEICE transactions on fundamentals of electronics, communications and computer sciences,* vol. 89, no. 3, pp. 654-659, 2006.

[90] M. Biagi, T. Borogovac, and T. D. Little, "Adaptive receiver for indoor visible light communications," *Journal of Lightwave Technology,* vol. 31, no. 23, pp. 3676-3686, 2013.

[91] A. G. Al-Ghamdi and J. M. Elmirghani, "Analysis of diffuse optical wireless channels employing spot-diffusing techniques, diversity receivers, and combining schemes," *Communications, IEEE Transactions on,* vol. 52, no. 10, pp. 1622-1631, 2004.

[92] S. Jivkova and M. Kavehrad, "Indoor wireless infrared local access, multi-spot diffusing with computer generated holographic beam-splitters," in *Communications, 1999. ICC'99. 1999 IEEE International Conference on*, 1999, vol. 1, pp. 604-608: IEEE.

[93] J. R. Barry, J. M. Kahn, W. J. Krause, E. Lee, and D. G. Messerschmitt, "Simulation of multipath impulse response for indoor wireless optical channels," *Selected Areas in Communications, IEEE Journal on,* vol. 11, no. 3, pp. 367-379, 1993.

[94] T. Komine and M. Nakagawa, "Fundamental analysis for visible-light communication system using LED lights," *Consumer Electronics, IEEE Transactions on,* vol. 50, no. 1, pp. 100-107, 2004.

[95] S. Jovkova and M. Kavehard, "Multispot diffusing configuration for wireless infrared access," *IEEE Transactions on Communications,* vol. 48, no. 6, pp. 970-978, 2000.

[96] A. T. Hussein and J. M. Elmirghani, "10 Gbps mobile visible light communication system employing angle diversity, imaging receivers, and relay nodes," *Journal of Optical Communications and Networking,* vol. 7, no. 8, pp. 718-735, 2015.

[97] J. Carruther and J. M. Kahn, "Angle diversity for nondirected wireless infrared communication," *IEEE Transactions on Communications,* vol. 48, no. 6, pp. 960-969, 2000.

[98] A. Al-Ghamdi and J. M. Elmirghani, "Optimization of a triangular PFDR antenna in a fully diffuse OW system influenced by background noise and multipath propagation," *IEEE transactions on communications,* vol. 51, no. 12, pp. 2103-2114, 2003.

[99] J. B. Carruthers and J. M. Kahn, "Modeling of nondirected wireless infrared channels," *IEEE transactions on communications,* vol. 45, no. 10, pp. 1260-1268, 1997.

[100] S. D. Personick, "Receiver design for digital fiber optic communication systems, I," *Bell Labs Technical Journal,* vol. 52, no. 6, pp. 843-874, 1973.

[101] F. E. Alsaadi and J. M. H. Elmirghani, "Mobile Multigigabit Indoor Optical Wireless Systems Employing Multibeam Power Adaptation and Imaging Diversity Receivers," *Optical Communications and Networking, IEEE/OSA Journal of,* vol. 3, no. 1, pp. 27-39, 2011.

[102] A. G. Al-Ghamdi and J. M. Elmirghani, "Line strip spot-diffusing transmitter configuration for optical wireless systems influenced by background noise and multipath dispersion," *Communications, IEEE Transactions on,* vol. 52, no. 1, pp. 37-45, 2004.

[103] P. Djahani and J. M. Kahn, "Analysis of infrared wireless links employing multibeam transmitters and imaging diversity receivers," *Communications, IEEE Transactions on,* vol. 48, no. 12, pp. 2077-2088, 2000.

[104] A. G. Al-Ghamdi and J. M. Elmirghani, "Triangular PFDR antenna optimisation under the restriction of background noise and multipath propagation in an optical wireless system," in *Communications, 2003. ICC'03. IEEE International Conference on*, 2003, vol. 3, pp. 2013-2019: IEEE.

[105] T. Komine, "Visible light wireless communications and its fundamental study," Ph. D. dissertation, Keio University, 2005.

[106] A. Al-Ghamdi and J. Elmirghani, "Performance analysis of mobile optical wireless systems employing a novel beam clustering method and diversity detection," in *Optoelectronics, IEE Proceedings-*, 2004, vol. 151, no. 4, pp. 223-231: IET.

[107] M. T. Alresheedi and J. M. Elmirghani, "10 Gb/s indoor optical wireless systems employing beam delay, power, and angle adaptation methods

with imaging detection," *Journal of Lightwave Technology,* vol. 30, no. 12, pp. 1843-1856, 2012.

[108] “European standard EN 12464-1: Lighting of indoor work places,”[online]Available:http://www.etaplighting.com/upoadedFiles/Downloadable_documentation/documentatie/EN12464_E_OK.pdf. Last access on 01/02/2015.

[109] M. T. Alresheedi and J. M. Elmirghani, "Hologram Selection in Realistic Indoor Optical Wireless Systems With Angle Diversity Receivers," *Journal of Optical Communications and Networking,* vol. 7, no. 8, pp. 797-813, 2015.

[110] A. Al-Ghamdi and J. Elmirghani, "Performance comparison of LSMS and conventional diffuse and hybrid optical wireless techniques in a real indoor environment," *IEE Proceedings-Optoelectronics,* vol. 152, no. 4, pp. 230-238, 2005.

[111] G. P. Agrawal, *Fiber-optic communication systems*. John Wiley & Sons, 2012.

[112] M. P. C. M. Krijn and M. J. J. Jak, "Eye-safe laser-based lighting," ed: Google Patents, 2008.

[113] A. Neumann, J. J. Wierer, W. Davis, Y. Ohno, S. R. Brueck, and J. Y. Tsao, "Four-color laser white illuminant demonstrating high color-rendering quality," *Optics express,* vol. 19, no. 104, pp. A982-A990, 2011.

[114] C. Basu, M. Meinhardt-Wollweber, and B. Roth, "Lighting with laser diodes," *Advanced Optical Technologies,* vol. 2, no. 4, pp. 313-321, 2013.

[115] R. Gatdula, J. Murray, A. Heizler, and M. Shah, "Solid state lighting with blue laser diodes," ed, 2015.

[116] F. E. Alsaadi and J. M. H. Elmirghani, "High-Speed Spot Diffusing Mobile Optical Wireless System Employing Beam Angle and Power Adaptation and Imaging Receivers," *Lightwave Technology, Journal of,* vol. 28, no. 16, pp. 2191-2206, 2010.

[117] F. E. Alsaadi, M. A. Alhartomi, and J. M. Elmirghani, "Fast and efficient adaptation algorithms for multi-gigabit wireless infrared systems," *Journal of Lightwave Technology,* vol. 31, no. 23, pp. 3735-3751, 2013.

[118] S.-M. Kim and S.-M. Kim, "Wireless optical energy transmission using optical beamforming," *Optical Engineering,* vol. 52, no. 4, pp. 043205-043205, 2013.

[119] S.-M. Kim and S.-M. Kim, "Performance improvement of visible light communications using optical beamforming," in *Ubiquitous and Future Networks (ICUFN), 2013 Fifth International Conference on*, 2013, pp. 362-365: IEEE.

[120] A. Gomez *et al.*, "Design and demonstration of a 400 Gb/s indoor optical wireless communications link," *Journal of Lightwave Technology,* vol. 34, no. 22, pp. 5332-5339, 2016.

[121] M. B. Rahaim, J. Morrison, and T. D. Little, "Beam control for indoor FSO and dynamic dual-use VLC lighting systems," *Journal of Communications and Information Networks,* vol. 2, no. 4, pp. 11-27, 2017.

[122] "PhotodiodeTutorial",[online]Available:https://www.thorlabs.com/ tutorials.cfm?tabID= 787382ff-26eb 4a7e-b021-bf65c5bf164b.

[123] A. P. Tang, J. M. Kahn, and K.-P. Ho, "Wireless infrared communication links using multi-beam transmitters and imaging receivers," in *Communications, 1996. ICC'96, Conference Record, Converging Technologies for Tomorrow's Applications. 1996 IEEE International Conference on*, 1996, vol. 1, pp. 180-186: IEEE.

[124] A. T. Hussein and J. M. H. Elmirghani, "10 Gbps mobile visible light communication system employing angle diversity, imaging receivers, and relay nodes," *Optical Communications and Networking, IEEE/OSA Journal of,* vol. 7, no. 8, pp. 718-735, 2015.

[125] J. M. Kahn, R. You, P. Djahani, A. G. Weisbin, B. K. Teik, and A. Tang, "Imaging diversity receivers for high-speed infrared wireless communication," *Communications Magazine, IEEE,* vol. 36, no. 12, pp. 88-94, 1998.

[126] F. E. Alsaadi and J. M. Elmirghani, "Mobile multigigabit indoor optical wireless systems employing multibeam power adaptation and imaging diversity receivers," *Journal of Optical Communications and Networking,* vol. 3, no. 1, pp. 27-39, 2011.

[127] F. E. Alsaadi and J. M. Elmirghani, "Adaptive mobile line strip multibeam MC-CDMA optical wireless system employing imaging detection in a real indoor environment," *IEEE Journal on Selected Areas in Communications,* vol. 27, no. 9, 2009.

[128] S. Jovkova and M. Kavehard, "Multispot diffusing configuration for wireless infrared access," *Communications, IEEE Transactions on,* vol. 48, no. 6, pp. 970-978, 2000.

[129] M. A. Seldowitz, J. P. Allebach, and D. W. Sweeney, "Synthesis of digital holograms by direct binary search," *Applied Optics,* vol. 26, no. 14, pp. 2788-2798, 1987.

[130] M. T. Alresheedi and J. M. H. Elmirghani, "High-Speed Indoor Optical Wireless Links Employing Fast Angle and Power Adaptive Computer-Generated Holograms With Imaging Receivers," *IEEE Transactions on Communications,* vol. 64, no. 4, pp. 1699-1710, 2016.

[131] P. Carnevali, L. Coletti, and S. Patarnello, "Image processing by simulated annealing," *IBM Journal of Research and Development,* vol. 29, no. 6, pp. 569-579, 1985.

[132] M. T. Alresheedi, A. T. Hussein, and J. M. H. Elmirghani, "Uplink design in VLC systems with IR sources and beam steering," *IET Communications,* vol. 11, no. 3, pp. 311-317, 2017.

[133] I. Stefan, H. Elgala, and H. Haas, "Study of dimming and LED nonlinearity for ACO-OFDM based VLC systems," in *Wireless*

Communications and Networking Conference (WCNC), 2012 IEEE, 2012, pp. 990-994: IEEE.

[134] S. Jivkova and M. Kavehrad, "Transceiver design concept for cellular and multispot diffusing regimes of transmission," *EURASIP Journal on Wireless Communications and Networking,* vol. 2005, no. 1, pp. 30-38, 2005.

[135] M. R. Pakravan and M. Kavehrad, "Design considerations for broadband indoor infrared wireless communication systems," *International Journal of Wireless Information Networks,* vol. 2, no. 4, pp. 223-238, 1995.

[136] R. Mesleh, R. Mehmood, H. Elgala, and H. Haas, "Indoor MIMO optical wireless communication using spatial modulation," in *Communications (ICC), 2010 IEEE International Conference on*, 2010, pp. 1-5: IEEE.

[137] A. H. Azhar, T. Tran, and D. O'Brien, "A Gigabit/s indoor wireless transmission using MIMO-OFDM visible-light communications," *Photonics Technology Letters, IEEE,* vol. 25, no. 2, pp. 171-174, 2013.

[138] A. Burton, H. Minh, Z. Ghassemlooy, E. Bentley, and C. Botella, "Experimental demonstration of 50-Mb/s visible light communications using 4× 4 MIMO," *IEEE Photonics Technology Letters,* vol. 26, no. 9, pp. 945-948, 2014.

[139] A. Nuwanpriya, S.-W. Ho, and C. S. Chen, "Indoor MIMO visible light communications: Novel angle diversity receivers for mobile users," *IEEE Journal on Selected Areas in Communications,* vol. 33, no. 9, pp. 1780-1792, 2015.

[140] T. Q. Wang, R. J. Green, and J. Armstrong, "MIMO optical wireless communications using ACO-OFDM and a prism-array receiver," *IEEE Journal on Selected Areas in Communications,* vol. 33, no. 9, pp. 1959-1971, 2015.

[141] K.-H. Park and M.-S. Alouini, "Optimization of an Angle-Aided Mirror Diversity Receiver for Indoor MIMO-VLC Systems," in *Global Communications Conference (GLOBECOM), 2016 IEEE*, 2016, pp. 1-6: IEEE.

[142] K.-P. Ho and J. M. Kahn, "Methods for crosstalk measurement and reduction in dense WDM systems," *Journal of lightwave technology,* vol. 14, no. 6, pp. 1127-1135, 1996.

[143] B. Lin, X. Tang, Z. Ghassemlooy, C. Lin, and Y. Li, "Experimental Demonstration of an Indoor VLC Positioning System Based on OFDMA," *IEEE Photonics Journal,* vol. 9, no. 2, pp. 1-9, 2017.

[144] J. Ding, I. Chih-Lin, and Z. Xu, "Indoor Optical Wireless Channel Characteristics With Distinct Source Radiation Patterns," *IEEE Photonics Journal,* vol. 8, no. 1, pp. 1-15, 2016.

[145] D. Wu, W.-D. Zhong, Z. Ghassemlooy, and C. Chen, "Short-range visible light ranging and detecting system using illumination light emitting diodes," *IET Optoelectronics,* vol. 10, no. 3, pp. 94-99, 2016.

[146] B. Leskovar, "Optical receivers for wide band data transmission systems," *Nuclear Science, IEEE Transactions on,* vol. 36, no. 1, pp. 787-793, 1989.

[147] R. Ziemer and W. H. Tranter, *Principles of communications: system modulation and noise*. John Wiley & Sons, 2006.

[148] F. Miramirkhani and M. Uysal, "Channel modeling and characterization for visible light communications," *IEEE Photonics Journal,* vol. 7, no. 6, pp. 1-16, 2015.

[149] M. Rahaim and T. D. Little, "Interference in IM/DD optical wireless communication networks," *IEEE/OSA Journal of Optical Communications and Networking,* vol. 9, no. 9, pp. D51-D63, 2017.

[150] F. E. Alsaadi and J. M. Elmirghani, "Performance evaluation of 2.5 Gbit/s and 5 Gbit/s optical wireless systems employing a two dimensional adaptive beam clustering method and imaging diversity detection," *IEEE Journal on Selected Areas in Communications,* vol. 27, no. 8, pp. 1507-1519, 2009.

[151] A. A. Al-Hameed, A. T. Hussein, M. T. Alresheedi, and J. M. Elmirghani, "Adaptive receiver for visible light communication system," in *Transparent Optical Networks (ICTON), 2016 18th International Conference on*, 2016, pp. 1-6: IEEE.

[152] A. Al-Hameed, A. T. Hussein, M. T. Alresheedi, S. H. Younus, and J. M. Elmirghani, "Transmitters Mapping of Visible Light Communication System," in *19th International Conference on Transparent Optical Networks (ICTON 2017)*, 2017: IEEE.

[153] N. Chi and J. Shi, "Investigation on overlapping interference on VLC networks consisting of multiple LEDs," *ICT Express,* 2015.

[154] P. H. Pathak, X. Feng, P. Hu, and P. Mohapatra, "Visible Light Communication, Networking, and Sensing: A Survey, Potential and Challenges," *Communications Surveys & Tutorials, IEEE,* vol. 17, no. 4, pp. 2047-2077, 2015.

[155] S. H. Younus, A. Al-Hameed, A. T. Hussein, M. T. Alresheedi and J. M. Elmirghani, "Parallel Data Transmission in Indoor Visible Light Communication Systems," *IEEE Access,* vol. 7, pp. 1126-1138, 2019.

[156] Q. Zhao, Y. Fan, L. Deng, and B. Kang, "A power-efficient ZF precoding scheme for multi-user indoor visible light communication systems," *Optics Communications,* vol. 384, pp. 101-106, 2017.

[157] Y. Hong, J. Chen, Z. Wang, and C. Yu, "Performance of a precoding MIMO system for decentralized multiuser indoor visible light communications," *Photonics Journal, IEEE,* vol. 5, no. 4, pp. 7800211-7800211, 2013.

[158] R. Feng, M. Dai, H. Wang, B. Chen, and X. Lin, "Linear Precoding for multiuser Visible Light Communication with Field of View Diversity."

[159] M. H. Shoreh, A. Fallahpour, and J. A. Salehi, "Design Concepts and Performance Analysis of Multicarrier CDMA for Indoor Visible Light

Communications," *Journal of Optical Communications and Networking,* vol. 7, no. 6, pp. 554-562, 2015.

[160] L. Yin, W. O. Popoola, X. Wu, and H. Haas, "Performance evaluation of non-orthogonal multiple access in visible light communication," *IEEE Transactions on Communications,* vol. 64, no. 12, pp. 5162-5175, 2016.

[161] H. Marshoud, P. C. Sofotasios, S. Muhaidat, G. K. Karagiannidis, and B. S. Sharif, "On the Performance of Visible Light Communications Systems with Non-Orthogonal Multiple Access," *IEEE Transactions on Wireless Communications,* 2017.

[162] D. Bykhovsky and S. Arnon, "Multiple access resource allocation in visible light communication systems," *Journal of Lightwave Technology,* vol. 32, no. 8, pp. 1594-1600, 2014.

[163] A. Sewaiwar, S. V. Tiwari, and Y. H. Chung, "Smart LED allocation scheme for efficient multiuser visible light communication networks," *Optics express,* vol. 23, no. 10, pp. 13015-13024, 2015.

[164] L. Miao, H. Qi, and W. E. Snyder, "A generic method for generating multispectral filter arrays," in *Image Processing, 2004. ICIP'04. 2004 International Conference on*, 2004, vol. 5, pp. 3343-3346: IEEE.

[165] R. Shrestha, J. Y. Hardeberg, and R. Khan, "Spatial arrangement of color filter array for multispectral image acquisition," in *IS&T/SPIE Electronic Imaging*, 2011, pp. 787503-787503-9: International Society for Optics and Photonics.

[166] Z. Chen and H. Haas, "Space division multiple access in visible light communications," in *Communications (ICC), 2015 IEEE International Conference on*, 2015, pp. 5115-5119: IEEE.

[167] Z. Chen, D. A. Basnayaka, and H. Haas, "Space Division Multiple Access for Optical Attocell Network Using Angle Diversity Transmitters," *Journal of Lightwave Technology,* vol. 35, no. 11, pp. 2118-2131, 2017.

[168] T. Cogalan, H. Haas, and E. Panayirci, "Power Control-Based Multi-User Li-Fi Using a Compound Eye Transmitter," in *Global Communications Conference (GLOBECOM), 2015 IEEE*, 2015, pp. 1-6: IEEE.

[169] A. Şahin, Y. S. Eroğlu, I. Güvenç, N. Pala, and M. Yüksel, "Hybrid 3-D localization for visible light communication systems," *Journal of Lightwave Technology,* vol. 33, no. 22, pp. 4589-4599, 2015.

[170] L. Yin, X. Wu, and H. Haas, "Indoor visible light positioning with angle diversity transmitter," in *Vehicular Technology Conference (VTC Fall), 2015 IEEE 82nd*, 2015, pp. 1-5: IEEE.

[171] Y. S. Eroğlu, İ. Güvenç, A. Şahin, Y. Yapıcı, N. Pala, and M. Yüksel, "Multi-element VLC networks: LED assignment, power control, and optimum combining," *IEEE Journal on Selected Areas in Communications,* vol. 36, no. 1, pp. 121-135, 2018.

A. Appendix A

1. Results of the Traditional VLC System

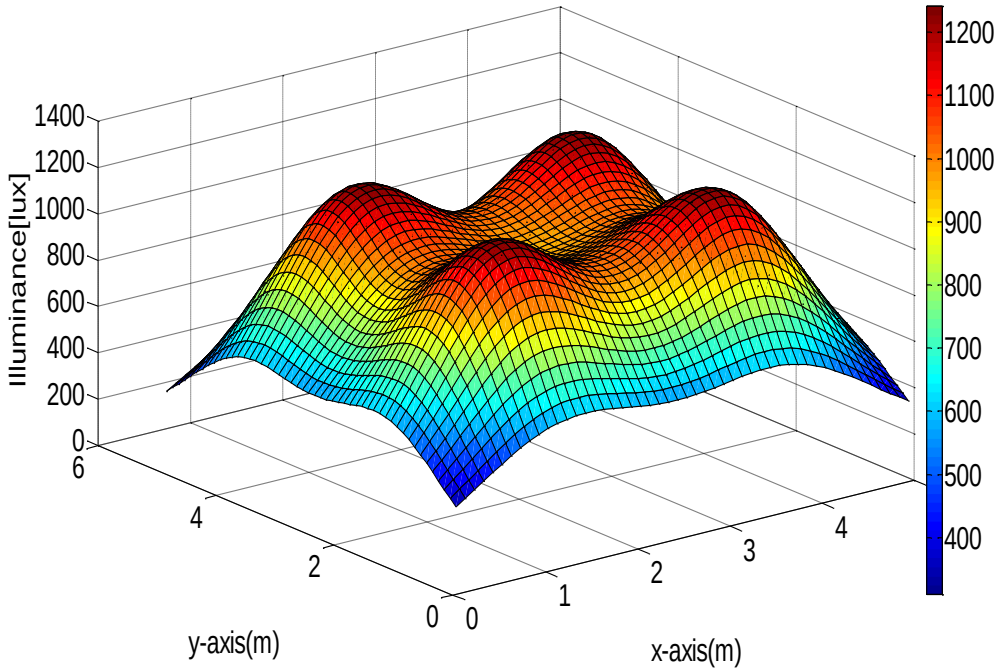

Figure A.1: Distribution of horizontal illumination at the communication plane (0.85m) in room with dimensions of 5 m × 5 m × 3 m.

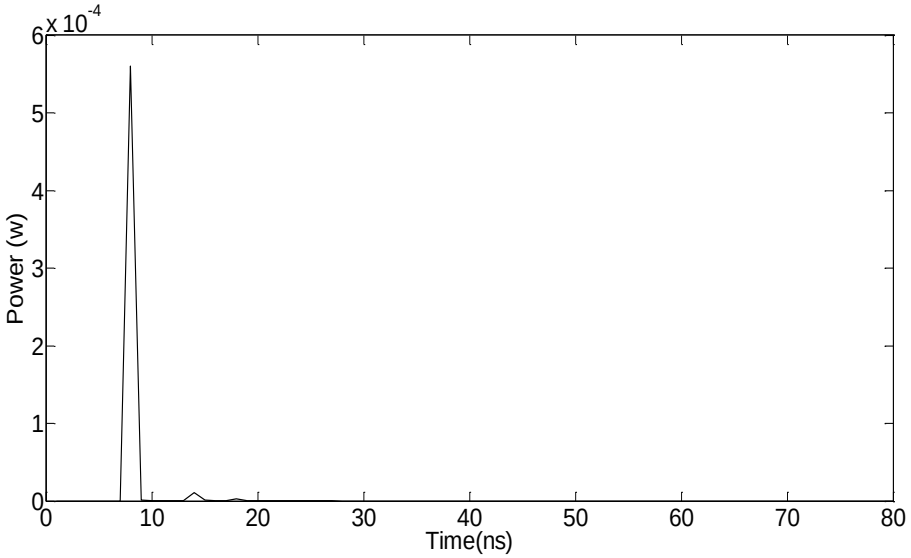

Figure A.2: Impulse response at 0.01 m, 0.01 m, 0.85 m in room with dimensions of 5 m × 5 m × 3 m.

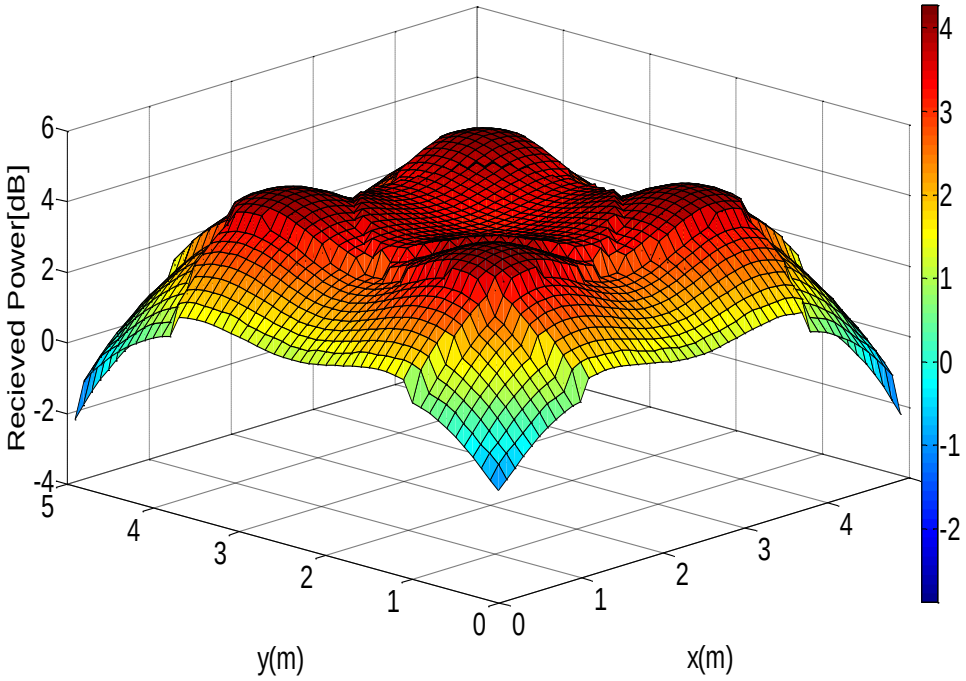

Figure A.3: The distribution of the received power from LOS and first reflection component. Min. -2.8 dBm and Max. 3.8 dBm.

2. Results of the Traditional IROW Systems

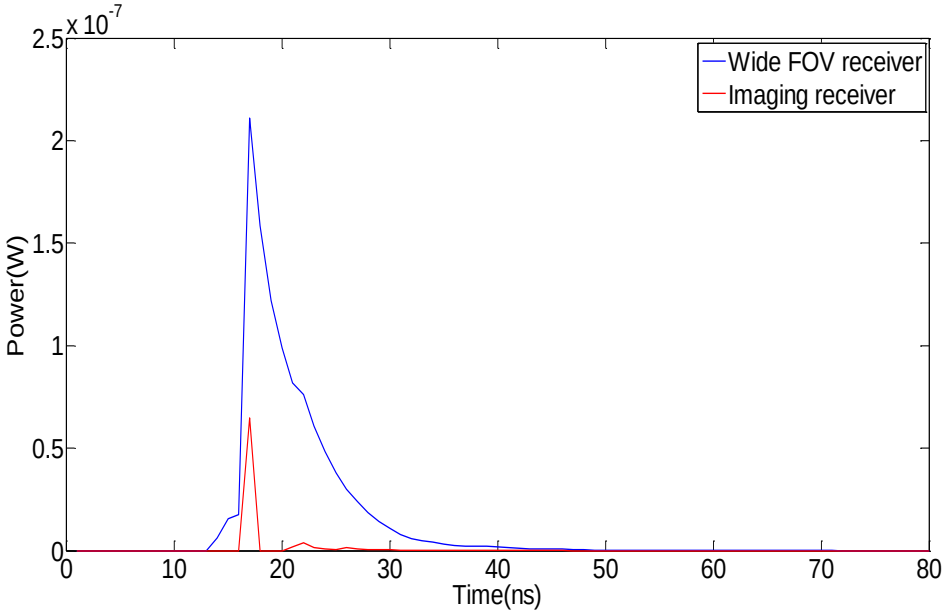

Figure A.4: Impulse response of CDS system with wide FOV receiver and an imaging receiver with 200 pixels.

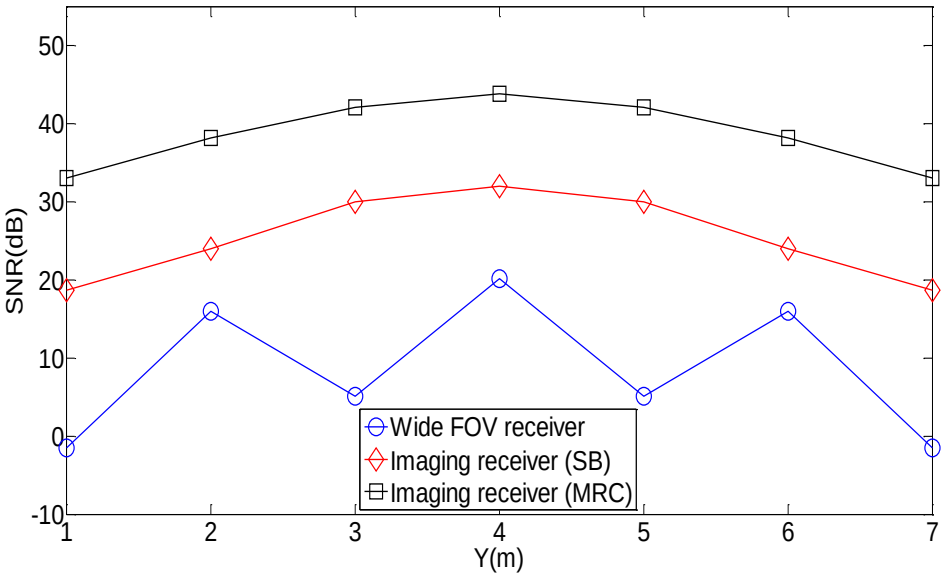

(a)

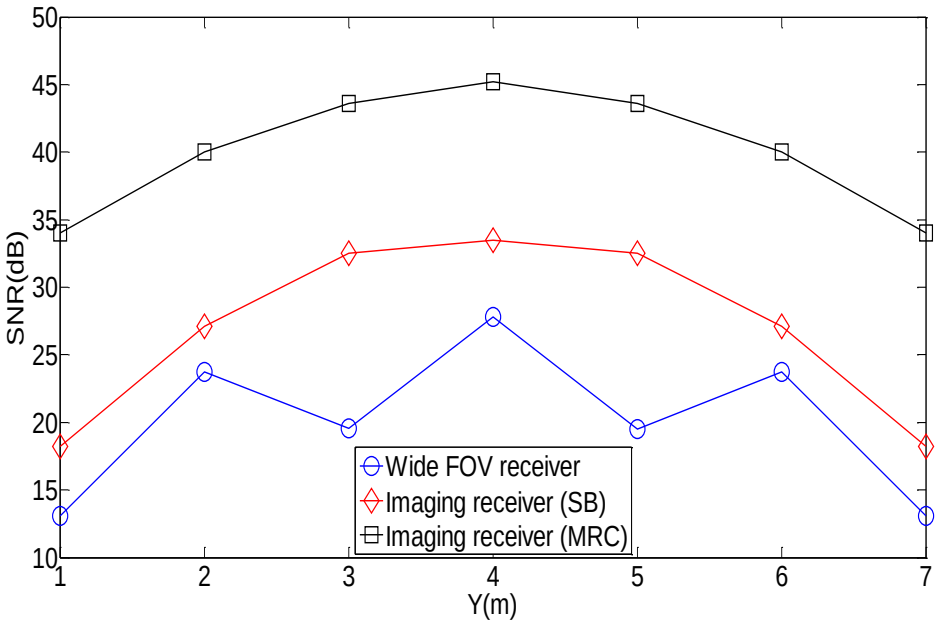

(b)

Figure A.7: The SNR of CDS system with wide-FOV receiver and imaging receiver (a) at x = 1 m and (b) at x = 2 m.

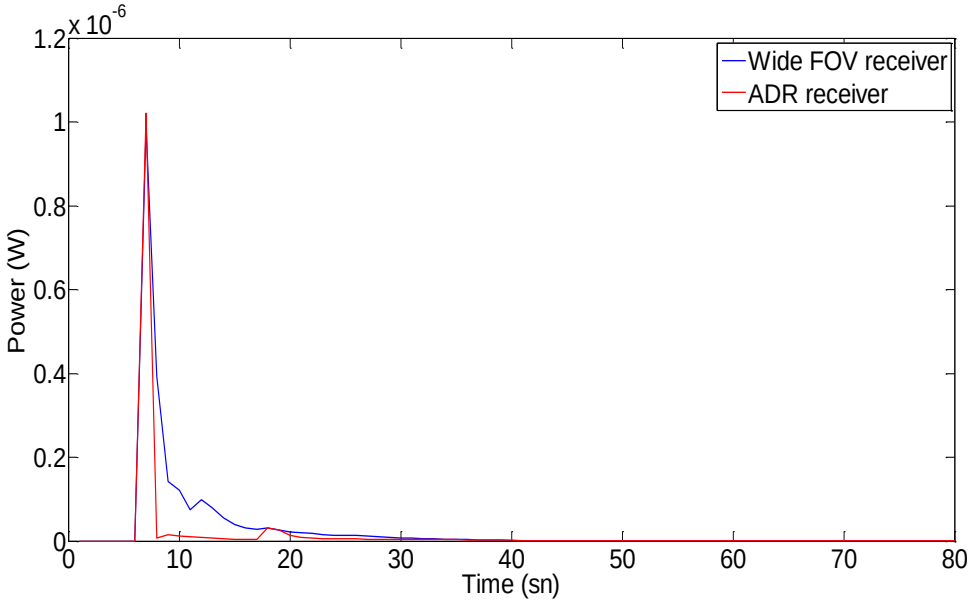

Figure A.10: Impulse response of LSMS system with wide-FOV receiver and ADR receiver (seven branches).

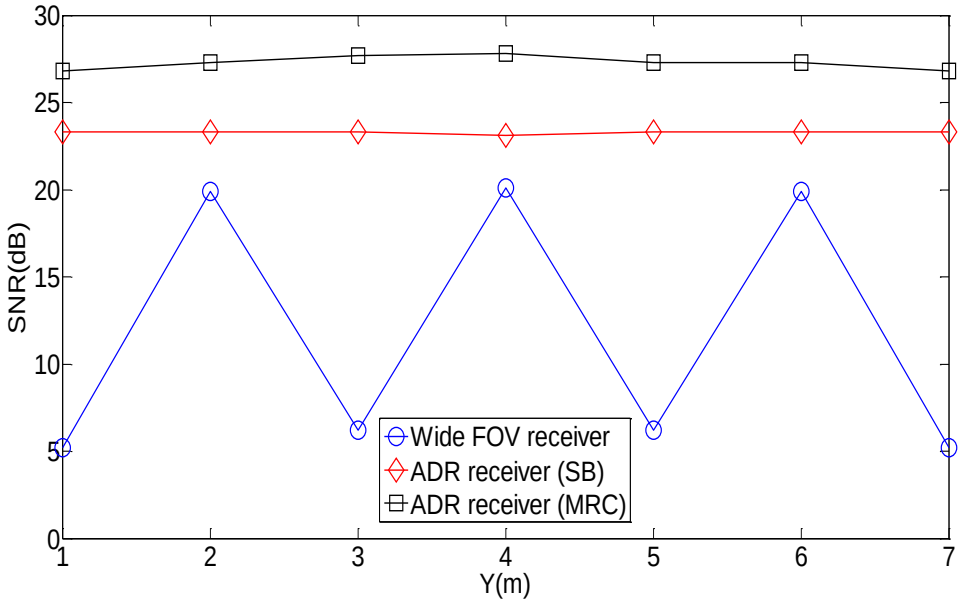

(a)

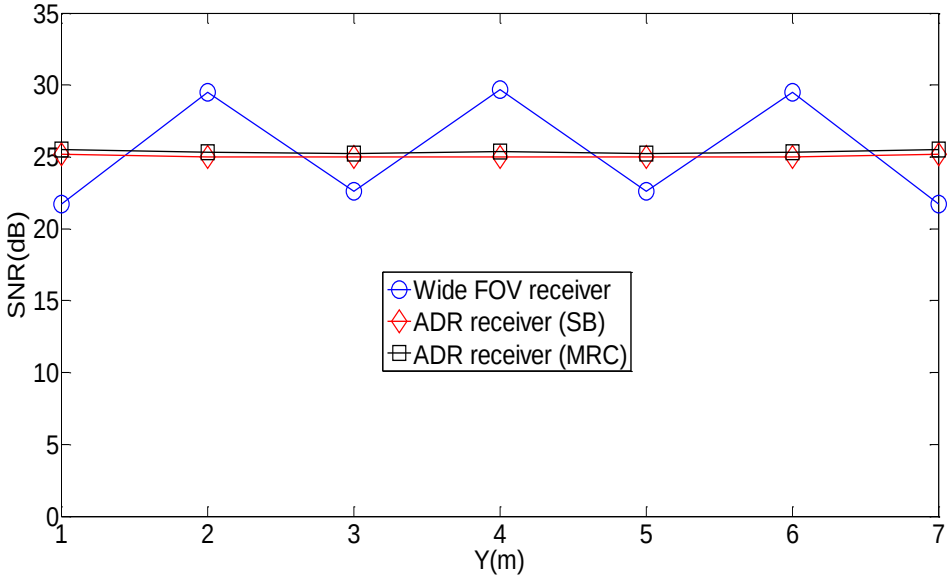

(b)

Figure A.12: SNR of LSMS system using wide-FOV receiver and ADR receiver (a) at x = 1 m and (b) at x = 2 m.

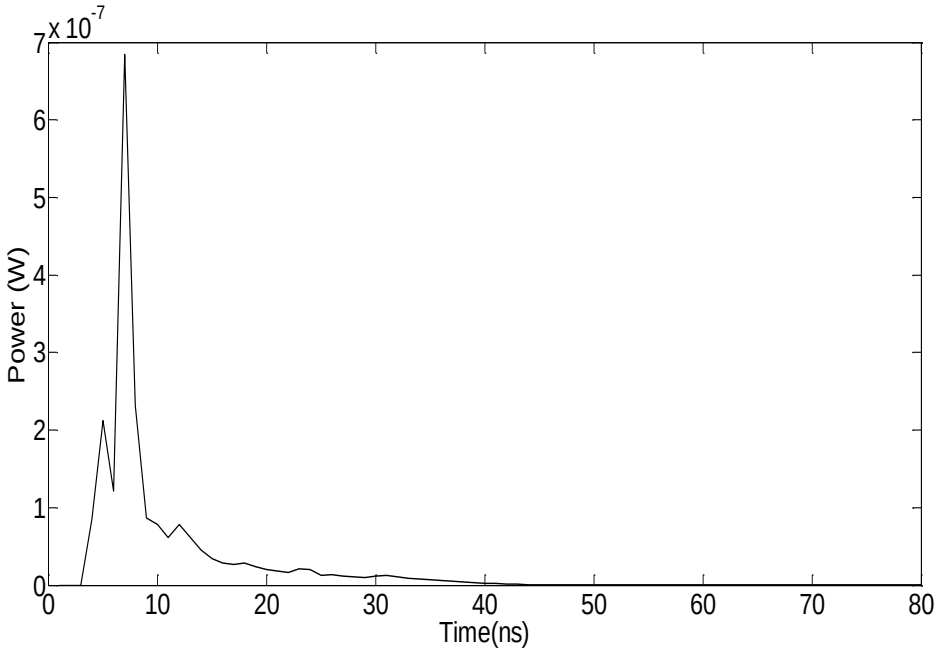

Figure A.14: Impulse response of BCM system with wide-FOV receiver at the room centre (x = 2 m, y = 4 m, z = 1 m).

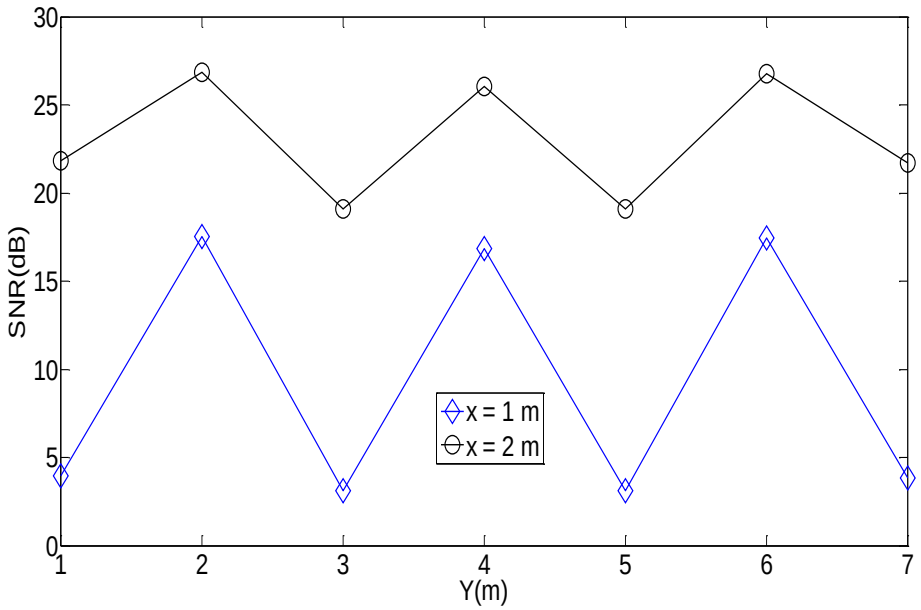

Figure A.17: SNR of BCM system using wide-FOV receiver.

B. Appendix B

1) Derivation the Convolution of Two Gaussian pdfs

In this section, the convolution of the two Gaussian pdfs, which used in chapter 5, will be derived. The first Gaussian pdf is a signal (a) that has a mean value m and a standard deviation σ_s and the second pdf is a white Gaussian noise (n) with zero mean and total standard deviation σ_t as below:

$$p(a) = \frac{1}{\sqrt{2\pi}\,\sigma_s} e^{-\left(\frac{a-m}{\sqrt{2}\sigma_s}\right)^2} \tag{B.1}$$

and

$$g(n) = \frac{1}{\sqrt{2\pi}\,\sigma_t} e^{-\left(\frac{n}{\sqrt{2}\sigma_t}\right)^2} \tag{B.2}$$

The convolution of two Gaussian pdfs is

$$f(z) = p(a) \otimes p(n) = \int_{-\infty}^{\infty} p(x)g(z-x)\,dx \tag{B.3}$$

$$f(z) = \int_{-\infty}^{\infty} \frac{1}{\sqrt{2\pi}\,\sigma_s} e^{-\left(\frac{x-m}{\sqrt{2}\sigma_s}\right)^2} \frac{1}{\sqrt{2\pi}\,\sigma_t} e^{-\left(\frac{z-x}{\sqrt{2}\sigma_t}\right)^2} dx \tag{B.4}$$

Simplify eq. (B.4)

$$f(z) = \frac{1}{\sqrt{2\pi}\,\sigma_s}\frac{1}{\sqrt{2\pi}\,\sigma_t}\int_{-\infty}^{\infty} e^{-\left(\frac{x^2(\sigma_s{}^2+\sigma_t{}^2)-2x(m\sigma_s{}^2+z\sigma_t{}^2)+m^2\sigma_s{}^2+z^2\sigma_t{}^2}{2\,\sigma_s{}^2\,\sigma_t{}^2}\right)} dx \tag{B.5}$$

$$f(z) = \frac{1}{\sqrt{2\pi}\,\sigma_s}\frac{1}{\sqrt{2\pi}\,\sigma_t}\int_{-\infty}^{\infty} e^{-\left(\frac{x^2-2x\frac{(m\sigma_s{}^2+z\sigma_t{}^2)}{(\sigma_s{}^2+\sigma_t{}^2)}+\frac{m^2\sigma_s{}^2+z^2\sigma_t{}^2}{(\sigma_s{}^2+\sigma_t{}^2)}}{\frac{2\,\sigma_s{}^2\sigma_t{}^2}{(\sigma_s{}^2+\sigma_t{}^2)}}\right)} dx \tag{B.6}$$

Let $c = \frac{(m{\sigma_s}^2 + z{\sigma_t}^2)}{({\sigma_s}^2 + {\sigma_t}^2)}$. To obtain square of the difference in the numerator of the exponential, we will add and sub c^2 to the numerator as:

$$f(z) = \frac{1}{\sqrt{2\pi}\,\sigma_s}\frac{1}{\sqrt{2\pi}\,\sigma_t}\int_{-\infty}^{\infty} e^{-\left(\frac{x^2-2xc+c^2-c^2+\frac{m^2{\sigma_s}^2+z^2{\sigma_t}^2}{({\sigma_s}^2+{\sigma_t}^2)}}{\frac{2\,{\sigma_s}^2{\sigma_t}^2}{({\sigma_s}^2+{\sigma_t}^2)}}\right)}dx \tag{B.7}$$

$$f(z) = \frac{1}{\sqrt{2\pi}\,\sigma_s}\frac{1}{\sqrt{2\pi}\,\sigma_t}\int_{-\infty}^{\infty} e^{-\left(\frac{(x-c)^2-c^2+\frac{m^2{\sigma_s}^2+z^2{\sigma_t}^2}{({\sigma_s}^2+{\sigma_t}^2)}}{\frac{2\,{\sigma_s}^2{\sigma_t}^2}{({\sigma_s}^2+{\sigma_t}^2)}}\right)}dx \tag{B.8}$$

$$f(z) = \frac{1}{\sqrt{2\pi}\,\sigma_s}\frac{1}{\sqrt{2\pi}\,\sigma_t}\int_{-\infty}^{\infty} e^{-\left(\frac{(x-c)^2}{\frac{2\,{\sigma_s}^2{\sigma_t}^2}{({\sigma_s}^2+{\sigma_t}^2)}}\right)} e^{-\left(\frac{-c^2+\frac{m^2{\sigma_s}^2+z^2{\sigma_t}^2}{({\sigma_s}^2+{\sigma_t}^2)}}{\frac{2\,{\sigma_s}^2{\sigma_t}^2}{{\sigma_s}^2+{\sigma_t}^2}}\right)}dx \tag{B.9}$$

$$f(z) = \frac{1}{\sqrt{2\pi}\,\sigma_s}\frac{1}{\sqrt{2\pi}\,\sigma_t} e^{-\left(\frac{-c^2+\frac{m^2{\sigma_s}^2+z^2{\sigma_t}^2}{({\sigma_s}^2+{\sigma_t}^2)}}{\frac{2\,{\sigma_s}^2{\sigma_t}^2}{{\sigma_s}^2+{\sigma_t}^2}}\right)}\int_{-\infty}^{\infty} e^{-\left(\frac{x-c}{\frac{\sqrt{2}\,\sigma_s\,\sigma_t}{\sqrt{{\sigma_s}^2+{\sigma_t}^2}}}\right)^2}dx \tag{B.10}$$

$$f(z) = \frac{1}{\sqrt{{\sigma_s}^2+{\sigma_t}^2}\sqrt{2\pi}} e^{-\left(\frac{-c^2+\frac{m^2{\sigma_s}^2+z^2{\sigma_t}^2}{({\sigma_s}^2+{\sigma_t}^2)}}{\frac{2\,{\sigma_s}^2{\sigma_t}^2}{{\sigma_s}^2+{\sigma_t}^2}}\right)}$$

$$\frac{1}{\sqrt{2\pi}\,\frac{\sigma_t\sigma_s}{\sqrt{{\sigma_s}^2+{\sigma_t}^2}}}\int_{-\infty}^{\infty} e^{-\left(\frac{x-c}{\frac{\sqrt{2}\,\sigma_s\,\sigma_t}{\sqrt{{\sigma_s}^2+{\sigma_t}^2}}}\right)^2}dx \tag{B.11}$$

However, the area of the normal distribution equal to one. Thus,

$$f(z) = \frac{1}{\sqrt{{\sigma_s}^2 + {\sigma_t}^2}\sqrt{2\pi}} e^{-\left(\frac{-c^2 + \frac{m^2{\sigma_s}^2 + z^2{\sigma_t}^2}{({\sigma_s}^2 + {\sigma_t}^2)}}{\frac{2\,{\sigma_s}^2{\sigma_t}^2}{{\sigma_s}^2 + {\sigma_t}^2}}\right)} \quad \text{(B.12)}$$

But, $c = \frac{(m{\sigma_s}^2 + z{\sigma_t}^2)}{({\sigma_s}^2 + {\sigma_t}^2)}$ henc,

$$f(z) = \frac{1}{\sqrt{{\sigma_s}^2 + {\sigma_t}^2}\sqrt{2\pi}} e^{-\left(\frac{-\left(\frac{(m{\sigma_s}^2 + z{\sigma_t}^2)}{({\sigma_s}^2 + {\sigma_t}^2)}\right)^2 + \frac{m^2{\sigma_s}^2 + z^2{\sigma_t}^2}{({\sigma_s}^2 + {\sigma_t}^2)}}{\frac{2\,{\sigma_s}^2{\sigma_t}^2}{{\sigma_s}^2 + {\sigma_t}^2}}\right)} \quad \text{(B.13)}$$

After simplified the above equation, we get:

$$f(z) = \frac{1}{\sqrt{2\pi({\sigma_s}^2 + {\sigma_t}^2)}} e^{-\left(\frac{z-m}{\sqrt{2({\sigma_s}^2 + {\sigma_t}^2)}}\right)^2} \quad \text{(B.14)}$$

2) Derivation the Optimum Threshold of the Two Hypotheses

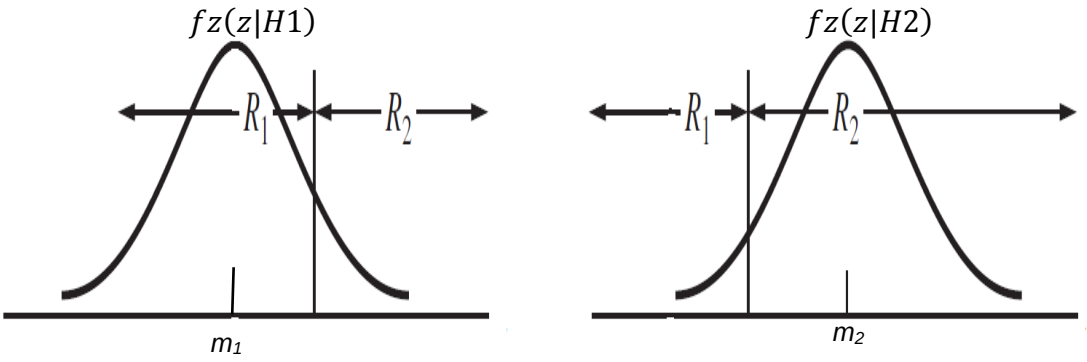

Figure B.2: The pdfs of two hypothesis.

Figure B.1 shows the pdf of the two hypothesis $fz(z|H1)$ and $fz(z|H2)$. As mentioned in chapter 5, $fz(z|H1)$, is the convolution of the noise pdf and the undesired SCM tone pdf while $fz(z|H1)$ is the convolution of the noise pdf

and the desired SCM tone pdf. Following [145], the observation space divided into two regions (see Figure B.1) R_1 and R_2. Hence, if Z falls into R_1, we decide hypothesis $H1$ is true, while if Z is in R_2, we decide $H2$ is true. The main goal is to minimize the cost of the decision. Thus, four a priori costs are required, since there are four types of decisions that we can make. These a prior costs are:

C_{11}: the cost of deciding in favour of $H1$ when $H1$ is actually true.

C_{12}: the cost of deciding in favour of $H1$ when $H2$ is actually true.

C_{21}: the cost of deciding in favour of $H2$ when $H1$ is actually true.

C_{22}: the cost of deciding in favour of $H2$ when $H2$ is actually true.

If $H1$ is true, the cost of making a decision is:

$$C(D|H1) = C_{11}P(\text{decide } H1|H1 \text{ true}) + C_{21}P(\text{decide } H2|H1 \text{ true}) \quad \text{(B.15)}$$

However, we can write the cost of the decision in term of pdf of Z given $H1$ as:

$$P(\text{decide } H1|H1 \text{ true}) = \int_{R_1} fz(z|H1)\, dz \quad \text{(B.16)}$$

$$P(\text{decide } H2|H1 \text{ true}) = \int_{R_2} fz(z|H1)\, dz \quad \text{(B.17)}$$

Z must lie in either R_1 or R_2. Hence,

$$P(\text{decide } H1|H1 \text{ true}) + P(\text{decide } H2|H1 \text{ true}) = 1 \quad \text{(B.18)}$$

and

$$\int_{R_2} fz(z|H1)\,dz = 1 - \int_{R_1} fz(z|H1)\,dz \tag{B.19}$$

The average cost given $H1$ can be written as:

$$C(D|H1) = C_{11}\int_{R_1} fz(z|H1)\,dz + C_{21}\left(1 - \int_{R_1} fz(z|H1)\,dz\right) \tag{B.20}$$

In the same way, we can write the average cost given $H2$ as:

$$C(D|H2) = C_{12}\int_{R_1} fz(z|H2)\,dz + C_{22}\left(1 - \int_{R_1} fz(z|H2)\,dz\right) \tag{B.21}$$

We can find the average cost without consider to which hypothesis is actually true. However, we must consider the prior probabilities of $H1$ and $H2$, $p = P[H1 \text{ true}]$ and $q = P[H2 \text{ true}] = 1 - p$. Hence, the average cost of making a decision is:

$$C(D) = p\,C(D|H1) + q\,C(D|H2) \tag{B.22}$$

$$\begin{aligned} C(D) = p\,&\left[C_{11}\int_{R_1} fz(z|H1)\,dz + C_{21}\left(1 - \int_{R_1} fz(z|H1)\,dz\right)\right] \\ &+ q\left[C_{12}\int_{R_1} fz(z|H2)\,dz + C_{22}\left(1 - \int_{R_1} fz(z|H2)\,dz\right)\right] \end{aligned} \tag{B.23}$$

However, we can collect all terms under common integral that involve integration over R_1 as:

$$\begin{aligned} C(D) = {} & (pC_{21} + qC_{12}) \\ & + \int_{R_1} \left[\left(q(C_{12} - C_{22})\right) fz(z|H2)\right. \\ & \left. - \left(p(C_{21} - C_{11})\right) fz(z|H1)\right] dz \end{aligned} \tag{B.24}$$

The term $(pC_{21} + qC_{21})$ represents a fixed cost. The integral represents the cost controlled by those points that are assigned to R_1. It should be noted that the wrong decision should be more costly than the right decision. Thus, we can assume that $(C_{21} > C_{11})$ and $(C_{12} > C_{22})$. If the first term of the integral larger than the second term, the decision is to select $H1$. If the first term of the integral less than the second term, the decision is to select $H2$. Thus, we can say:

$$\big(q(C_{12} - C_{22})\big)\, fz(z|H2) \underset{H1}{\overset{H2}{\gtrless}} \big(p(C_{21} - C_{11})\big) fz(z|H1) \tag{B.25}$$

$$\frac{fz(z|H2)}{fz(z|H1)} \underset{H1}{\overset{H2}{\gtrless}} \frac{\big(p(C_{21} - C_{11})\big)}{\big(q(C_{12} - C_{22})\big)} \tag{B.26}$$

The left hand side of (B.26) is called likelihood ratio, while the right hand side is called the threshold of the test. If an observed value for Z results in the left-hand ratio of pdfs being greater than the right-hand ratio of constants, choose $H2$; if not, choose $H1$. In our system in chapter 5, $C_{11} = C_{22} = 0$ as there is no cost to decide the desired SCM tone when it is true or to decide the undesired SCM tone when it is true. In addition, $C_{12} = C_{21} = 0.5$ because the cost to decide the desired SCM tone when it is not true equal to the cost to decide the undesired SCM tone when it is not true. Besides that, $p = q = 0.5$ as the prior probability of $H1$ equal to the prior probability of $H2$. Hence, (eq. B.26) can be rewrite as:

$$\frac{fz(z|H2)}{fz(z|H1)} \underset{H1}{\overset{H2}{\gtrless}} 1 \tag{B.27}$$

In chapter 5, we obtained $fz(z|H2)$ and $fz(z|H1)$. Thus, we can write (B.27) as:

$$\frac{\frac{1}{\sqrt{2\pi({\sigma_1}^2+{\sigma_t}^2)}}e^{-\left(\frac{z-m_2}{\sqrt{2({\sigma_1}^2+{\sigma_t}^2)}}\right)^2}}{\frac{1}{\sqrt{2\pi({\sigma_2}^2+{\sigma_t}^2)}}e^{-\left(\frac{z-m_1}{\sqrt{2({\sigma_2}^2+{\sigma_t}^2)}}\right)^2}} \underset{H1}{\overset{H2}{\gtrless}} 1 \tag{B.28}$$

here, m_2 and σ_2 are the mean value and the standard deviation of the desired SCM tone, respectively, m_1 and σ_1 are the mean value and the standard deviation of the undesired SCM tone, respectively and σ_t the standard deviation of the noise. To find the optimum threshold, we can write (B.28) as:

$$e^{-\left(\frac{z-m_2}{\sqrt{2({\sigma_1}^2+{\sigma_t}^2)}}\right)^2+\left(\frac{z-m_1}{\sqrt{2({\sigma_2}^2+{\sigma_t}^2)}}\right)^2} \underset{H1}{\overset{H2}{\gtrless}} \frac{\sqrt{({\sigma_1}^2+{\sigma_t}^2)}}{\sqrt{({\sigma_2}^2+{\sigma_t}^2)}} \tag{B.29}$$

Taking the natural logarithm of both sides, we obtain:

$$-\left(\frac{z-m_2}{\sqrt{2({\sigma_1}^2+{\sigma_t}^2)}}\right)^2+\left(\frac{z-m_1}{\sqrt{2({\sigma_2}^2+{\sigma_t}^2)}}\right)^2 \underset{H1}{\overset{H2}{\gtrless}} \ln\left(\frac{\sqrt{({\sigma_1}^2+{\sigma_t}^2)}}{\sqrt{({\sigma_2}^2+{\sigma_t}^2)}}\right) \tag{B.30}$$

By simplifying (eq. B.30) and using Quadratic equation, we can find Z that gives the optimum threshold as:

$$z \underset{H1}{\overset{H2}{\gtrless}} \frac{1}{{\sigma_2}^2-{\sigma_1}^2}\left(m_{us}({\sigma_2}^2+{\sigma_t}^2)-m_2({\sigma_1}^2+{\sigma_t}^2) + \sqrt{\begin{pmatrix}{\sigma_2}^2{\sigma_1}^4+{\sigma_t}^4{\sigma_1}^2+{\sigma_t}^2{\sigma_1}^4\\ -{\sigma_2}^4{\sigma_t}^2-{\sigma_2}^4{\sigma_1}^2-{\sigma_2}^2{\sigma_t}^4\end{pmatrix}\ln\left(\frac{{\sigma_1}^2+{\sigma_t}^2}{{\sigma_2}^2+{\sigma_t}^2}\right)+ (m_2-m_1)^2({\sigma_t}^2{\sigma_2}^2+{\sigma_2}^2{\sigma_1}^2+{\sigma_t}^4+{\sigma_t}^2{\sigma_1}^2)}\right) \tag{B.31}$$